



The
University
Of
Sheffield.

Functional Analysis of a Novel Player in Single Strand Break Repair

PhD Thesis Submission

by

Kirsty Emma Liversidge

Department of Molecular Biology and Biotechnology
University of Sheffield
Sheffield, United Kingdom

March 2018

Acknowledgements

Firstly, I would like to thank my supervisor Professor Sherif El-Khamisy for providing me with the opportunity to undertake this project and for all the support throughout the process. The advice given has been invaluable and I will be forever grateful for your wealth of knowledge and belief in me. I would like to express huge gratitude to Dr. Swagat Ray, for providing extremely helpful feedback during the thesis writing process, for the vital help with experimental procedures and your patience during lengthy discussions. I can't thank you enough. Thanks to all the members of the El-Khamisy lab, with extra special thanks to Dr. Jude Chiang. Your amazing knowledge base, calm demeanour and willingness to talk just about anything through is so appreciated and will never be forgotten.

Thanks to Dr. Jason King from the Department of Biomedical Science for helpful discussions during the mechanical stress experiments, along with providing me with specialist inserts to use during this process. Thanks also to Ben Phillips, for all the help during the live cell imaging studies. Your expertise in this area was so useful.

I would like to thank my amazing, supportive parents for being there, always. Your belief in me and your constant encouragement through this process is immeasurable and more appreciated than you know. To my little sister, who has shown me first hand that hard work really does pay off. I would also like to acknowledge my grandad, who may not always be in the best of health, but never fails to say 'you can do it Kirst'. Love you all.

To all my friends who have managed to (just about) keep me sane throughout this PhD process, I thank you for being there. Last, but certainly not least, I give the biggest thanks of all to my partner, Arthur. My best friend, my love. I couldn't have completed this process if it wasn't for your sacrifice, patience and your ability to cheer me up almost instantly. I will be forever grateful for your support.

Thank you!

Table of Contents

Table of Contents	i	
List of Abbreviations	vii	
Abstract	x	
 <u>Chapter 1 - Introduction</u>		
1.1	Genome Stability & Regulation	1
1.2	Types of DNA Damage	1
1.2.1	Base Modifications	3
1.2.1.1	Base Damage and AP sites	3
1.2.1.2	Alkylation and Methylation	3
1.2.1.3	Oxidation	4
1.2.1.4	Hydrolysis	5
1.2.2	Bulky Adducts	6
1.2.3	Inter-strand Cross Links	6
1.2.4	Single-strand Breaks	7
1.2.5	Double-strand Breaks	7
1.3	The DNA Damage Response	8
1.3.1	Cell Cycle Checkpoints	8
1.3.1.1	Phosphatidyl-inositol-3 kinase-like kinases (PIKKs)	9
1.3.1.2	G1, Intra-S and G2/M Checkpoints	10
1.3.2	DNA Repair	11
1.3.2.1	Direct Reversal	11
1.3.2.2	Mismatch Repair	11
1.3.2.3	Base Excision Repair	12
1.3.3.4	Nucleotide Excision Repair	14

1.3.3.5	Fanconi Anaemia Pathway	15
1.3.3.6	Single Strand Break Repair	16
1.3.3.7	Double Strand Break Repair	19
1.3.3.8	Homologous Recombination	19
1.3.3.9	Non-Homologous End Joining	22
1.4	DNA Topoisomerases	24
1.4.1	Topoisomerase Classification	24
1.4.2	Mechanism of Action	24
1.4.3	Roles of Topoisomerases in Cellular Processes	25
1.4.3.1	Transcription	25
1.4.3.2	Replication	25
1.4.3.3	Remodeling of Chromatin	26
1.4.4	Topoisomerase 1-cleavage complexes (TOP1cc)	26
1.4.5	Usage of TOP1 Poisons in a Clinical Setting	29
1.5	TDP1	30
1.5.1	TDP1 Structure	30
1.5.2	TDP1 Cellular Processes and Interacting Proteins	32
1.5.3	TDP1 Deficiencies and Clinical Relevance	33
1.6	Linking Structural Proteins to the DNA Damage Response	33
1.7	Nuclear Mitotic Apparatus Protein 1 (NuMA)	34
1.7.1	NuMA Structure	34
1.7.2	NuMA Cellular Processes and Interacting Proteins	37
1.7.3	NuMA/Related Protein Deficiencies and Clinical Relevance	39
1.8	Aims and Objectives	40

Chapter 2 – Materials and Methods

2.1 General Chemicals and Equipment	41
2.2 Bacterial Transformation and Cloning Techniques	41
2.2.1 DNA Plasmids	41
2.2.2 Bacterial Transformations – Propagation of Plasmid DNA	42
2.2.3 Colony Selection	42
2.2.4 Mini-Prep	42
2.2.5 Midi-Prep	42
2.2.6 DNA Quantification	43
2.2.7 Primer Design	43
2.2.8 Gibson Assembly	43
2.2.9 PCR Mixes & Reaction Times	44
2.2.10 Agarose Gel Electrophoresis	46
2.2.11 Gel Extraction	46
2.2.12 Restriction Digest	47
2.2.13 Ligation	47
2.2.14 DNA Sequencing	47
2.2.15 Standard Solutions for Transformations and Cloning	48
2.3 Mammalian Cell Culture	48
2.3.1 Cell Lines	48
2.3.2 Media	49
2.3.3 Passaging of Cells	49
2.3.4 Cell Counting	50
2.3.5 Differentiation of SH-SY5Y Cells	50
2.3.6 Solutions required for mammalian cell culture	50
2.4 Transfection (DNA and RNA)	51
2.4.1 DNA/RNA Transfection	51
2.4.2 Solutions required for DNA/RNA transfection	52
2.5 Protein Analysis of Cellular Extracts	53
2.5.1 Cell Lysis – Preparation of Whole Cell Extract	53
2.5.2 Co-Immunoprecipitation	54
2.5.3 Bradford Assay	55
2.5.4 SDS-PAGE	55

2.5.5 Loading of Samples	57
2.5.6 Western Blotting	57
2.5.6.1 Transfer	57
2.5.6.2 Blocking of Membranes	57
2.5.6.3 Probing with Antibodies	57
2.5.6.4 Stripping of Membranes	59
2.5.7 Solutions required for Protein Analysis and Western Blotting	59
2.6 DNA Damage and Repair Assays	60
2.6.1 Alkaline Comet Assay	60
2.6.2 Clonogenic Survival Assay	62
2.6.3 Immunofluorescence Studies	62
2.7 Mechanical Stress of Cells	64
2.7.1 Preparation of Agarose	64
2.7.2 Cutting of Agarose	64
2.7.3 Addition of Plastic Inserts	65
2.7.4 Removal of Inserts and Agarose Discs	65
2.7.5 Schematic of Application of Mechanical Stress	66
2.8 Statistical Analysis	66

Chapter 3 – SSBR and DSBR

3.1 Introduction	67
3.2 NuMA depletion results in accumulation of DSBs	67
3.3 NuMA depletion results in accumulation of PDBs	71
3.4. NuMA depletion results in a cellular repair defect in response to oxidative stress	78
3.5 NuMA depletion affects cell survival	84
3.6 Discussion	86

Chapter 4 – Interacting Partners of NuMA

4.1 Introduction	95
-------------------------	-----------

4.2 TDP1 physically interacts with PARP1	95
4.3 NuMA physically interacts with TDP1	97
4.4 PARP1 and NuMA bind to different regions of TDP1	103
4.5 TDP1, PARP1 and NuMA are epistatic for the repair of SSBs	111
4.6 Discussion	124

Chapter 5 – Proteomic Analysis of NuMA

5.1 Introduction	132
5.2 Long isoform complementation rescues the NuMA depletion associated repair defect	133
5.3 Truncated versions of NuMA rescue the repair defect associated with NuMA depletion	150
5.4 Discussion	161

Chapter 6 – Functional Analysis of the Effect of Mechanical Stress on Mammalian Cells

6.1 Introduction	165
6.2 Mechanical stress increases the level of SSBs	165
6.3 Imaging of cells after application of mechanical stress	173
6.4 Discussion	178

Chapter 7 – General Discussion

7.1 NuMA is involved in SSBR	184
7.2 NuMA interacts with TDP1, a key player in resolution of PDBs	185
7.3 Long isoform of NuMA rescues the repair defect observed when NuMA is depleted to a greater extent than the short isoform	186
7.4 The globular tail domain of NuMA is sufficient to rescue	187

the repair defect associated with NuMA depletion

7.5 The deletion of the microtubule binding domain still allows for the rescue of the repair defect associated with the knockdown of NuMA	188
7.6 Mechanical stress prevents the repair of TOP1-linked and oxidative-induced SSBs	188
7.7 Future Work	189
7.8 Conclusion	191
References	192

Abbreviations

3'OH – 3' Hydroxyl

5'drp – 5' Deoxyribose Phosphate

7MeG – N7-Methylguanine

8-oxoG – 8-oxoguanine

AGTs – Alkylguanine-DNA-Alkyltransferases

ALS – Amyotrophic Lateral Sclerosis

AOA1 – Ataxia with Oculomotor Apraxia Type 1

AOA2 – Ataxia with Oculomotor Apraxia Type 2

AP – Apurinic/Apyrimidinic

APC – Aphidicolin

APE1 – AP Endonuclease 1

APLF – Aprataxin-and-PNK-Like Factor

APT X – Aprataxin

A-T – Ataxia Telangiectasia

ATM – Ataxia Telangiectasia Mutated

ATR – Ataxia Telangiectasia Mutated and Rad3-related

ATRIP – ATR interacting protein

BER – Base Excision Repair

BLM – Bloom Syndrome RecQ like Helicase

CDK – Cyclin-Dependent Kinase

CHK – Checkpoint Kinases

Chk1 – Checkpoint Kinase 1

Chk2 – Checkpoint Kinase 2

CPD – Cyclobutane-Pyrimidine Dimer

CPT – Camptothecin

CRL4 – Cullin-Ring Finger Ligase-4

CSA – Cockayne syndrome A

CSB – Cockayne syndrome B

DDB1-DDB2 – DNA damage binding protein 1/2

DDR – DNA Damage Response

DNA – Deoxyribonucleic Acid

DNA-PKcs – DNA-dependent protein kinases
DRB – 5,6-dichloro-1-beta-D-ribofuranosylbenzimidazole
DSB – Double Strand Break
DSBR – Double Strand Break Repair
FA – Fanconi Anaemia
FEN1 – Flap Endonuclease 1
G₀ – Gap 0/Senescence
G₁ – Gap 1 phase
G₂ – Gap 2 phase
GG-NER – global-genome Nucleotide Excision Repair
H₂O₂ - Hydrogen Peroxide
H2AX – Histone H2A variant X
HGPS – Hutchinson-Gilford progeria syndrome
HNPCC – Hereditary Non-Polyposis Colorectal Cancer
ICLs –Interstrand cross links
IR – Ionising Radiation
LP-BER – Long Patch Base Excision Repair
M – Mitosis phase
MBD – Microtubule Binding Domain
MGMT – O6-methylguanine DNA methyltransferase
MMR – Mismatch Repair
MMS – Methyl Methanesulfonate
MNU – *N*-methyl-*N* -nitrosourea
MRN – Mre11-Rad50-Nbs1
NER – Nucleotide Excision Repair
NuMA – Nuclear Mitotic Apparatus Protein 1
O6-MeG – O6-methylguanine
p53 – Tumour protein 53
PAR – Poly ADP-ribose
PARG – Poly ADP-ribose Glycohydrolase
PARP1 – Poly(ADP-ribose) Polymerase 1
PARP3 – Poly(ADP-ribose) Polymerase 3
PCNA – Proliferating Cell Nuclear Antigen

PDBs – Protein-linked DNA Breaks
PIKK – Phosphatidylinositol-3 kinase-like kinases
PLD – Phospholipase D
PNKP – Polynucleotide Kinase Phosphatase
PTM – Post-translational Modification
RD – Restrictive Dermopathy
RNA – Ribonucleic Acid
RNaseH1 – Ribonuclease H1
ROS – Reactive Oxygen Species
RPA – Replication Protein A
S – Synthesis phase
SCAN1 – Spinocerebellar Ataxia with Axonal Neuropathy 1
siRNA – Small/Short Interfering RNA
SMC – Structural Maintenance of Chromosomes 1
SP-BER – Short Patch Base Excision Repair
ssDNA – Single-Stranded DNA
SSB – Single Strand Break
SSBR – Single Strand Break Repair
SUMO – Small Ubiquitin-like Modifiers
TC-NER – transcription-coupled Nucleotide Excision Repair
TDP1 – Tyrosyl-DNA Phosphodiesterase 1
TOP1 – Topoisomerase 1
TOP1cc – Topoisomerase 1 Complex Complex
TOP2 – Topoisomerase 2
TOP3 – Topoisomerase 3
TLS – Trans-lesion Synthesis
UV – Ultraviolet
XLF – XRCC4-like factor
XPA – *Xeroderma pigmentosum* group A
XPC – *Xeroderma pigmentosum* group C
XPE – *Xeroderma pigmentosum* group E
XPF – *Xeroderma pigmentosum* group F
XRCC1 – X-ray Cross Complementing Protein 1

Abstract

Over the past few decades, the understanding of DNA damage and associated repair mechanisms has greatly increased. To maintain the integrity of the genome, damaged DNA must be repaired quickly and accurately. If breaks are unrepaired, diseases such as cancer and neurodegeneration can occur. Single-stranded DNA breaks (SSBs) are the most common type of damage in vertebrate cells. SSBs can arise from oxidative attack on the DNA backbone, or from trapping of endogenous enzymes such as DNA topoisomerases. Much is known about the mechanisms whereby cells resolve SSBs but little is known about how these are coordinated with nuclear structure. Growing evidence suggests that defects in structural components of cells, e.g. lamins, can cause defects in the DNA damage response. It was decided to examine the interplay between SSB repair and nuclear structural proteins. In my doctoral work, I have tried to investigate the underlying mechanism between nuclear mitotic apparatus protein 1 (NuMA), a protein which is involved in mitotic spindle orientation during mitosis, and the DNA damage response (DDR). siRNA knockdowns showed that NuMA depletion leads to the accumulation of both topoisomerase 1 (TOP1)-linked and oxidative-induced SSBs. Cells with depleted levels of NuMA also exhibit a repair defect after H₂O₂ treatment. Tyrosyl-DNA Phosphodiesterase 1 (TDP1) is a DNA repair enzyme that can remove a variety of covalent adducts from DNA through hydrolysis of a 3'-phosphodiester bond and primarily repairs abortive TOP1 linked DNA breaks. Using co-immunoprecipitation, it was shown that TDP1 physically interacts with NuMA. TDP1 and NuMA have been shown to exist in a complex with poly(ADP-ribose) polymerase 1 (PARP1), and have displayed epistasis in single strand break repair (SSBR). The studies into NuMA and its involvement with the DDR were facilitated through a multi-experimental approach, aimed to give a well-rounded view of NuMA's role within the DDR.

Chapter 1

Introduction

1.1 Genome Stability & Regulation

The human genome encodes all genetic material, including DNA which codes for proteins and mitochondrial DNA. There are an estimated 20,000-25,000 genes within the human genome, as discovered upon the completion of 'The Human Genome Project' in 2003. Genetic material is subjected to alterations constantly by both intracellular mechanisms and environmental stimuli. Intracellular processes such as transcription and replication are 'programmed', however internal errors can result in DNA damage. Reactive oxygen species are also a major cause of damage to the genetic material. The external environment can pose a variety of damaging threats, including ultraviolet radiation (UV), ionising radiation (IR) and a wealth of chemical agents. Although genetic variations via adaptation is a necessity for the continuation of evolution, it is also imperative to keep DNA alterations under control. The regulation of DNA insults is especially important during reproduction as intact, undamaged genetic information is required to be passed on to progeny, so to avoid germline mutations. If the DNA becomes damaged before, or as reproduction occurs, there are many potentially devastating issues which may arise. In order to keep DNA damage levels in check, higher eukaryotes have a plentiful, established network of tools to rectify any insults that may occur. This is vital as endogenous lesions alone amount to around 20,000 lesions per cell, per day and under normal physiological conditions, do not lead to cell death (Drabløs, et al., 2004). There are many different DNA repair pathways which are specifically tailored to different types of DNA damage. As the area of DNA damage and repair continues to expand and develop, scientists delve deeper into understanding mechanisms further.

1.2 Types of DNA Damage

There are many causative agents of DNA damage, both of endogenous and exogenous origin. The types of damage can be loosely grouped by mechanism of action and by which part of the DNA it targets. Damage can primarily target nucleotide residues, the bonds

between residues, or the sugar phosphate backbone itself. The general blanket term base modifications refers to processes such as alkylation, methylation, oxidation and hydrolysis. These lesions most often arise due to ROS. Interstrand cross links (ICLs) can arise due to chemical agents, of which a proportion of cross link-inducing agents are used to day as chemotherapeutic drugs. ICLs act via preventing the DNA helix from separating. This is a process which is essential for the transcription and replication of genetic material. ICLs have become heavily studied in the context of Fanconi Anaemia (FA) as patients exhibit a severe sensitivity to ICLs which leads to genome instability (Deans & West, 2011). Bulky lesions can arise from cytotoxic chemicals, including those in cigarette smoke. These lesions tend to be carcinogenic due the chemical having the ability to covalently bind to DNA, creating a bulky adduct. If bulky adducts fail to be repaired, they can lead to more detrimental events such as strand breaks (Hang, 2010). Single-strand breaks (SSBs) are lesions which arise when one strand of the DNA duplex is broken. They form due to disruptions within the DNA backbone, which can lead to genomic instability. Double-strand breaks (DSBs) are breaks which arise when both strands of the DNA duplex are broken. They can arise via the exposure to many exogenous agents, e.g. UV radiation, but also due to endogenous machineries failing, such as replication fork collapse as a response to unrepaired DNA damage. DSBs are deadly lesions which unless repair can be carried out effectively, ultimately result in cell death (Chapman, et al., 2012). Figure 1.1 shows the main categories of DNA damage.

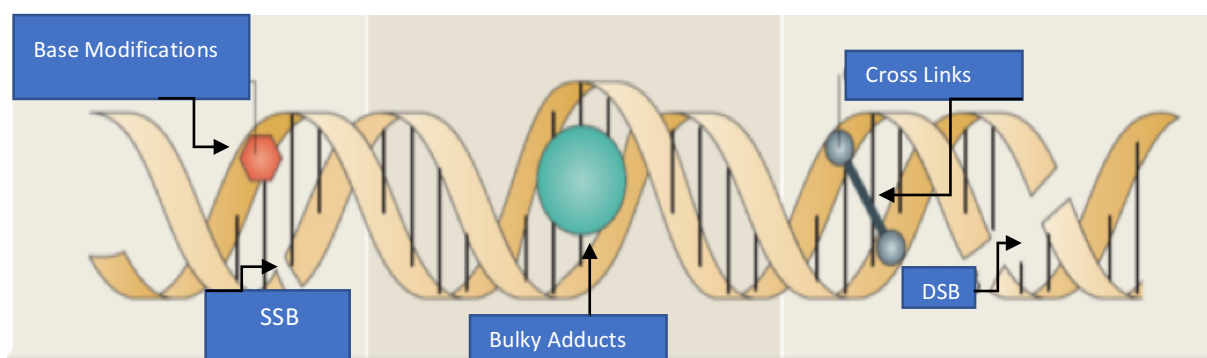


Figure 1.1 Types of DNA Damage. Visual representation of the most common forms of DNA damage are shown in the schematic. **Adapted from Wells & El-Khamisy, 2014.**

1.2.1 Base Modifications

1.2.1.1 Base Damage and AP sites

Damage targeting bases or at apurinic/apyrimidinic (AP) sites (abasic sites) is common, from both endogenous and exogenous sources. This type of damage totals approximately 10^4 lesions per cell, per day (Lindahl & Nyberg, 1972). Endogenous damage to bases usually arises from base modification by processes such as oxidation. The exogenous causes of base damage include exposure to a vast array of alkylating agents such as harmful smoke from tobacco and cytotoxic chemicals (Alagoz, et al., 2014). AP sites also arise very readily, usually as a by-product of the base excision repair (BER) process. During the repair of a damaged base via BER, the recognition of the damaged base is coordinated by a DNA glycosylase, which leads to the cleavage of an N-glycosidic bond. This event can leave behind an AP intermediate residue, which has the potential to cause strand breaks (Mohammed, et al., 2011).

1.2.1.2 Alkylation and Methylation

Substances which allow for the transfer of alkyl groups to nucleotides within the DNA backbone are broadly classified as alkylating agents (Soll, et al., 2017). Damage to DNA caused by alkylation lesions can arise through endogenous complexes such as S-adenosylmethionine, environmental stimuli such as carcinogenic combustion fumes and cytotoxic chemicals called alkylating agents (Drabløs, et al., 2004). The most common and simplest form of alkylation is that of methylation. This process involves the transfer of methyl group(s) to DNA base(s) (Soll, et al., 2017). As the methyl groups are transferred to DNA, they can cause bulky adducts within the DNA, leading to blocking of replication. They can also disrupt the pairing of bases, which leads to mutagenesis. The most prevalent methylation lesion within the body, accounting for around 75% of adducts produced is N7-methylguanine (7MeG) (Beranek., 1990). Although the most common, this lesion alone is reasonably harmless. However, it is susceptible to spontaneous depurination which can lead to further base damage and AP site generation. This, as mentioned previously, has the potential to become a greater deleterious threat (Soll, et al., 2017). Less common methylation lesions include N3-methyladenine and N1-methyladenine. These lesions, although they occur less regularly, are naturally cytotoxic. This is due to the fact that the methyl group added at the N3 or N1 positions of the

nucleotide prevent DNA polymerases from binding to the DNA and therefore physically block the process of replication. As previously mentioned, this is a highly cytotoxic event (Fronza & Gold, 2004). One other major methylation which occurs due to SN1 alkylating agents (react directly with bases) such as *N*-methyl-*N*-nitrosourea (MNU) is that of O6-methylguanine (O6-MeG). O6-MeG poses a large mutagenic threat as when position O6 is methylated, DNA polymerases have a tendency to mis-insert a thymine (T) residue instead of a cytosine (C) residue opposite the O6-MeG moiety. This leads to a mismatch of bases and therefore gives rise to the potential of carcinogenesis (Warren, et al., 2006; Klapacz, et al., 2008). Methylation events are very diverse and can affect many different DNA sites, and hence the body has a wealth of pathways to combat alkylation and methylation events. One very specific mechanism which recognises and resolves SN1-mediated alkylation is the DNA repair enzyme O6-methylguanine DNA methyltransferase (MGMT). This enzyme has the ability to demethylate the O6-methylguanine residue, therefore preventing mismatch of bases (Martin, et al., 2009) (Soll, et al., 2017). This process is however much more specific to SN1-type agents rather than SN2-type agents (forms a reactive intermediate which reacts with bases) such as methyl methanesulfonate (MMS). Alkylating agents, such as cyclophosphamide and temozolomide have been exploited in recent years for their DNA transcription- and replication- blocking properties for usage as anti-cancer therapies.

1.2.1.3 Oxidation

The oxidation of bases and subsequent damage to cellular DNA is ubiquitous in nature and one which is particularly prevalent in aerobic organisms. Oxidation is one of the most common type of base damage within the human body, causing a high level of the daily cellular DNA damage (Maynard, et al., 2009). The oxidation is caused through a family of chemically reactive molecules called reactive oxygen species (ROS) (Cadet, et al., 2017). Exogenous stimuli can be a source of ROS production; these include pollutants, types of radiation (IR and UV) and harmful chemicals (Maynard, et al. 2014). However, the main source of ROS is endogenously produced radicals from certain organelles. The most prevalent producer of ROS is the mitochondria, during the process of oxidative phosphorylation (Holmström & Finkel, 2014). The predominant ROS generated by the mitochondria are the free radicals, superoxides (O_2^-). These can arise from electron leakage from the electron transport chain which results in the spontaneous conversion to oxygen. This event occurs in around 1-2% of consumed oxygen during oxidative

phosphorylation (West, et al., 2011, Cui, et al., 2012). The superoxides can be converted to non-radical ROS such as H₂O₂. This can happen in one of two ways; via a catalyzed reaction involving superoxide dismutase (SOD) or as a spontaneous event (Cui, et al. 2012). Other organelles which are a source of ROS production are the endoplasmic reticulum, and peroxisomes. Peroxisomes can generate ROS during fatty acid metabolism (Holmström & Finkel, 2014). Other enzymatic processes within cells can also bring about the production of ROS. The formation of dangerous hydroxyl radicals can be caused by the reduction of H₂O₂ by ferrous ions, in a process named the Fenton reaction (Cadet, et al., 2017). The generation of intracellular ROS, can also bring about base oxidation, most notably the oxidation of guanine residues. Guanine can be oxidised to form 8-oxoguanine (8-oxoG) which has been reported as being a cytotoxic and potentially mutagenic modification (Singh, et al., 2011). Due to the mutagenic nature of the modification, it is required to be removed. The removal of the lesion is usually performed by the repair enzyme 8-oxoguanine-DNA glycosylase (Singh, et al., 2011).

1.2.1.4 Hydrolysis

Processes such as alkylation and excessive heating can lead to the glycosidic bonds between DNA molecules becoming very susceptible to alterations (De Bont & van Larebeke, 2004). The labile glycosidic bonds can be enzymatically cleaved, spontaneously, by DNA glycosylases which leads to the formation of AP sites. This process is often alluded to as depurination (Gates, 2009). As previously discussed, these abasic sites have the potential to cause strand breaks. The production of ROS also has the capability of causing these hydrolytic events. Another type of damage via hydrolysis is that of the hydrolytic deamination of bases (Lindahl, 1993). Deamination of nucleotides occurs much more readily on single stranded DNA (ssDNA) compared to double stranded DNA (dsDNA) (Gates, 2009). The main target of deamination is cytosine residues and the methylated version of cytosine, 5-methylcytosine (De Bont & van Larebeke, 2004). The cytosine residue can be spontaneously deaminated to an uracil residue. This is then effectively removed due to the non-DNA base nature of uracil via the activity of uracil-DNA glycosylase (Cooper, et al., 2010). However, 5-methylcytosine residues are often the subject of spontaneous deamination, due to the deamination of these residues occurring around 3 times quicker than on that of cytosines (De Bont & van Larebeke, 2004). The deamination of 5-methylcytosine also poses a greater mutagenic potential than that of

cytosine residues. This is due to the deamination of 5-methylcytosine yielding thymine residues, rather than uracil in the case of cytosine deamination. As thymine is a recognized DNA base, the recognition of the incorrect base substitution is not as rapid as the activity of uracil-DNA glycosylase. This can give rise to the mismatch of bases and therefore can lead to strand breaks (Cooper, et al., 2010).

1.2.1.5 Bulky Adducts

Bulky lesions are compounds which can bind to the DNA covalently, posing a high mutagenic risk (Hang., 2009). Bulky lesions tend to stem largely from exogenous sources, usually from toxic chemicals such as those in tobacco smoke and UV damage. Due to the nature of the source, most bulky adduct formation are of a carcinogenic nature. It has been discovered that the most common mutation arising from bulky lesions are substitutions in guanine for the base thymine (Denissenko, et al., 1998). As with the deamination of bases, this can lead to the mismatch of bases and gives rise to more deleterious events such as DSBs. The repair pathway of choice for the removal of these type of lesions is nucleotide excision repair (NER). This pathway facilitates the repair of the bulky adduct relatively slowly and it is thought that this could give rise to their carcinogenic potential (Denissenko, et al., 1998).

1.2.2 Inter-strand Cross Links

Inter-strand cross links (ICLs) are lesions which inhibit the separation of the strands of the DNA duplex, hence blocking the necessary transcription and replication of DNA (Deans & West, 2011). The major stimuli for the formation of ICLs arise from environmental factors, mostly chemical mutagens which can pose a great threat to the integrity of DNA (Deans & West, 2011). ICL forming agents include nitrogen mustard-related chemicals, such as cyclophosphamide. There are a few endogenous sources which can form ICLs, such as by-products of cellular processes such as lipid peroxidation and nitric oxides (Schärer, 2005). Another well-documented endogenous source of the introduction of ICLs is that of formaldehyde and its ability to react with DNA. Although the initial reaction introduces ICLs, this is a reversible process. As the damage can be reversed, the precise detection and subsequent repair of this type of lesion can prove difficult.

1.2.3 Single-strand Breaks

Single-strand breaks (SSBs) form due to disruptions within the DNA backbone, which can lead to genomic instability. This lesion is the most commonly occurring type of DNA damage within the human body. There can be in excess of tens of thousands of SSBs per cell, per day (Lindahl & Nyberg, 1972). The DNA break usually involves the loss of a nucleotide, including damage to the 3' and 5' termini surrounding the break (Neil, et al., 2012). There are many situations in which DNA SSBs can arise, and may be caused by both endogenous and exogenous agents. The main endogenous causative agent of SSBs is that of reactive oxygen species (ROS), which can directly attack the DNA sugar phosphate backbone (Neil, et al., 2012). The enzymatic activities of DNA topoisomerase I can also give rise to SSBs (McKinnon & Caldecott, 2007) (Katyal, et al., 2007). Exogenous agents which can produce SSBs include ionising radiation, which can permanently damage DNA via the oxidation of bases in the absence of adequate repair mechanisms. (Lomax, et al., 2002).

1.2.4 Double-strand Breaks

Double-strand breaks (DSB) are the least frequent of all lesions discussed, as most DSBs are formed if other types of damage are not repaired effectively. There are many well established repair pathways that aim to deal with initial, less severe damage, but the DDR is also equipped to deal with deleterious lesions such as DSBs. DSBs form due to two individual SSBs simultaneously occurring on complementary strands of DNA, hence compromising the stability of the sugar phosphate backbone (Mehta & Haber, 2014). The main source of DSBs is ionizing radiation (IR). As little as a single radiation track can induce a DSB, and hence high doses of IR can be highly dangerous and has huge carcinogenic potential (Rothkamm & Löbrich, 2003). Insults on the DNA caused by IR can be highly cytotoxic and due to them affecting both strands of the DNA, results in a loss of genomic material, leading to genome instability (Rastogi, et al., 2010). Endogenous causes of DSBs include ROS and clashes of DNA transcription and replication, such as transcription machinery collisions (Mehta & Haber, 2014). Although many DSBs are brought about in a mutagenic setting, not all DSBs are spontaneous. Programmed DSB introduction is a key process in meiosis, as it enables the induction of the homologous recombination (HR) pathway, which allows for the efficient and precise segregation of

chromosomes (Murakami & Keeney, 2008; Cannan & Pedersen, 2016). If DSBs are not repaired in a timely and effective manner, genetic stability is severely compromised and hence can lead to carcinogenesis and potential cell death.

1.3 The DNA Damage Response

As explained, there are many internal and external stimuli which can cause various types of DNA damage. To combat the many insults encountered on a daily basis, cells must be armed with a vast array of tools to deal with damage in an efficient and timely manner. The DNA damage response (DDR) is an intricate signal transduction pathway which enables the recognition of damage and the timely transmission of information to cells in order to elicit the appropriate response. The responses must be kept under tight regulations, to provide the precise action to match the specific type of DNA damage, which makes for quick and accurate repair of the damage (Ciccia & Elledge, 2010). This is required to prevent potentially deleterious modifications from being passed on to progeny cells. The DDR is a very important pathway and there are many conditions arising from defective DDR factors. These include an increased sensitivity to DNA-damaging agents, a predisposition to cancer and neurodegenerative conditions, as well as many other human disease states (Jackson & Bartek, 2009).

1.3.1 Cell Cycle Checkpoints

Stringent regulation of pathways is common practice in many systems throughout the body, including eukaryotic DNA replication. It is imperative that each chromosome only replicates once during each cell cycle (Sclafani & Holzen, 2007). There are 4 stages to the cell cycle; 3 stages collectively referred to as interphase Gap 1 (G_1), Synthesis (S) and Gap 2 (G_2) and the stage of Mitosis (M). G_1 is the phase where the cells are duplicating cellular material in preparation for DNA synthesis. S phase is where the DNA replication is carried out, which results in the duplication of chromosomes into sister chromatids. G_2 phase is the preparation of cells for entering mitosis, whereby the newly duplicated DNA is assessed for damage. M phase is made up of 4 stages; anaphase, prophase, metaphase and telophase by the end of which the chromosomes will have been efficiently segregated into two daughter cells. After the completion of mitosis, there are two options for cells. They can begin the interphase cycle again and return to G_1 phase, or they can exit the cycle and reside in G_0 phase. G_0 is a cellular state outside the cell cycle, of which cells are 'resting';

this resting can be reversible (quiescent cells) or irreversible (senescent or differentiated) (Vermeulen, et al., 2003).

The progression of cells into each of the 4 phases is tightly controlled by cyclin-dependent kinases (CDKs). CDKs belong to the serine/threonine protein kinase family and are activated at various points of the cell cycle. They have the ability to phosphorylate important substrates in order to promote the synthesis of DNA and the entrance into mitosis (Vermeulen, et al., 2003; Barnum & O'Connell, 2014). The inhibition of CDKs can halt or severely slow the progression of cells through the cell cycle. This is facilitated by the use of cell cycle checkpoints (Jackson & Bartek, 2009). There are 3 major cell cycle checkpoints; G₁/S, intra-S and G₂/M. The utilisation of checkpoints ensures that cells do not enter the next phase of the cell cycle before the current phase is completed (Kastan & Bartek, 2004). Checkpoints are employed at these stages in the cell cycle to ensure that adequate time is available to repair any damaged DNA, or to eradicate cells which are beyond the point of repair, before further progression through the cell cycle (Jackson & Bartek, 2009).

1.3.1.2 Phosphatidyl-inositol-3 kinase-like kinases (PIKKs)

The phosphatidyl-inositol-3 kinase-like kinases (PIKKs) ATM (ataxia telangiectasia mutated) and ATR (ATM and Rad3-related) are the major factors in regulating the DDR-signaling pathways in mammalian cells (Jackson & Bartek, 2009). The activation of ATM and ATR is accepted as the first step in the signal transduction pathway which leads to cell cycle arrest after recognition of DNA damage. ATM and ATR along with DNA-dependent protein kinases (DNA-PKcs) are the furthest upstream components of the DDR (Maréchal & Zou, 2013). The recognition of DNA damage leads to a downstream cascade of signals, leading to the phosphorylation of various targets at serine, threonine or glutamine residues, often in a ATM or ATR-dependent manner. A wealth of reversible post-translational modifications (PTMs) such as phosphorylation or ubiquitylation events by small molecules such as SUMO (small ubiquitin-like modifiers) also occur in response to DNA damage (Schimmel, et al., 2014; Maréchal & Zou, 2013).

The main players in the DDR downstream of ATM and ATR are the checkpoint kinases, Chk1 and Chk2. Chk1 and Chk2 are serine/threonine protein kinases which are activated and regulated by ATR and ATM, respectively, in response to DNA damage (Zhou & Elledge, 2000). Briefly, ATM activation is mostly associated in response to DSB recognition by the MRN (Mre11-Rad50-Nbs1) complex. The MRN complex upon detection of a DSB localizes to the site of damage and recruits ATM, which in turn autophosphorylates to form the active monomer (Patil, et al., 2014). In contrast, ATR is usually recruited to sites of SSB often caused by UV radiation damage or SSBs arising from replicative stress. ATR is recruited by the sensor of the SSB, RPA (replication protein A) which binds to ssDNA to form an RPA coating. In turn this event recruits ATR to sites of damage by means of its interacting partner, ATRIP (ATR interacting protein) (Patil, et al., 2014).

1.3.1.2 G₁, Intra-S and G₂/M Checkpoints

Genotoxic stress encountered within the G₁-phase of the cell cycle promotes the phosphorylation of the tumour suppressor p53. The CDK inhibitor, p21, is a major activation target of p53. Once activated in a p53-dependent manner, p21s elevated levels lead to the inhibition of cyclin E and the suppression of CDK2, of which activity is associated with Cyclin A. These events result in the prevention of cells residing in G₁ phase progressing into S phase (Abraham, 2001). p21 can also activate many downstream genes to determine the induction of apoptosis (Abbas & Dutta, 2009; Abraham, 2001). The major role of the S-phase checkpoint is to significantly reduce the rate of DNA replication upon detection of DNA damage (Willis & Rhind, 2009). The halting of DNA replication is can be in response to IR-induced DSBs (Sørensen, et al., 2003). This enables more available time to repair any damage whilst still in S-phase, before the cells reach G₂ phase. Another major event during S-phase is in response to the recognition of bulky lesions mostly caused by UV damage. The response to lesions of this kind require ATR and the activation of Chk1 to act on downstream target proteins in order to prevent DNA replication. This process can also prevent DNA strand elongation. The G₂/M checkpoint is the final checkpoint of the cell cycle and its main role is to prevent cells with damaged DNA from entering mitosis. Arrest in this stage allows adequate time for the

DNA damage to be repaired, and as chromosome segregation occurs in mitosis, this checkpoint is particularly important in preventing genomic instability (Abraham, 2001).

1.3.2 DNA Repair

As discussed, there are many different types of DNA damage. Depending on the nature of the damage sustained and the stage of the cell cycle the cell has entered, the cell has many options by which it can repair the damage. A wealth of repair pathways enable detection of a lesion and the subsequent effective repair.

1.3.2.1 Direct Reversal

There are many well established DNA repair pathways which are very complex. However, a small cohort of DNA lesions can be repaired by the process called direct reversal. This process involves the direct repair of the damage without having to make a cut in the DNA backbone or affect the molecular integrity. As mentioned, this type of repair is only applicable to a small subset of lesions; namely the reversal of UV radiation induced photolesions and the reversal of damage caused by O-alkylation by O6-alkylguanine-DNA-alkyltransferases (AGTs) (Chenggi & Chuan, 2013).

1.3.2.2 Mismatch Repair

Mismatch repair (MMR) is a process which carries out the switching of mispaired DNA bases, for the correct base. These mispairings can arise due to errors during the replication of DNA (Hombauer, et al., 2011). MMR is instigated by the mismatch being recognised by MutS-related Msh2-Msh6 (MutS α) and/or the Msh2-Msh3 (MutS β) heterodimers. MutS α is predominantly involved in small-loop MMR and base substitutions. MutS β also plays a role in small-loop MMR, but is also involved in large-loop (>10 nucleotides) MMR; MutS β is unable to repair base substitutions. To note, the MutS α is greatly more abundant and hence this most likely initiates MMR in eukaryotic cells. This being said, MutS β has the important role of fixing any mismatches of bases which have not been efficiently repaired by MutS α . Once mispairing has been identified by mismatch recognition proteins, the Mlh1-Pms2 (MutL α - involved in the co-ordination of MMR) (in humans) and Mlh1-Mlh3 complexes are recruited to the site of damage. This recruitment allows for the formation of a ternary complex with the MutS-complexes and facilitates repair by excision of the mismatched base (Hong, et al., 2008). The repair of

the mismatched base can be carried out bi-directionally; 3' to 5' excision, or 5' to 3' excision. The MutS α and MutS β proteins contain N-terminal binding sites for the proliferating cell nuclear antigen (PCNA). As well as the importance of the loading of PCNA onto the nicked daughter strand in 3' to 5' excision, PCNA is also thought to be involved in damage recognition (Stoimenov & Helleday, 2009; Hombauer, et al., 2011). Exo1 is also an important factor in the repair of mismatched bases, being indispensable for the 5' to 3' excision. Other factors involved in the repair process include the single-stranded binding protein RPA, DNA polymerase δ and DNA ligase (Peltomäki, 2001; Li, 2008). If there are defects in MMR factors, disease states arise. The notable disease related to defective MMR is that of hereditary non-polyposis colorectal cancer (HNPCC) or Lynch Syndrome. The main mutations which give rise to the pathology are those in key MMR factors, Mlh1 and Msh2. Individuals diagnosed with HNPCC have a significant risk of early onset cancer, especially that of colon cancer, with around an 80% chance of cancer development. HNPCC also heightens the risk of other cancers such as skin, gastric and gynaecological cancers in women (Hsieh & Yamane, 2008; Peltomäki, 2001; Li, 2008).

1.3.2.3 Base Excision Repair

Damage to bases is the most common pre-cursor of endogenous DNA breaks, with exogenous stress also accounting to the thousands of lesions per cell, which occur each day. As this damage is very commonly occurring, a pathway evolved to deal with the vast base alterations quickly and effectively. This pathway is known as base excision repair (BER) (Neil, et al., 2012) (Parsons, et al., 2007). This mechanism is used when repairing damage resulting from small lesions which do not affect the integrity of the DNA helix. The pathway is the primary response to the endogenous base damage caused by ROS and the alkylation and hydrolysis of bases (Hedge, et al., 2008). As there is such a high frequency of this type of damage, BER is hugely important in preventing genomic instability. Firstly, a DNA glycosylase recognises the damaged base and performs the removal of the base from the DNA. There have been eleven identified DNA glycosylases in mammals and they can either be monofunctional or bifunctional in nature (Whitaker, et al., 2017; Jacobs & Schär, 2012). Although, in principle, DNA glycosylases all search for, recognise and deal with base damage, their mechanism of action differs depending on classification. Monofunctional glycosylases, as the name suggests, performs just one event; the excision of the base. This is facilitated by nucleophilic attack on the N-

glycosidic bond, performed by a water molecule. The bifunctional glycosylases also excise the damaged base, but in doing so, create a nick in the DNA. The excision of the base performed by bifunctional glycosylases occurs via the use of an amino group of a catalytic lysine side chain, which facilitates nucleophilic attack to cleave the damaged base. This mechanism results in the formation of a base intermediate, which upon resolution, leads to a nick in the DNA and the formation of a 3' blocking residue, which must be processed further before nick sealing can occur (Jacobs & Schär, 2012; Kim & Wilson, 2012). Once basal cleavage has been completed, the glycosylase remains bound to the AP site. In order to repair the AP site, the enzyme APE1 (AP endonuclease 1) is recruited. This enzyme creates a nick in the DNA (if base excision was completed by a monofunctional glycosylase) 5' to the AP site and leaves 3'OH (3' hydroxyl) and 5'dRP (5' deoxyribose phosphate) termini. If base excision was carried out by a bifunctional glycosylase, APE1 removes the 3' blocking residue and creates 3'OH and 5'dRP ends. The 5'dRP is recognised and removal is facilitated by the lyase region of DNA polymerase β , returning the 5'phosphate terminus which is required for ligation to take place. The scaffold protein X-ray cross complementing protein 1 (XRCC1) is recruited to the site, allowing for the filling of the excised base by the nucleotidyl transferase property of DNA polymerase β (Whitaker, et al., 2017; Freudenthal, et al., 2013; Hedge, et al., 2008). The DNA strand is then sealed by DNA ligase 3 α (Parsons, et al., 2007). Certain base lesions are known to be resistant to the process of BER. In this instance it has been found that the 3'-5' exonuclease activity of DNA polymerase δ is the major enzyme involved in the repair of these particular lesions (Parsons et al., 2007). As a single stranded nick is created in BER, there are a number of other key factors which are involved in SSB repair also involved in repairing the breaks and subsequent end processing such as Polynucleotide Kinase Phosphatase (PNKP), Tyrosyl-DNA Phosphodiesterase 1 (TDP1) and Aprataxin (APTX) (Caldecott, 2008; Ward & La Spada, 2015).

1.3.3.4 Nucleotide Excision Repair

An attractive trait in a DNA repair pathway is the capability to recognise many types of damage caused by many endogenous and exogenous agents. The nucleotide excision repair (NER) pathway has the ability to recognise damage caused from a vast array of different agents (de Boer & Hoeijmakers, 2000). It resolves lesions which cause more extensive damage (involving damage to multiple bases) than those which could be repaired by BER (Ciccia & Elledge, 2010). NER removes the damaged DNA by excising an extended section of DNA of approximately 30 base pairs, including the damaged bases. Although the NER pathway has the ability to recognise lesions caused by many stimuli, the most relevant damage which NER targets for repair is that of cyclobutane-pyrimidine dimers (CPDs) and other bulky lesions caused by UV damage (de Boer & Hoeijmakers, 2000). The NER pathway can be categorized into two sub-pathways; transcription-coupled NER (TC-NER) or global-genome NER (GG-NER). TC-NER acts to recognise damage occurring at sites of stalled replication machinery, whereas (as the name suggests) the GG-NER pathway has the ability to recognise damaging lesions throughout the entire genome. Although the damage detection of the sub-pathways vary in nature, the repair of the lesion occurs through a common pathway (Vermeulen & Fousteri, 2013; Schärer, 2013). TC-NER is triggered by the blockage of RNA polymerase II, which occurs as a result of replication fork collapse. This stalling of the RNA polymerase triggers the TC-NER pathway to respond. The mechanisms behind this pathway are not fully understood, however it is accepted that the Cockayne syndrome complementation group proteins A (CSA) and B (CSB) are involved. Compared with CSB, less is known about the role of CSA in the recruitment of the NER machinery, however CSB is known to interact directly with RNA polymerase II and this interaction is thought to be sufficient for the dislodging of the stalled polymerase (Melis, et al., 2013). In the case of GG-NER, the recognition of the lesion is mediated through XPC-RAD23B (*Xeroderma Pigmentosum* complementation group C-RAD23B) and DDB1-DDB2/XPE (DNA damage binding protein 1/2; *Xeroderma Pigmentosum* complementation group E) protein complexes (Hakem, 2008). The XPC protein is instrumental in recruiting the repair machinery to the site of damage. As GG-NER is tasked with scanning the whole genome for damage, it is thought to be a more inefficient repair pathway than that of TC-NER (Melis, et al., 2013). The excision and repair of the lesion is mostly carried out via the same pathway, with small changes depending on whether the damage was detected via TC-NER or GG-NER. The

complex recruited to the damage site is a ubiquitin ligase complex known as CRL4 (cullin-ring finger ligase-4) with the substitution of one constituent of the complex depending on the recognition pathway. In TC-NER the complex consists of CSA-DDB1-CUL4-RBX1 E3 ligase as CSA is involved in the recognition of the stalled RNA polymerase II, although it does not function in the removal of the stalled polymerase. In GG-NER the complex is the same, except the CSA protein is replaced with DDB2 (Melis, et al., 2013). Pathologies arising from defects in TC-NER include cockayne syndrome. This condition results in neurological defects and premature ageing, as well as a severe photosensitivity. GG-NER defects cause the Xeroderma Pigmentosum family of disease states, of which there are 7, with varying ranges of severity. The condition causes a predisposition to skin cancer, due to the extreme photosensitivity leading to profuse lentigine accumulation (de Laat, et al., 1999).

1.3.3.5 Fanconi Anaemia Pathway

The Fanconi Anaemia (FA) pathway is a repair process which acts to repair DNA inter-strand crosslinks (ICLs), acting predominantly in S-phase (Haynes, et al., 2015). The process involves phosphorylation of the FA factor FANCI, which in turn leads to the ubiquitination of both FANCD2 and FANCI, resulting in a FANCD2/FANCI complex forming at the ICL site. It is then thought that removal of the ICL and the subsequent gap-filling stages are carried out by low fidelity polymerases (perhaps by initiated by RAD6/RAD18-induced PCNA monoubiquitination) of the NER and TLS (trans-lesion synthesis) pathways, although this has not been proven (Haynes, et al., 2015). By resolving crosslinks in the DNA, genomic integrity is maintained. Defects in the FA pathway are indicative of the disease of the same name, which is a diverse but rare autosomal inherited disorder, which displays profound genomic instability. FA is the most common of a group of diseases called inherited bone marrow failure syndromes. The disease is characterised by pancytopenia and ultimately the failure of the bone marrow; the pathophysiology of this is yet to be elucidated (Ceccaldi, et al., 2012). FA patients are usually more susceptible to cancers, with onset occurring from a young age (averaging at around 16 years old); to note, cells from FA patients are highly sensitive to DNA crosslinking chemotherapeutic agents such as mitomycin C (Garner & Smogorzewska, 2011).

1.3.3.6 *Single Strand Break Repair*

Single-strand breaks (SSBs) form due to disruptions within the DNA backbone, which result from genomic instability. The DNA break arises from damage to the 3' and 5' termini of the DNA (Neil, et al., 2012). Both endogenous and exogenous stimuli can lead to the formation of DNA SSBs. The main endogenous causative agent inducing SSBs is that of reactive oxygen species (ROS), which can directly attack the DNA sugar phosphate backbone (Neil, et al., 2012). Abortive TOP1 activity can also bring about SSBs (Katyal, et al., 2007). SSB repair (SSBR) is recognised as a more specific sub-pathway of the BER pathway. Initially, the damage is recognised by poly(ADP-ribose) polymerase 1 (PARP1), which binds directly to the site of damage (Ikejima, et al., 1990). This binding to damaged DNA increases the enzymatic action of PARP1 by around 500 times (Abbotts & Wilson, 2017). The binding event leads to the automodification of PARP1 to produce poly ADP-ribose (PAR) chains, which are essential for other key proteins involved in SSBR such as XRCC1. XRCC1 exhibits favourable binding to the automodified version of PARP1 and hence leads to early recruitment of the protein to sites of damage (El-Khamisy, et al., 2003). Once XRCC1 has been recruited to the site of damage, it acts as a scaffold protein and facilitates the recruitment of other factors needed for the processing and subsequent repair of the break. This is required as the PAR chains produced by the automodification of PARP1 are under tight regulation, as they are degraded swiftly by poly ADP-ribose glycohydrolase (PARG) (Wei, et al., 2013). After the recruitment of key factors, the SSB can be repaired in two ways; by short-patch BER (SP-BER) or long-patch BER (LP-BER). Figure 1.2 is a visual representation of the pathways. The SP-BER pathway mechanism was detailed in chapter 1.3.2.3. If the genotoxic insult has damaged more than a single base (usually up to 8 nucleotides), LP-BER is required to repair the DNA. As with SP-BER, APE creates a nick in the DNA 5' to the site of damage and creates a 5'dRP end. DNA polymerases β (proliferating cell nuclear antigen-independent (PCNA)), δ and/or ϵ along with PCNA are able to synthesise the appropriate amount of nucleotides required to fill the gap, and in doing so they displace the 5'dRP strand (Meas & Smerdon, 2016; Prasad, et al., 2000). It is thought that PCNA can bind to flap endonuclease 1 (FEN1), triggering its nuclease activity (Gary, et al., 1999). This strand displacement event creates a 'flap' which is removed by FEN1, returning the 5' phosphate end, which allows for re-ligation of the nick via DNA ligase 1 (Meas & Smerdon, 2016; Sattler, et al., 2003).

As mentioned, various enzymatic processes can bring about SSBs and often there are specific pathways enlisted to deal with such damage. An example of which, is damage brought about by stalled Topoisomerase 1 cleavage complexes (see section 1.4.4). Another key pathway to repair SSBs is the nucleolytic cleavage pathway, which is a non-specific repair mechanism. This pathway results in the loss of genetic material as the damaged bases are removed in a non-specific manner; this potentially gives rise to mutations (Ashour, et al., 2015). There are many end processing factors involved in aspects of SSBR of which, if defects occur, disease states arise. Many of these involve neurological symptoms, indicative of neurodegeneration. Mutations in Aprataxin (APTX), for example, results in the disease Ataxia with oculomotor apraxia type 1 (AOA1). The disease results in cerebellar ataxia and motor neuropathy (Sykora, et al. 2011).

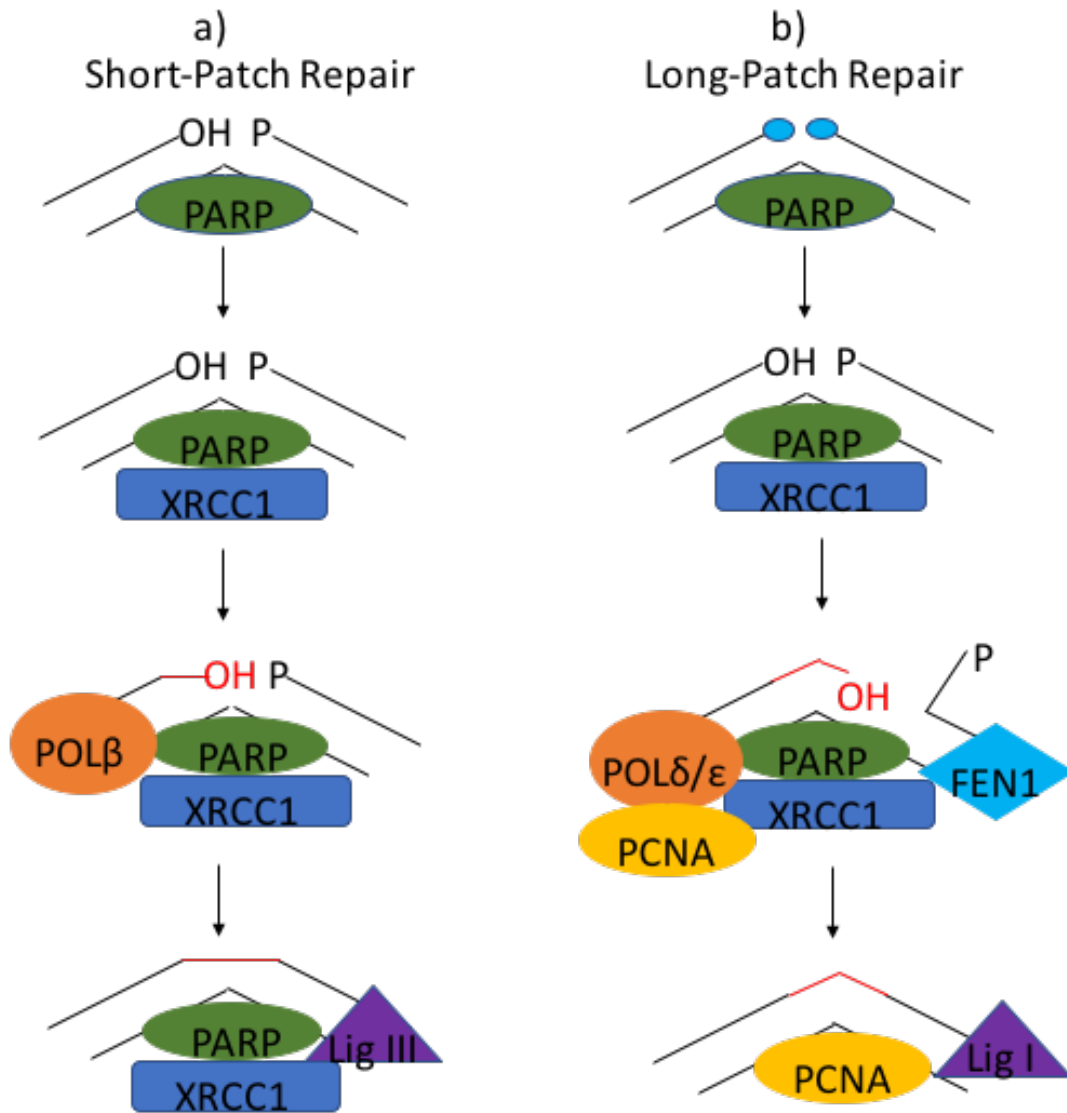


Figure 1.2. **Short-patch and long-patch BER.** a) shows the SP-BER pathway, adopted when only a single base is damaged. PARP1 senses damage and binds to the site. Automodification of PARP1 recruits XRCC1. Polβ fills in the gap with a nucleotide and the break is re-ligated by Ligase 3α. b) shows the LP-BER pathway, involving more proteins. This pathway is utilised when more than one bases are damaged. PARP1 senses damage and binds to the site. Automodification of PARP1 recruits XRCC1. Either Polβ or Polδ/ε (as shown above) along with PCNA synthesise new nucleotides to replace the damaged bases. This displaces the DNA strand creating a ‘flap’ which is cleaved by FEN1. The break is then re-ligated by ligase 1. **Adapted from Curtin, 2005.**

1.3.3.7 Double Strand Break Repair

DNA double strand breaks (DSBs) arise when nicks in both strands of the DNA double helix are created. Such events can be caused by endogenous processes, such as the collapse of replication machinery upon encountering DNA lesions, or exogenous processes such as ionising radiation (Chapman, et al., 2012). DSBs are highly dangerous lesions. If left unrepaired, they can result in cell death or the occurrence of many genetic mutations such as chromosomal rearrangements. These can give rise to genomic instability, a major hallmark of cancer (Shrivastav, et al., 2008). Defects in three major proteins involved in DSB repair (DSBR), NBS1, ATM and ATR, result in the diseases NBS (Nijmegen breakage syndrome) A-T (ataxia telangiectasia) and Seckel syndrome, respectively. NBS is an autosomal recessive disorder which is characterised by growth retardation, microcephaly, immunodeficiency and a predisposition to cancers (Cheung & Ewens, 2006). A-T is a disease state which is typified by cerebellar ataxia (which is progressive) immunodeficiency, as well as the predisposition to develop certain types of lymphoid cancer. Seckel syndrome is characterised by microcephaly, delays in development and pronounced facial features (Bohgaki, et al., 2010). There are two major pathways enlisted to resolve DSBs and depending on cell cycle stage and the severity of the DNA damage sustained are factors of which pathway is selected. They are distinctly different in mechanism and produce different outcomes (Chang, et al., 2017).

1.3.3.8 Homologous Recombination

Homologous recombination (HR) is the one of the main pathways involved in the repair of DSBs. It acts to maintain genomic stability via resolving DSBs as well as various other lesions which could arise endogenously or exogenously, with direct DSBs being caused by IR (Moynahan & Jasin, 2010). It is considered the most precise of the DSB repair mechanisms, due to the utilisation of a homologous chromosome as a DNA template (Jasin & Rothstein, 2013). HR is most prevalent in late S phase/ G₂ phase of the cell cycle, due to the pathway enlisting a homologous donor sequence as the template for the repair activity (Kass, et al., 2013) (Moynahan & Jasin, 2010). As well as the repair of DSBs, the HR pathway is also required to maintain telomeres, restart stalled replication forks and provide accurate segregation of homologous chromosomes during meiosis (Bugreev, et al., 2014). As DSBs are formed, the MRN complex (mre11-RAD50-NBS1) and ATM

become activated and in turn phosphorylate a number of downstream factors in the DDR such as H2AX, and BLM; the order in which MRN and ATM are activated in response to DSB still remains unclear (Uziel, et al., 2003). Figure 1.3 shows a schematic of the pathway. During HR, there is a key strand invasion event, which allows error-free repair via the utilisation of a homologous chromosome. For this event to take place, a small section of nucleotides are removed via the MRN complex and CtIP. The 5' end of the DNA is then resected (a step which is initiated by CDK phosphorylation) to generate a 3' ssDNA overhang, via the action of the complex DNA2-BLM or through Exo1, with the aid of RPA (Pfister, et al., 2014). RPA coats the ssDNA which, with help from BRCA2 and RAD54, gives rise to the nucleofilament formation of RAD51 which initiates the strand invasion event (Pfister, et al., 2014; Bakr, et al., 2015). To note, BRCA1 is an interacting partner of both the MRN complex and CtIP and is involved in the promotion of HR. It is also thought to have a role in the end resection process (Jasin & Rothstein, 2013). There are two outcomes of the strand invasion, after end resection. In the synthesis-dependent strand annealing (SDSA) pathway, a 'non-crossover' results from the newly synthesised strand being displaced before annealing to the previous DNA end (Moynahan & Jasin, 2010). In the canonical DSB repair (DSBR) pathway, there are two alternative outcomes, arising from double Holliday junctions. The first is that one DNA end is 'secured' in order to form two Holliday junctions, which can be dissolved by the BLM helicase-Topoisomerase III α -RMI1- RMI2 (BTR) complex to form a 'non-crossover' (Shah Punatar, et al., 2016). The second option is that the Holliday junction can be resolved by proteins such as GEN1, Mus81-EME1 or SLX1-SLX4 to create a 'crossover' or a 'non-crossover' (Moynahan & Jasin, 2010; Matos & West, 2014). It was published in 2007 that CtIP complex is necessary for DNA end resection, and individuals which lack the protein, or have a defect within the protein show defects in the HR pathway (Sartori, et al., 2007). ATM defects also result in disease phenotypes and DSB dysfunction.

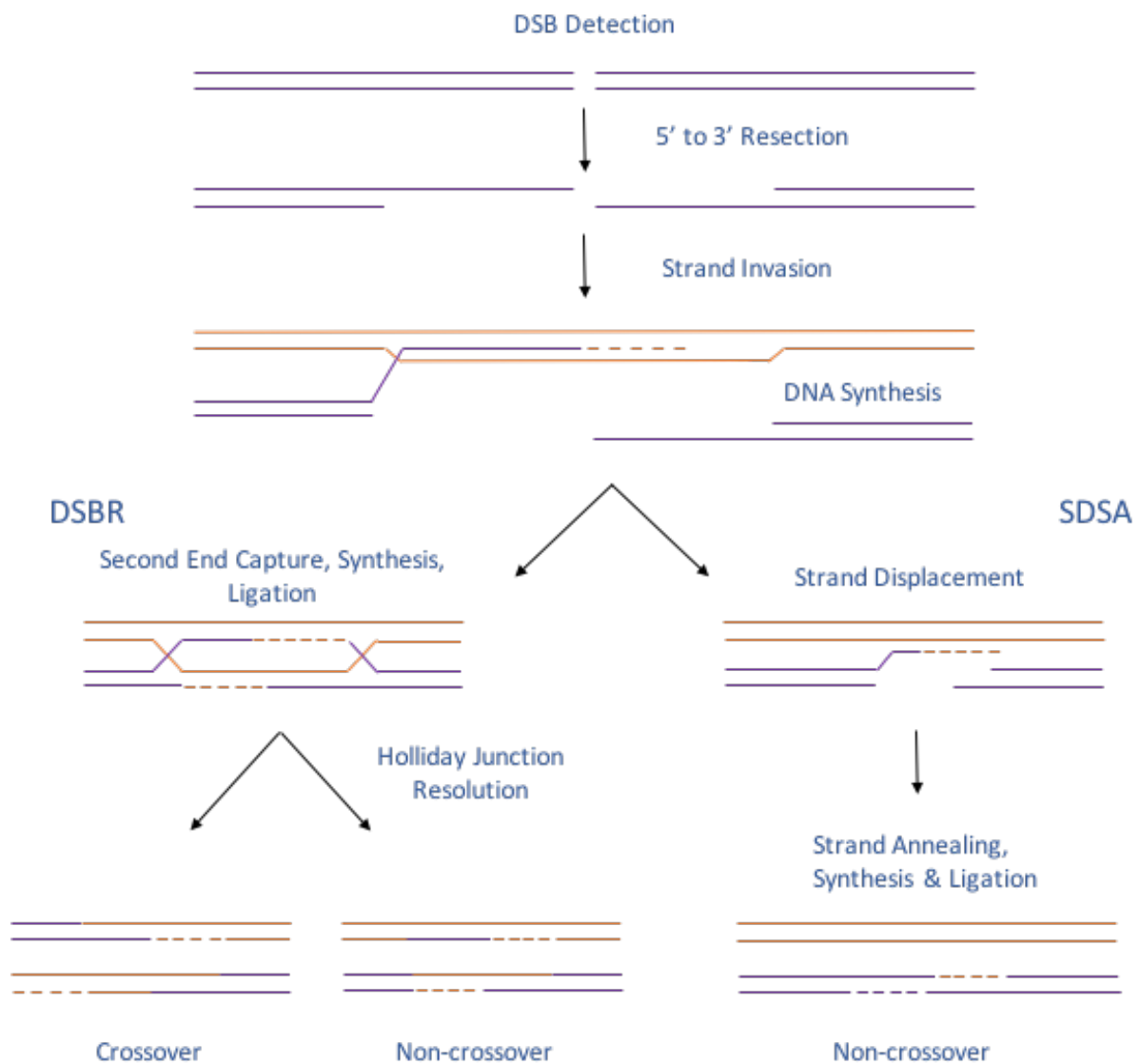


Figure 1.3. **Repair of DSB via Homologous Recombination.** After detection of a DSB, a number of proteins are recruited to perform end resection and the strand invasion event; the recruitment order of proteins has not yet been established. The choice is then made whether to perform repair via the SDSA pathway to form a non-cross over event or to repair via the DSBR pathway which involves double holliday junction resolution. The resolution of a double holliday junction can either result in a crossover or a non-crossover. **Adapted from Allers & Lichten, 2001.**

1.3.3.9 Non-Homologous End Joining

Non-homologous end joining (NHEJ) is the major repair pathway for DSBs that occur in mammalian somatic cells and unlike HR, NHEJ occurs in all stages of the cell cycle (Felgentreff, et al., 2014). This therefore means that the process of NHEJ repairs most of DSBs occurring from exogenous agents such as IR (Kakarougkas, et al., 2013). Figure 1.5 shows visual representation of the pathway. NHEJ acts to try and repair the DSBs as quickly as possible; if the DSB occurs within the euchromatin, then NHEJ can repair the break without the need for any associated DDR proteins or the serine/threonine protein kinase ATM (Woodbine, et al., 2014). If the break is not repaired by the end of G₂, i.e. there is a failure in the NHEJ pathway, then the DNA is subjected to end resection and therefore repair must be completed by HR (Kakarougkas, et al., 2013). The process of NHEJ involves the rapid binding of Ku70/Ku80 heterodimer to the DNA DSB. This results in the recruitment of the two DNA PK catalytic subunits, which can form the DNA PK holoenzyme. The DNA PKs interact with the structure-specific endonuclease Artemis, which can process the DNA ends. In order for genomic integrity to be maintained, DNA Ligase 4 complex processes and ligates the DNA ends. This final process is catalysed by the XRCC4-like factor (XLF) (Felgentreff, et al., 2014; Woodbine, et al., 2014). NHEJ is generally considered to be an error-prone pathway, due to the absence of a homology sequence, which can give rise to translocations and loss of genetic material. The NHEJ pathway is associated with the introduction of insertion and deletion mutations (indels) at the breakage site, which in turn can rise to genomic instability and cell death (Rodgers & McVey, 2016). Figure 1.4 shows visual representation of the pathway.

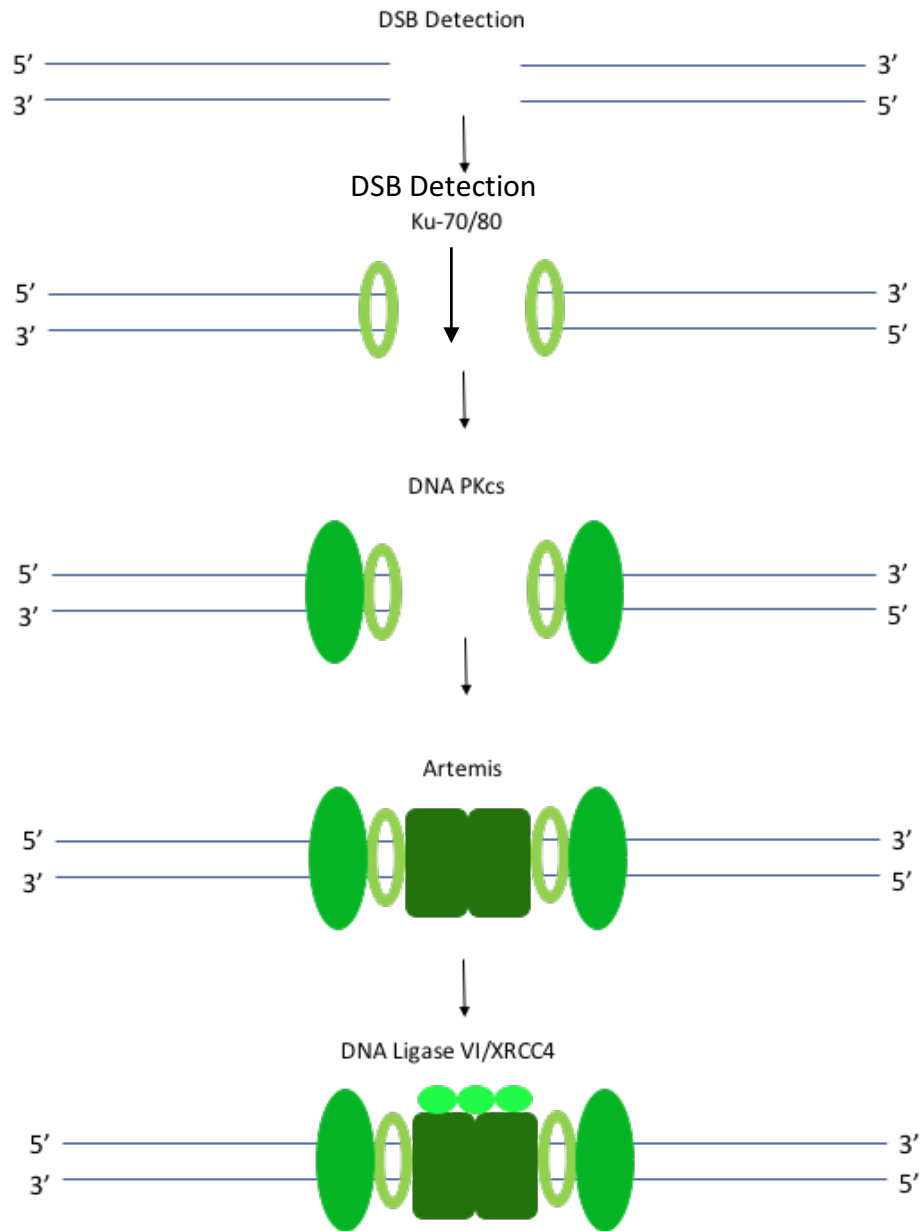


Figure 1.4. **Non-Homologous End Joining simplified schematic.** Upon detection of the DSB, Ku-70/80 binds to the DSB, which in turn recruits DNA PKcs to subsequently bind to the DNA. DNA PKcs can interact with the end processing factor Artemis, to prime the DNA ends ready for break resealing by the DNA ligase 4/XRCC4 complex. **Adapted from De Lorenzo, et al., 2013.**

1.4 DNA Topoisomerases

DNA topoisomerases are naturally occurring enzymes within the body and are employed to help resolve topological problems within the DNA when undergoing processes such as transcription and replication. They resolve torsional stress via inducing transient breaks in the DNA, which are either single stranded, introduced by type I topoisomerases or double stranded via type II topoisomerases (Champoux, 2001). The two different types of topoisomerase enzyme exhibit distinctly separate mechanisms of action.

1.4.1 Topoisomerase Classification

Although there are two main types of topoisomerases, there are different sub-types within these. In humans, there are 6 different topoisomerase enzymes, which fall into 3 categories; TOP1 and TOP1mt (type IB), TOP2 α and TOP2 β (type IIA) and TOP3 α and TOP3 β (type IA) (Pommier, et al., 2016).

1.4.2 Mechanism of Action

Regardless of the sub-type, topoisomerases all have the ability to create nicks in the DNA, through a transesterification reaction. This nucleophilic attack breaks the DNA phosphodiester bond, leading to a covalent linkage between the topoisomerase and the DNA (Champoux, 2001). Type IA and IIA enzymes both act in a similar way; they enable the nicking of the DNA (either single or double stranded) via the binding to the 5' phosphate. This is distinct from the action of type IB topoisomerases, which bind covalently to the 3' phosphate (Pommier, 2013). The type IA and IIA enzymes also have a different mechanism in which to relieve the torsional stress and reseal the break, in comparison to the type IB topoisomerases. Type IA and IIA act by facilitating a strand passing event (either single stranded or duplex DNA) from the complimentary (type IA) or another intact DNA strand, as in supercoiled DNA (type IB) through the nick created by the topoisomerase, before being resealed. Type IB, on the other hand, facilitate a rotation movement of the nicked strand around the unbroken strand, thus alleviating the DNA supercoiling (Pommier, 2013).

1.4.3 Roles of Topoisomerases in Cellular Processes

Topoisomerases are physiologically relevant in a myriad of processes involving DNA activity, due to their properties allowing the relaxation of torsional stress, via the alleviation of both positive and negative supercoils.

1.4.3.1 Transcription

Transcription is an essential process for the proliferation of cells. During transcription, the DNA has the propensity to form positive supercoils, ahead of the transcription machinery. Additionally, this creates negative supercoils behind the transcription machinery (French, et al., 2011). DNA topoisomerases are important enzymes enlisted to introduce nicks in the DNA, to facilitate the relief of torsional stress. This relief of supercoiling is an important process, as, in the case of negative supercoils, can cause unwanted DNA-RNA hybrid structures known as R-loops which can interfere with the process of transcription. R loops are very stable structures which form due to the binding of the elongating nascent RNA strand to negative supercoils. The accumulation of R-loops, which are regulated by proteins such as Senataxin, can give rise to neurodegenerative disease states such as AOA2 (Ataxia with oculomotor apraxia type 2) and ALS (Amyotrophic Lateral Sclerosis) (Ghilarov & Shkundina, 2012; Walker, et al., 2017). Topoisomerases also have an important role in gene expression and transcription, with particular emphasis on the transcription of long genes (Ashour, et al., 2015). Topoisomerases also have the ability to prevent the collision of transcription and replication machineries, via the relief of torsional stress (García-Muse & Aguilera, 2016). Tuduri, et al., showed that transcription can impede the progression of replication forks in TOP1-deficient cells. The proposed mechanism suggested that this was occurring through the formation of R-loops. To confirm, Ribonuclease H1 (RNaseH1) which enables the cleavage of the RNA strand of the R-loop structure, was shown to be able to resolve the halting of the progression of replication forks and reduced strand breaks (Tuduri, et al., 2009; Pileur, et al., 2003).

1.4.3.2 Replication

The progression of replication forks during the process of replication gives rise to the amassing of positive upstream supercoils (Ghilarov & Shkundina, 2012). Type IB topoisomerases are usually employed to relieve this kind of replication-associated

torsional stress. If the replication machinery has the ability to rotate around the DNA helix, this can shift the positive supercoiling downstream of the replication fork, which can lead to the collision of two daughter strands of DNA, as a consequence of the convergence of replication forks. These strands require decatenation, which is carried out by type IIA topoisomerases (Masai, et al., 2010; Ghilarov & Shkundina, 2012; Wang, 2002).

1.4.3.3 Remodeling of Chromatin

As access to genetic material is critical for various cellular processes such as transcription and replication, it is unsurprising that there is a role for topoisomerases in the dynamic modulation of chromatin (Ehrenhofer-Murray, 2004). The remodeling of chromatin is an essential process in the maintenance in genomic stability, therefore it has been shown that mutations in various members of the SWI/SNF family of remodelers result in cancer. One member of the SWI/SNF family, SMARCA4, is a transcription activator which utilises ATPase activity to perform many roles within the chromatin such as the destabilisation and the restructure of nucleosomes (Husain, et al., 2016). It has been detailed that SMARCA4 is instrumental in the recruitment of TOP1 to chromatin. It has also been shown that TOP2 is a key component of the scaffolding of chromatin, with its activity implicated in global chromatin remodeling events (Bermejo, et al., 2007; Husain, et al., 2016).

1.4.4 **Topoisomerase 1-cleavage complexes (TOP1cc)**

The nicking event caused by type IB topoisomerases (as previously described) creates the topoisomerase-linked DNA break, which is often referred to as a cleavage complex (TOP1cc). Under normal physiological conditions, these complexes are reversible, catalytic intermediates, resolved as the breaks are resealed (Strumberg, et al., 2000). However, if TOP1 is exposed to an agent damaging to DNA, the stalling of transcription occurs (via various mechanisms) (see section 1.4.3.1). If TOP1 encounters the collision of replication machinery (see section 1.4.3.2), TOP1 can become stalled on the DNA, resulting in the cleavage complex becoming irreversible (Pommier, et al., 2014; Das, et al., 2014; Edenberg, et al., 2014). The trapping of topoisomerases on the DNA can also be referred to as the production of protein-linked DNA breaks (PDBs). PDBs, if not

effectively repaired, can lead to the formation of DSBs and potentially cell death (Walker, et al., 2014). One major pathway to deal with the resolution of TOP1ccs is the TOP1-TDP1-SSBR (topoisomerase 1-tyrosyl-DNA phosphodiesterase 1-single strand break repair) pathway (Hubert Jr, et al., 2011). A schematic of this is shown in figure 1.5. Tyrosyl-DNA Phosphodiesterase 1 (TDP1) is an important protein in the repair of PDBs, which cleaves covalently bound tyrosine residues in order for DNA nicks to be resealed via the recruitment of end processing factors (Ashour, et al., 2015). One instrumental protein which acts in response to the PDB is PARP1 (Poly(ADP-Ribose) Polymerase 1). PARP1 is activated by DNA which has been damaged, which allows for the synthesis of poly(ADP-ribose) polymers which can then bind to a myriad of protein acceptors. PARP1 is also involved with regulating the base excision repair, homologous recombination and non-homologous end joining pathways of the DNA damage response (Patel, et al., 2012). Importantly, PARP1 is an interacting partner of TDP1 and is imperative for the stability and recruitment of TDP1 to the stalled TOP1cc. This pathway is discussed in greater detail in section 1.5). The other pathway to resolve PDBs is the less precise repair mechanism of non-specific nucleolytic cleavage. This involves incising the DNA to remove the PDB, however this can result in the loss of genetic material due to the lack of precision, compared to phosphodiesterases. It is currently unclear how the choice of pathway is determined; however, recent evidence shows the involvement of PARP in channeling TOP1-mediated PDBs to the non-specific nucleolytic cleavage pathway. It is also not clear whether prior proteolytic degradation of TOP1 is required prior to the action of PDB nucleases, as is the case for TDP1 (Ashour, et al., 2015).

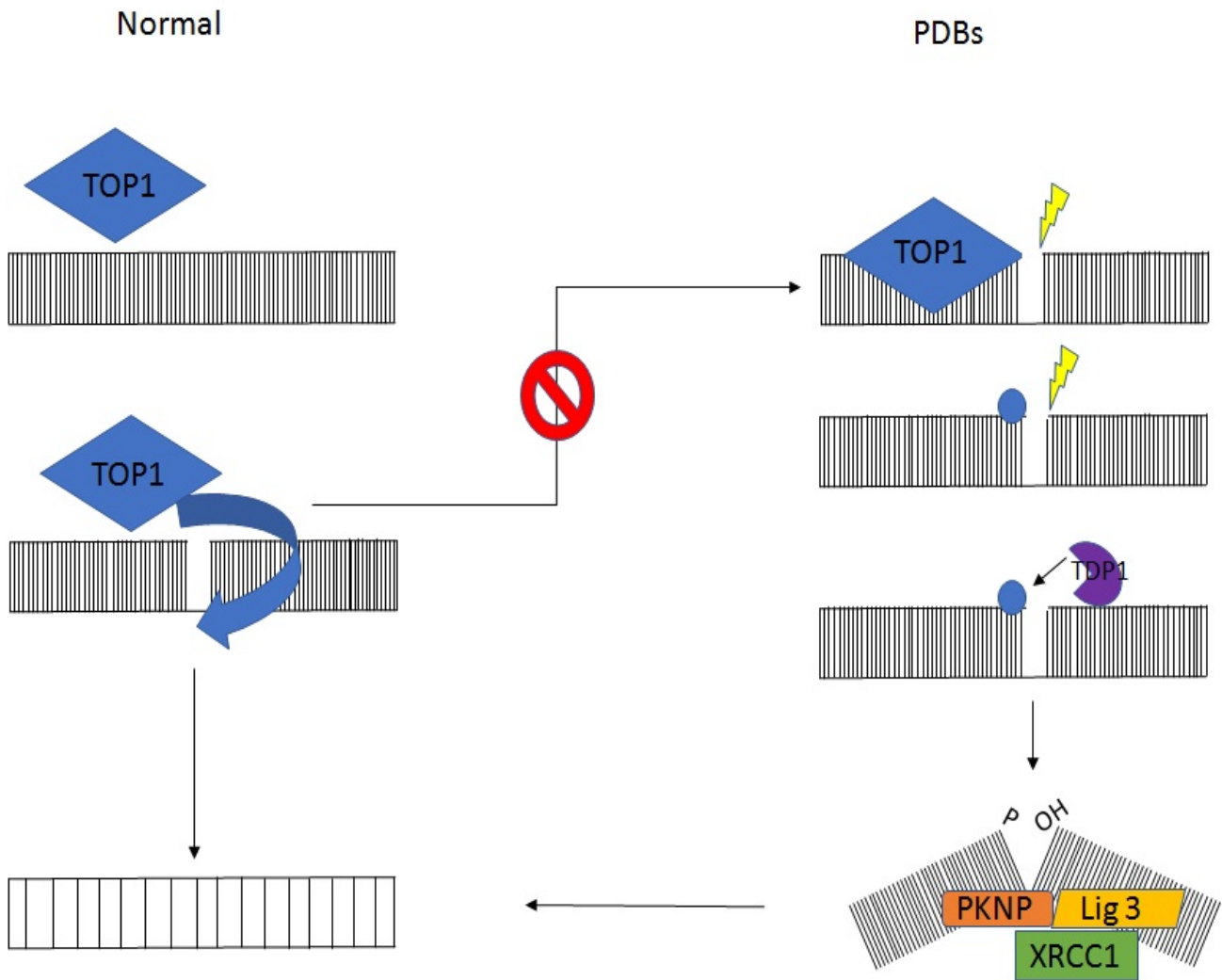


Figure 1.5. Resolution of supercoiling when PDBs occur. Under normal physiological conditions, topoisomerases are recruited to relax supercoiled DNA by reversibly cleaving one strand of DNA (forming a cleavage complex) which allows the efficient unwinding and subsequent re-ligation of DNA. However, if the cleavage complex becomes trapped due to a drug such as CPT, the DNA cannot be resealed. In order to resolve this, the topoisomerase 1 (TOP1) is degraded to a small peptide in an event which is most likely orchestrated by ATM, leaving a covalently bound tyrosine residue. TDP1 can then cleave the tyrosine residue and bind to the DNA. The binding to the DNA allows for other repair factors to be recruited, including PKNP to facilitate the termini to be rectified to 5' phosphate group and 3' hydroxyl group. XRCC1 acts as a scaffold protein and ligase 3 allows for the nick to be re-ligated, resolving the superhelical tension and permitting the progression of transcription and replication without compromising genomic integrity. **Adapted from Ashour, et al., 2015.**

1.4.5 Usage of TOP1 Poisons in a Clinical Setting

The stalling of TOP1 on DNA by chemical agents is a phenomenon exploited by various chemotherapeutic agents, notably the TOP1-trapping agent Camptothecin (CPT) and its analogues. Camptothecin is derived from the *Camptotheca acuminata* tree, which is indigenous to China. Although it was traditionally used in Chinese remedies, it was first isolated and purified for further biochemical investigations by Wall, et al., in 1958 (Legarza & Yang, 2006). CPT was used as a chemotherapeutic agent, showing potent anti-tumour activity in many cancers, mainly ovarian cancer and bowel cancer. CPT was shown to exhibit severe side effects, including extreme vomiting and diarrhoea, due to the administration of CPT as a salt, due to solubility issues in water (Kingsbury, et al., 1991; O'Leary & Muggia, 1998). However, the main issue with the utilization of CPT as an anti-cancer drug was the inadequate solubility of the compound in water (Kingsbury, et al., 1991). As the solubility of CPT was poor, derivatives which had more water soluble properties were designed, namely irinotecan and topotecan (Zhao, et al., 2014; O'Leary & Muggia, 1998). CPT and its derivatives inhibit the action of TOP1 by binding to the TOP1cc and stabilising the complex. Its activity upon binding slows down the resealing of the strand break (Legarza & Yang, 2006). As CPT stabilises the TOP1 on the DNA, in a TOP1-stalled intermediate, DNA strand breaks can occur during mitosis. This leads to the premature termination of replication which in turn leads to the inhibition of transcription and ultimately results in the cell entering apoptosis (Hentze, et al., 2004). TDP1 is one enzyme employed to resolve these kinds of breaks and has become a potentially 'druggable' target, as inhibition could lead to cell death (Ward, et al., 2014). As previously mentioned, there are a myriad of DNA repair pathways which have compensatory properties. If TOP1cc become stalled and cannot be repaired, they can be converted to different lesions, i.e. DSB which would then lead to the repair of the break via a different pathway. Taking this information into account, the derivatives of CPT are often used in combination therapy with inhibitors of other pathways, which can target cells for death due to defects in the repair pathways (Solier, et al., 2012). An example of this is using irinotecan along with 5-fluorouracil and or/oxaliplatin as a first-line treatment for colorectal cancer (Köhne, et al., 2008).

1.5 TDP1

Tyrosyl-DNA Phosphodiesterase 1 (TDP1) is a DNA repair enzyme that can remove a variety of covalent adducts from DNA through hydrolysis of a 3'-phosphodiester bond (Nitiss & Nitiss, 2013; McKinnon & Caldecott, 2007). TDP1 and its activity are known for resolving various 3' lesions, including acting on the covalently bound tyrosine residue in order to help repair TOP1-linked strand breaks (Alagoz, et al., 2014).

1.5.1 TDP1 Structure

Human TDP1 is a 68.5kDa structure consisting of 608 amino acids. TDP1 is a member of the phospholipase D (PLD) family of proteins (Interthal, et al., 2013). The protein consists of both N and C-terminal domains, of which the C-terminal domain is responsible for the catalytic activity of TDP1. The N-terminal region of TDP1 is not required for the enzymatic catalytic nature, but is involved in the stabilising and control of the protein (Pommier, et al., 2014). Figure 1.6 shows a simple schematic of TDP1. The TDP1 protein contains two separate HKN motifs, of which crystallography studies elucidated from a tertiary structure encompassing the active site (Huang, et al., 2011). In TDP1, the motifs are H₂₆₃K₂₆₅N₂₈₃ and H₄₉₃K₄₉₅N₅₁₆, which is the difference between the other members of the family, as they contain HKD domains, in which the asparagines found in the TDP1 HKN motif are replaced with aspartate residues (HKD motifs) (Pommier, et al., 2014).



Figure 1.6. **Schematic of TDP1.** TDP1 is a 608 amino acid protein with N and C terminal domains. There are two stretches within the protein which contain the nuclear localisation signal (NLS). The residues spanning the NLS regions are amino acids 56-74 and 216-223 (shown in orange). There are also 2 HKN motifs within the protein, at residues H₂₆₃K₂₆₅N₂₈₃ and H₄₉₃K₄₉₅N₅₁₆ (shown in red). **Adapted from Dexheimer, et al., 2008.**

1.5.2 TDP1 Cellular Processes and Interacting Proteins

The conserved role of TDP1 is to remove abortive TOP1 complexes, in order for the break to be resealed, maintaining genomic integrity. One of the major interacting proteins of TDP1 which is heavily involved in this process is PARP1. PARP1 is able to respond rapidly to DNA damage and is instrumental in the recruitment and subsequent stabilisation of the TDP1 protein. It has been shown by Das, et al., in 2014 that PARP1 binds to the N-terminal region of TDP1. The PARylation (addition of poly(ADP-ribose) chains) to TDP1 further increases its stability, without the modification affecting TDP1s catalytic activity. This may be due to the C-terminal region of TDP1 being responsible for the phosphodiesterase properties. The recruitment and stabilisation of TDP1 by PARP1 to sites of PDBs leads to the subsequent interaction and recruitment of the scaffold protein XRCC1. For the termini to be returned to the correct orientation, PNKP is recruited, along with DNA Ligase 3, which is required for nick re-ligation (Pommier, et al., 2014). As PARP1 is a vital factor in the recruitment of TDP1 in response to stalled TOP1-ccs, and its role in the signaling and recruitment of central BER factors, it has become an attractive target for chemotherapy, with many drugs targeting PARP1 in pre-clinical trials or having already been approved for use in clinic (Rouleau, et al., 2010).

After the recruitment of TDP1 to sites of trapped TOP1ccs (via PARP1), there are two key post-translational modifications which occur on TDP1. These modifications allow for the accumulation and maintenance of TDP1 at sites of TOP1ccs, but also allow for the recruitment of downstream repair factors. It has been shown that, as TDP1 has a pivotal role in resolving abortive TOP1 activity, there is a link between TDP1 and key factors of the DDR. A phosphorylation event on TDP1 at serine 81 increases the abundance of TDP1 and its stability at sites of damage; this event is orchestrated by DDR factors ATM and DNA-PK (Das, et al., 2009). Another post-translational modification event is the SUMOylation of TDP1 at lysine residue 111. This modification occurs under physiological (non-damaging) conditions and is not a direct response to sites of TOP1-linked DNA damage, however SUMOylation at this residue does increase the accumulation of TDP1 to stalled-TOP1ccs. It also leads to the stimulation of DNA repair (Hudson, et al., 2012). A paper published in 2014 reported that the depletion of TDP1 can increase sensitivity of human cells to alkylation damage. It has also been reported that TDP1 has a role in the

response to damaged bases, which is independent of apurinic/apyridimic endonuclease 1 (APE1) (Alagoz, et al., 2014).

TDP1 has been shown to have a more general role in DNA repair; as well as repairing TOP1-mediated DNA damage, a role for TDP1 in many different types of base damage has also been confirmed. Specifically, TDP1 has been shown to have a crucial role in the repair of Top2-mediated damage in yeast (Nitiss, et al., 2006). Deleting the TDP1 gene in yeast led to hypersensitivity of Top2 targeting agents; this was also the case when TOP1 was deleted. In addition, TDP1 mutants with combined deletions of various genes involved in repair pathways such as NHEJ and NER confirmed greater lethality than single mutant alone; these data suggest that TDP1 plays a role in other types of DNA damage (Nitiss, et al., 2006).

1.5.3 TDP1 Deficiencies and Clinical Relevance

Deficiencies in TDP1 have been linked with the neurodegenerative condition Spinocerebellar Ataxia with Axonal Neuropathy 1 (SCAN1). SCAN1 is a hereditary disease, acquired in an autosomal recessive manner. The key mutation found to correlate to the SCAN1 phenotype is a homozygous mutation in the H493R residue, which is located in the active site of TDP1 (Huang, et al., 2011; Hawkins, et al., 2009). The onset of SCAN1 is usually observed around the early teenage years, with patients having problems associated with chromosomal instability as well as exhibiting peripheral neuropathy and cerebellar atrophy (Caldecott, 2008).

1.6 Linking Structural Proteins to the DNA Damage Response

In recent years, great interest has arisen in the link between structural proteins and protein complexes to the DDR, especially the repair of DNA breaks. One example of this is the formation of nuclear actin filaments in response to DNA damage (Belin, et al., 2015). Actin is a filament protein which provides a cytoskeletal structure to cells amongst many other roles. It is a very abundant protein, usually the most abundant in eukaryotic cells (Dominguez & Holmes, 2011). Nuclear actin filaments have been shown to accumulate in response to processes such as protein misfolding. Belin, et al., discovered that nuclear actin filaments are produced in response to DNA damage, with a dependence on the action of actin nucleation factors formin-2 (involved in actin cytoskeleton assembly and

re-organisation) and Spire-1/Spire-2 (involved in actin cytoskeleton re-organisation and polymerisation) (Belin, et al., 2015; Baum & Kunda, 2005). Another nuclear protein, Nuclear Mitotic Apparatus Protein 1 (NuMA) (see section 1.7) has been linked tenuously with the DNA damage response through its interaction with a member of the PARP family PARP3. PARP3 is thought to be involved in the progression of cells through mitosis, additional to playing a role in genome stability (Boehler, et al., 2011). It was shown that PARP3 is a member of a protein complex involving NuMA and Tankyrase 1 (see 1.7.2). PARP3 has been shown to have a role, working together with PARP1, in response to DSBs. It has also been shown to function in the same pathway as Aprataxin-and-PNK-Like Factor (APLF) to increase repair of DSBs, via NHEJ (Boehler, et al., 2011; Rulten, et al., 2011). However, in the context of SSBs, it was determined that there was not a role for PARP3 in response to SSBs. This was due to the lack of sensitisation of cells to TOP1-poison CPT, when levels of PARP3 were depleted via gene silencing (using specific siRNAs), compared with the sensitisation of PARP1 depleted cells to CPT (Loseva, et al., 2010). The emerging area of the involvement of structural proteins in response to DNA damage and the evidence linking NuMA to the DNA damage response warranted further investigations.

1.7 Nuclear Mitotic Apparatus Protein 1 (NuMA)

Nuclear mitotic apparatus protein 1 (NuMA) is a large, abundant protein which is situated in the nucleus through interphase. As cells progress through the cell cycle and the nuclear envelope breaks down, NuMA quickly localises to mitotic spindle poles (Cleveland, 1985).

1.7.1 NuMA Structure

NuMA is a 238kDa protein containing 2115 amino acids. Of note, there are a number of variants of NuMA, the most studied and clinically relevant forms are variant 1 (2115 amino acids) and variant 2 (2101 amino acids) which, within this thesis, have been referred to as the long and short isoforms of NuMA, respectively. The long isoform contains an extra 14 amino acids at positions 1536-1549 with an amino acid sequence of QVEQLEVFQREQTK. For the case of domain positions, all residue numbers refer to the long isoform. NuMA was discovered approximately 30 years ago by Lyderson and Pettijohn, who named it based on the proteins localisation to interphase nuclei and the link to the spindle poles (Lyderson & Pettijohn, 1980; Radulescu & Cleveland, 2014).

Figure 1.7 shows a simple schematic of NuMA. It is a protein which contains a large coiled-coil region, central to both N- and C-terminal domains, with globular domains at the head (1-216) and tail (1700-2115) of the protein (Compter, et al., 1992). The coiled-coil domain spans 1487 amino acids, from residues 213-1699, which is important in roles relating to the positioning and lengthening of the mitotic spindle during mitosis (Truebestein & Leonard, 2016). The NuMA protein also contains a nuclear localisation signal (NLS) from 1984 to 1989 and a microtubule binding domain (MBD), a feature which spans 70 amino acids (residues 1866-1936). Both the NLS and MBD are positioned in the C-terminal domain of NuMA (Radulescu & Cleveland, 2014). Another key feature of NuMA is the occurrence of 13 distinct S/TPXX putative DNA binding motifs; these motifs are found in both N-terminal and C-terminal regions of NuMA, with 6 and 7 distinct motifs respectively (Ludérus, et al. 1994).



Figure 1.7. **Schematic of NuMA.** NuMA is a 2115 amino acid structure with N- and C-terminal domains. NuMA consists of two globular domains, the head (N-terminal) and the tail (C-terminal) which are separated by approximately 1500 residues which make up the α -helical coiled-coil domain. The NuMA protein also consists of a microtubule binding domain (MBD) spanning residues 1866-1936 (shown in green) and a nuclear localisation signal (NLS) spanning residues 1984-1989 (shown in yellow), both of which lie within the C-terminus. **Adapted from Uchida, et al., 2013.**

1.7.2 NuMA Cellular Processes and Interacting Proteins

Although NuMA is poorly characterised, especially in the context of its involvement in the DNA damage response, initial studies have shown that NuMA is heavily involved in a number of cellular processes. The discovery of NuMA elucidated the role as a nuclear protein during interphase with the ability to rapidly re-disperse to spindle poles during prometaphase (Cleveland, 1985). It was recently discovered that the MBD of NuMA allows localisation of NuMA to the tips of microtubules. It is also known that NuMA plays a large role in spindle pole maintenance, via the tethering of microtubules to centrosomes and the concentration of microtubules to the spindle poles (Radulescu & Cleveland, 2014). NuMA was found to be a key member of a complex of cortical proteins including LGN and dynein/dynactin, which are involved in establishing proper spindle orientation during asymmetric divisions (Seldin, et al., 2013). Dynein, through its specific activator Dynactin, binds to the N-terminal region of NuMA, whereas LGN binds to NuMA at residues 1818-1930, located in the C-terminus (Haren & Merdes, 2002; Merdes, et al., 2000; Seldin, et al., 2016). It has been shown that defects in any of the cortical complex constituents results in defects in the orientation of spindle poles and splayed microtubules (Seldin, et al., 2013; Radulescu & Cleveland, 2014). After the breakdown of the nuclear membrane, in order for NuMA to rapidly re-localise to the spindle poles, hyper-phosphorylation by the CDK1/Cyclin B complex occurs at 4 putative sites within NuMA to increase its interaction with Dynein and control NuMA's localisation to the mitotic spindle (Kotak, et al., 2013). NuMA has also been shown to interact with the nuclear pore complex component Rae1 (Wong, et al., 2006). It is proposed that the mRNA export factor, Rae1 (a.k.a. Gle2) can bind to NuMA at the C-terminus, through the utilisation of the microtubule binding domain (MBD), however specific binding residues are yet to be identified (these residues are thought to be in the coiled-coil region) (Wong, et al., 2006). Rae1 is a constituent of the nuclear pore complex and has been shown to be able to bind to both the nucleoporin Nup98, and the mitotic checkpoint kinase Bub1. The binding of Rae1 to both Nup98 and Bub1 is facilitated by the GLEBS (Gle2-binding domain) domain present in Nup98 and Bub1 (Wong, et al., 2006). A nucleoporin complex including Rae1 is required for the stabilisation of microtubules, a process which is coordinated by RanGTP/Importin β (Blower, et al., 2005). RanGTP has a role in the promotion of spindle assembly, and Importin β (regulated by RanGTP) is involved in the negative regulation of spindle assembly, as well as a role in nuclear import (Harel &

Forbes, 2004). The depletion or conversely, the over-expression of Rae1 leads to the formation of abnormal spindle fibres (Yokoyama & Gruss, 2013; Wong, et al., 2006).

One important interaction is the binding of NuMA to Tankyrase 1. Tankyrase 1 (a.k.a. PARP5a) is a poly(ADP-ribose) polymerase and is localised at the centromeres during mitosis. It has a major role in the regulation of telomere length and cohesion of sister telomeres (Chang, et al., 2005). Tankyrase 1 binds to NuMA through the RXXPDG motif in the C-terminal region of NuMA (Sbodio & Chi, 2002). It is thought that through the binding at this region, Tankyrase 1 PARylates NuMA during mitosis and promotes the interaction between the two proteins as the cells enter mitosis (Chang, et al., 2005). It is also thought that Tankyrase 1 is required for mitotic progression (Chiang, et al., 2008). It has been discovered that Tankyrase 1 and NuMA are components of a protein complex, along with the poly(ADP-ribose) polymerase, PARP3. A role for PARP3 in the stabilisation of the mitotic spindle has been described, along with the maintenance of integrity of telomeres, largely thought to be through the interaction and subsequent regulation of NuMA and Tankyrase 1 (Fernández-Marcelo, et al., 2014; Boehler, et al., 2011).

More recently, and in a different cellular setting, it has emerged that NuMA functionally and physically interacts with the chromatin remodeler SNF2h/SMARCA5 (Vidi, et al., 2014). Experiments showed that NuMA is able to regulate the diffusion of SNF2h, which can control the accumulation of SNF2h at DNA breaks. It was also discovered that NuMA can accumulate at sites of DNA damage in a PARylation dependent manner, with the acceptance of PAR chains from PARP3 also resulting in PARP3s accumulation at damage sites. This study revealed the potential role for a scaffold protein such as NuMA to have a key role in the maintenance of the genome via orchestrating remodelers of chromatin (Vidi, et al., 2014). It is known that SMARCA5 is recruited with the E3 ubiquitin ligase RNF168 to sites of DNA damage, in a PARP1-dependent manner (Aydin, et al., 2014). As described, SMARCA5 interacts with both NuMA and PARP3; SMARCA5 is required for efficient HR and hence depletion of NuMA could lead to the misrepair, or lack of repair of DSBs which can lead to genomic instability. This suggests NuMA could be implicated in the repair of DSBs due to the interaction of various chromatin remodelers (Aydin, et al., 2014).

1.7.3 NuMA/Related Protein Deficiencies and Clinical Relevance

It was previously alluded to that depleting levels of NuMA results in aberrant mitotic spindle formation. In a cancer setting, epithelial ovarian cancer cells have been shown to have increased levels of NuMA (Brüning-Richardson, et al., 2012). However, NuMA is a relatively uncharacterised protein. A protein family which is related to NuMA, the lamin family, have been studied much more comprehensively, and defects are associated with various disease pathologies (Yang, et al., 1992; Vidi, et al., 2014). Lamins are intermediate filament proteins which are components of the nuclear lamina, a network located between inner nuclear membrane and chromatin (Peravanovic, et al., 2016; Swift, et al., 2013). They have many roles within the cell and are implicated in chromatin organization, gene regulation and genome stability amongst others (Gruenbaum & Foisner, 2015). NuMA is structurally related to lamins due to the large coiled-coil domain which many structural proteins, such as myosin heavy chains, contain (Yang, et al., 1992; Vidi, et al., 2014).

Abnormalities in the structure or processing of the *LMNA/C* gene, which codes for the Lamin A/C proteins (alternately spliced from a single transcript) can result in disease pathology (Kamat, et al., 1993; Musich & Zou, 2011). The abnormalities in the gene leads to truncated versions of the protein being produced. This family of diseases are dubbed laminopathies (Broers, et al. 2006). Examples of laminopathies include Hutchinson-Gilford progeria syndrome (HGPS), and restrictive dermopathy (RD). In these conditions, genome instability is observed even though genome maintenance and repair genes appear normal (Musich & Zou, 2011). As the mutant lamin proteins accumulate they sequester replication and repair factors, leading to stalled replication forks which collapse into DSBs (Barboro, et al., 2002). In a reaction unique to HGPS and RD cells, *Xeroderma pigmentosum* group A (XPA) protein becomes unexpectedly trapped at DSB sites, which excludes normal binding by DNA DSB repair proteins. The bound XPA also signals activation of ATM and ATR, arresting cell cycle progression, leading to arrested growth (Musich & Zou, 2011). HGPS patients exhibit premature aging, as the name of the condition suggests. Other characteristics include dwarfism, baldness and premature arteriosclerosis (Ghosh & Zhou, 2014). Due to the structural similarities between NuMA and lamins, it could be hypothesized that defective NuMA proteins may work in a similar manner.

1.8 Aims and Objectives

The main aims of this project were to investigate the potentially novel role of NuMA in the setting of DNA damage, specifically the role of NuMA within the repair of SSBs. The investigations into the unresolved role of NuMA in the context of genome maintenance adopted a multi-experimental approach of biochemical techniques; namely alkaline comet assay, co-immunoprecipitation, immunofluorescence and clonogenic survival assays. The studies utilised mammalian cellular systems (HEK 293, MRC5 and SH-SY5Y cells), to elucidate novel interactions and complexes. Through the varied experimental approach, different aspects of the role of NuMA was studied. This involved using techniques such as gene silencing (specific siRNAs), live cell imaging and the application of mechanical stress. It was hoped that this project could further elucidate additional roles for NuMA in the expanse of genomic maintenance and stability, through discovering new interactions with members of the DNA damage response, notably the interaction protein of interest, TDP1.

Chapter 2

Materials and Methods

2.1 General Chemicals and Equipment

All the chemicals were obtained from Fisher Scientific or Sigma Aldrich, unless otherwise stated. The DNA restriction enzymes were obtained from Roche or New England Biosciences, unless otherwise specified. The DNA/RNA primers (oligonucleotides) were synthesised by Integrated DNA Technologies (IDT) or Eurofins Scientific. The cell culture medium and foetal calf serum was purchased from Sigma Aldrich or Gibco (Fisher Scientific). The plasticware was sourced from Nunc, Falcon (BD Biosciences) or Corning.

2.2 Bacterial Transformation and Cloning Techniques

2.2.1 *DNA Plasmids*

Plasmid/Construct	Source/Reference
pci-puro-Myc	Prof. Keith Caldecott
pci-Puro-Myc-TDP1	Dr Shih-Chieh Chiang
pci-Puro-Myc-TDP1(150-608)	Dr Shih-Chieh Chiang
pci-Puro-Myc-TDP1(168-608)	This Thesis
pEGFP-N1	Dr Majid Hafezparast
pEGFP-C1-NuMA	Purchased from Addgene (Plasmid # 81209)
pEGFP-C1-NuMA LTR	This Thesis
pEGFP-C1-NuMA STR	This Thesis
pEGFP-C1-NuMA 1700-2115	This Thesis
pEGFP-C1-NuMA LTR - MBD	Dr. Swagat Ray

Table 2.1. DNA Constructs. List of plasmids and their sources which were used throughout this doctoral thesis.

2.2.2 Bacterial Transformations – Propagation of Plasmid DNA

50µl competent bacterial cells (DH5α *E. coli*) were thawed on ice before the introduction of DNA (1µg DNA prep, 15µl ligation reaction). Cells were left on ice for a further 30 minutes before heat-shocking cells at 42°C for 45 seconds. Cells were returned to the ice for approximately 2 minutes. 200µl LB broth was added to the cells, before shaking cells in a rotating incubator at 37°C for 1 hour. Cells were then plated on an LB agar plate, containing appropriate selection (Ampicillin, final concentration; 100µg/ml; Kanamycin, final concentration 50µg/ml), using strict aseptic technique. Plate(s) were left to incubate at 37°C overnight.

2.2.3 Colony Selection

Single bacterial colonies were selected and grown in LB broth (plus appropriate selection antibiotic) overnight, in a shaking incubator set to 37°C. The required volume of LB broth varied depending on type of DNA preparation to be completed; for mini-prep a volume of 10ml was used, for midi-prep a volume of 100ml was selected.

2.2.4 Mini-Prep

DNA preparations were carried out using the step by step guide in the QIAprep® Spin Mini-prep kit (Qiagen, Catalogue Number: 101674Z). Cells were initially centrifuged at 2000 RCF for 7 minutes, before discarding the supernatant. Cells were then re-suspended, lysed and then neutralised, sequentially, before removing all insoluble protein fractions. The DNA was then precipitated using ethanol. After all steps were carried out, DNA was eluted with 50µl elution buffer.

2.2.5 Midi-Prep

DNA preparations were carried out using the step by step guide in the QIAGEN® Plasmid Plus Midi-prep kit (Qiagen, Catalogue Number: 12243). Cells were initially centrifuged at 2000 RCF for 20 minutes, before discarding the supernatant. Cells were then re-suspended, lysed and then neutralised, sequentially, before removing all insoluble protein fractions. The DNA was then precipitated using ethanol. After all steps were carried out, DNA was eluted with 200µl elution buffer.

2.2.6 DNA Quantification

The concentration of DNA was determined using the Thermo Scientific ND-1000 Nanodrop Spectrophotometer. The instrument was installed by using 1µl ddH₂O, before being 'blanked' by using 1µl elution buffer. 1µl of sample was then measured. Concentration of the DNA was given in ng/µl. Observation of the DNA curve and 260/280 values were noted, as an indication of DNA quality.

2.2.7 Primer Design

Primers were designed using the open reading frame (ORF) and the DNA sequence in FASTA format. GC caps were added to the beginning of the primer sequence, to help eliminate degradation of the DNA when performing the PCR. Appropriate restriction sites were also incorporated into the primer. Reverse complement sequence was determined and primers were ordered through Integrated DNA Technologies (IDT). DNA primer 'rules' were abided by, ensuring that the melting temperatures of the primer pair were within 5°C. Primers were designed in a non-overlapping manner, so to avoid annealing of the primer pairs. Site-Directed mutagenesis (SDM) primers were designed utilising the amino acid tool, available at www.sigmaaldrich.com.

2.2.8 Gibson Assembly

The NEBuilder Assembly tool was utilised for the designing of PCR primers to amplify sections of DNA, with overlapping regions of the vector backbone. General guidelines for Gibson assembly primers were taken into consideration. The PCR was performed with specific primers, using 10ng plasmid DNA and other constituents detailed in the table in section 2.2.10. The PCR product was run on 1% agarose gel, before completing a gel extraction protocol (see 2.2.11 and 2.2.12). The assembly of PCR fragments was carried out using 0.02-0.5pmols of fragments; a maximal amount of 100ng of vector (range between 50-100ng) and 2-3 times more of the insert. The fragments were assembled in a PCR tube, in a thermocycler (30 minutes at 50°C), according to the reaction make up provided by NEB. Following fragment assembly, a transformation protocol was followed (see section 2.2.2) with the slight alteration that the bacterial strain of NEB-5α competent *E. coli* was used. Around 5 colonies were selected before adding to LB broth with appropriate selection antibiotics. The cultures were grown overnight (see section 2.2.3) before performing mini-preps (see section 2.2.4). The samples were sent for sequencing,

with sequencing data analysed to check correct in-frame orientation of the insert and backbone.

2.2.9 *PCR Mixes & Reaction Times*

The PCR mixes utilised varied slightly depending on the purpose of the reaction and the polymerase used. The polymerase used in the reactions was KOD Hot Start DNA Polymerase (Merck Millipore, Catalogue Number: 71086-5).

Constituents	Amount Required/Reaction: Standard/Gibson - PCR	Amount Required/Reaction: Site- Directed Mutagenesis
10 x KOD Buffer	5µl	5µl
dNTPs	5µl	5µl
MgSO ₄	2µl	2µl
DMSO	1µl	1µl
Forward Primer (10µM)	1.5µl	1.5µl
Reverse Primer (10µM)	1.5µl	1.5µl
DNA (20ng/µl)	0.5/1µl	2-4µl
KOD Polymerase	1µl	1µl
ddH ₂ O	32/32.5µl	29-31µl

Table 2.2. PCR Reaction Mixes. List of typical constituents of PCR reactions depending on application which were used throughout this doctoral thesis.

Reaction Times & Conditions

Amplification of DNA and Creation of Truncations (Standard PCR/Gibson Assembly):

5 minutes initial denaturing - 94°C

35 Cycles of:

- Denaturation - 94°C (1 minute)
- Annealing - 5°C lower than lowest primer melting temperature (1 minute)
- Elongation - 68°C (30 seconds/kb)

Final extension - 68°C (1 minute/kb)

Annealing temperatures were changed accordingly as part of the troubleshooting process. For troublesome PCRs, a 2 step PCR programme was adopted (anneal and elongate at the same temperature).

Site-Directed Mutagenesis:

5 minutes initial denaturing - 94°C

18 Cycles of:

- Denaturation - 94°C (1 minute)
- Annealing - 5°C lower than lowest primer melting temperature (1 minute)
- Elongation - 68°C (1 minute/kb)

Final extension - 68°C (1 minute/kb)

Once the PCR run was complete, 1µl DPN1 was added to the reaction before placing at 37°C for 1 hour. The reaction was then placed back into the thermocycler for 20 minutes at 80°C. This was to digest any remaining template DNA. The DNA concentration was adjusted up to 100ng if required. The annealing temperatures were changed accordingly as part of the troubleshooting process. For troublesome PCRs, a 2 step PCR programme was adopted (anneal and elongate at the same temperature).

Primer Name	Sequence
Myc-TDP1 168-608 F1	GGGCCCCGGGCCGAATTCAATGACTSGAGTCTCTGGAGTTAA
Myc-TDP1 168-608 R1	GCGCGCCGCGGATCCTCTAGATCAGGA
NuMA Backbone F1	GGTGCAGCAGCAGAAGCT
NuMA Backbone R1	CCTTGACCTTGGCACCCCTC
Exon Top Strand	TGAGGGTGCCAAGGTCAAGGTCCTGG
Exon Bottom Strand	TCAGCTTCTGCTGCTGCACCTTGCTGG
pEGFP-c1 F1	AGGGCCAGTACCAGTGAG
pEGFP-c1 R1	AGATCTGAGTCCGGACTTG
SDM siNuMA F1	GCAAATCCAAGTAGCTACAGACGCGTTGAAGAGCCGTGAG
SDM siNuMA R1	CTTCAACGCGTCTGTAGCTACTGGGAATTTGCCAGGTCTCG
SDM 1700-2115 F1	CTTTCCAAGTAGCTACAGACGCGTTGAAGAGCCGTGAGCCC
SDM 1700-2115 R1	CTCTTCAACGCGTCTGTAGCTACTTGGAAAGATCTGAGTCCG

Table 2.3. Primers. List of primers and sequences used for cloning throughout this doctoral thesis.

2.2.10 Agarose Gel Electrophoresis

Agarose gel was prepared by dissolving 0.5-2% (w/v) agarose (depending on the size of the protein of investigation) in 1 x TBE buffer. The solution was heated until the agarose had dissolved and left to cool. Ethidium Bromide was added to the molten liquid to a final concentration (20ug/ml). The gel was poured into gel setting equipment and a comb was added. Once set, the gel was transferred to a gel electrophoresis tank, and submerged in 1 x TBE buffer. 6 x DNA loading buffer was added to DNA samples to give a 1 x final concentration, before loading the samples into the wells. A DNA ladder was also loaded into the gel to give approximate DNA fragment sizes. The DNA samples were separated via electrophoresis; typically, gel ran at 100V for 60 minutes. The DNA samples were visualised via UV light, using the ChemiDoc MP system.

2.2.11 Gel Extraction

DNA samples were prepared before performing electrophoresis (see section 2.2.10). Gels were visualised on the BioRad ChemiDoc™ MP Imaging System, before performing band excision of a discrete DNA band using the UV transilluminator. The gel extraction protocol was carried out using the step by step guide in the QIAquick® Gel Extraction kit (Qiagen,

Catalogue Number: 101676Z). Once the gel extraction protocol was completed, DNA quantification was performed using the Thermo Scientific ND-1000 Nanodrop Spectrophotometer (see section 2.2.6).

2.2.12 Restriction Digest

Once the PCR product had been purified via gel extraction, an appropriate amount of DNA was digested. This was performed utilising the restriction enzymes corresponding to the restriction sites incorporated into the DNA primers. 0.1µl enzyme was enough to digest 1µg DNA. The specific enzymes and the compatible buffers were adopted, according to the manufacturer's recommendations. The digestion was carried out at 37°C for 1 hour. The digested product was then run on a 1% agarose gel and visualized using the ChemiDoc MP system. The gel extraction protocol was completed once again.

2.2.13 Ligation

The ligation of DNA fragments was carried out with a 'digested' vector and the digested PCR product (insert). The digestion ensured that the DNA was linearised. T4 ligase and compatible buffer was required for the efficient ligation of the fragments (Roche, Catalogue Number: 10481220001). The total reaction volume was 20µl. The below equations determine how much of the vector and insert was added to the reaction.

$$\text{Vector (ng)} = 0.057 \times 0.649 \times \text{size of vector (kDa)} / 2$$

$$\text{Insert (ng)} = \text{vector (ng)} \times 3 \times \text{size of insert (kDa)} / \text{size of vector (kDa)}$$

The ligation reaction was completed at 4°C overnight. This reaction could also be performed at room temperature, for approximately 4 hours. Half of the ligation product was then transformed, with additional water being added to the transformation reaction to help decrease the salt concentration.

2.2.14 DNA Sequencing

The sequencing of DNA was carried out using GATC-Sanger sequencing (samples sent to GATC Biotech via airmail). DNA sequencing was facilitated via the adoption of plasmid-specific sequencing primers. The DNA sequences were analysed to check that the

sequence was in-frame and that no mutations had been introduced during the PCR process.

2.2.15 Standard Solutions for Transformations and Cloning

LB Broth

8g of LB Broth (10g/L Tryptone, 5g/L yeast extract, 5g/L NaCl) powder (Sigma Aldrich, Catalogue Number: L3022-1KG) was added to 400ml ddH₂O. The solution was sterilised at 121^oC for 15 minutes under a pressure of 15 psi, before storing at room temperature.

LB Agar

14g of LB Agar (10g/L Tryptone, 5g/L yeast extract, 5g/L NaCl, 15g/L Agar) powder (Sigma Aldrich, Catalogue Number: L2897-1KG) was added to 400ml ddH₂O. The solution was sterilised at 121^oC for 15 minutes under a pressure of 15 psi, before storing at room temperature.

10 x Tris-Borate-EDTA (TBE) Buffer

108g of Tris base, 55g of Boric acid and 40ml of 0.5M EDTA (pH 8) were dissolved in 1 litre of ddH₂O. The solution was stored at room temperature.

6 x DNA Loading Buffer

6 x loading buffer purchased from NEB (Catalogue Number: B7024S). The solution was stored at room temperature.

2.3 Mammalian Cell Culture

2.3.1 Cell Lines

All cell lines were obtained from a central cell stock at the Genome Damage and Stability Centre, The University of Sussex, UK.

All cells used within this thesis were grown as monolayers.

- Human Embryonic Kidney 293 (HEK 293) cells (human epithelial kidney cells-normal)
- MRC5 cells - human lung cells (fibroblasts - normal)

- SH-SY5Y cells – human bone marrow (derived from neuroblastoma tissue - disease)

All cell lines were routinely checked for mycoplasma using a specific mycoplasma testing kit .

2.3.2 Media

Minimum Essential Medium (MEM)

MEM (Sigma Aldrich, Catalogue Number: M2279) was supplemented with 10% FCS (Sigma Aldrich, Catalogue Number: F7524), 1% L-Glutamine (Gibco, Catalogue Number: 25030-024) and 1% Pen-Strep (Gibco, Catalogue Number: 15140-122). The media was stored at 4^oC, being warmed before use.

Dulbecco's Modified Eagle Medium (DMEM)

DMEM (Sigma Aldrich, Catalogue Number: D6546) was supplemented with 10% FCS (Sigma Aldrich, Catalogue Number: F7524), 1% L-Glutamine (Gibco, Catalogue Number: 25030-024) and 1% Penicillin/Streptomycin (Gibco, Catalogue Number: 15140-122). The media was stored at 4^oC, being warmed before use.

2.3.3 Passaging of Cells

Adherent Cells

HEK 293 cells were passaged twice weekly, usually at a ratio of 1:10. The media was removed from the T75 flask and placed into a universal. 2ml of Trypsin/EDTA was added to the flask, before gently agitating to detach the cells. 8ml of Phosphate Buffered Saline (PBS) was added to the flask to ensure all cells were detached. All the solution was removed and 1ml was added to the universal. A further 10ml of PBS added to the flask to wash. 9ml of the PBS was added to the universal. The cells were centrifuged for 5 minutes at approximately 300 RCF, to pellet. The supernatant was removed, before re-suspending pellet in 12ml of complete MEM and being returned to the T75 flask.

MRC5 cells were passaged twice weekly, usually at a ratio of 1:5. As the MRC5 cells are very adherent, once the 2ml of Trypsin/EDTA was added to the flask, the T75 was placed in the 37^oC incubator, to help with the detachment of cells. 8ml of PBS added to the flask

to ensure all cells were detached. All the solution was removed and 2ml was added to the universal. A further 8ml of PBS was added to the flask to wash. 8ml of the PBS was added to the universal. The cells were centrifuged for 5 minutes at 300 RCF, to pellet. The supernatant was removed, before re-suspending pellet in 12ml of complete MEM and being returned to the T75 flask.

SH-SY5Y cells were passaged weekly, usually at a ratio of 1:10. 2ml of Trypsin/EDTA was added to the flask, before gently agitating to detach the cells. 8ml of PBS added to the flask to ensure all cells detached. All the solution was removed and 1ml was added to the universal. A further 10ml of PBS was added to the flask to wash. 9ml was added to the universal. The cells were centrifuged for 5 minutes at 300 RCF, to pellet. The supernatant was removed, before re-suspending pellet in 12ml of complete MEM and being returned to the T75 flask.

2.3.4 Cell Counting

Before performing the cell count, all cells were checked for contamination by eye, using an inverted microscope. The concentration of cells was established using an Improved Neubauer Haemocytometer, counting 10 μ l of cell suspension. This allowed for accurate numbers of cells to be plated as necessary.

2.3.5 Differentiation of SH-SY5Y Cells

The cells were maintained in media complemented with 2% FCS and 20 μ M retinoic acid until the desired percentage (approximately 75%) of the cell population exhibited a neuronal phenotype. The medium and retinoic acid were replaced as necessary. Due to the light sensitive nature of retinoic acid, plates were kept covered with aluminium foil in the incubator.

2.3.6 Solutions required for mammalian cell culture

1 x Phosphate Buffered Saline (PBS)

1 PBS tablet (Fisher Scientific, Catalogue Number: 11510546) was added to 500ml ddH₂O. The solution was sterilised at 121^oC for 15 minutes under a pressure of 15 psi, before storing at room temperature.

0.25% Trypsin

500mg of Trypsin 1:250 powder (Gibco, Catalogue Number: 27250-018) was dissolved in 10ml sterile PBS. The solution was filter sterilised before being made up to 200ml with sterile PBS. The solution was stored at 4°C.

4% Ethylenediaminetetraacetic Acid (EDTA)

27.397ml of 0.5M filter sterilised EDTA stock solution was added to 72.603ml ddH₂O. The solution was stored at 4°C.

Trypsin/EDTA

6.5ml of 4% EDTA, 30ml of 0.25% Trypsin and 37.5ml of PBS were mixed together before storing at 4°C.

2.4 Transfection (DNA and RNA)

2.4.1 DNA/RNA Transfection

Calcium Phosphate Transfection

10µg DNA was transfected into a 10cm dish. 2 x HBS was thawed, before adding 500µl to an Eppendorf tube. (x)µl DNA was added to 61µl calcium chloride (CaCl₂) and the appropriate amount of ddH₂O (to make volume up to 500µl). 2 x HBS was 'bubbled' with a sterile glass pipette to avoid calcium precipitation as the solution containing the DNA was added to the 2 x HBS dropwise. The bubbling continued for a short period of time once the solution has been added, before adding to the 10cm plate, drop by drop. The cells were incubated at 37°C for a minimum of 48 hours, before harvesting. The media was changed in the plates after 24 hours to prevent any precipitated calcium chloride becoming toxic to the cells.

Liposome-Based Transfection

200µl of warm Opti-MEM (Thermo Fisher Scientific, Catalogue Number: 11058021) was added to an Eppendorf tube. 3µl of Gene Juice (Merck Millipore, Catalogue Number: 70967-3) per µg DNA was incubated with the media for 5 minutes at room temperature. The appropriate amount of DNA was then added to the media, and incubated for 15 minutes at room temperature. The media containing the DNA was then added to the

appropriate well in a 6 well plate. The cells were incubated at 37°C for a minimum of 48 hours, before harvesting.

siRNA Transfection

100µl of warm Opti-MEM was added to two Eppendorf tubes. 1.2µl of Dharmafect 1 was added to one tube, and 3µl of 20µM siRNA was added to the other tube (final concentration: 50nM). Each tube was incubated for 5 minutes, before combining. The tubes were incubated for 20 minutes at room temperature. The media containing the siRNA was then added to the appropriate well in a 6 well plate (final volume 1.2ml). The cells were incubated at 37°C for a minimum of 48 hours, before harvesting. For NuMA knockdown, cells were re-transfected with siRNA in the above manner and incubated for a further 24 hours before harvesting.

siRNA Name	siRNA Sequences
SMARTpool NuMA Seq. 1	GGUGGCAACUGAUGCUUUA
SMARTpool NuMA Seq. 2	GAACCAGCCUCACCUAUCU
SMARTpool NuMA Seq. 3	GCAAACGGGUCUCCUAGA
SMARTpool NuMA Seq. 4	GGAGUUCGCUACCCUGCAA
SMARTpool TDP1 Seq. 5	GGAGUUAAGCCAAAGUAUA
SMARTpool TDP1 Seq. 6	UCAGUUACUUGAUGGCUUA
SMARTpool TDP1 Seq. 7	GACCAUAUCUAGUAGUGAU
SMARTpool TDP1 Seq. 8	CUAGACAGUUUCAAGUGA
Scrambled siRNA (Low GC)	UAAUGUAUUGGAACGCAUA

Table 2.4. siRNA sequences. Table detailing each of the siRNA sequences utilised throughout this doctoral thesis.

2.4.2 Solutions required for DNA/RNA transfection

2 x HBS

8g of Sodium Chloride (NaCl), 0.2g of Sodium Hydrophosphate (Na₂HPO₄) and 6.5g of HEPES (4-(2-hydroxyethyl)-1-piperazineethanesulfonic acid) was dissolved in 500ml ddH₂O. The pH was adjusted to 7 by the addition of concentrated hydrochloric acid. Aliquots for single usage were made and stored at -20°C.

2.5 Protein Analysis of Cellular Extracts

2.5.1 Cell Lysis – Preparation of Whole Cell Extract

Whole cell extracts were prepared by washing plates (6 well/10cm dish) with ice cold PBS (appropriate amount for well size). An appropriate amount of immunoprecipitation (IP) lysis buffer was added to each well (N.B. each step is carried out on ice). Table 2.5 shows the IP lysis buffer constituents. The cells were then scraped and re-suspended gently before transferring to a labelled Eppendorf tube. The cells were left to lyse for 30 minutes, on ice. Once lysed, the cells were centrifuged at 17,000 RCF for 15 minutes at 4°C. This step was carried out to remove the insoluble fractions from the whole cell extracts. The supernatant was decanted into a clean tube, before quantification.

Constituents	Stock Concentration	Final Concentration	Amount Required/1ml
HEPES (pH 7.4)	1M	20mM	20µl
NaCl	5M	39mM (40mM)	8µl
MgCl ₂	1M	2mM	2µl
Triton	2%	0.5%	250µl
Protease Inhibitor (Roche, Catalogue Number: P8340-1ML)	20 x	1 x	50µl
Phosphatase Inhibitor (Roche, Catalogue Number: 4906837001)	20 x	1 x	50µl
Benzonase Nuclease (Merck Millipore, Catalogue Number: 71205)	1µl/ml	0.1%	1µl
ddH ₂ O	-	-	619µl

Table 2.5. Constituents of Lysis Buffer. Standard constituents of IP lysis buffer, for lysis cells in the preparation of whole cell extracts, throughout this doctoral thesis.

2.5.2 Co-Immunoprecipitation

HEK 293 cells were transfected with DNA using either calcium phosphate (homemade) or GeneJuice (EMD Millipore) as the transfection reagent. After a 48-hour incubation post DNA transfection, the cells were lysed in an appropriate volume of buffer (20mM HEPES, 40mM NaCl (adjusted to 150mM/300mM), 2mM MgCl₂, 0.5% Triton X-100, 1x protease and phosphatase inhibitor cocktail (Roche) and 10 units/ml of Benzonase/Basemuncher for 30 minutes on ice). The cellular debris was removed by centrifugation at 17,000 RCF for 15 minutes. The NaCl concentration was adjusted to 150mM and the Triton X-100

levels were adjusted to 0.1%. The Anti-Myc antibody (9E10) was added to the lysate, adding 5µl per sample (1mg/ml). 30µl of Protein G Dynabeads (ThermoFisher) were washed with PBS + 0.01% TBST before adding the cell lysate to them. The cell lysates were incubated on a rotator at 4⁰C for a minimum of 2 hours, before removing the lysate. Protein G beads were washed 3 times with wash buffer (20mM HEPES, 150mM NaCl), before boiling in SDS loading buffer. After SDS-PAGE, the IP samples were analysed via immunoblotting. Early experiments in this doctoral thesis were performed using protein G sepharose beads. The samples were analysed in the same way, taking more care when removing supernatant, as the agarose beads were more easily disturbed than the magnetic beads.

2.5.3 Bradford Assay

The quantification of proteins was carried out using Coomassie protein assay reagent (Thermo Scientific, Catalogue Number: 1856209). 998µl of the reagent was added to 2µl sample/blank(ddH₂O)/control(BSA) in a cuvette before spectrophotometric analysis at an optical density of 595nm. The protein concentration was calculated ensuring the sample values were standardised against the BSA control.

2.5.4 SDS-PAGE

The analysis of proteins was carried out using a Sodium Dodecyl Sulphate – Polyacrylamide Gel Electrophoresis (SDS-PAGE) system, in which the percentage of gel selected varied depending on the molecular weight (kDa) of the protein of interest. In order to select the appropriate percentage of gel, the protein size was taken into account; the larger the protein, the lower the percentage of gel used.

Constituents	6% Resolving Gel (10ml)	8% Resolving Gel (10ml)	10% Resolving Gel (10ml)	4% Stacking Gel (5ml)
ddH ₂ O	5.3ml	4.6ml	4ml	3.736ml
30% Acrylamide	2ml	2.7ml	3.3ml	680µl
1.5M Tris (pH 8.8)	2.5ml	2.5ml	2.5ml	-
1M Tris (pH 6.8)	-	-	-	500µl
10% SDS	100µl	100µl	100µl	40µl
10% APS	100µl	100µl	100µl	40µl
UltraPure™ TEMED	8µl	6µl	4µl	10µl

Table 2.6. SDS-PAGE gel constituents. The amounts of each chemical required for different percentage gels are detailed, utilised throughout this doctoral thesis. 4% stacking gel was utilised for each gel, regardless of the percentage of the resolving gel.

The resolving gel was poured into cassettes (Fisher Scientific, Catalogue Number: NC2010), before adding a small amount of isopropanol (Sigma Aldrich, Catalogue Number: 59300-1L) to remove bubbles. Once the resolving gel was set, isopropanol was removed and rinsed; the stacking gel was then poured into the cassette, before adding a comb (10 well/12 well).

On occasions where large molecular weight proteins and small proteins were required to be analysed simultaneously during the same experiment, a gradient gel (BioRad) was utilised. This provided a 4-15% gradient, allowing the smaller proteins to travel less distance at the bottom of the gel, whilst yielding good separation of the larger proteins.

The gels were loaded into an electrophoresis tank, before the addition of 1 x SDS running buffer. The protein samples were loaded (see 2.5.5). The gels were run at 150-200V for the appropriate time to achieve the desired protein separation.

2.5.5 Loading of Samples

24µl of lysate (+ddH₂O) and 6µl of 5 x PLB was typically loaded per well. The protein concentration was accounted for, so to load the exact same amount of protein per well. The samples were boiled for 10 minutes at 95⁰C on a heat block before centrifuging quickly, to remove condensation. The samples were then loaded with a gel loading tip. Precision Plus Protein™ Dual Color Standard (BioRad, Catalogue Number: 161-0374) was used as a molecular weight marker. The gel was run for the desired time, depending on application.

2.5.6 Western Blotting

After the SDS-PAGE protocol had been completed (see section 2.5.4), the gel was transferred to a blotting membrane, in order to perform the western blotting protocol.

2.5.6.1 Transfer

The transfer of the gel to either a polyvinylidene difluoride (PVDF) (BioRad, Catalogue Number: 162-0264) or a nitrocellulose (BioRad, Catalogue Number: 162-0115) membrane was completed using a BioRad Trans-Blot® Turbo™ Transfer System, utilising filter papers soaked in 1 x Trans-Blot® Turbo™ transfer buffer. The transfer was carried out using the desired setting, depending on the size of the protein of interest.

2.5.6.2 Blocking of Membranes

The membrane was blocked for 1 hour with 5% milk solution (milk powder dissolved in 1 x TBST), with constant shaking in order to block the non-specific protein binding sites.

2.5.6.3 Probing with Antibodies

The blot was probed with the appropriate primary antibody, made up in 5% milk, at the appropriate dilution. This was left overnight, at 4⁰C, with constant shaking. It was also possible to incubate with certain antibodies at room temperature for 1 hour. Table 2.7 details antibodies used.

Antibody	Host Species	Source/Catalogue Number	Dilution
α -Actin	Mouse	Sigma Aldrich/A4700	1:1000
α -GFP	Rabbit	Abcam/ab290	1:2000
Myc (9E10)	Mouse	BioServ/9E10	1:2000
NuMA H-300	Rabbit	Santa Cruz/sc-48773	1:250
PARP1	Mouse	Santa Cruz/sc-8007	1:1000
TDP1	Rabbit	Abcam/ab4166	1:500-1:1000
pXRCC1 (s485, T488)	Rabbit	Bethyl Labs/A300-231A	1:2000

Table 2.7. Primary Antibodies. List of primary antibodies used throughout this doctoral thesis, with the dilutions detailed, along with company obtained from.

Once the blot was retrieved from cold room, it was washed 3 times (for a minimum of 5 minutes per wash) with TBST. The blot was probed with appropriate secondary antibody (anti-Mouse or anti-Rabbit) made up in 5% milk solution for 1 hour, at room temperature. The wash steps were carried out again, before visualisation using enhanced chemiluminescence (ECL) - Clarity™ Western ECL substrate (BioRad, Catalogue Number: 170-5061). The visualisation of the blot was performed on a BioRad ChemiDoc™ MP Imaging System.

Antibody	Host Species	Source/Catalogue Number	Dilution
Mouse IgG (H + L)- HRP Conjugate	Goat	BioRad (170-6516)	1:4000
Rabbit IgG (H + L)- HRP Conjugate	Goat	BioRad (170-6522)	1:4000

Table 2.8. Secondary Antibodies. List of secondary antibodies used throughout this doctoral thesis, with the dilutions detailed, along with company obtained from.

2.5.6.4 Stripping of Membranes

The membranes were stripped using Restore™ PLUS stripping buffer (Thermo Scientific, Catalogue Number: 46428). The membranes were submerged in the stripping buffer, before being incubated at 37°C for approximately 30 minutes, shaking at 80rpm. The blots were washed thoroughly with TBST, before blocking with 5% milk solution. The blots were then probed with primary antibodies (see section 2.5.6.3).

2.5.7 Solutions required for Protein Analysis and Western Blotting

10 x Tris Buffered Saline (TBS)

24.2g of Tris base and 80g of NaCl was added to 500ml of ddH₂O. The pH was adjusted to 7.6 by the addition of concentrated hydrochloric acid, before making the solution up to 1 litre with ddH₂O. The solution was stored at room temperature.

1 x TBST

100ml of 10 x TBS was added to 900ml of ddH₂O. 1ml of TWEEN® 20 was dissolved in the solution. The solution was stored at room temperature.

10 x Running Buffer

30.3g of Tris base, 144g of glycine and 10g of SDS were dissolved in 1 litre of ddH₂O. The solution was stored at room temperature. The running buffer was diluted to 1 x using 100ml of 10 x running buffer and 900ml ddH₂O.

1 x Transfer Buffer

200ml of 5 x Trans-Blot® Turbo™ transfer buffer was mixed with 600ml of ddH₂O and 200ml of 100% ethanol to give 1 litre of 1 x buffer. Once the transfer buffer was made to 1 x, the solution was stored at room temperature; 5 x buffer was stored at 4°C.

1M Tris

131.14g of Tris base was added to 500ml of ddH₂O. The pH was adjusted to 6.8 by the addition of concentrated hydrochloric acid, before making the solution up to 1 litre with ddH₂O. The solution was stored at room temperature.

1.5M Tris

181.71g of Tris base was added to 500ml of ddH₂O. The pH was adjusted to 8.8 by the addition of concentrated hydrochloric acid, before making the solution up to 1 litre with ddH₂O. The solution was stored at room temperature.

10% Ammonium Persulphate (APS)

1g of APS was dissolved in 10ml of ddH₂O. Aliquots of 1ml were stored at -20°C.

10% Sodium Dodecyl Sulphate (SDS)

100g of SDS was dissolved in 1 litre ddH₂O. The solution was stored at room temperature.

5 x Protein Loading Buffer (PLB)

Constituents	Amount Required/10ml
250mM Tris-HCl, pH 6.8	1M Tris-HCl, pH 6.8 – 2.5ml
500mM Dithiothreitol (DTT)	DTT – 771.25mg
10% w/v SDS	SDS – 1g
0.5% Bromophenol Blue	Bromophenol Blue – 50mg
50% w/v Glycerol	100% Glycerol – 5ml
ddH ₂ O	ddH ₂ O – 2.5ml

Table 2.9. Protein Loading Buffer Constituents. Chemicals required for 5 x Protein Loading Buffer, utilised throughout this doctoral thesis. Weights/volumes detailed yield 10ml 5 x PLB.

All the measuring of reagents was carried out in a fume cupboard, due to the toxic nature of DTT. 1ml aliquots of 5 x PLB were stored at -20°C.

2.6 DNA Damage and Repair Assays

2.6.1 Alkaline Comet Assay

MRC5 cells which had been transfected with siRNA were treated with 50µm CPT for 20/60 minutes at 37°C/10µm H₂O₂ in pre-chilled PBS, on ice, for 10 minutes. For H₂O₂ treated cells, following treatment the cells were left to recover in complete media for

varying periods of time at 37°C. After treatment, the cells were washed 1x with PBS. A thin layer of 0.6% agarose (Sigma) was laid onto frosted slides (Thermo Scientific). The cells were suspended in ice cold PBS before being mixed with an equal volume of 1.2% low melting temperature agarose (Sigma, Type VII), maintained at 42°C; the slides were then placed at 4°C to set. The cells (embedded in the agarose) were lysed in a pre-chilled lysis buffer (2.5M NaCl, 10mM Tris-HCl, 100mM EDTA pH 8.0, 1% Triton X-100, 1% DMSO; pH 10) for 1 hour at 4°C, before submerging in pre-chilled alkaline electrophoresis buffer (50mM NaOH, 1mM EDTA, 1% DMSO) for 45 minutes at 4°C. The process of electrophoresis was performed; running at 12V for 25 minutes, at 4°C, followed by addition of 400 mM Tris-HCl pH 7 to neutralise. Lastly, DNA was stained with Sybr Green (1:10,000 in PBS), before measuring the average tail moments of 50 cells/sample, using Comet Assay IV software (Perceptive Instruments, UK). Figure 2.1 shows representative images of partly and greatly damaged cells.

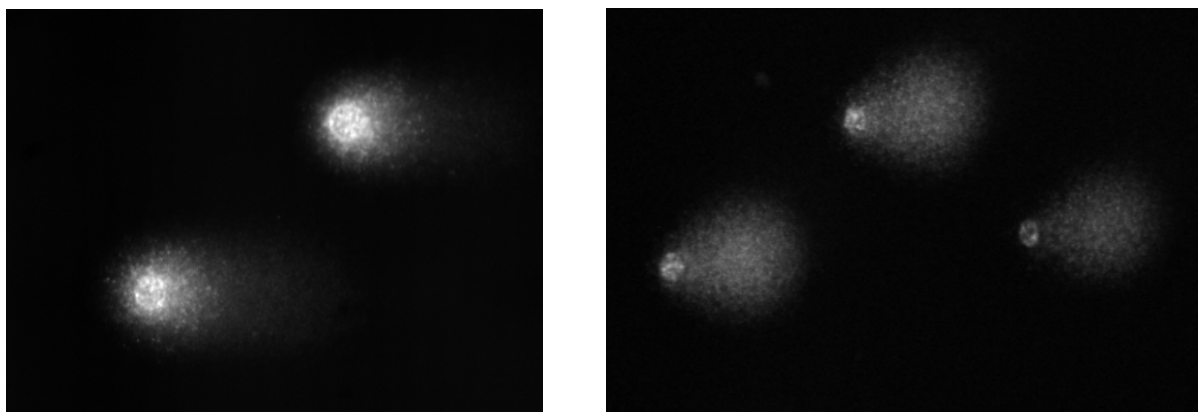


Figure 2.1. Representative images of cells with minimal damage (left) and cells which are severely damaged (right). Images taken from demo provided as part of the Comet Assay IV software (Perceptive Instruments, UK).

2.6.2 Clonogenic Survival Assay

The cells were plated in 6 well dishes and transfected with either siRNA (final concentration 50nM) or DNA (1µg) for the desired incubation periods. The cells were trypsinised, counted and then varying concentration of cells were re-plated on 10cm dishes (Corning) in triplicate. Concentration ranges varied depending on treatment drug. The cells were left to adhere for 24 hours, before being treated with DMSO or with the specified doses of CPT for 1 hour at 37°C, H₂O₂ in ice cold PBS for 10 minutes on ice, or Olaparib overnight at 37°C. The plates were washed with 1 x PBS before replacing the fresh media on to plates. Colonies were left to form for 7-10 days at 37°C. The colonies were fixed with 80% ethanol, left to air-dry and stained with 2% Methylene Blue for 1 hour before washing with distilled water. Colonies were counted and adjusted for cell number, before being normalised against control samples. This was completed by accounting for the concentration of cells plated; e.g. if 1000 cells plated on control plate, but 10,000 cells plated for a high treatment condition, the amount of colonies on the plate was multiplied by 10.

2.6.3 Immunofluorescence Studies

The cells (HEK 293/MRC5) were transfected in a 6 well plate using Gene Juice, having placed a sterile coverslip in the well(s). The cells were incubated at 37°C for a minimum of 24 hours, before harvesting. All the media was removed from the wells (N.B. all steps prior to fixation must be completed very slowly). 200µl of 4% Paraformaldehyde (PFA) (Science Services, Catalogue Number: 15710) was added to the well and was left to incubate at room temperature for a maximum of 10 minutes. The PFA was removed before washing twice with 200µl PBS. The PBS was removed and 200µl 0.2% Triton-X (Sigma Aldrich, Catalogue Number: X100) was added and left to incubate for 5-10 minutes. The wells were washed twice with PBS. The PBS was removed and coverslips blocked with 3% filter sterilised BSA in PBS for 30 minutes at room temperature. The coverslips were then incubated with 200µl primary antibody in 3% BSA for 45 minutes at room temperature. The primary antibody was then removed, before washing twice with PBS. The coverslips were then incubated with secondary antibody complemented with 4',6-diamidino-2-phenylindole (DAPI) (Fisher Scientific, Catalogue Number: VXD1306) at a concentration of 1:10000 for 30 minutes at room temperature. During this incubation, the plate was protected from light. The secondary antibody was removed

before coverslips were washed twice with PBS. The microscope slides were labelled, and the coverslips were carefully lifted from the well. The coverslips were mounted with Immuno Mount™ (GeneTex, Catalogue Number: GTX30928) and left to set for a minimum of 30 minutes. In the later stages of this thesis, the DAPI step in the secondary antibody incubation was omitted, as the lab switched from using Immuno Mount™ as mounting agent, to Vectashield® Hard Set Mounting Medium with DAPI (Vector Laboratories, Catalogue Number: H-1500).

For DSB repair experiments (foci counting), 100 cells were counted per condition. The total number of foci counted was then divided by 100 to give the average number of foci/cell.

A

Antibody	Host Species	Source/Catalogue Number	Dilution
53BP1	Rabbit	Bethyl Labs/A300-231A	1:1000
γ H2AX (Ser 139)	Mouse	Millipore (05-636)	1:1000
NuMA (H-300)	Rabbit	Santa Cruz/sc-48773	1:250

B

Antibody	Host Species	Source/Catalogue Number	Dilution
Goat Anti-Mouse IgG(H+L)-Alexa Fluor 488	Goat	Molecular Probes (A28175)	1:1000
Goat Anti-Rabbit IgG(H+L)-Alexa Fluor 488	Goat	Molecular Probes (A27039)	1:1000

Table 2.10. Antibodies used for Immunofluorescence. A) shows primary antibodies used, and B) secondary antibodies used throughout this doctoral thesis, with the dilutions detailed, along with company obtained from.

2.7 Mechanical Stress of Cells

2.7.1 *Preparation of Agarose*

1% of agarose (w/v) was dissolved in the desired volume of MEM, before pouring into dish (25ml/25cm dish). The agarose was left in 5% CO₂ incubator overnight to equilibrate.

2.7.2 *Cutting of Agarose*

A small disc of agarose was cut using a purpose made plastic 'lid' which was of a similar size to the insert. The disk was placed gently on top of the media in a 6 well plate.

2.7.3 Addition of Plastic Inserts

The plastic inserts were specially made to fit 6 well plates. The inserts contained small holes in the base, in order to allow media to flow into the insert and to allow cells to breathe (see Figure 2.2) The plastic inserts were washed with ethanol and allowed to dry before placing on agarose disc, to sterilise. A small amount of media was added directly to the agarose disc before the addition of the insert, in order to lubricate the gel disc, which prevents cell shearing.



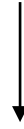
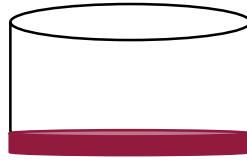
Figure 2.2. Plastic insert used for mechanical stress experiments. These inserts were specially designed for use with cells, with small holes in the base. They were developed to use in conjunction with 6 well plates.

2.7.4 Removal of Inserts and Agarose Discs

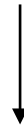
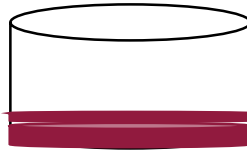
After the desired treatment time, the inserts were removed and cleaned with ethanol. The agarose discs were very carefully removed using a long, thin spatula. Great care was taken to remove the disc with minimal movement, due to the risk of shearing the cells.

2.7.5 Schematic of Application of Mechanical Stress

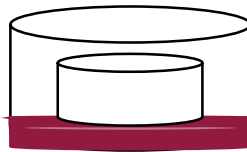
1. Plate cells in 6 well plate



2. Lay thin layer of agarose on cells



3. Place insert on cells



4. Carefully remove insert and agarose disk



N.B. This schematic is for illustration purposes only.

2.8 Statistical Analysis

All statistical tests performed were paired, two-tailed, student's T-Test. Statistical tests were performed using Microsoft Excel.

All graphed data was created using GraphPad Prism.

Results

Chapter 3

The role of NuMA in SSBR and DSBR

3.1 Introduction

Over recent years, there has been a development of interest in the crosstalk between structural proteins and functional cellular processes. It is known that NuMA plays an important role in spindle pole maintenance and correct spindle pole orientation (Radulescu & Cleveland, 2014). However, the link between NuMA and the DNA damage response is relatively unexplored. Vidi, et al. reported in 2014 that there is a role for NuMA in response to DSBs through the interaction of NuMA with various chromatin remodelers, notably SNF2h/SMARCA5 (Vidi, et al., 2014; Aydin, et al., 2014). The aim of this project was to confirm whether NuMA is involved in the DNA damage response. The initial studies began with exploration into the role of NuMA in response to DSBs, then focused on the role of NuMA in the repair of chromosomal SSBR. Further characterisation studies were also performed to further elucidate its function within this novel setting.

3.2 NuMA depletion results in accumulation of DSBs

The growing evidence linking structural proteins and the cellular DNA damage response led to the further investigation into this emerging area (Vidi, et al., 2014). As previously mentioned, the protein of interest was NuMA. NuMA was selected due to the structural relation to the protein family lamins, in which defects have shown to result in genomic instability (Musich & Zou, 2011). Additionally, other nuclear structural proteins have been shown to accumulate in response to DNA damage (Belin, et al., 2015). The first question asked was 'does NuMA play a role in the DNA damage response?'. In most of the investigative DNA damage assessing experiments, siRNA specific to NuMA and a scrambled siRNA as a control sequence were utilised. The cell line of choice was the lung fibroblast MRC5 cells. These cells were initially chosen for the immunofluorescence experiments as they exhibit a greater level of adherence compared HEK 293 cells, and they are a cell line which are derived from normal tissue. Taking this into account, it was

decided they would provide an easier platform to work with when performing delicate immunofluorescence work. As the initial optimisation of the knockdown was completed in MRC5 cells and as fibroblasts are particularly good at taking up siRNA, MRC5 cells were utilised for the majority of the experiments performed. The first set of experiments aimed to confirm that NuMA plays a role in double strand break (DSB) repair (Vidi, et al., 2014). In order to determine whether the depletion of NuMA results in accumulation of endogenous DNA breaks, the immunofluorescence technique was adopted. The immunofluorescence studies looked at the accumulation of foci, measured by the p53 binding protein 1 (53BP1) and the phosphorylated variant of histone H2A (γ H2AX) immunostaining following camptothecin (CPT) treatment. CPT is a specific inducer of TOP1-linked breaks and acts by binding to and stabilizing the covalent 3'phosphotyrosyl intermediate (Staker, et al., 2002). This prevents the protein-linked DNA break (PDB) from being repaired and can give rise to DSBs and/or apoptosis (Cristini, et al., 2016). These proteins were selected as analysis tools due to 53BP1 often being used as a marker of DSB formation due to the interaction of the protein with the chromatin associated with the DSB (Lassmann, et al., 2010). γ H2AX was chosen as a DSB marker as the H2A variant H2AX becomes phosphorylated at Serine 139 upon detection of DSB (Cleaver, et al., 2011). The extent of DNA damage was determined by quantifying the focal accumulation of both 53BP1 and γ H2AX by utilizing specific antibodies. Figure 3.2.1 shows the results obtained.

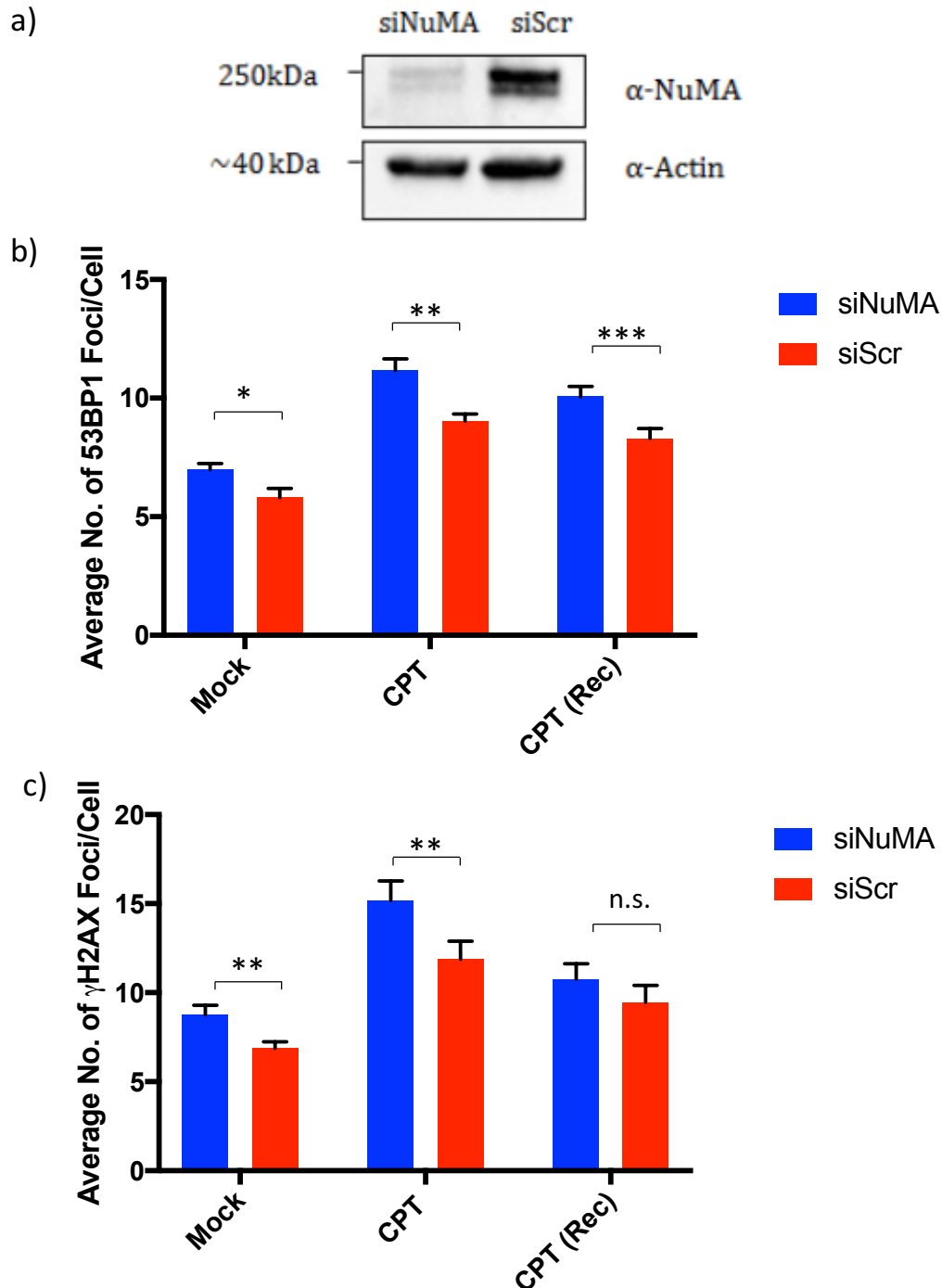


Figure 3.2.1 Depletion of NuMA results in the accumulation of double strand breaks. MRC5 cells were transfected with either scrambled (siScr) or NuMA (siNuMA) siRNA (50nM) for 72 hours. Cells were then treated with DMSO (Mock) or 5 μ M CPT for 1 hour before fixation. For recovery experiment, CPT treated cells were incubated at 37°C for 1 hour in complete medium after CPT treatment. Immunofluorescence was performed to assess 53BP1 and γ H2AX focal accumulation, as a marker of DSB induction. a) Western Immunoblotting to confirm NuMA knockdown with siRNA transfection. Actin serves as loading control. b) and c) Measurement of DNA damage levels modulated by NuMA. The bars represent average number of 53BP1 and γ H2AX foci/cell, respectively. The error bars represent S.E.M from 3 biological repeats (n=3). * = <0.05, ** = <0.005, *** = <0.0005, n.s. = not significant (Student T-test).

Figure 3.2.1 a) shows that there is a significant reduction in the level of NuMA expression after siNuMA siRNA transfection. Confidence can be taken that a true reduction in the level of NuMA present in the cells is occurring after transfection with specific siRNA, as equal levels of actin are detected in both the NuMA knockdown and control conditions. Figure 3.2.1 b) shows that as the cells are challenged with a cytotoxic drug, the amount of average foci in both NuMA depleted cells and control treated cells increases. The increase observed, however, is more pronounced in the NuMA depleted cells. This increase is also evident in the mock-treated cells; depletion of NuMA alone increases the average number of 53BP1 foci, compared to control. The CPT condition shows a significant difference in the average number of foci when comparing the NuMA knockdown and the control conditions; $p = 0.0095$ (student t-test). The CPT recovery condition shows a slight reduction in the average number of foci counted in both the NuMA depleted setting and the control. A significant difference was still evident in knockdown condition compared to control; $p = 0.00000037$. Figure 3.2.1 c) shows a similar trend as b) with a slightly greater average number of γ H2AX foci. The CPT treatment appears to induce more γ H2AX foci than 53BP1 foci, as well as a slightly quicker resolution of foci. This is shown by the quicker disappearance of γ H2AX foci, after a 60-minute recovery period in media. The CPT treated samples exhibit statistical significance between the samples with depleted levels of NuMA and the control samples; $p = 0.0021$. The CPT recovery condition exhibits a difference in number of foci, but not to a statistically significant level; $p = 0.069$.

Analysing the data from the immunofluorescence, a subtle but significant difference in the NuMA depleted cells, compared to the control was observed. This suggests a role for NuMA in the response to DSBs. However, the results do exhibit a very subtle difference upon depletion of NuMA, and for that reason it was decided to explore other potential roles of NuMA within the DNA damage response (DDR).

3.3 NuMA depletion results in accumulation of PDBs

After the findings relating to DSBs and taking into account the DSB response was relatively small, the next question posed was 'does NuMA play a more important role in SSB repair?'. Therefore, it was decided to investigate the accumulation of endogenous DNA SSBs as measured by alkaline comet assays (see materials and methods, section 2.6.1 for representative images of damaged cells).

Single cell gel electrophoresis, or the comet assay, is a technique first established in 1984 by Ostling and Johanson, with the 'comet' aspect of the name attributed to the shape of the damaged DNA. This method used a very basic neutral detergent to lyse mammalian cells embedded in agarose, before brief electrophoresis and staining with acridine orange to facilitate visualisation of the damaged DNA via fluorescence microscopy (Ostling & Johanson, 1984). There was a modified version introduced by Singh et al., 4 years later (Singh, et al., 1988). There are two main types of comet assay; neutral and alkaline. Neutral comet assays are used to detect the presence of DSBs, with the alkaline method also detecting DSBs but mainly SSBs. The protocol for both techniques are largely similar. Both methods involve embedding cells in agarose and degrading cellular proteins before performing the electrophoresis of the cells. This can either be completed using a neutral pH buffer or an alkali buffer. The electrophoresis step allows for the migration of damaged DNA, which has accumulated breaks and therefore lost the supercoiled property hence leading to migration from the 'head' of the comet tail. A fluorescent dye is used to determine the level of DNA damage according to the amount of tail migration, which is proportional to the amount of DNA damage (Olive & Banáth, 2006). For the purpose of this study, the alkaline comet assay was the adopted technique. The alkaline comet assay is the accepted method used to detect SSBs, due to two main reasons. Firstly, lesions such as AP sites which can arise due to ROS and other stimuli are known as alkali-labile lesions. The alkaline nature of the electrophoresis buffer enables the conversion the AP sites to SSBs (Collins, et al., 2008; Fairbairn, et al., 1995). Secondly, there are a high level of hydroxide ions within the electrophoresis buffer, which are negatively charged. The positive nature of hydrogen ions, which are indispensable for the hydrogen bonding between DNA bases, leads to attraction to the hydroxide ions in the buffer which in turn results in disruption of the hydrogen bonding within the DNA duplex. This leads to the

separation of the duplex to yield ssDNA and therefore the detection of SSBs (Fairbairn, et al., 1995).

The first comet assay experiments were performed using CPT as the damaging agent. This induces mostly SSBs via the stabilisation of the TOP1-DNA complex, however it is known to also induce DSB in the event of replication fork collapse during S-phase (Xu, et al., 2015). The siRNA specific to NuMA and a scrambled control was utilised for these experiments. The level of DNA damage caused by treating with 50 μ M CPT for 20 and 60 minutes was examined. The knockdown level was consistently similar to the blot shown in Figure 3.2.1. If knockdown levels were inadequate, the results were discounted and the experiment was repeated. Figure 3.3.1 shows the results obtained.

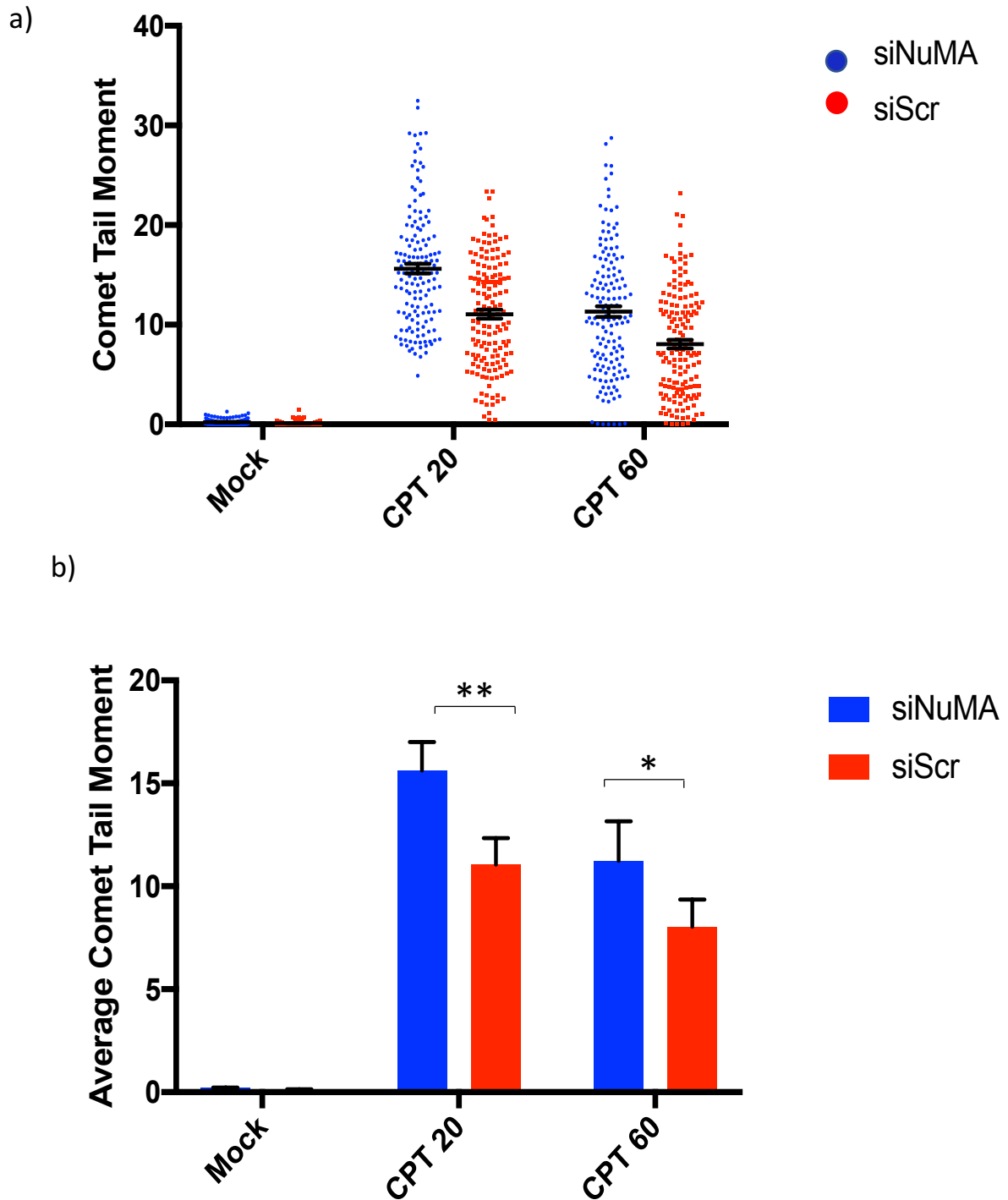


Figure 3.3.1. The depletion of NuMA results in the accumulation of TOP1-linked single strand breaks. MRC5 cells were transfected with either scrambled (siScr) or NuMA (siNuMA) siRNA (50nM) for 72 hours. Cells were then treated with DMSO (mock) or 50 μ M CPT for 20 or 60min before harvest. Alkaline comet assay was performed to assess DNA damage in single cells after gel electrophoresis. a) Representative scatter graph showing spread of comet tail moments from 150 scored nuclei in presence (red dots) or absence of NuMA (blue dots). b) SSBR modulated by NuMA. The bars represent CPT induced average comet tail moments, after 20 and 60min of CPT treatment. The error bars represent S.E.M from 3 biological repeats (n=3) * = <0.05, ** = <0.005, *** = <0.0005 (Student T-test).

Figure 3.3.1 a) shows each individual data point scored across 3 biological replicates (150 total), represented as a dot. The data represents 50 μ M CPT treated MRC5 cells. This scatter plot shows the spread of the data, with error bars representing the standard error of the mean. The scatter plot shows a similar trend across each of the conditions. There are notably bigger comet tail moments associated with the NuMA depleted cell population, at both 20 minutes and 60 minutes of CPT treatment. Figure 3.3.1 b) shows the data from a) represented as a bar chart, with averages of the 150 data points calculated; error bars represent standard error of the mean. There is a significant difference between NuMA depleted and control cells after 20 minutes of CPT treatment ($p= 0.0091$). There is a reduction in average comet tail moment after 60 minutes of CPT treatment, however this is still statistically significant ($p= 0.045$). There is not a statistically significant difference between mock-treated samples ($p= 0.067$).

Following on from the initial CPT comet assay data, it was decided to use 5,6-dichloro-1-beta-D-ribofuranosylbenzimidazole (DRB) as a drug tool to study the effect of transcription halting on accumulation of SSBs. DRB is a well-established agent utilised to inhibit mRNA synthesis (Zandomeni, et al., 1982). DRB acts to inhibit both CDK7 and CDK9 which are required for the phosphorylation of the C-terminal domain of RNA Polymerase II (Pol II), for efficient Pol II- dependent transcription (Turinetto, et al., 2009). The inhibition of these kinases causes the untimely termination of transcription, without affecting the initiation of mRNA transcripts (Baumli, et al., 2010). DRB is a good tool to stall transcription as it is reversible in nature. The aim of the experiments was to examine whether the increase in average comet tail moments associated with the depletion of NuMA was dependent on transcription. Figure 3.3.2 shows the results.

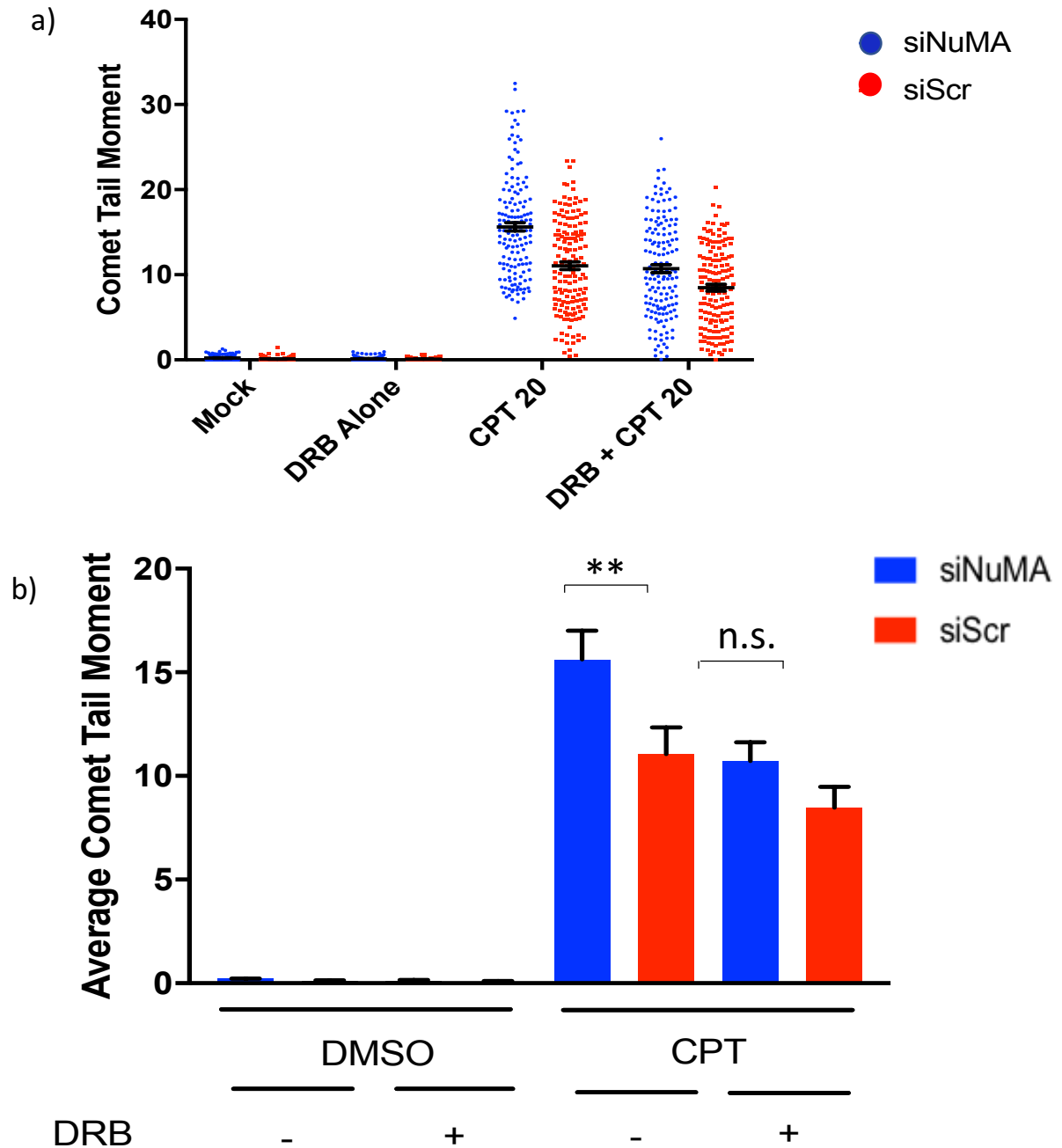


Figure 3.3.2. The depletion of NuMA results in the accumulation of TOP1-linked single strand breaks in a transcription dependent manner. MRC5 cells were transfected with either scrambled (siScr) or NuMA (siNuMA) siRNA (50nM) for 72 hours. Cells were pre-incubated with either mock (DMSO) or transcription inhibitor, DRB (10 μ M) for 2 hours, before treatment DMSO or CPT (50 μ M) for 20 or 60min before harvest. Alkaline comet assay was performed to assess DNA damage in single cells after gel electrophoresis. a) Representative scatter graph showing spread of comet tail moments from 200 scored nuclei in presence (red dots) or absence of NuMA (blue dots) between CPT and CPT + DRB treated cells. b) NuMA modulates SSB repair in transcriptionally active cells. The bars represent CPT induced average comet tail moments in presence or absence of DRB treatment, after 20 min CPT treatment. The error bars represent S.E.M from 4 biological repeats (n=4). ** = <0.005, n.s. not significant (Student T-test).

Figure 3.3.2 a) shows each scored comet, across 4 biological replicates (150 total), representing DRB pre-treated, 50 μ M CPT treated MRC5 cells. The scatter plot shows there is a similar trend to that seen at the 20 minute CPT point in Figure 3.3.1 a) when the cells are not treated with DRB. The cells which were subjected to DRB treatment exhibit noticeably smaller comet tail moments. Figure 3.3.2 b) shows the data from a) represented as an average in bar chart form. The CPT 20 time point with no DRB treatment, mirrors the results shown in b) with a significant difference between the NuMA depleted and the control cells after 20 minutes of CPT treatment ($p= 0.0091$). After DRB pre-treatment, both the NuMA depleted and control cells average comet tail moment reduces. The NuMA depleted cells average reduces to a greater extent, resulting in the statistical significance disappearing ($p= 0.10$). The mock-treated control cells and the NuMA depleted cells show no significant statistical difference when pre-treated with DRB ($p= 0.52$) or with a DMSO pre-incubation ($p= 0.067$). To note, there was also a significant difference between the NuMA depleted cells without the stalling of transcription and after DRB pre-treatment ($p= 0.0098$).

Second to the transcription-stalling studies, the next step was to investigate whether the NuMA depletion phenotype of impaired repair or increase in DNA damage was replication dependent, or independent. To study this, the utilisation of the replication inhibitor aphidicolin was adopted. Aphidicolin is a specific inhibitor of DNA polymerase α which is responsible for DNA replication. Aphidicolin works to inhibit the B family of polymerases, predominantly that of pol α without inhibiting additional processes such as methylation of DNA, or RNA and protein synthesis (Baranovskiy et al. 2014). Figure 3.3.3 shows the results.

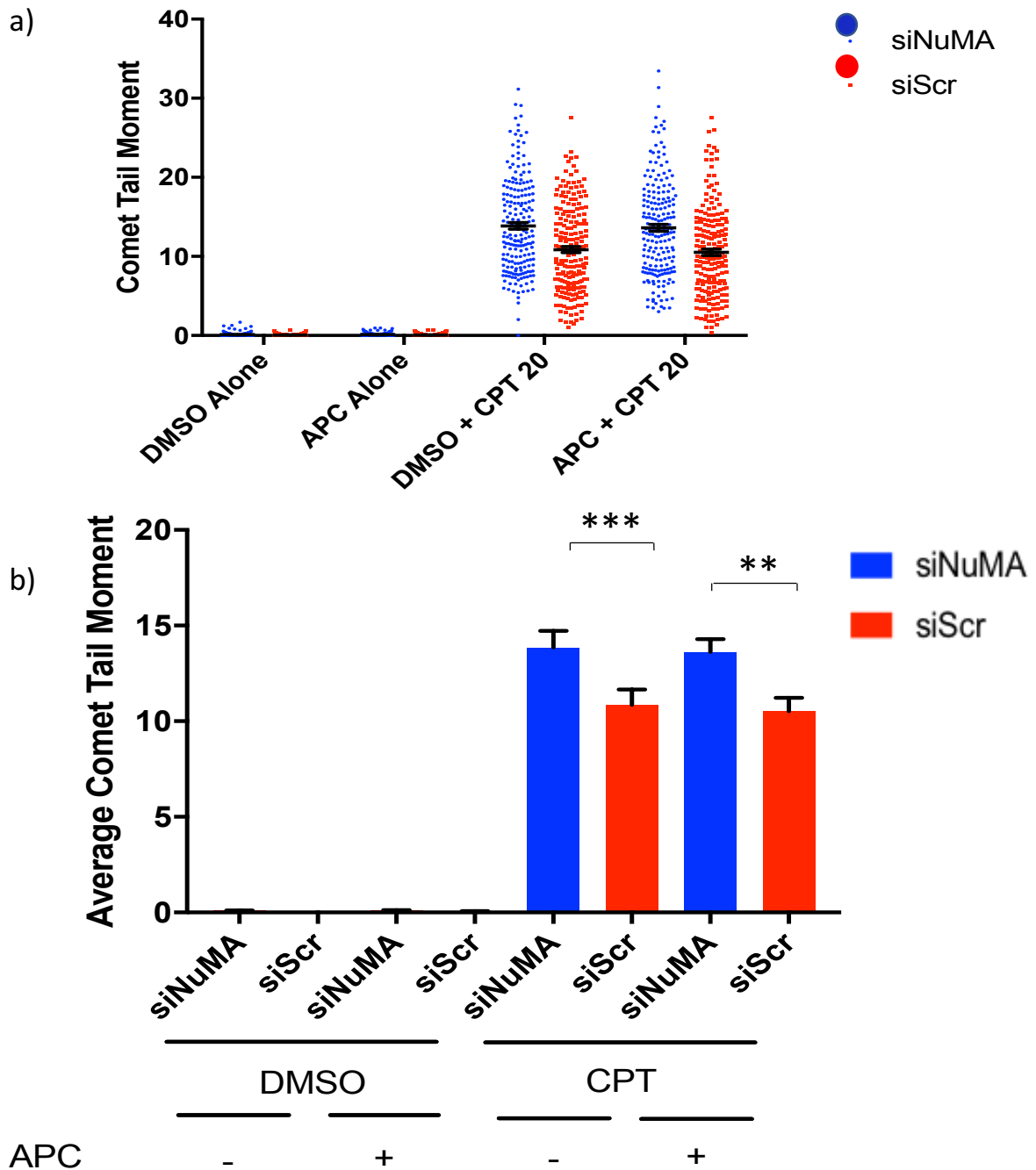


Figure 3.3.3. The depletion of NuMA results in the accumulation of TOP1-linked single strand breaks, in a replication independent manner. MRC5 cells were transfected with either scrambled (siScr) or NuMA (siNuMA) siRNA (50nM) for 72 hours. Cells were pre-incubated with either mock (DMSO) or replication inhibitor, aphidicolin (APC) (50 μ M) overnight, before treatment DMSO or CPT (50 μ M) for 20 or 60min before harvest. Alkaline comet assay was performed to assess DNA damage in single cells after gel electrophoresis. a) Representative scatter graph showing spread of comet tail moments from 200 scored nuclei in presence (red dots) or absence of NuMA (blue dots) between CPT and CPT + APC treated cells. b) NuMA does not further modulate SSB repair in replication-arrested cells. The bars represent CPT induced average comet tail moments in presence or absence of APC treatment, after 20 min CPT treatment. The error bars represent S.E.M from 4 biological repeats (n=4). ** = <0.005, *** = <0.0005 (student t-test).

Figure 3.3.3 a) shows each individual comet tail moment scored, across 4 biological experiments (200 total), representing aphidicolin pre-treated, 50 μ M CPT treated MRC5 cells. The scatter plot shows that with both aphidicolin pre-treatment and without, after 20 minutes of CPT treatment the sets of points are very similar. Figure 3.3.3. b) shows the data from a) represented as a bar chart, with averages calculated. It is clear that there has not been much of a change in the average comet tail moments between siNuMA and siScr cells respectively, regardless of aphidicolin treatment. In both settings, the NuMA depleted cells show a statistically significant difference, compared to control, with DMSO pre-incubation ($p = 0.00000080$) and after APC pre-incubation ($p = 0.0063$). There is no statistical significance between mock-treated siNuMA depleted samples compared to control either with DMSO pre-incubation ($p = 0.13$) or APC pre-incubation ($p = 0.22$). In order to be sure that replication was inhibited, the technique of fluorescent-activated cell sorting could have been used to sort cells into the separate stages of the cell cycle, hence giving an indication of the proportion of cells not replicating.

3.4. NuMA depletion results in a cellular repair defect in response to oxidative stress

One of the major causes of SSBs within the body is reactive oxygen species (ROS). ROS are a class of molecules which include free radicals (both oxygen and hydroxyl radicals) and non-radical oxidants, of which H_2O_2 is an example (Gough & Cotter, 2011). H_2O_2 has become a popular tool to investigate the cellular response to oxidative stress as high levels can induce a high level of cellular toxicity, through the damage of many important molecular structures. It was discovered that there seemed to be a relationship between high levels of ROS, especially H_2O_2 and an increase in genomic instability and oncogenic tendency of cells (Jeffrey, 1958). As H_2O_2 is a source of oxidative stress it was selected as the damaging agent, due to the established usage in cellular systems and its affordability. This use of H_2O_2 would allow for the selective induction of almost wholly SSBs. This tool would also allow for the creation of a repair kinetic profile of the NuMA depleted cells, by recovering the cells after H_2O_2 damage in complete media, at 37 $^{\circ}$ C, for a range of time points. The time points initially adopted were the maximal damage point (R'0), and recovery time points at 7.5 minutes, 15 minutes, 30 minutes and 60 minutes (R'7.5, R'15, R'30 and R'60). Figure 3.4.1 shows the results obtained.

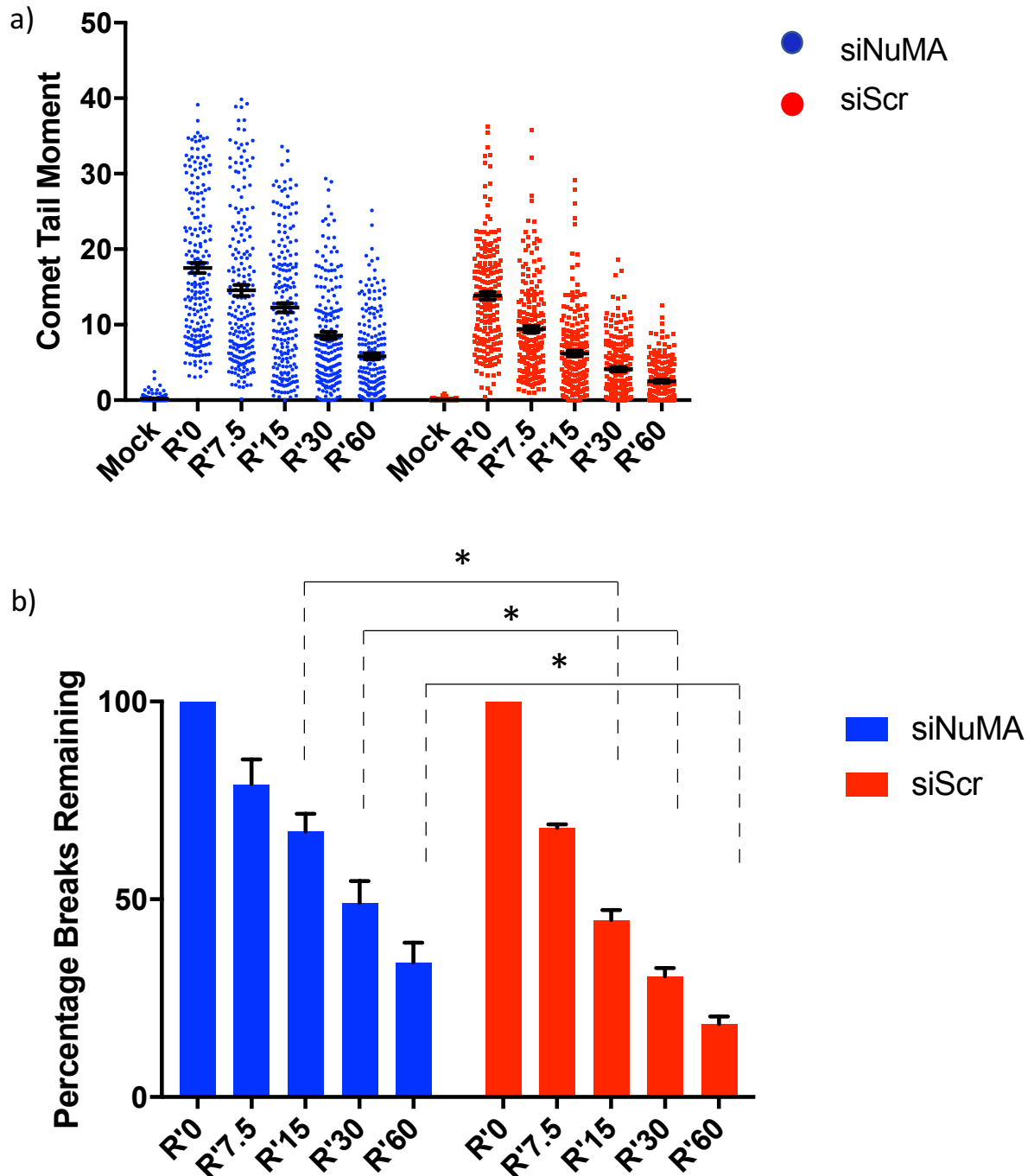


Figure 3.4.1. The depletion of NuMA results in the accumulation of oxidative stress-induced single strand breaks. MRC5 cells were transfected with either scrambled (siScr) or NuMA (siNuMA) siRNA (50nM) for 72 hours. Cells were treated with H₂O₂ (10μM) for 10 minutes on ice, followed by recovery at 37°C in complete medium for 0, 7.5, 15, 30 and 60 minutes respectively. Alkaline comet assay was performed to assess DNA damage in single cells after gel electrophoresis. a) Representative scatter graph showing spread of comet tail moments from 200 scored nuclei in presence (red dots) or absence of NuMA (blue dots). b) SSBR modulated by NuMA. The bars represent percentage breaks remaining (as a measure of average comet tail moment) after removal of oxidative stress and recovery in complete medium between siScr and siNuMA transfected cells. The error bars represent S.E.M from 4 biological repeats (n=4). * = <0.05 (Student T-test).

Figure 3.4.1 a) shows each individual data point scored across 4 biological replicates (200 total), represented as dots. The data represents 10 μ M H₂O₂ treated MRC5 cells. This scatter plot shows the spread of the data, with error bars representing the standard error of the mean. Both the NuMA depleted and the control cells shows a similar stepwise reduction in the average comet tail moment after the initial insult and as the cells recover, with a higher level of breaks attributed to the cells with reduced levels of NuMA. Figure 3.4.1 b) shows data from a) represented as a repair kinetic bar graph. Each R'0 (NuMA depleted and control cells) was respectively assigned as 100% as this was the initial insult, and a repair kinetic profile was created by dividing each of the subsequent recovery points by the R'0 figure. This allows for the assessment of how well the cells recover after H₂O₂ insult. There is a significant statistical difference in the recovery of NuMA depleted cells at R'15 (p= 0.036), R'30 (p= 0.044) and R'60 (p= 0.031) time points, which suggests a repair defect when NuMA levels are diminished. The R'7.5 time point was not of statistical significance (p= 0.163). Moving forward, analysis of the the R'7.5 and R'15 time points was not carried out. The R'7.5. time point did not show a significant difference compared to control. This may have been due to the very short time period left for cells to recover, and that cells require a greater time period to respond to the damage and begin repair. The decision was taken to also omit the 15-minute recovery point and therefore chose to concentrate on the R'30 and R'60 recovery points. By eliminating a couple of the time points, this helped with the experiments becoming higher throughput and for a greater amount of drug/knockdown conditions to be analysed within the same experiment. This was due to length of experiment and equipment limitations as the electrophoresis tank used can only hold 20 slides per experiment.

As with the CPT data shown in section 3.3, the next set of experiments utilised DRB as a tool to stall transcription. The experiments aimed to address whether the repair defect (H₂O₂) associated with the depletion of NuMA was dependent on transcription. Figure 3.4.2 shows the results.

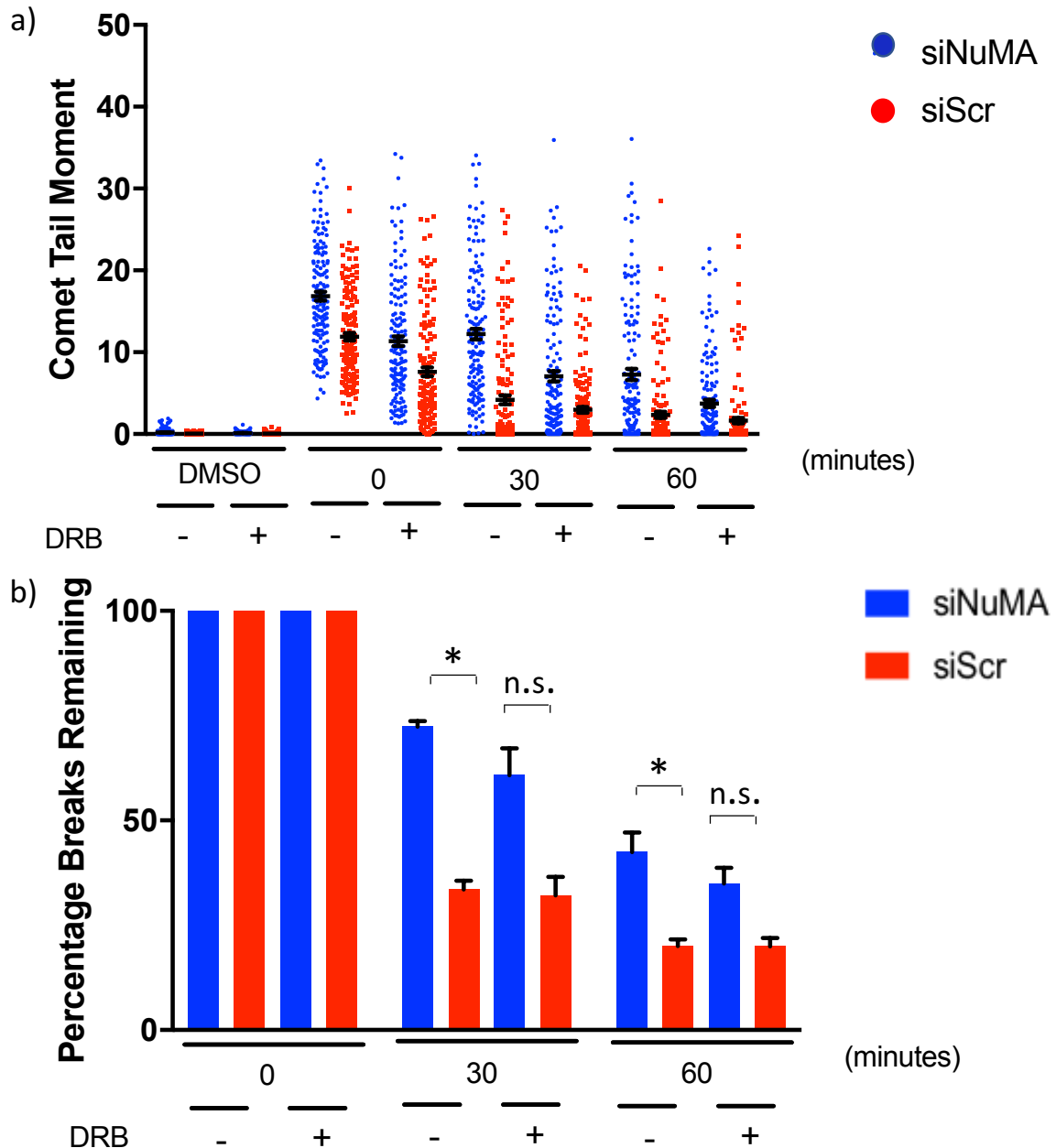


Figure 3.4.2. The depletion of NuMA results in the accumulation of oxidative stress-induced single strand breaks in a transcription dependent manner. MRC5 cells were transfected with either scrambled (siScr) or NuMA (siNuMA) siRNA (50nM) for 72 hours. Cells were pre-incubated with either mock (DMSO) or transcription inhibitor, DRB (10 μ M) for 2 hours, before treatment with H₂O₂ (10 μ M) for 10 minutes on ice. Cells were recovered at 37°C in complete medium for 30 and 60 minutes respectively. Alkaline comet assay was performed to assess DNA damage in single cells after gel electrophoresis. a) Representative scatter graph showing spread of comet tail moments from 150 scored nuclei in presence (red dots) or absence of NuMA (blue dots). b) SSBR modulated by NuMA. The bars represent percentage breaks remaining (as a measure of average comet tail moment) after removal of oxidative stress and recovery in complete medium between siScr and siNuMA transfected cells. The error bars represent S.E.M from 3 biological repeats (n=3). * = <0.05, n.s. = not significant (Student T-test).

Figure 3.4.2 a) shows each scored comet, across 3 biological replicates (150 total), representing DRB pre-treated, 10 μ M H₂O₂ treated MRC5 cells. As mentioned, only R'0, R'30 and R'60 time points were assessed in further experiments. The scatter plots show a reduction in both siNuMA and siScr comet tail moments corresponding to the DRB treated cells at all time points, compared to untreated controls. Figure 3.4.2 b) shows the representation of the data shown in a) as a repair kinetic bar chart. It clearly shows that the NuMA depleted cells which were not pre-treated with DRB have a statistically significant repair defect, compared to control (R'30; p= 0.0011, R'60; p= 0.042). The DRB treatment of NuMA depleted cells reduces the repair defect, as it is no longer statistically significant compared with the control (R'30; p= 0.100, R'60; p= 0.144).

To corroborate the data attained with CPT plus aphidicolin treatment, the tool of SH-SY5Y cells was chosen. This was as an alternative to treating MRC5 cells with aphidicolin. SH-SY5Y are an undifferentiated cell line exhibiting a morphology similar to neuroblasts, which can be differentiated into neuroblastoma epithelial cells under a low foetal calf serum (2%) setting along with the addition of 20 μ M retinoic acid. Once differentiated, they exhibit a similar morphology to primary neurons (Gordon, et al., 2013). It was decided to utilise these particular cells as a tool due to the cells' potential to differentiate into a neuronal cell subtype under specific conditions previously stated (Shipley, et al., 2016). Once differentiated, the cells phenotype changes dramatically and they exhibit a dendritic phenotype, with long, axonal branches to the cells. This allowed for confidence in the fact that cells were differentiated efficiently. As the SH-SY5Y cells are undifferentiated cells derived from bone marrow, once differentiated they are classified as a neuronal cell type and hence could be dubbed post-mitotic cells (Gordon, et al., 2013). As neuronal cells do not have the ability to proliferate, they are usually classed as quiescent and therefore the cells are no longer cycling (Frade & Ovejero-Benito, 2015). This allows us to corroborate the aphidicolin data already attained using CPT as the damaging agent, due to the lack of replication occurring in neuronal cells. The results obtained also showed the same profile as the aphidicolin data set. This data set is shown in figure 3.4.3.

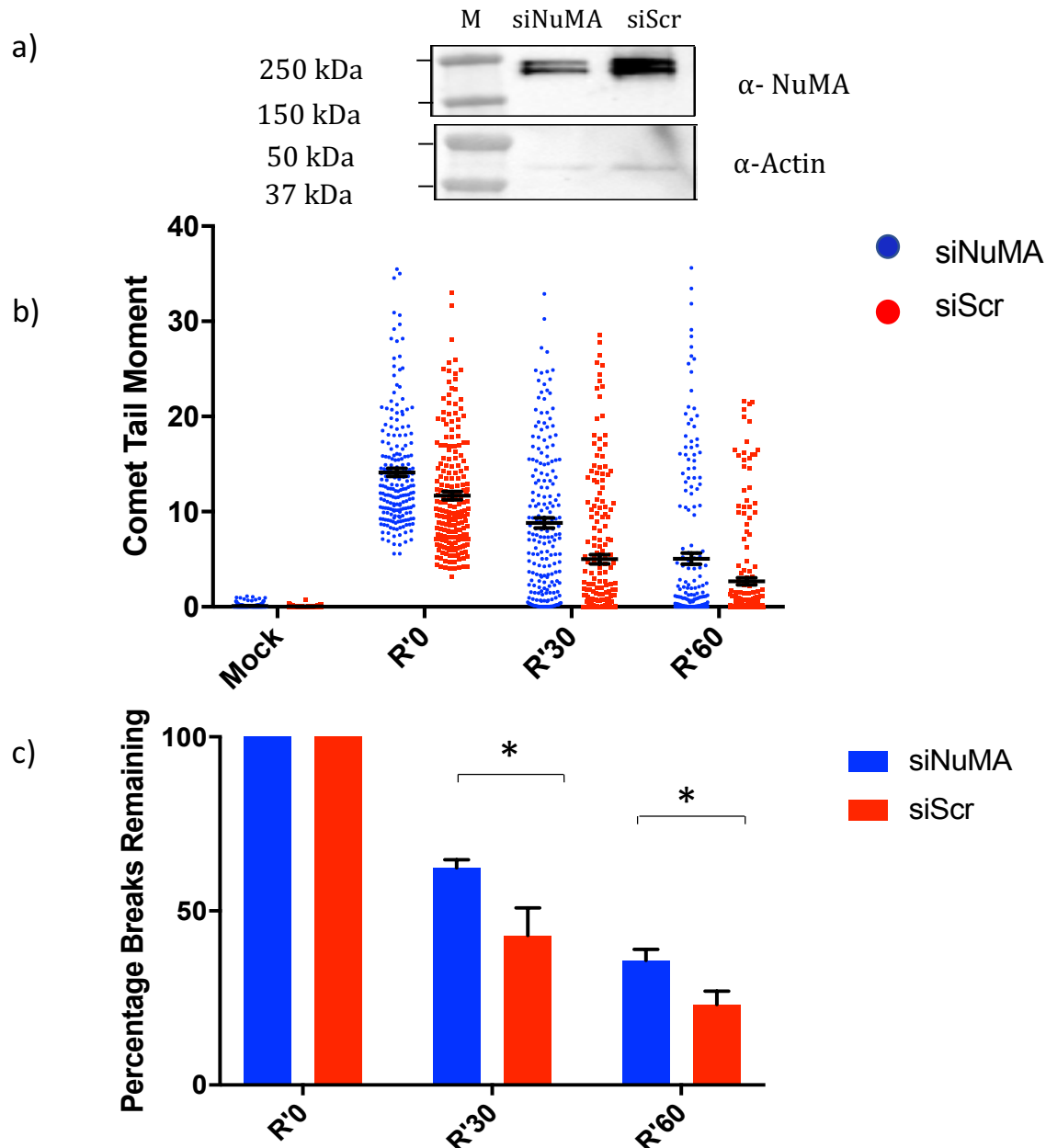


Figure 3.4.3. The depletion of NuMA results in the accumulation of oxidative stress-induced single strand breaks in a replication independent manner. SH-SY5Y cells were transfected with either scrambled (siScr) or NuMA (siNuMA) siRNA (50nM) for 72 hours. Cells differentiated with low serum and 20 μ M retinoic acid until cells exhibited dendritic phenotype. Cells were treated with H₂O₂ (10 μ M) for 10 minutes on ice, followed by recovery at 37°C in complete medium for 30 or 60 minutes. Alkaline comet assay performed to assess DNA damage in single cells after gel electrophoresis. a) Western Immunoblotting to confirm NuMA knockdown with siRNA transfection. Actin serves as loading control. b) Representative scatter graph showing spread of comet tail moments from 200 scored nuclei in presence (red dots) or absence of NuMA (blue dots). c) NuMA does not further modulate SSB repair in differentiated SH-SY5Y cells. The bars represent percentage breaks remaining (as a measure of average comet tail moment) after removal of oxidative stress and recovery in complete medium between siScr and siNuMA transfected cells. The error bars represent S.E.M from 4 biological repeats (n=4). * = <0.05 (Student T-test).

Figure 3.4.3 a) shows scatter plot of each individual data point scored across 4 biological replicates (200 total) representing aphidicolin pre-treated, 10 μ M H₂O₂ treated SH-SY5Y cells. The scatter plot shows a similar reduction in comet tail moments as cells recover in both siNuMA and siScr treated cells. Figure 3.3.4 b) is a repair kinetic bar chart, representing the data shown in a). The graph shows that after 30 and 60 minutes of recovery, there is a significant difference between the repair of cells which have a depleted pool of NuMA and those which do not (R₃₀; p= 0.0402, R'₆₀; p= 0.0063).

3.5 NuMA depletion affects cell survival

After the completion of the comet assays described above, a rounder knowledge of how the depletion of NuMA affects the cellular response to CPT, H₂O₂ and the effect of transcription and replication-stalling drugs under the same conditions was acquired. To further extend the knowledge in this area, the adoption of the technique of clonogenic survival assay was selected. This was mainly due to the fact that one disadvantage of the alkaline comet assay is that it cannot show the ultimate fate or the viability of the cell, which would be useful information (Olive & Banáth, 2006). Clonogenic survival assays assess the relationship between the dosage of selected drug and the ability of the cells to replicate and therefore form a clone, providing an insight into cell fate. The proportionality of the amount of clones present at each given concentration point allows a clonogenic curve to be constructed. The clonogenic survival assay was chosen to further strengthen the data previously ascertained from the comet assay and provide further information relating to the fate of the cell. Both CPT and H₂O₂ clonogenics showed a reduction in survival when NuMA is depleted. The results are show in figure 3.5.1. These results are concurrent with the findings from the comet assays. This result further points to a role for NuMA in the repair of damaged cells; if the cells can't repair the initial damage caused by CPT or H₂O₂, they fail to survive and hence can't go on to form colonies. This observation requires further investigations.

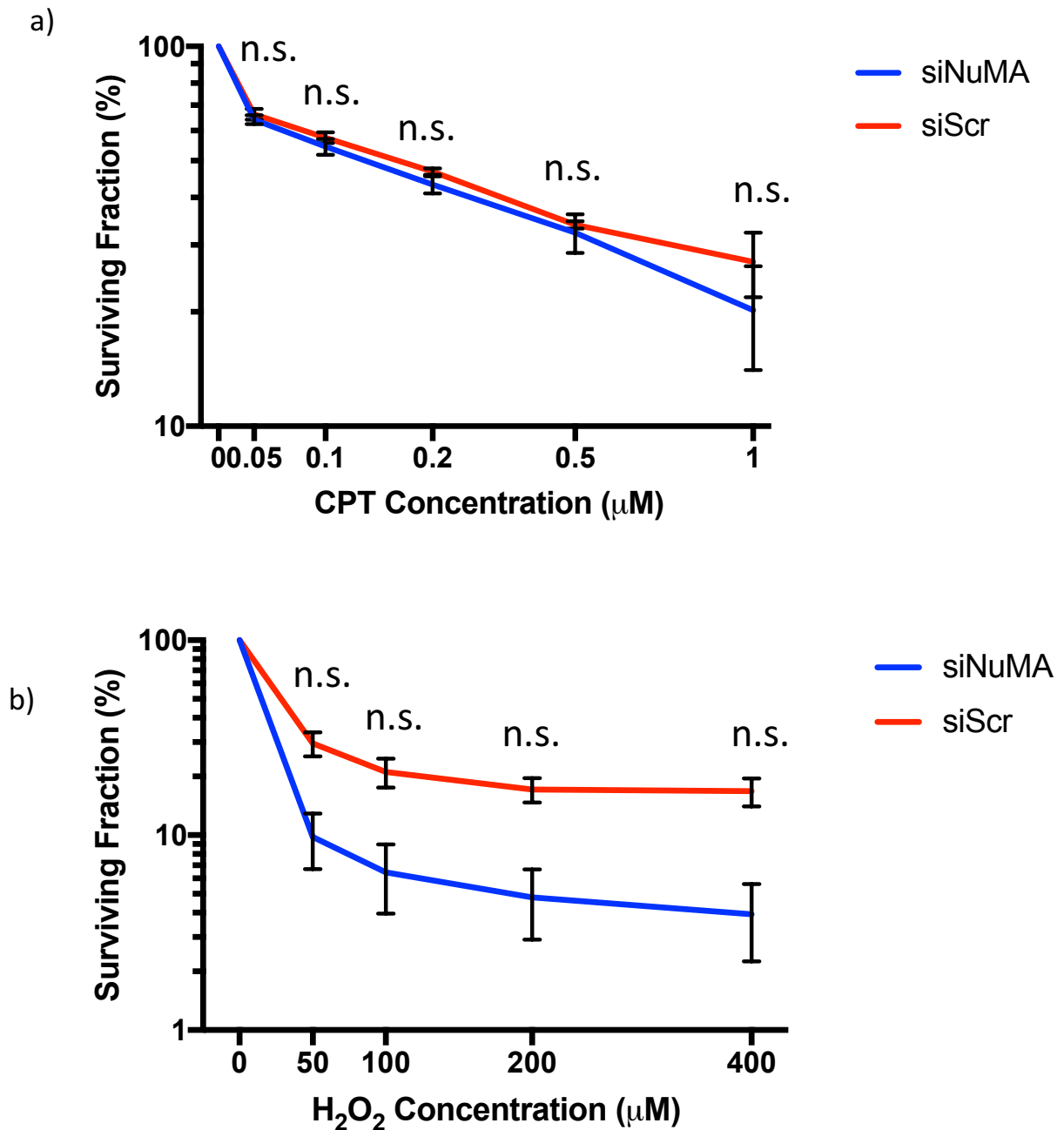


Figure 3.5.1. The depletion of NuMA results in greater cell death. MRC5 cells were transfected with either scrambled (siScr) or NuMA (siNuMA) siRNA (50nM) for 72 hours. Cells were then re-plated on to 10cm dishes in varying cell concentrations and were left to adhere overnight. Cells were then treated with DMSO (mock) or varying concentrations of CPT for 1 hour before washing with PBS (a); cells were treated with varying concentrations of H_2O_2 for 10 minutes on ice before washing with PBS (b). The medium was replaced and cells were left to form colonies for 10 days at 37°C . a) NuMA depletion has a minimal effect on survival. Log10 scale graph showing the surviving cellular fractions following CPT treatment. b) NuMA mediates cell survival. Log10 scale graph showing the surviving cellular fractions following H_2O_2 treatment. The error bars represent S.E.M from 4 biological repeats ($n=4$) for (a) and S.E.M from 3 biological repeats ($n=3$) for (b). n.s. = not significant (Student T-test).

Figure 3.5.1 a) shows a line graph using a log₁₀ scale, detailing the percentage of surviving cells after treatment with varying concentrations of CPT. The results were analysed by taking plating densities and dividing by the appropriate factor to equal the same density as was plated on the control plate (see materials and methods). This allowed for accurate plating and similar numbers of colonies per plates to count. The results do not show a significant difference in the survival of the NuMA depleted cells compared to the control. Notably, mock treated samples (represented as 100% on the graph) for both NuMA depleted and Scr treated samples were not statistically significant when calculated from raw values (average of 162.5 colonies siNuMA; 160.3 colonies siScr) ($p= 0.184$). Figure 3.5.1 b) shows a line graph using a log₁₀ scale, detailing the percentage of surviving cells after treatment with varying concentrations of H₂O₂. Similarly to a) the number of colonies per plate were normalised to the same density as control plates. The results show there is not a significant difference in the percentage survival of cells which have depleted levels of NuMA, compared to control. The mock treated samples (adjusted to 100% on the graph) did not exhibit any statistical significance between NuMA depleted and control cells when calculated from raw values (average of 172 colonies siNuMA; 177 colonies siScr) ($p= 0.869$).

3.6 Discussion

In this study, the investigation into the potential role of NuMA in the DNA damage response was intended. The utilisation of specific siRNA sequences to silence the *NUMA1* gene allowed us to study the response to SSB and DSB upon depletion of the NuMA protein. siRNA works to degrade the mRNA after transcription which results in a stoppage of or reduced level of protein translation and hence reduced levels of protein expression. As is shown by the western blotting in Figure 3.2.1 the depletion of NuMA is only a partial knockdown. There were many initial issues with the optimisation of the NuMA knockdown. Ordinarily, a 48 hour incubation post transfection of the siRNA was sufficient to provide partial or even complete knockdown of protein expression, evidently depending on the gene of interest. It was discovered that NuMA seemed more difficult than anticipated to transiently knockdown, however a good level of knockdown was achieved via adopting a double knockdown method; two transfections were used, the second after 48 hour incubation which was left for a further 24 hours before harvest. A hypothesis was proposed that perhaps the reason it was so difficult to achieve a good

level of knockdown was that as the protein is large (2115 amino acids), that it has a long half life and hence protein turn over may be relatively slow. One way to have further explored this possibility would have been to use the drug cyclohexamide (CHX) in order to stall protein production. CHX facilitates the shut-down of protein synthesis by affecting the elongation step of translation in higher eukaryotes (Schneider-Poetsch et al., 2010). By stalling translation and monitoring protein levels over a time course of a number of hours (usually up to 24 hours) it can give an indication of how long the protein remains without levels decreasing, in the absence of new protein synthesis. Another explanation is that as NuMA is a structural protein, with a large coiled-coil domain; this could account for the high level of stability of the protein and hence the difficulty in reduction in protein levels. Once the desired knockdown was achievable, the DSB repair studies could begin.

As the initial plan was to gain insight into DSBR, assessment of focal accumulation of γ H2AX and 53BP1 after reduction of NuMA levels was of paramount interest. Adopting the immunofluorescence assay not only allowed the achievement of a relatively high-throughput stream of data, but also allowed for the validation that the chosen cytotoxic drugs were working as expected. The initial immunofluorescence experiments used CPT as the damaging agent. As TOP-1 stalling allows for accumulation of SSBs and the conversion to DSBs in the absence of repair mechanisms, the increase in both γ H2AX and 53BP1 foci should be proportional to CPT treatment. There was a high level of confidence that CPT was working as hoped due to the increase in foci number. Referring to figure 3.2.1, the results showed a small but significant increase in both γ H2AX and 53BP1 foci when NuMA was depleted. This finding means that the depletion of NuMA does increase the accumulation of DSBs, however the increase compared to control is quite small, which led to exploring other channels. Furthermore, the results were reassuring that there was a role for NuMA within the DNA damage response (DDR), however as the results showed a very subtle difference, investigating SSBR after NuMA depletion was an interesting prospect. As CPT had been previously utilised and there was confidence that the drug was having the desired effect in causing the accumulation of PDBs and hence CPT was chosen as the damaging agent for the preliminary comet assay experiments.

The comet assay is an extremely useful tool to assess both SSBs and DSBs. There are two different types of comet assay; neutral and alkaline. The neutral assay is used to assess

DSBs, as due to the neutral pH of the electrophoresis buffer, both DNA strands remain annealed. The alkaline comet assay is more often adopted to study SSBs (as well as DSBs) as the use of NaOH in both the lysis buffer and the electrophoresis buffer yields SSBs. The usage of NaOH acts to disorder the hydrogen bonding between the DNA bases which allows for the separation of the DNA strands, hence unveiling SSBs (Collins, et al., 2008). Before setting up a large-scale comet experiment, lengthy optimisation of CPT concentration was performed in order to determine a concentration which would produce enough breaks to detect relatively large comet tail moments but not introduce so many breaks that the cells are damaged to the extent that they become exceptionally difficult to score accurately. After testing a number of different CPT concentrations, it was decided to move forward with 50 μ M. Cells were subjected to either 20 minutes or 60 minutes of CPT treatment. Cells were then embedded in agarose and mounted on to slides and performing the comet assay. Referring to figure 3.3.1 a) and b), the results show that both untreated samples (siNuMA and siScr) exhibit a very low level of damage, as expected. This was reassuring that the cells were relatively healthy, even after trypsinisation. The 20-minute time point showed a high level of damage in both NuMA depleted and control cells, however a significant increase in comet tail moment in the siNuMA sample was observed, compared to the control. This means that CPT is damaging both NuMA depleted and control cells, but there is a greater extent of damage in the cells which have reduced levels of NuMA. This could be due to NuMA potentially having a protective role within the DDR. Another explanation could be that NuMA is a fundamental protein within the cell and its depletion combined with CPT damage means that the cells accumulate significantly more damage. The 60-minute time point indicates a situation where although the cells are still being damaged by the maintenance of the CPT insult, the cells repair mechanisms have also begun to recognize the damage and start to repair it. This is indicative of the general reduction in comet tail moments observed after 60 minutes CPT treatment in both knockdown and control settings. This pointed to a role in NuMA in SSB formation or SSBR as the NuMA knockdown either exacerbated the effect of CPT on cells, or prevented the cells to be repaired as the moments were increased, compared to control. There was a significant difference in average comet tail moment of the NuMA depleted cells compared to control, which further pointed to a requirement for NuMA in SSBR.

It was decided that the results obtained were interesting enough to investigate further into the link between NuMA and SSBs. To obtain a more rounded vision of how damage and NuMA depletion correlate, it was decided that a different damaging agent would be utilised. As it was a possibility that the depletion of NuMA was preventing the initiated SSBs from being repaired, it was proposed to attempt to formulate a repair kinetic profile to visualise how quickly cells recover from the cytotoxic insult. In order to study NuMA and the specific repair kinetics associated with the depletion of NuMA, H₂O₂ was adopted as the damaging agent and it was decided to use the alkaline comet assay as a tool to study SSBs. ROS is one of the major causes of SSBs, which are the most commonly occurring lesions within the human body. H₂O₂ was selected as the damaging agent as it is an excellent source of oxidative damage, which induces predominantly SSBs. As H₂O₂ treatment is very short, it allowed for the creation of a kinetic repair profile, by allowing cells to recover in complete media for varying amounts of time post H₂O₂ exposure.

Akin to the CPT experiments, H₂O₂ was first optimised to determine the required concentration to induce the desired level of comet tail moment. After testing a number of concentrations, 10µM for 10 minutes (in ice cold PBS) on ice was opted for. This was chosen as it induced a significant level of damage to score efficiently without creating too much which could make scoring the comet tail moments difficult and inaccurate. After removing the H₂O₂, cells were allowed to recover in complete media, before being mounted on slides for analysis via comet assay. Referring to figure 3.4.1 a) and b) the results showed that there was a significant difference in the repair kinetics of the NuMA depleted cells compared to control after 15, 30 and 60 minutes of recovery, post H₂O₂ insult. It is important to note that the R'0 time point which is indicative of the highest level of damage, directly after the drug was removed, was normalised to 100 for both siNuMA and siScr samples. It can be seen in the scatter graph that the absolute levels of damage are higher in the NuMA depleted cells. This was an expected observation as there were a higher amount of average comet tail moments when treated with CPT. We believe that this could be due to the fact that *NUMA1* is potentially an essential gene (NuMA was found to be essential in at least one aspect of murine embryonic development) and a fellow lab members' attempt to attain a CRISPR knockout cell line proved unsuccessful (Silk, et al., 2009). As the levels of NuMA protein expression was significantly reduced when siRNA transfected, the cells are perhaps less healthy than cells which are treated

with control siRNA. The mock treated cells also have a slightly higher level of damage in the NuMA knockdown cells, but this is very subtle, which points to an exacerbation of the amount of damage caused when treated with the drugs when NuMA levels are depleted. The reason for the normalisation was to see a comparative repair kinetic profile. The results obtained mean that the reduction of NuMA results in cells recovering less well. Although an exact explanation to this is yet to be elucidated, it can be said that there is a repair defect when NuMA depleted cells are treated with an acute dose of H₂O₂ and allowed to recover for up to one hour.

One issue encountered when performing the H₂O₂ comet assays was that the output was sometimes unpredictable. To explain further, huge levels of variation were noticed with the comet tail moment measurements with comparable samples across experiments. It was hypothesised that this difference was perhaps as a result of the instability of H₂O₂, every time a new vial was opened that some potency could be being lost. To overcome this it was decided to aliquot the H₂O₂ before use and use each vial only once, in an attempt to minimise the loss of efficacy and standardise any potential loss across consecutive experiments. The results show an evident defect in repair when cells had depleted levels of NuMA. There was a decent level of confidence that there was perhaps a role for NuMA in SSB repair specifically, and this led to further investigations into the protein and its emerging role within the DDR.

Taking into account the data collected from both the CPT and H₂O₂, it was decided to look into whether the increased comet tail moments when NuMA is depleted are dependent on, or independent of, both transcription and replication. In order to assess this, two different drugs were adopted as tools which specifically inhibit transcription and replication. DRB was adopted as the drug tool to study the effect of transcription halting on accumulation of SSBs. DRB acts to inhibit CDK7 and CDK9 to prevent the phosphorylation of RNA Polymerase II, resulting in the untimely termination of transcription (Turinetti, et al., 2009). Being aware of the reversible nature of DRB, a 2 hour pre-treatment with 50µM DRB was determined an optimal concentration to stall transcription. However, as the drug treatment followed the pre-incubation, the DRB needed to be replaced during the drug incubation/recovery period. This was a precaution taken to prevent the restarting of transcription during this time. Referring to both figures

3.3.2 a) and b) and 3.4.2 a) and b), when transcription is inhibited, the significance of increase in comet tail moment/repair defect of NuMA depleted cells compared to control disappears – i.e. when transcription is stalled, although there are still slightly higher comet tail moment averages and a slightly slower repair kinetic profile in the NuMA knockdown cells, this is not to a significant extent. This suggests that the NuMA knockdown profile we observe with both CPT and H₂O₂ treatment is dependent on transcription. As can be seen for both the CPT and H₂O₂ DRB comet assay results (figures 3.3.2 a) and b) and 3.4.2 a) and b)), there was a reduction in the average comet tail moment. This reduction resulted in a loss of significance between the siNuMA and siScr samples. This means that if transcription is stalled, the average comet tail moment of the NuMA depleted samples are not significantly greater than that of the siScr samples. Notably, the DRB treated siScr cells does not show much of a reduction in average comet tail moment, or indeed a change in amount of recovery, which is converse to the effect seen on DRB treated siNuMA cells. This points to a role for transcription in the increase in both CPT induced and H₂O₂ induced breaks when NuMA is depleted. It can be seen that NuMA cells don't recover to the same extent as the control cells, even when transcription has been stalled. This could be due to the fact that NuMA is required in the SSBR process and hence this becomes impaired, albeit to a lesser extent when transcription has been shut down.

Following on from the transcription-stalling experiment, investigating the role of replication on NuMA depletion was the next experiment. Aphidicolin was selected as the drug to stall replication. Aphidicolin is derived from *Nigrospora sphaerica* and is a reversible inhibitor of replication via the specific inhibition of DNA polymerase α . As with DRB, aphidicolin is a reversible antagonist and therefore the drug was replaced during CPT treatment/H₂O₂ recovery. Although the potential for any restarting of replication in such a small window of treatment/recovery to skew the results is small, it was felt the precaution was necessary. Referring to figure 3.3.3 a) and b), there was a high level of significance between siNuMA and siScr at both conditions, as assessed using a two-tailed paired T-test. This suggests that the accumulation of CPT-induced breaks is independent of replication. When replication is inhibited, the significance of increase in comet tail moment/repair defect of NuMA depleted cells compared to control is maintained – i.e. when replication is stalled, the profile observed is very similar to that of standard

knockdown conditions and the difference between NuMA knockdown and control cells is still significant. This means that the NuMA depleted cells still exhibit a repair defect, after replication has been stalled. From this inference can be drawn that the repair profile observed when NuMA is depleted is replication independent, shown by the persistence of the repair defect when replication is halted.

Following on from this finding, it was thought that there may be a need to confirm this using another tool. The tool utilised was SH-SY5Y cells. SH-SY5Y are a stem cell line which can be differentiated into cells with neuronal characteristics (see section 3.4). This allows for the corroboration of the aphidicolin data already attained using CPT as the damaging agent, due to the lack of replication occurring in neuronal cells. The initial experiments with the SH-SY5Y cells were to ascertain whether it would be possible to transfect the cells with siRNA and deplete the levels of NuMA to a sufficient level. As the transfection protocol for NuMA siRNA amounts to 72 hours post initial transfection, it was not known whether once we differentiated the cells after 72 hours of transfection the knockdown status of NuMA would remain once the cells had differentiated. The cells were allowed to differentiate for around 72 further hours post transfection, until around 70% of the cell population had a dendritic phenotype. As the goal was to be satisfied that the cells were no longer replicating, the requirement for the whole population to have differentiated was unnecessary as this process can sometimes be quite lengthy. As previously mentioned there was a worry that the silencing of the NuMA gene might not be maintained, and therefore the process was somewhat time-sensitive. After western blot analysis, the NuMA knockdown profile was very similar to that seen in MRC5 cells when harvested after 72 hours post siRNA transfection and hence the level of confidence was attained in order for progression. Once the ascertainment that the siRNA seemed to still have the desired effect after a further 72 hours differentiation, the comet assay experiments were started. For this subset of experiments, H₂O₂ was selected as the treatment of choice. This was selected due to the fact that the aphidicolin experiments were performed with CPT and hence it would be ideal to show that in a replication-stalled setting, the same profile is observed with two different drugs. Referring to figure 3.4.3 a) and b), the results show that there is still a significant difference between siNuMA and siScr at both R'30 and R'60 time points. This is the same profile that was seen with the H₂O₂ alone treatment, hence the SH-SY5Y cells exhibit the same trend, which supports

the aphidicolin data set that the stoppage of replication does not affect significance. This means that there is still a significant difference between the NuMA depleted cells and control cells, when replication is halted. Both the aphidicolin and the SH-SY5Y data show that the increase in CPT induced breaks in MRC5 cells and the repair defect associated with the depletion of NuMA (H_2O_2 treatment- SH-SY5Y cells) are not dependent on replication.

The clonogenic survival assay is a useful tool to assess the viability of cells after exposure to stimuli. The technique can provide a large output of data, however the variability between data sets can be relatively great. This can be due to plating tiny amounts of cells per plate, and especially with CPT, very small amounts of drug. These can allow for a high level of error, hence each concentration point was carried out in triplicate. In these particular experiments, the siRNA protocol as previously described was adopted to deplete the levels of NuMA, before treating with either CPT or H_2O_2 . As with the comet assays, first a series of optimisation experiments were performed. Initially, a much higher concentration of CPT was used, due to the concentrations used for comet assays. It was quickly realised that the higher doses of CPT were mostly lethal, which left only a very small amount of colonies left to count. This led to the change of drug concentrations. To note, the initial insult needed to take place whilst the cells still had a reduced level of NuMA in order to ascertain the knockdown effect on cell survival. As the cells were left for 7-10 to incubate post drug treatment, the siRNA would no longer be effective and the protein levels would return to normal. However, as the insult occurred whilst the gene was still knocked down, it was thought that the treatment occurred at a time which would allow for the results obtained to be a true reflection of the knockdown phenotype. It came to light that another condition that would need to be changed after preliminary experiments was the plating densities. Originally, the amount of cells plated was the same for each of the conditions of drug, including the untreated samples. This was an issue as there was a much higher level of cell death with the highest concentration of drug, and hardly any cell death in the untreated samples. This meant that there were huge amounts of colonies on the untreated plates and none on the higher concentration plates. This issue was rectified by plating varying amounts of cells, with much fewer cells on the untreated plates and up to 10x more cells for the high concentration plates. This allowed for a standardization of colony counting, whereby similar amounts of colonies were

counted per condition, so to provide an easier counting experience without too many colonies merging into each other. The difference in cell density was then accounted for when analysing the data collected.

To begin with, experiments were not carried out in triplicate. As the experiment was repeated, it quickly became evident that the variation was so large that each concentration of drug required multiple plates per condition. This allowed for an increased confidence in the accuracy and precision of both plating density and concentration of drug treatment. Referring to figure 3.5.1 a) and b) it can be seen with both the CPT (4 biological repeats) and H₂O₂ (3 biological repeats) that there is not a significant difference in the percentage cell survival of the cells which had reduced levels of NuMA, compared to control. This graphs show that the cells with depleted levels of NuMA are more sensitive to the cytotoxic drugs, albeit very subtly (both CPT and H₂O₂). There was a good level of satisfaction that the plating efficiency was accurate as there was no significant difference between the two untreated samples (siNuMA and siScr). This is shown through the fact that after the 10 day incubation, although there were slightly more colonies on the untreated siScr plates on average, this was not to a significant extent (CPT: average of 162.5 colonies siNuMA; 160.3 colonies siScr. H₂O₂: average of 172 colonies siNuMA; 177 colonies siScr). This means that the NuMA depletion alone does not have a significantly greater lethality. It was apparent that there was a much more obvious difference in survival rates when H₂O₂ was used as the damaging agent. This could be due to the fact that there was very high concentrations of H₂O₂ used. It also could be due to the specific SSB induction that H₂O₂ causes and hence why a much larger difference in NuMA depleted cells compared to control. This result is also backed up by the comet assay data, as a greater level of damage was observed when H₂O₂ was chosen as the damaging agent.

Through a multi-experimental approach to investigating NuMA and the effect its depletion has on the DDR, it was agreed that substantial amount of evidence had been collected to support the hypothesis that NuMA plays a role in SSBR. Therefore, it was decided to further explore this area, expanding the focus area. As there was a particular interest in the role of NuMA in the DNA damage response and specifically in SSBR, investigations into potential interactions with other elements of the SSBR machinery were undertaken.

Chapter 4

Interacting Partners of NuMA

4.1 Introduction

Following on from the results obtained which pointed to a potential role for NuMA within the DDR, it was decided to explore this area further. As there seemed to be a more important role for NuMA in the repair of SSBs, wider knowledge of how NuMA functions within the SSBR process was desired. Investigations into potential proteins which may functionally or physically interact with NuMA were undertaken. These studies centred around known SSB repair factors, in particular factors involved in the repair of PDBs. In chapter 3, CPT was used as a tool to study PDBs. Since NuMA depletion showed sensitisation to TOP1-mediated DNA damage, the possibility that NuMA physically interacts with enzymes which are implicated in the repair of TOP1 breaks was examined.

4.2 TDP1 physically interacts with PARP1

It was shown in 2014 that TDP1 and PARP1 directly interact (Das, et al., 2014). As an initial experiment, it was decided to confirm the interaction via the utilisation of co-immunoprecipitation (co-IP), whilst ensuring the protocol was effectively optimised in order to detect a physical interaction of the proteins. Figure 4.2.1 shows the western blotting performed after completion of the co-IP.

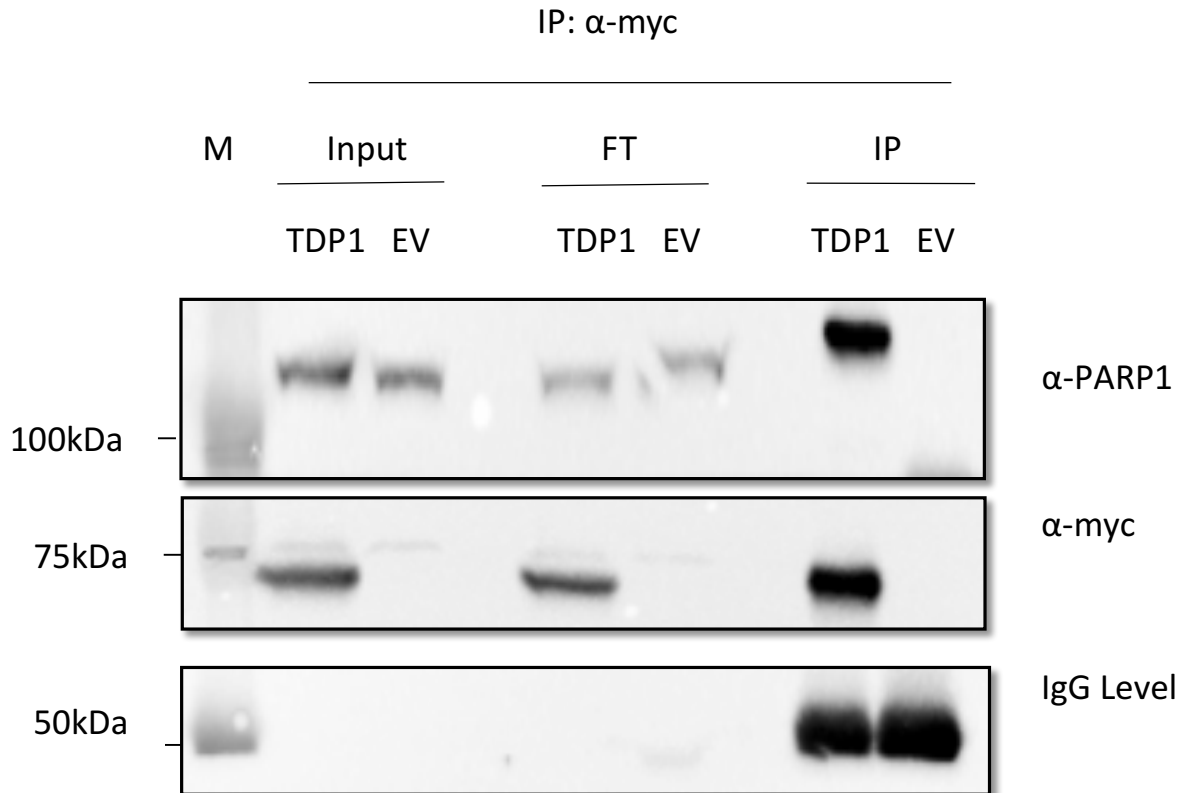


Figure 4.2.1. **TDP1 physically interacts with PARP1.** HEK 293 cells were transfected with myc-TDP1(TDP1) alone, or empty myc vector (EV, empty vector) for 48 hours before harvest. TDP1 was immunoprecipitated from whole cell extracts using myc antibody (9E10; mouse). Immunoprecipitated complexes were analysed by western immunoblotting using antibodies specific to human PARP1 (mouse) or c-myc (mouse). IgG level was used as a loading control. Inputs (5% of total lysate)-lanes 1,2; Flow through (FT)-lanes 3,4; myc-IP-lanes 5,6. Position of pre-stained molecular weight markers (kDa) is indicated (ladder). Protein sample analysis was carried out via SDS-PAGE, using a 6% polyacrylamide gel. Gel transferred to nitrocellulose membrane, using a Trans-Blot transfer system (Bio-Rad).

Figure 4.2.1. shows the western blot analysis following co-immunoprecipitation. This is determined by the presence of an intense protein band in the IP lane corresponding to the HEK 293 cells which were transfected with myc-TDP1, when probed with α -PARP1 antibody. The absence of a protein band in the lane which corresponds to the HEK 293 cells which were transfected with the myc empty vector (EV) suggests that the PARP1 band detected in the cells over-expressing TDP1 is specific. The anti-myc 9E10 antibody is also shown to be very specific, with an absence of detectable myc protein in the EV lanes. The myc EV plasmid is used as a control for the tag expressed on the TDP1 construct. The amount of material pulled down in the IP is comparable, as the IgG levels of the two IP sample lanes show a very similar level of IgG, however there is still an absence of PARP1 protein in the control sample. The results showed that there is a physical interaction between TDP1 and PARP1 and hence this IP led to using PARP1 as the positive control in all subsequent IP experiments.

4.3 NuMA physically interacts with TDP1

After the confirmation that the co-IP experimental protocol was working as hoped due to the TDP1 and PARP1 physical interaction detected, it was decided to implement the protocol to investigate whether NuMA and TDP1 physically interact. The initial approach to this IP was to overexpress both NuMA and TDP1 in the hope that we would see a physical interaction. This approach was employed as a literature search appeared to show that this particular interaction had not been investigated previously and hence increasing the chance to see an interaction via over-expression was the thought process. The other reason for the over-expression of both plasmids was that endogenous TDP1 levels are very low in normal physiological conditions. It was thought that working with extremely low levels of TDP1 might prevent us seeing an interaction, even if there was one present. This experimental procedure was facilitated by the purchase of a GFP-NuMA plasmid from Addgene (Plasmid no. 81209) and the utilisation of the myc-TDP1 plasmid used in the TDP1-PARP1 IP. The purchase of a GFP-tagged NuMA plasmid meant that an interaction could be determined by probing blots with a α -GFP antibody, due to the lack of a NuMA antibody at this time. Figure 4.3.1 shows the western blotting from this experiment.

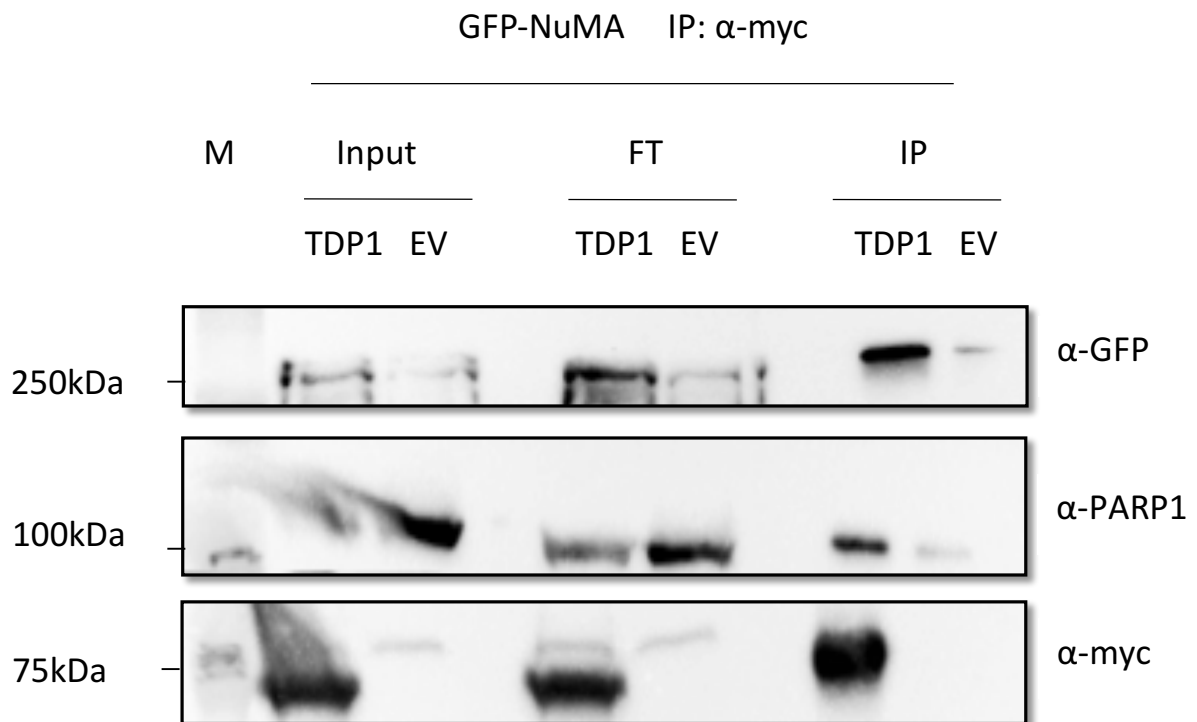


Figure 4.3.1. **NuMA physically interacts with TDP1.** HEK 293 cells were transfected with GFP-NuMA in combination with either myc-TDP1 (TDP1), or empty myc vector (EV, empty vector) for 48 hours before harvest. TDP1 was immunoprecipitated from whole cell extracts using myc antibody (mouse). Immunoprecipitated complexes were analysed by western immunoblotting using antibodies specific to GFP (rabbit), PARP1 (mouse) or c-myc (mouse). Inputs (5% of total lysate)-lanes 1,2; Flow through (FT)-lanes 3,4; myc-IP-lanes 5,6. Position of pre-stained molecular weight markers (kDa) is indicated (ladder). Protein sample analysis was carried out via SDS-PAGE, using a 6% polyacrylamide gel. Gel transferred to nitrocellulose membrane, using a Trans-Blot transfer system (Bio-Rad).

Figure 4.3.1 shows the western blot analysis following co-immunoprecipitation. The labelling of the blot shows that all cells (HEK 293) were co-transfected with GFP-NuMA and either myc-TDP1 or myc EV. The input lanes (5% of lysate) show that there is a good level of protein expression. There also appears to be a substantial amount of material in the flow-through lanes. This is an indication that there is a saturation of the protein G beads. This could be rectified by the addition of more beads in the co-IP, which would help to increase the binding of additional proteins. Confidence in the results can be taken due to the presence of a PARP1 band in the band which corresponds to GFP-NuMA and myc-TDP1 transfected cells. This confirms the TDP1-PARP1 interaction previously observed. There is also an absence of myc-TDP1 in the GFP-NuMA and myc-EV transfected cells, which shows that there is a high level of antibody specificity. There is a presence of both GFP and PARP1 bands in the GFP-NuMA-EV IP lanes. In the case of PARP1, this could point to a slight interaction of PARP1 with GFP-NuMA. It could however, be protein carry over from neighbouring wells; it has relative low intensity compared to the GFP-NuMA and myc-TDP1 IP lane. This could have occurred when loading the gel. This explanation is backed up by the presence of GFP in the GFP-NuMA-EV IP lane. The expectation was to see an absence of protein in this lane due to GFP-NuMA being targeted for pull down by α -myc and although the cells are expressing a myc-EV, there is no interacting protein to bind to. The blots ultimately show that there is a physical interaction between NuMA and TDP1.

An additional experiment performed was a co-IP with the over-expression of myc-TDP1 and either GFP-NuMA or a pEGFP-N1 empty vector. This would allow for the control of the GFP tagged NuMA plasmid, rather than controlling for the myc-tagged TDP1. Upon performing this experiment, there was an unexpected observation. Figure 4.3.2 shows the results.

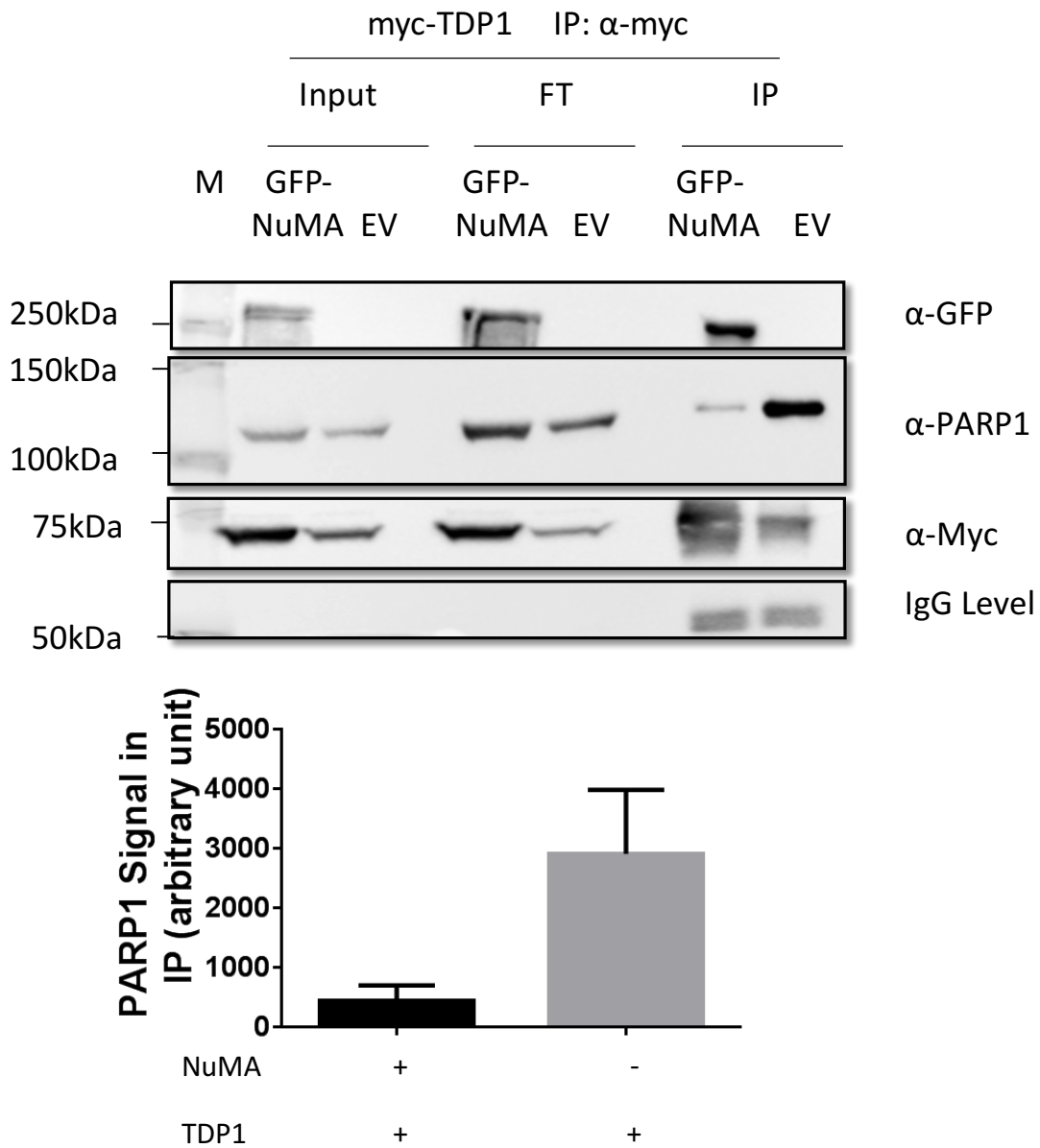


Figure 4.3.2. NuMA physically interacts with TDP1, but co-expression of NuMA and TDP1 depletes PARP1 levels. HEK 293 cells were transfected with myc-TDP1 in combination with either GFP-NuMA, or pEGFP-N1 (EV, empty GFP vector) for 48 hours before harvest. TDP1 was immunoprecipitated from whole cell extracts using myc antibody (mouse). Immunoprecipitated complexes were analysed by western immunoblotting using antibodies specific to GFP (rabbit), PARP1 (mouse) or c-myc (mouse). IgG level was used as a loading control. Inputs (5% of total lysate)-lanes 1,2; Flow through (FT)-lanes 3,4; myc-IP-lanes 5,6. Position of pre-stained molecular weight markers (kDa) is indicated (ladder). Protein sample analysis was carried out via SDS-PAGE, using a 6% polyacrylamide gel. Gel transferred to nitrocellulose membrane, using a Trans-Blot transfer system (Bio-Rad). Quantification represents relative densitometry performed on the band intensities of 5 biological repeats (n=5).

Figure 4.3.2 shows the western blot analysis following co-immunoprecipitation and subsequent band densitometry. a) further confirms the interaction between NuMA and TDP1, when both GFP NuMA and myc-TDP1 are over-expressed. As the cells (HEK 293) were all transfected with myc-TDP1 and either GFP-NuMA or pEGFP-N1 empty vector, it was expected that an interaction with PARP1 would be detected in both IP lanes. For this reason, there was a good level of satisfaction that the IP had worked effectively. It is noticeable that there appears to be a reduction in the pool of interacting PARP1. There is an obvious reduction in the amount of PARP1 present in the pulldown when both TDP1 and NuMA are over-expressed. It was unexpected that the interaction between PARP1 and TDP1 appeared to be significantly reduced when both GFP-NuMA and myc-TDP1 were simultaneously over-expressed. This led to the discussion of what could be causing this depletion in the amount of PARP1 being pulled down. It was originally thought that it was just an artefact of one experiment and that perhaps there had been an issue with the transfer of the gel or that there was an issue with the loading of samples. However, as there seemed to be if anything more myc-tagged TDP1 pulled down in the GFP-NuMA and myc-TDP1 IP lane, this explanation seemed unlikely. It was therefore decided to repeat the experiment. This observation was consistent across 5 independent biological replicates; figure 4.3.2 shows the relative densitometry performed on the band intensities from each of the 5 western blots. As this was an unexpected observation, the rationale behind this was of interest. As it appears that the simultaneous over-expression of NuMA and TDP1 suppresses TDP1 interaction with PARP1, a hypothesis was formulated. It was proposed that perhaps NuMA and PARP1 were competing for the same binding site on TDP1. Figure 4.3.3 shows the proposed TDP1 schematic.

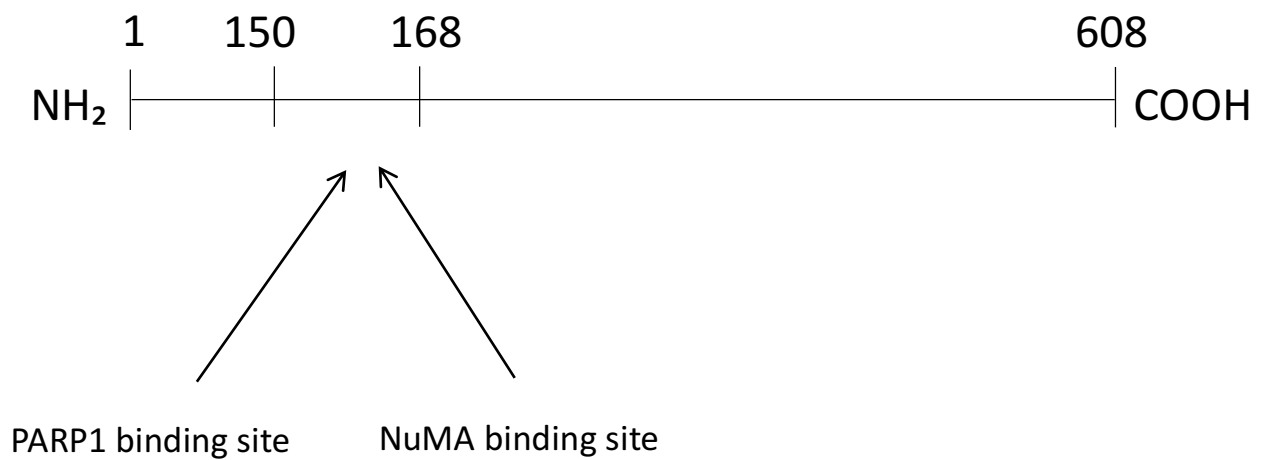


Figure 4.3.3. **Proposed model of PARP1 and NuMA binding to TDP1.** Schematic of TDP1 protein. It is hypothesised that NuMA and PARP1 are competing for the same binding site on TDP1, hence the reduction in levels of PARP1 when both TDP1 and NuMA are over-expressed. It is known that PARP1 binds to the N-terminal region of TDP1 (1-185) (Das, et al. 2014).

Figure 4.3.3. is schematic representation of the TDP1 protein. The arrows depict proposed binding sites of NuMA and PARP1 on TDP1. As data suggests, it is hypothesised that NuMA and PARP1 are competing for the same binding site. This was discussed as a potential explanation for the reduction in PARP1 level when both NuMA and TDP1 were overexpressed. As this was a novel, unexpected observation, further experiments were designed to help answer the question posed.

4.4 PARP1 and NuMA bind to different regions of TDP1

As the above model shows, the hypothesis was that NuMA and PARP1 were competing for the same binding site on TDP1. In order to investigate this hypothesis, truncations in the TDP1 protein were made. Discussions were held to decide which truncations to start with. Within the El-Khamisy lab, various truncations in TDP1 have been made previously. Truncated versions of TDP1 with both 1-150 amino acids only (C-terminal truncation) and 150-608 amino acids only have been made during other investigations into both SUMOylation of TDP1 and DNA Ligase III interactions and have been shown to express well in a mammalian cellular systems (Hudson, et al., 2012). As previously mentioned, PARP1 and TDP1 interaction has already been confirmed. Das et. al., showed that PARP1 binds to TDP1 within the N-terminal region, and that 1-185 amino acids was sufficient for this interaction. Careful consideration of the information led to the decision to utilise the truncated version of TDP1 expressing amino acids 150-608. This truncation had been previously used within the lab, and it had the appropriate myc-tag required for IP experiments using 9E10 myc antibody to pull interacting proteins down, so no further cloning was required. Another truncation that was also decided upon was a construct expressing the 168-608 region of TDP1. As the 1-185 amino acid stretch has been shown to be sufficient to bind PARP1, it was thought that trying to narrow down the binding region of PARP1 on TDP1 would be a good idea. It was decided that a truncated version of TDP1 expressing amino acids 168-608 would be a good starting point, as it was within the range of 150-185. The truncation was also made in the myc-tagged TDP1 plasmid. Truncations were made via the introduction of a start codon at the beginning of the desired truncation. This allowed for the open reading frame to not be disrupted and hence no frame shifts should occur during the cloning process. A traditional cloning method of PCR, restriction digest and ligation was adopted (see materials and methods;

section 2.2). Once truncations had been made, sequenced and checked for expression in HEK 293 cells, optimisation for the co-IP experiment began. It was quickly realised that using the same amount of cells as were used for the previous co-IP's would not be sufficient to look for interactions with NuMA and PARP1. This was partly due to the fact that the truncations were not expressed as well as the full length plasmids. To overcome this, a higher number of cells were plated in larger culture dishes. A greater amount of DNA was also transfected in to the cells. Figure 4.4.1 shows the initial western blotting.

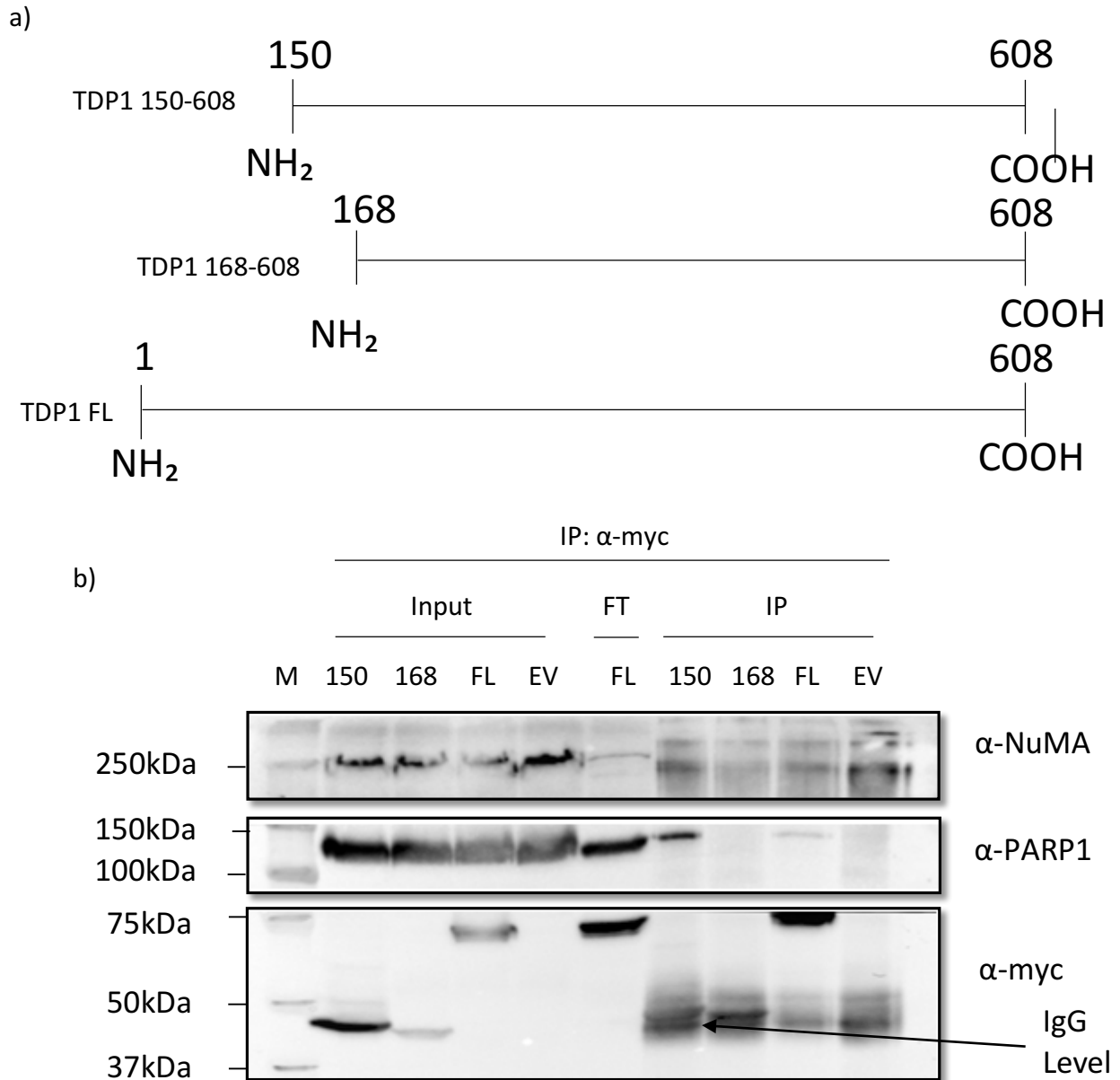


Figure 4.4.1 PARP1 and NuMA bind to different regions of TDP1. HEK 293 cells were transfected with either full-length myc-TDP1 (FL), myc-EV (EV) or truncated versions of the protein namely 150-608aa (158) and 168-608aa (168) for 48 hours before harvest. a) various truncations made within the TDP1 protein. b) TDP1 was immunoprecipitated from whole cell extracts using myc antibody (mouse) or IgG. Immunoprecipitated complexes were analysed by western immunoblotting using antibodies specific to human NuMA (rabbit), PARP1 (mouse) and c-myc (mouse). Inputs (5% of total lysate)-lanes 1-4; Flow through (FT)- lane 5; myc-IP-lanes 6-9. Position of pre-stained molecular weight markers (kDa) is indicated (ladder). Protein sample analysis was carried out via SDS-PAGE, using a 4-15% polyacrylamide gel (Bio-Rad). Gel transferred to nitrocellulose membrane, using a Trans-Blot transfer system (Bio-Rad).

Figure 4.4.1 a) shows the schematics of the truncated proteins, with figure 4.4.1 b) showing western blotting performed post co-IP experiment. Of note, this is an experiment which detects the endogenous levels of NuMA, as only the bait protein (myc-TDP1 truncation variants) was over-expressed for the purpose of the pull down. The α -myc blot inputs show the different sizes of the truncations (TDP1 150-608; ~ 50kDa, TDP1 168-608; ~48kDa, Full length; ~68kDa – N.B. myc-tagged TDP1 detected at around 75kDa). To note, there does appear to be a little less full length TDP1 in the inputs, which may explain why there are quite low levels of full length TDP1 protein detected in the IP samples probed with α -NuMA and α -PARP1.

The IP samples mirror the band positions detected in the whole cell lysates (inputs). This is however difficult to decipher for the two truncations, as the IgG heavy chain runs at around the same molecular weight. The EV control appears to have worked as there is no detection of a myc band in the IP lane (only IgG detected, as a result of the antibody bound to the beads). There is a band detected in the NuMA panel, as this corresponds to endogenous levels of NuMA. This level looks slightly higher than the other samples in the NuMA IP panel, however, there is a larger IgG band, suggesting there was perhaps a higher concentration of protein within this sample. One criticism of this result could be that the NuMA band seen is not specific to TDP1 interaction, as there is binding with myc-EV control. To eliminate any doubt, when repeating the experiment, an IgG bead control was adopted to ensure there is no non-specific binding. With reference to figure 4.4.1, there is no detection of a PARP1 band in the myc EV lane, which also indicates the IP has worked appropriately, as there is no TDP1 to interact with PARP1.

The PARP1 blot shows relatively equal levels of protein across samples in the inputs. However, in the IP lanes, it appears that the TDP1 168-608 stretch cannot bind to TDP1 and hence there is an absence of a protein band. The NuMA blot also appears to have a slightly reduced level of bound protein in the TDP1 168-608 IP lane. Although there seems to be a reduced level in the NuMA levels bound to TDP1 in this truncation, there appears to be lower expression levels of this truncation, compared to the TDP1 150-608 and full length constructs. Taking this into account, for future experiments it was decided to run the gel for a longer period of time to enable a better separation from the IgG heavy chains. It was also decided that an IgG control be adopted, to control for the specificity of

antibody binding. IgG is an antibody which lacks a myc recognition site; it is adopted as a negative control as will distinguish non-specific background from primary specific signals. In this case, the lysate would be from cells over-expressing full length myc-TDP1. The need of an IgG control for each of the truncations was deemed unnecessary. In attempt to overcome the TDP1 168-608 overexpression issue, many troubleshooting steps were undertaken, such as protein quantification in order to load exactly the same amount of protein (μg). Even when this step had been undertaken, there still seemed to be a reduction in expression in this truncation. It was decided to try to increase the cellular material used to create the whole cell extracts, in just this truncation. For this, 5 x the initial starting material was used, but cells were lysed in the same volume as other conditions, giving a 5 x concentrated cell lysate. The same amount of inputs (5%) and volume of lysate from each condition were added to the beads. Figure 4.4.2 shows the results.

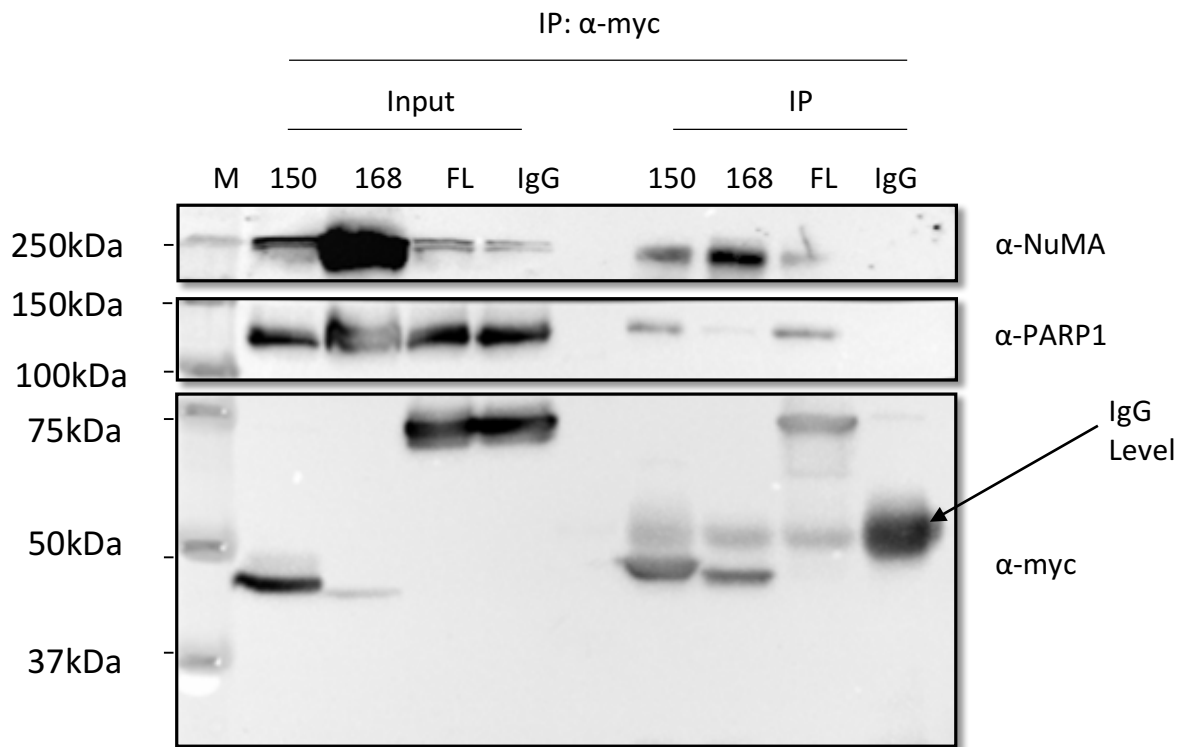
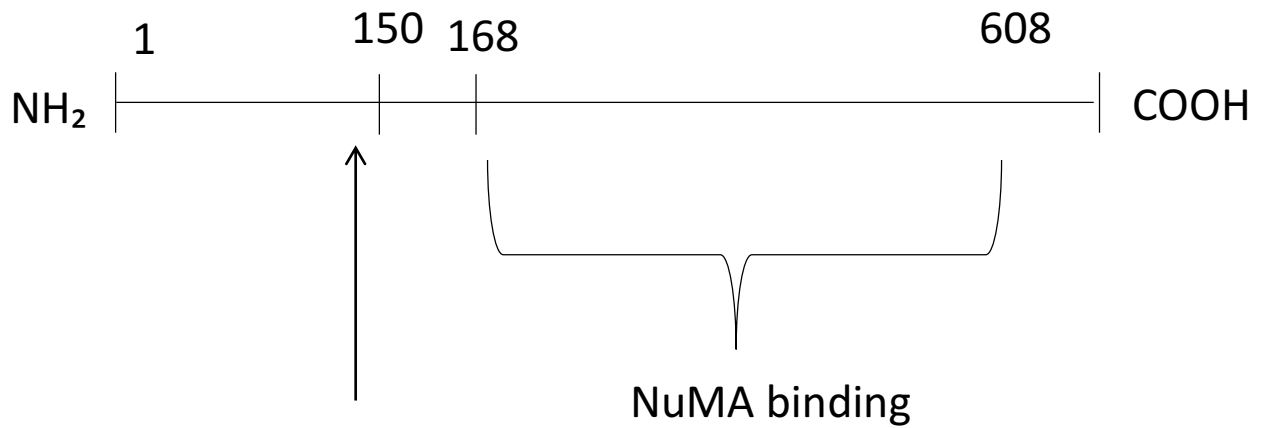


Figure 4.4.2 PARP1 and NuMA bind to different regions of TDP1. HEK 293 cells were transfected with either full-length myc-TDP1 (FL), truncated versions of the protein namely 150-608aa (158) and 168-608aa (168) or IgG bead control (FL lysate) for 48 hours before harvest. TDP1 was immunoprecipitated from whole cell extracts using myc antibody (mouse) or IgG. Immunoprecipitated complexes were analysed by western immunoblotting using antibodies specific to human NuMA (rabbit), PARP1 (mouse) and c-myc (mouse). Inputs (5% of total lysate)-lanes 1-4; myc-IP-lanes 6-9. Position of pre-stained molecular weight markers (kDa) is indicated (ladder). Protein sample analysis was carried out via SDS-PAGE, using a 4-15% polyacrylamide gel (Bio-Rad). Gel transferred to nitrocellulose membrane, using a Trans-Blot transfer system (Bio-Rad).

Figure 4.4.2 confirms the data shown in figure 4.4.1, with the main difference being that the myc-EV control has been replaced with an IgG bead control, in order to check that the interactions observed are specific. The gel was run for a longer period of time than previous repeats of this experiment to separate the IP samples of the truncations from the IgG level. Levels of protein within the IP lanes of the myc blot show there is a good amount of protein being pulled down in the IP. As expected, the IgG IP lane shows an increased level of IgG heavy chain compared to the other samples. Also, there is no interaction with PARP1 or NuMA, which shows the experiment is working as expected and in a specific manner. One thing to note is the increase in material put in to the TDP1 168-608 IP. Both the input and the IP samples were 5 x concentrated compared to that of the TDP1 150-608, full length TDP1 and full length TDP1 IgG control. This can be seen by the very high intensity band in the input lane of the NuMA blot. Notably, there is still a very low level of protein detected in the input lane of the myc blot in comparison to the other samples. The NuMA IP blot shows that both truncations appear to interact with TDP1. There is an increase in the band intensity in the band corresponding to the TDP1 168-608 pull down, however, this is to be expected as 5 x the material was used in this sample. In stark contrast, there appears to be a significant reduction in the band intensity in the same condition when probed with PARP1. Although it does not seem to be a complete abrogation of the band as seen in figure 4.4.1, however as mentioned there was 5 x the material used. Considering the data from figure 4.4.1 and 4.4.2, re-assessment of the initial model was required. A new proposed model was formulated, in which the amino acid stretch of 150-168 is sufficient for PARP1 binding to TDP1 and that NuMA binds somewhere downstream of this, in the C-terminal region. Figure 4.4.3 is visual representation of this.



PARP1 binding site

Figure 4.4.3. **Adapted proposed model of PARP1 and NuMA binding to TDP1.** Schematic of TDP1 protein. Following on from the data collected for the co-IP experiments, the proposed model has been adapted to encompass the findings that NuMA and PARP1 appear to bind to two independent regions of TDP1 and hence competition for the binding site is not taking place.

Figure 4.4.3 shows a schematic of the 608 amino acid structure of TDP1 depicting the N-terminal amine group and the C-terminal carboxylic acid group. The amino acids pointed out on the schematic were the amino acid residues of particular interest for creating truncations within the TDP1 protein. The experiments performed suggested that the 150-608 stretch of TDP1 allows the binding of PARP1 to TDP1, however the 168-608 section of TDP1 does not facilitate the binding of PARP1. This suggests that the 150-168 region of TDP1 is sufficient to bind PARP1. Contrary to the TDP1 168-608 region not allowing the binding of PARP1, this stretch of the protein is sufficient to bind NuMA and hence suggests that the binding site of NuMA on TDP1 is downstream of the PARP1 binding site, somewhere within the C-terminal region.

4.5 TDP1, PARP1 and NuMA are epistatic for the repair of SSBs

In the previous chapters, allusion to the epistatic nature of TDP1 and PARP1 in the repair of SSBs, in particular PDBs was made. Expanding on the results collected that NuMA is involved in the repair of SSBs and that a truncated form of TDP1 is not expressed particularly well, does not bind PARP1 and to some extent reduces the binding affinity of NuMA, it was thought that maybe NuMA is within the same repair pathway as TDP1 and PARP1. It is worth noting that the slightly more direct explanation for this is that NuMA interaction with TDP1 is PARylation dependent. It is already known that TDP1 is PARylated which increases the stability, and the results in 4.4.1 seem to suggest that if PARP1 binding is inhibited, a reduction in the amount of NuMA binding to TDP1 is observed. Results obtained from Dr Swagat Ray, of the El-Khamisy lab, has been able to confirm that TDP1 and NuMA interact in a PARylation dependent manner. Nevertheless, confirming TDP1, NuMA and PARP1 epistasis was a channel which was thought interesting enough to explore further. In order to test the hypothesis that NuMA, TDP1 and PARP1 were epistatic and hence functioned along the same pathway, working on the assumption that TDP1 and PARP1 were epistatic was paramount. The original strategy was to adopt 3 separate siRNAs, targeted to NuMA, TDP1 and PARP1. However, attempting to knockdown 3 different genes to halt protein expression was something which was deemed to be very difficult. This left the option of performing a double knockdown (both NuMA and TDP1) alongside single knockdowns of both TDP1 and NuMA. To achieve the knockdown desired, specific siRNA pools to both TDP1 and NuMA were utilised. The NuMA siRNA had already been optimised for the comet assay

experiments discussed in chapter 3. The TDP1 siRNA was optimised, which proved difficult due to the relatively low abundance of endogenous TDP1. This made ascertaining whether the siRNA had knocked down TDP1 challenging. The double knockdown condition used half the usual amount of siRNA for both TDP1 and NuMA, so the final concentration equalled 50nM, in line with the single knockdowns. A scrambled control was also adopted. Figure 4.5.1 shows the western blotting associated with the knockdown of both NuMA and TDP1.

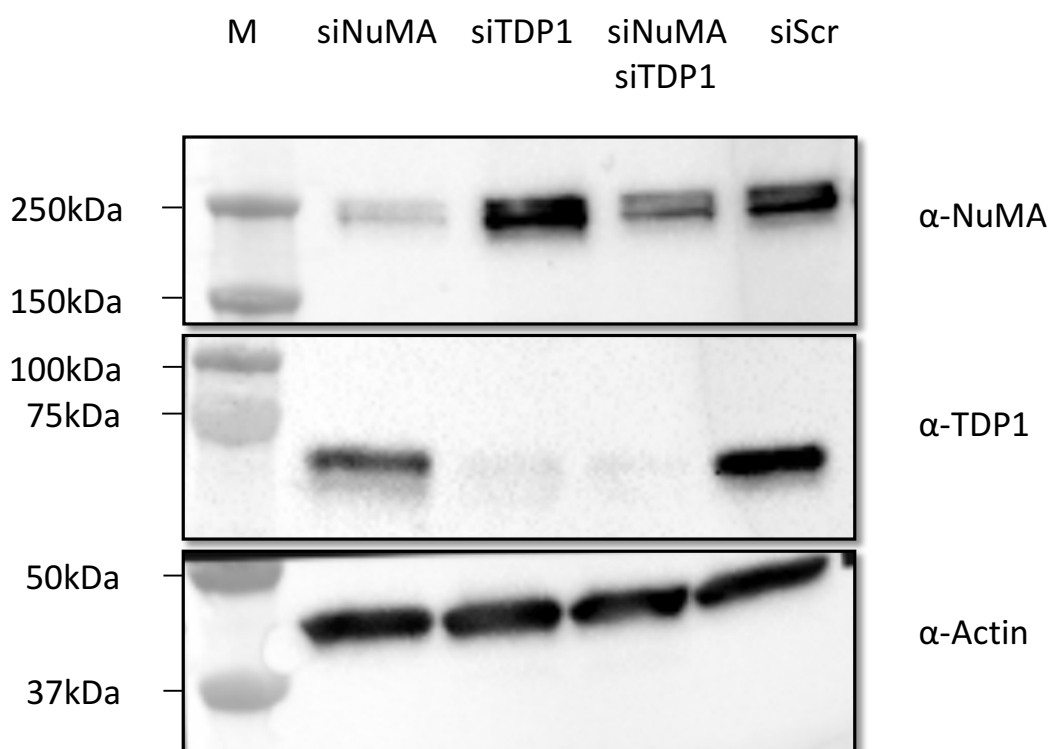


Figure 4.5.1. **Knockdown validation of NuMA, TDP1 and the simultaneous knockdown of NuMA and TDP1.** MRC5 cells were transfected with either siRNA specific to NuMA (siNuMA), to TDP1 (siTDP1), a combination of TDP1 and NuMA (siNuMA-siTDP1) or scrambled siRNA (siScr) (final concentration - 50nM) for 72 hours. Western Immunoblotting to confirm NuMA knockdown with siRNA transfection. Actin serves as loading control. Protein sample analysis was carried out via SDS-PAGE, using a 4-15% polyacrylamide gel (Bio-Rad). The gel was transferred to nitrocellulose membrane, using a Trans-Blot transfer system (Bio-Rad).

Figure 4.5.1 shows the western blotting produced to determine the representative level of knockdown of NuMA, TDP1 and both NuMA and TDP1 simultaneously, compared to normal endogenous levels of protein (scrambled control). The level of knockdown of NuMA is very similar to that shown in figure 3.2.1. The level of TDP1 also appears to be mostly reduced, with only a very small band detected in both the single TDP1 and the double TDP1 and NuMA knockdown conditions. The control siRNA does not seem to have any effect on the endogenous levels of NuMA, TDP1 and actin as expected. As there are equal levels of actin detected in each condition, the assumption can be made that the siRNA transfected in to the cells is acting specifically, with minimal (if any) off target effects. All the western blotting performed for the single and double knockdown set of experiments exhibited a similar reduction in the relevant protein otherwise results obtained were discounted. After optimisation had been completed, both CPT and H₂O₂ comet assays were performed. The experimental design was akin to the comet assay experiments performed in chapter 3. Figure 4.5.2 and figure 4.5.3 show the CPT and H₂O₂ comet data, respectively.

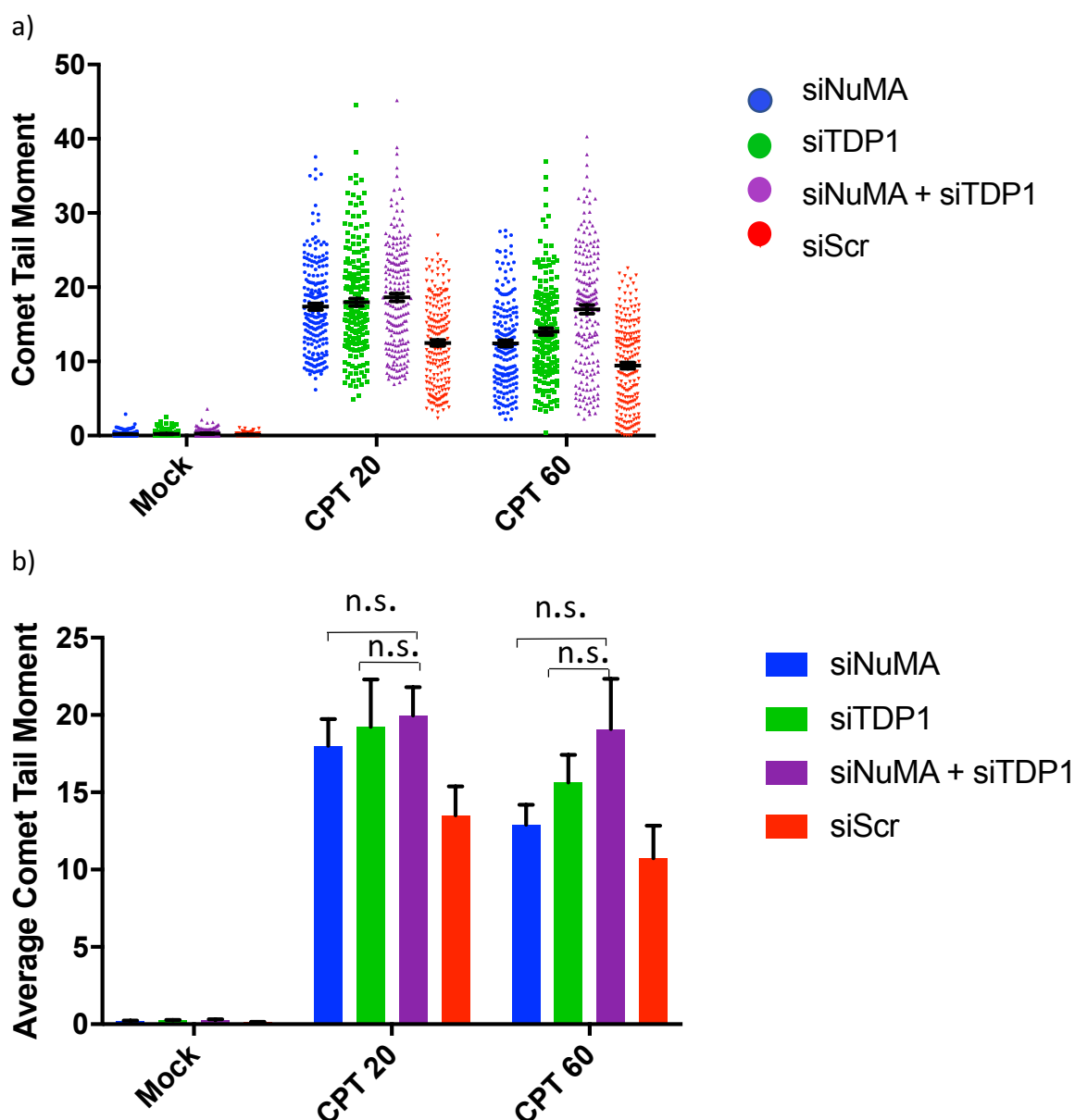


Figure 4.5.2. **NuMA and TDP1 are epistatic in the regulation of CPT-induced single strand breaks.** MRC5 cells were transfected with scrambled (siScr), NuMA (siNuMA) or TDP1 (siTDP1) siRNA (50nM) either individually or in combination for 72 hours. Cells were treated with CPT (50uM) for 20 and 60 minutes respectively before harvest. Alkaline comet assay was performed to assess DNA damage in single cells after gel electrophoresis. a) Representative scatter graph showing spread of comet tail moments from 200 scored nuclei in presence (red dots) or absence of NuMA (blue dots), TDP1 (green dots) or both (purple dots). b) The bars represent average comet tail moments after 20 minute and 60 minute of CPT treatment between cells either depleted of NuMA and TDP1 individually, or in combination. The error bars represent S.E.M from 4 biological repeats (n=4). n.s. = not significant (Student T-test). Some statistical asterices omitted to avoid confusion.

The experiment aimed to ascertain whether the dual knockdown of TDP1 and NuMA would result in a greater level of TOP1-linked PDBs compared to single knockdown alone. Figure 4.5.2 shows each individual data point scored across 4 biological replicates (200 total), represented as dots. The data represents 50 μ M CPT treated MRC5 cells. The scatter plot shows the data spread, with error bars representing the standard error of the mean. The scatter plot shows a very similar trend across the single and double knockdowns at both the 20 and 60 minute CPT treatments, with a slight reduction in the comet tail moment length after 60 minutes of CPT treatments. The single NuMA, TDP1 and double knockdown conditions all exhibit a similar spread of comet tail moments scored, with all these conditions registering larger comet tail moments compared to the scrambled control. Figure 4.5.2 b) shows the data from a) represented as a bar chart, with averages of the 150 data points calculated; error bars represent standard error of the mean. Referring to figure 4.5.2 b) it is slightly easier to see the trend with the data represented in bar chart form. There is a greater amount of DNA damage registered in TDP1 knockdown samples (both single and double knockdown) compared to that of NuMA knockdown alone and control. However, there is still a significant difference in the average comet tail length in the NuMA knockdown compared to control (CPT 20-minute $p=0.0014$), as was consistently presented in chapter 3. There are similar average comet tail moment levels in the single and double knockdown conditions after 20 minutes of CPT treatment, which do not exhibit statistical significance (siNuMA compared with siNuMA-TDP1; $p= 0.42$, siTDP1 compared with siNuMA-TDP1; $p= 0.66$). It is notable that there does appear to be less of a reduction in average comet tail moments at the 60-minute treatment time in the double knockdown condition compared to single knockdown and control. This however is not to a statistically significant extent (siNuMA compared with siNuMA-TDP1 CPT 60; $p= 0.088$, siTDP1 compared with siNuMA-TDP1 CPT 60; $p= 0.142$).

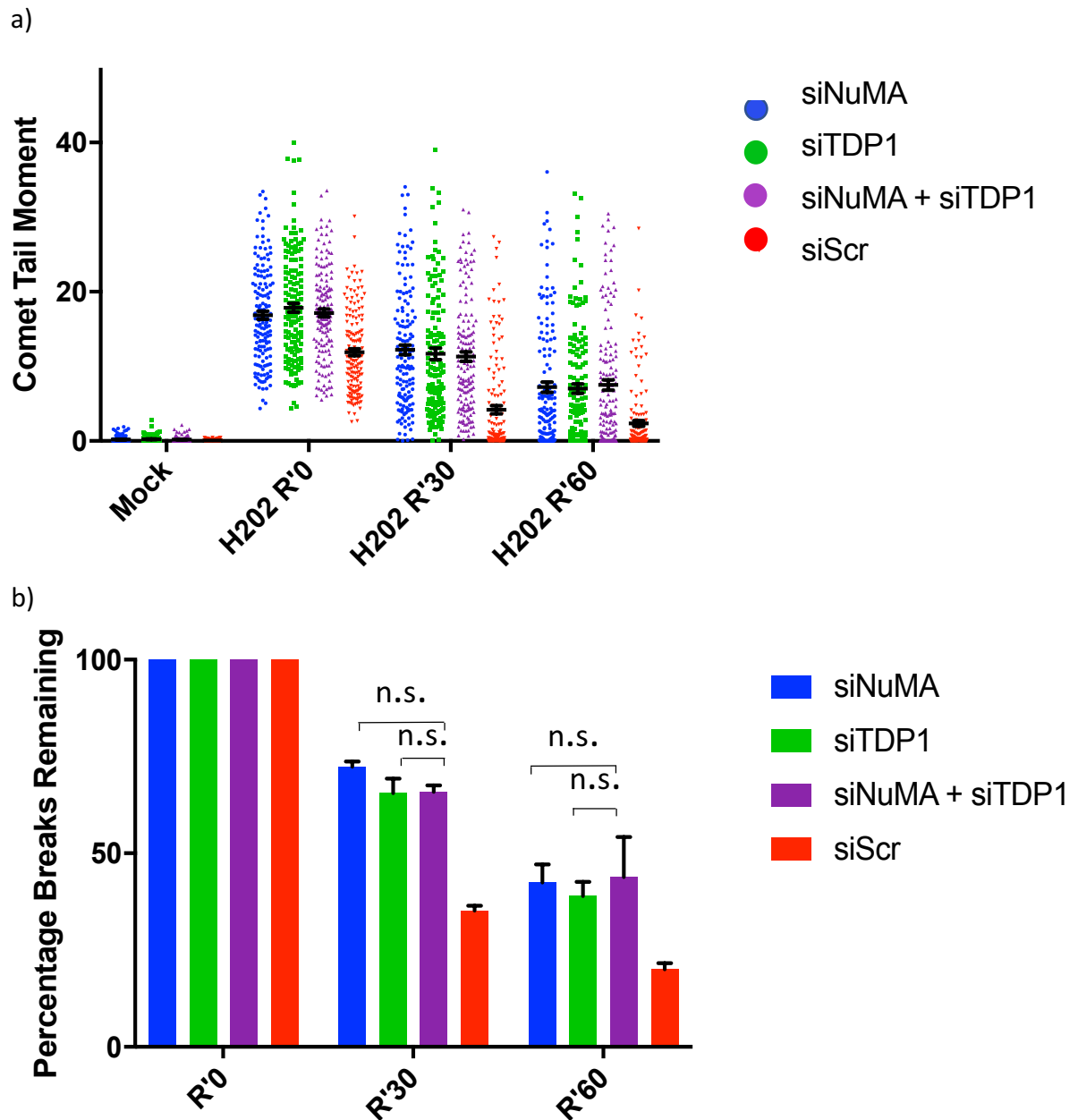


Figure 4.5.3. **NuMA and TDP1 are epistatic in the regulation of oxidative-induced single strand breaks.** MRC5 cells were transfected with scrambled (siScr), NuMA (siNuMA) or TDP1 (siTDP1) siRNA (50nM) either individually or in combination for 72 hours. Cells were treated with H₂O₂ (10μM) for 10 minutes on ice, followed by recovery at 37°C in complete medium for 30 or 60 minutes. Alkaline comet assay was performed to assess DNA damage in single cells after gel electrophoresis. a) Representative scatter graph showing spread of comet tail moments from 150 scored nuclei in presence (red dots) or absence of NuMA (blue dots), TDP1 (green dots) or both (purple dots). b) The bars represent percentage breaks remaining (as a measure of average comet tail moment) after removal of oxidative stress and recovery in complete medium between cells either depleted of NuMA and TDP1 individually, or in combination. The error bars represent S.E.M from 3 biological repeats (n=3). n.s. = not significant (Student T-test). Some statistical asterices omitted to avoid confusion.

The experiment aimed to ascertain whether the dual knockdown of TDP1 and NuMA would result in a greater level of oxidative-induced DNA damage compared to single knockdown alone. Figure 4.5.3 shows each individual data point scored across 3 biological replicates (150 total), represented as dots. The data represents 10 μ M H₂O₂ treated MRC5 cells. The scatter plot shows the spread of the data, with error bars representing the standard error of the mean. The mock treated cells in all transfected conditions exhibit a similar amount of damage, which is minimal. This is indicative of healthy cells and is reassuring that the knockdown of the genes isn't too detrimental to the cells health. The maximal damage point (R'0) shows that there is a comparable level of damage between the TDP1, NuMA and double knockdown condition, with generally smaller comet tail moments associated with the scrambled control. There is a reduction in comet tail moments across all conditions after 30 and 60-minutes recovery of the cells in media. Figure 4.5.3 b) shows data from a) represented as a repair kinetic bar graph. R'0 was taken as 100 from each condition. The repair kinetic graph shows that there is not much of a difference in the percentage of cells which are still damaged after 30 minutes recovery comparing the TDP1, NuMA and double knockdown condition. There is still however a significant difference between the percentage recovery of NuMA depleted and control cells (R'30; p= 0.013, R'60; p= 0.048). There is no statistical significance between the single and double knockdowns after 30 minutes of recovery (siNuMA compared with siNuMA-TDP1; p= 0.40, siTDP1 compared with siNuMA-TDP1; p= 0.72). At the R'60 time point, it appears the repair of cells with both NuMA and TDP1 depleted is slightly slower than that of the single knockdowns. This however is not to a statistically significant level (siNuMA compared with siNuMA-TDP1; p= 0.92, siTDP1 compared with siNuMA-TDP1; p= 0.80). Following on from these experiments, it was decided to test whether the epistasis trend exhibited under CPT and H₂O₂ treatments remained if transcription was stalled. This experiment was performed using the RNA Polymerase II inhibitor DRB to stall transcription (see chapter 3 for further information on DRB). Due to time constraints, the transcription-stalling experiments were only carried out in an oxidative damage setting, utilising H₂O₂ as the damaging agent (see figure 4.5.4).

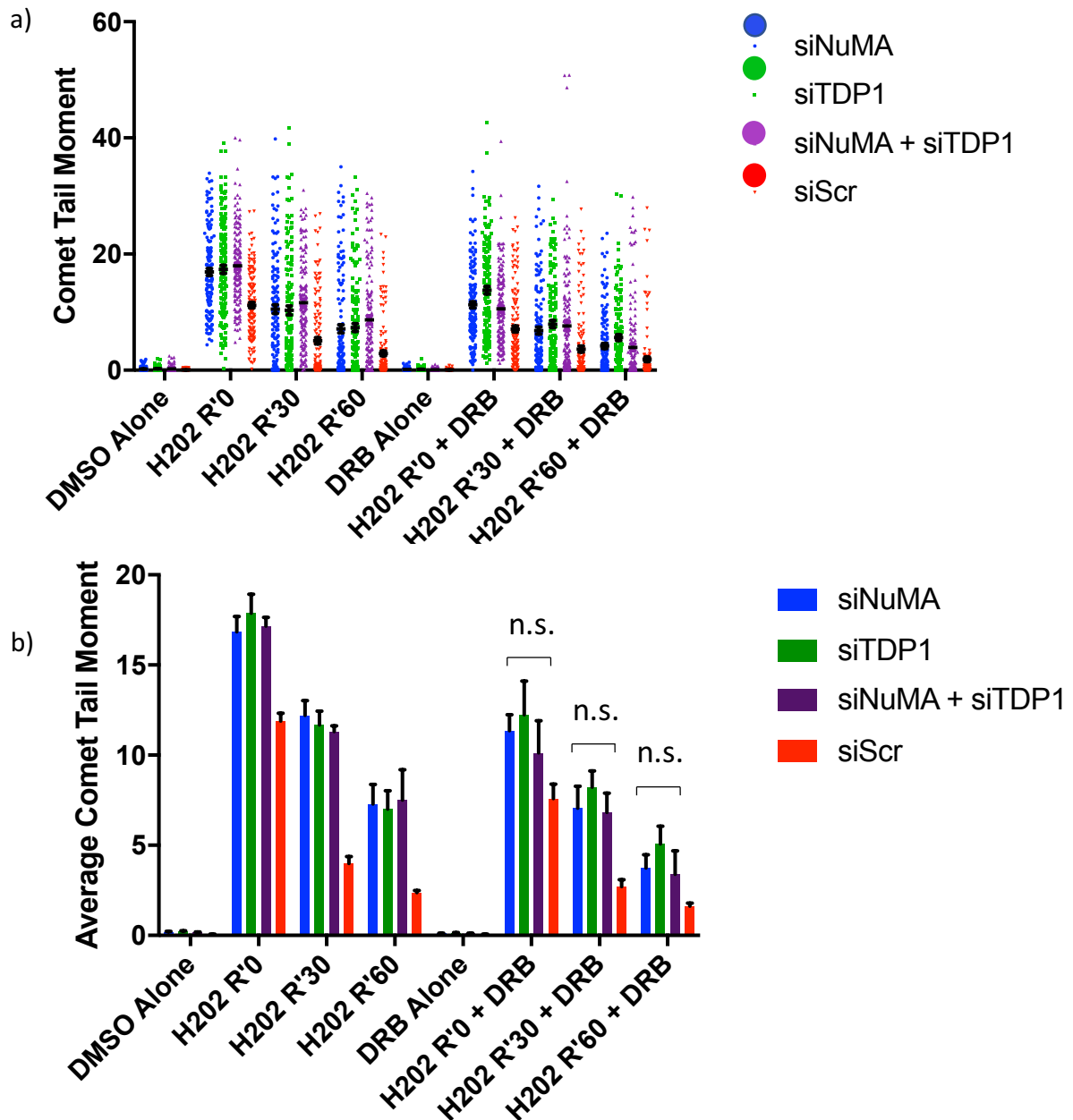


Figure 4.5.4 TDP1, NuMA and double knockdown results in the accumulation of oxidative stress-induced single strand breaks in a transcription dependent manner. MRC5 cells were transfected with scrambled (siScr), NuMA (siNuMA) or TDP1 (siTDP1) siRNA (50nM) either individually or in combination for 72 hours. Cells were pre-incubated with either mock (DMSO) or transcription inhibitor, DRB (10 μ M) for 2 hours, before treatment with H₂O₂ (10 μ M) for 10 minutes on ice. Cells were recovered at 37°C in complete medium for 30 and 60 minutes respectively. Alkaline comet assay was performed to assess DNA damage in single cells after gel electrophoresis. a) Representative scatter graph showing spread of comet tail moments from 150 scored nuclei in presence (red dots) or absence of NuMA (blue dots), TDP1 (green dots) or both (purple dots). b) The bars represent percentage breaks remaining (as a measure of average comet tail moment) after removal of oxidative stress and recovery in complete medium between cells either depleted of NuMA and TDP1 individually, or in combination. The error bars represent S.E.M from 3 biological repeats (n=3). n.s. = not significant (Student T-test). Some statistical asterices omitted to avoid confusion.

The experiment aimed to ascertain whether the dual knockdown of TDP1 and NuMA would result in a greater level of oxidative-induced DNA damage compared to single knockdown alone, and whether this damage accumulation was dependent on transcription. Figure 4.5.4 shows each individual data point scored across 3 biological replicates (150 total), represented as dots. The data represents DMSO or DRB pretreated MRC5 cells which were then treated with mock or 10 μ M H₂O₂. The scatter plot shows the spread of the data, with error bars representing the standard error of the mean. Referring to figure 4.5.4 a) the scatter plot shows a global reduction in the accumulation of SSBs after treatment with DRB (comparing right hand side of plot to left). As shown previously, without DRB treatment the comet tail moment length is similar between the single and double knockdowns which exhibits no significance between the single and double knockdown, with a significant amount less in the control (the p values for the samples not treated with have been previously stated). Figure 4.5.4 b) shows the data from a) represented as a repair kinetic bar chart. The DRB reduces the length of comet tail moments across all conditions, as expected. As was seen with the NuMA knockdown data shown in chapter 3, DRB pre-treatment results in a loss of statistical significance between the NuMA depleted cells and the control (R'30; p= 0.080, R'60; p= 0.10). There is also no significant difference between the single and double knockdowns, as expected (siNuMA compared with siNuMA-TDP1; R'30: p= 0.91, R'60: 0.063; siTDP1 compared with siNuMA-TDP1; R'30: p= 0.72, R'60: p= 0.45). Taking this data along with figures 4.5.2 and 4.5.3, it can be inferred that TDP1 and NuMA are epistatic for the repair of SSBs.

After the collection of the comet assay data with TDP1, NuMA and the simultaneous knockdown of both TDP1 and NuMA, it was felt that the finding of NuMA and TDP1 being epistatic in the repair of SSBs required further consolidation. To achieve this, the clonogenic survival assay was utilised (refer to materials and methods/chapter 3). The experimental set up was very similar to that of the comet assay, and the assay was performed with H₂O₂ as the damaging agent. Due to time constraints, full data sets of the clonogenic assay with CPT as the damaging agent were not completed. Figure 4.5.5 shows the data obtained.

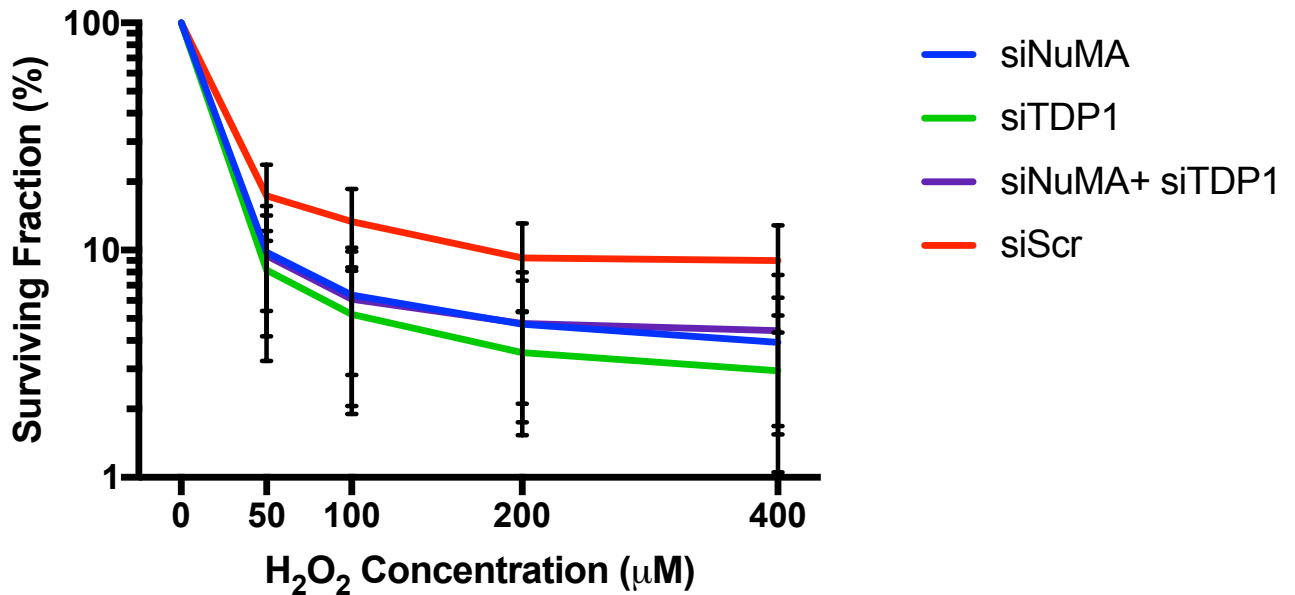


Figure 4.5.5. NuMA and TDP1 are epistatic in the regulation of oxidative-induced single strand breaks and results in a similar cell fate when compared to single knockdown alone. MRC5 cells were transfected with scrambled (siScr), NuMA (siNuMA) or TDP1 (siTDP1) siRNA (50nM) either individually or in combination for 72 hours. Cells were then re-plated on to 10cm dishes in varying cell concentrations and were left to adhere overnight. Cells were then treated with varying concentrations of H₂O₂ for 10 minutes on ice before washing with PBS. The medium was replaced and cells were left to form colonies for 10 days at 37°C. NuMA mediates cell survival. Log₁₀ scale graph showing the surviving cellular fractions following H₂O₂ treatment. The error bars represent S.E.M from 3 biological repeats (n=3). Statistical asterices omitted to avoid confusion.

The experiment aimed to ascertain whether the dual knockdown of TDP1 and NuMA would result in a greater level of cell death following oxidative-induced DNA damage compared to single knockdown alone. Figure 4.5.5 shows a line graph using a log₁₀ scale, detailing the percentage survival of cells which were transfected with specific siRNA to deplete levels of NuMA, TDP1 or NuMA and TDP1 simultaneously. Control cells were transfected with a scrambled siRNA sequence. Cells were then treated with varying concentrations of H₂O₂. The results are representative of 3 biological replicates (n=3). The results were analysed by taking plating densities and dividing by the appropriate factor to equal the same density as plated on the control plate. This allowed for accurate plating and similar numbers of colonies per plates to count. The graph shows that cells with depleted levels of NuMA, TDP1 and NuMA and TDP1 are more sensitive to H₂O₂ treatment and hence survive less well. The survival curve of the NuMA, TDP1 and NuMA and TDP1 depleted samples do not exhibit any statistical significance and hence this supports the hypothesis that NuMA and TDP1 are epistatic for the repair of SSBs.

Following on from these experiments, it was decided to further explore the potential epistasis between the proteins of interest. The approach was to adopt a PARP inhibitor, Olaparib. Olaparib has been shown to inhibit several members of the PARP family of enzymes, however studies have mostly focused on PARP1 inhibition (Knezevic, et al., 2016) (Nile, et al., 2016). Olaparib is an inhibitor of the catalytic activity of the PARP family and although does not physically deplete PARP1 itself, it eradicates the enzymatic activity. This occurs via the competition for the catalytic site of PARP1 with NAD⁺ (nicotinamide adenine dinucleotide), which is required for the PARylation activity of PARP1, leading to the recruitment of DNA damage repair proteins (Krishnakumar & Kraus, 2010; Murai, et al., 2014). This is a useful tool as it allowed for the exploration into the pathway with relative ease, as the treatment is relatively short. It was hypothesised that if TDP1, NuMA and PARP1 do indeed all work within the same repair pathway, then Olaparib treatment should not further sensitise cells which have TDP1 or NuMA depletion, when treated with a cytotoxic drug. In this preliminary experiment, it was decided to determine an Olaparib treatment concentration which would not cause major cell death. This was investigated using the clonogenic survival assay, using NuMA depleted cells and siScr controls. Figure 4.5.6. shows the results.

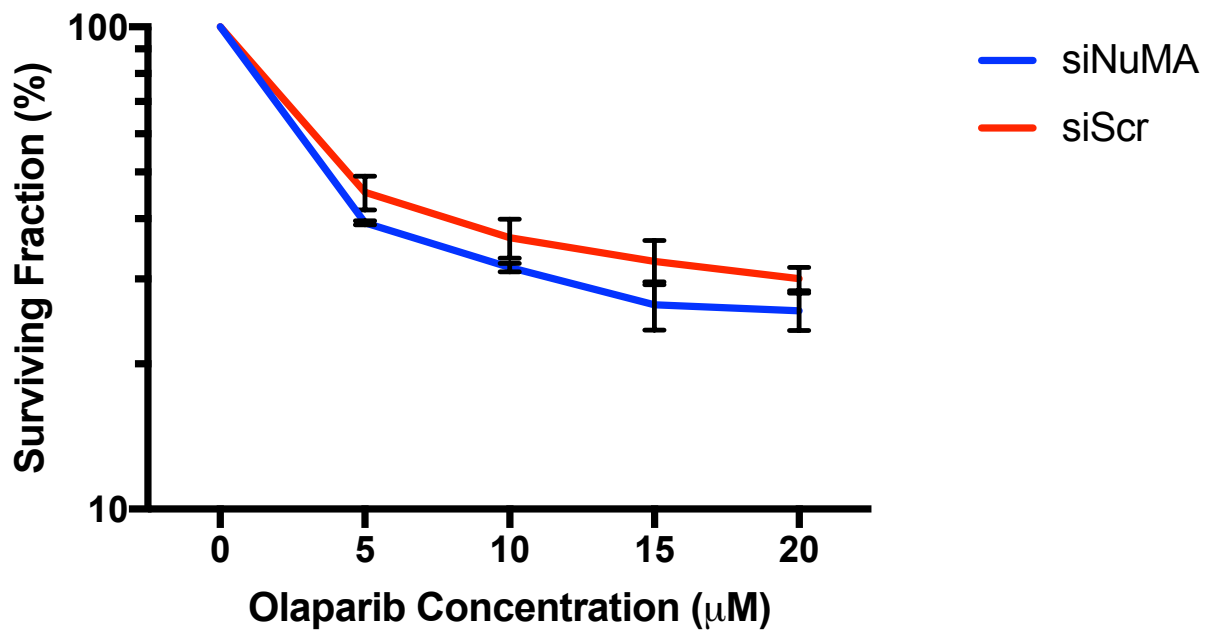


Figure 4.5.6. Olaparib treatment of NuMA depleted cells does not significantly increase cell death, compared to control cells. MRC5 cells were transfected with either scrambled (siScr) or NuMA (siNuMA) siRNA (50nM) for 72 hours. Cells were then replated on to 10cm dishes in varying cell concentrations and were left to adhere overnight. Cells were treated with varying concentrations of Olaparib in media overnight at 37°C. Plates were then washed thoroughly with PBS. The medium was replaced and cells were left to form colonies for 10 days at 37°C. Log10 scale graph showing the surviving cellular fractions following H₂O₂ treatment. The error bars represent S.E.M from 2 biological repeats (n=2).

Figure 4.5.6 shows a line graph using a log₁₀ scale, detailing the percentage survival of cells which were transfected with specific siRNA to deplete levels of NuMA, or a scrambled sequence as a control. Cells were then treated with varying concentrations of Olaparib. The results are representative of 2 biological replicates. The results were analysed by dividing plating densities by the appropriate factor to equal the same density as the control plates. This allowed for accurate cell plating and resulted in similar numbers of colonies per plates to count. The results of this preliminary experiment to determine an Olaparib treatment concentration which would not cause major cell death show that there is a slight increase in sensitivity to Olaparib in the cells which have reduced levels of NuMA. If there was more time, a concentration of Olaparib would have been selected to use in conjunction with H₂O₂ treatment in order to perform synthetic lethality studies. This data could support the hypothesis that NuMA and PARP1 act within the same pathways. With the previous data obtained and the knowledge that PARP1 and TDP1 are interacting partners, it would also suggest that TDP1 also works within the same pathway.

4.6 Discussion

This study set out to investigate whether any protein interactions existed between proteins involved in the DNA damaged response and NuMA. The findings in chapter 3, showed the discovery that the nuclear protein NuMA has a role in the accumulation of TOP1-linked and oxidative induced SSBs, additional to NuMA depleted cells exhibiting a repair defect when exposed to oxidative damage. Following on from these findings, it was decided to explore whether the DNA repair protein, TDP1, which is involved in the repair of stalled topoisomerase 1 complexes on DNA interacted with NuMA. Initial experiments were performed to determine whether NuMA and TDP1 interact *in vivo*. The technique adopted to assess the presence of an interaction was that of co-immunoprecipitation (co-IP). Simply, the co-IP protocol allows for the detection of protein-protein interactions by using a bait protein as the known protein in a complex, which binds to antibody incubated/conjugated beads in order to detect any other members of a protein complex (for further information see chapter 2). The initial probing experiment into the potential interaction between NuMA and TDP1 was that of a control experiment. This IP was performed in order to reproduce an already well-established interaction between TDP1

and PARP1. It is already known that TDP1 and PARP1 are epistatic for the repair of TOP1-linked DNA breaks and that TDP1 and PARP1 bind directly in order to do this (Das et al., 2014). It is also known that TDP1 is PARylated by PARP1; PARylation stabilises TDP1 together with the SUMOylation of TDP1 (Alagoz, et al., 2014; Ray Chaudhuri & Nussenzweig, 2017). The PARylation of TDP1 enhances its recruitment to the DNA damage sites without interfering with TDP1 catalytic activity. TDP1-PARP1 complexes in turn recruit XRCC1 (Pommier, et al., 2014). Referring to figure 4.2.1, the western blotting shows that there is a specific physiological interaction between TDP1 and PARP1. As mentioned, the purpose of this experiment was to confirm the interaction and to determine the conditions needed to enable the detection of an interaction. This would give more confidence in experiments designed to probe for novel interactions, as the experimental procedure had previously been optimised. As the interaction between PARP1 and TDP1 was established, the presence of this interaction in subsequent IP experiments was taken as the positive control. This would give assurance that the IP experiment had worked.

The next step was to test whether there was an interaction between NuMA and TDP1. Figure 4.3.1 shows that when both a GFP-tagged NuMA plasmid and a myc-tagged TDP1 plasmid are over-expressed in a mammalian cellular system, there is a physical interaction between the two proteins. The initial reason for the over-expression of both proteins is that there are very low levels of endogenous TDP1 in cells which have only a basal level of stress. As TDP1 is recruited in response to TOP1-stalled DNA complexes which only occur if they become trapped by endogenous or exogenous stress, relative abundance is low. It was thought that if there are low endogenous levels of TDP1 then a potential interaction with NuMA may be quite difficult to detect. If there wasn't an interaction detected then it could be due to this fact rather than due to there being an absent protein complex. This was also the reason for the initial over-expression of NuMA. As NuMA was a relatively new protein of interest, expression levels in various cell types were unknown and overexpression aimed to prevent a false negative result due to low expression levels. Whilst performing these experiments it was decided that as there were two plasmids being overexpressed, each with different tags, that extra controls might need to be included. This gave IP experiments which utilised a myc empty vector (EV) plasmid as the control. These IPs allowed for both myc-TDP1 and GFP-NuMA to be

simultaneously overexpressed with the controls only overexpressing GFP-NuMA and a myc-EV. The second set of IP experiments used GFP-EV as the control. This second condition of using a GFP-EV as the control plasmid allowed for both myc-TDP1 and GFP-NuMA to be overexpressed, with just myc-TDP1 and GFP-EV as the comparative control. Referring to figure 4.3.2, it was encouraging that the interaction had been confirmed whilst employing a different control. However, it was not expected that the interaction between PARP1 and TDP1 appeared to be significantly reduced when both GFP-NuMA and myc-TDP1 were simultaneously over-expressed. This led to the discussion of what could be causing this depletion in the amount of PARP1 being pulled down. It was originally thought that it was just an artefact of one experiment and that perhaps there had been an issue with the transfer of the gel or that there was an issue with the loading of samples. However, as there seemed to be if anything more myc-tagged TDP1 pulled down in the GFP-NuMA and myc-TDP1 IP lane, this explanation seemed unlikely. It was therefore decided to repeat the experiment. This observation was consistent across 5 independent biological replicates and figure 4.3.2 b) shows the relative densitometry performed on the band intensities from each of the 5 western blots. As this was an unexpected observation, the reason for this was of interest. As it appears that the simultaneous over-expression of NuMA and TDP1 suppresses TDP1 interaction with PARP1, the mechanism behind this was of great interest and hence was the next line of investigation.

The hypothesis suggested to explain the reduction in the amount of PARP1 detected in the TDP1 pulldown when both NuMA and TDP1 were overexpressed was due to competition. It was proposed that PARP1 and NuMA were competing for the same binding site on TDP1 (see figure 4.3.3 for schematic). It was thought that as NuMA is a very large structural protein that maybe it was causing a scaffold-like block to the PARP1 binding site and hence a reduction of PARP1 was observed in the IP lane. In order to investigate this hypothesis, it was decided to make truncations in the TDP1 protein. The truncations were a key tool in mapping the binding sites of both NuMA and PARP1 on TDP1. Once the truncations had been made, and expression tested, the IP experiments were carried out. Referring to figure 4.4.1, the preliminary figure suggests that 168-608 TDP1 truncation is unable to bind to PARP1. There is also a slight reduction in the NuMA binding affinity in this truncation, as can be seen by a reduction in band intensity. Notably,

the 168-608 stretch of TDP1 appears to express less well than the 150-608 region and the full length TDP1. As to an explanation for this, it might be that losing slightly more of the N-terminal region of TDP1 accounts for a reduction in expression. Another explanation could be that as the 168-608 truncation seems to not bind PARP1, and it is known that PARP1 and the PARylation of TDP1 helps stabilise the protein, that perhaps the loss of this interaction reduces the stability of TDP1 and hence the reduction in expression (Ray Chaudhuri & Nussenzweig, 2017). In an attempt to overcome the poor expression of the 168-608 stretch of TDP1, it was finally decided to bulk up the starting material of this truncation. With reference to figure 4.4.2, the results are very similar to those obtained in figure 4.4.1. It is obvious that in the NuMA and PARP1 blots there is significantly more material in the 168-608 input lane. There is however significantly less in the Myc blot. Even though the starting material for this truncation was increased 5-fold compared to the other truncations, there still appears to be a very low level of expression. With comparison to figure 4.4.1, there does appear to be a slight band in the PARP1 IP lane corresponding to the 168-608 region of TDP1. As mentioned, the material in this IP was increased 5-fold. This could account for the very slight band observed. Another explanation could be that there was a slight overspill from one lane to another, accounting for the very slight band observed. Taking both results into account, it was decided that confidence was high enough to refute the original hypothesis that PARP1 and NuMA were competing for the same binding site. A new model was proposed, which suggested that the respective binding domains of NuMA and PARP1 on TDP1 were distinct from each other, with PARP1 binding somewhere within the 150-168 region and NuMA binds downstream of this, within the C-terminal region of TDP1. If there were more time available, further truncations within TDP1 would have been made in order to narrow the binding of NuMA to TDP1 to a much more specific area than the generalisation of 168-608. It would have also been a nice experiment to further investigate the PARP1 binding to TDP1 residues. As mentioned in chapter 3, glutamic acid residues are the main acceptors of PAR chains and hence they are a main site of PARylation. It is hypothesised that PARP1 binds to the glutamic residue at amino acid position 150. The alteration of the protein by site directed mutagenesis (SDM) of this putative site could have helped pinpoint the interaction site to one residue, as hopefully the mutation would have prevented the binding of PARP1 to TDP1.

Following on from the finding that TDP1 and NuMA physically interact, and that PARP1 and NuMA bind to independent regions of TDP1, further investigations to the role of TDP1 and NuMA were begun. It was hypothesised that NuMA and TDP1 may function within the same pathway. In order to test this hypothesis, siRNA was once again utilised. The hope was that if TDP1 and NuMA levels were simultaneously depleted, that a significant increase in the amount of DNA damage or an exacerbated repair defect would not be observed. The siRNA specific to NuMA had already been optimised for use in previous experiments (see chapter 3), however the TDP1 siRNA did require optimisation. The main issue which arose with the knockdown of TDP1 was the relative abundance of endogenous TDP1 in MRC5 cells. Under normal physiological conditions the TDP1 level is low, as TDP1 is required for the repair of TOP1-stalled complexes on DNA. Once the antibody concentration had been optimised and an ideal concentration of protein was determined, the experiments could begin. The western blotting shown in figure 4.5.1 gives confidence that the siRNAs are working as expected, as in the corresponding lanes of NuMA, TDP1 and the double knockdown of NuMA and TDP1 there are observable reductions in the protein level, compared to the scrambled control. The actin levels are all equal which is a good indicator that the reduction in the NuMA and TDP1 protein bands aren't due to less protein being loaded. This western blotting was used as the standard level of knockdown. For all experiments, the protein levels were checked after siRNA treatment and if they were not to a parallel level as in 4.5.1, results were discounted.

Figure 4.5.2 a) and b) shows the spread of comet tail moments and the average comet tail moments yielded from cells which have had NuMA and TDP1 levels depleted, both independently and simultaneously. It is noticeable that there does appear to be slightly more breaks at both 20 and 60 minutes of CPT treatment when both TDP1 and NuMA levels are depleted. It is also notable that the length of comet tail moment does not reduce as much as the single knockdowns, or the control. However, both of these observations did not pose too much worry that the hypothesis may be incorrect as they were not statistically significant compared to TDP1 and NuMA knockdown alone. Due to the siNuMA and siScr data sets exhibiting statistical significance as previously shown in chapter 3, it was deemed that the experiment had worked satisfactorily. An explanation to the slightly greater length of comet tail moments observed could be that as two

different genes are being targeted, cells may be slightly healthier as two proteins are being downregulated, compared to just one. The conclusion drawn from the CPT data is that the dual knockdown of TDP1 and NuMA does not significantly increase the accumulation of PDBs.

After using CPT as the damaging agent, it was decided to perform the same experiment using H₂O₂ to induce specific SSBs. This is in keeping with previous experiments detailed in chapter 3. Figure 4.5.3 a) represents the spread of each individual comet tail moment scored, and figure 4.5.3 b) shows the repair kinetic profile associated with 30 and 60 minutes of cell recovery. The data shows that there are similar comet tail lengths scored at the peak damage point, before the cells have been allowed to recover (R'0). This means that the double knockdown of TDP1 and NuMA after H₂O₂ does not induce a greater amount of DNA damage, which supports the hypothesis. The R'30 and R'60 time points also exhibit similar spreads of comet tail moment length. With reference to b) there appears to be slightly more breaks remaining in the NuMA depleted cells compared to the other conditions after 30 minutes of recovery. After 60 minutes, there was a reduction in the percentage of breaks remaining as expected, although there are slightly more persisting in the double knockdown condition. This however is not to a significant extent. As with the CPT data, the greater amount of breaks remaining in the TDP1 and NuMA depleted cells were not significantly greater than that of the NuMA or TDP1 alone knockdowns. The percentage breaks remaining in the NuMA knockdown were significantly greater than the control, which mirrors the data shown in chapter 3. This supports the hypothesis proposed.

Next, it was decided that the effect of transcription-stalling would also be assessed. For this experiment, DRB was adopted as the agent to stall transcription (see chapter 3). Due to time restrictions, the damaging agent of choice for this experiment was H₂O₂. If there was more available time, the experiment would have also been performed with CPT as the damaging agent. Figure 4.5.4 a) and b) show the samples which are not treated with DRB (left hand side) and the samples pre-treated with DRB (right hand side). As expected, the average length of comet tail moment was reduced following DRB treatment. One striking observation is that after DRB treatment, although there is a general reduction in average comet tail moment and more efficient repair taking place, there appears to be

slightly more breaks remaining in the TDP1 depleted cells. This could be due to the key role TDP1 plays in the repair of SSBs. It is hard to explain as to why the same profile is not seen with the simultaneous TDP1 and NuMA knockdown, especially as the western blotting shown in figure 4.5.1 shows a similar level of TDP1 depletion. As this set of experiments were only performed 3 times, perhaps if a wider pool of cells had been examined then the repair kinetic profile might have been slightly different. It is also important to note that the treating of cells with H₂O₂ is well known for its variability and hence this may have also played a role. This being said, the slight increase in the comet tail length and the slightly greater impaired repair kinetics compared to the other conditions is still not of statistical significance. Collectively, the data shown in figures 4.5.1, 4.5.2 and 4.5.3 point to the epistatic nature of TDP1 and NuMA. This can be inferred due to the double knockdown failing to produce significantly greater comet tail moments or exhibit a further impaired repair defect, compared to the single knockdowns alone. The conclusion drawn from the analysis of this data is that NuMA, TDP1 and therefore PARP1 are all within the same repair pathway and should demonstrate epistasis.

Following on from these findings, clonogenic survival assays were carried out. As with the DRB experiments, the damaging agent of choice was H₂O₂. The clonogenics were set up as described in chapter 2. Figure 4.5.5 shows the survival curve of the four conditions (siNuMA, siTDP1, siNuMA-TDP1 and siScr) where cells were treated with a high dose of H₂O₂ for 10 minutes on ice, before being left to form colonies in complete media, at 37°C for 10 days. It can be seen that all of the 3 knockdown conditions are more sensitive to H₂O₂ treatment. This is due to an element of the DNA SSB repair pathway being inhibited. However, there is not a greater sensitivity to H₂O₂ when both NuMA and TDP1 are simultaneously depleted, hence supporting the theory that NuMA and TDP1 are epistatic for the repair of SSBs. It is of note that the TDP1 alone knockdown yields the poorest survival, however this is not to a significant extent when compared with the NuMA and NuMA/TDP1 double knockdown results. The control condition and the NuMA knockdown is statistically significant, as previously shown in chapter 3.

The previous data discussed has pointed to the epistasis of NuMA, PARP1 and TDP1. This was further explored by the utilisation of the PARP inhibitor Olaparib. Olaparib gained excitement surrounding the potential of PARP inhibition, due to the increased selectivity

of targeting PARP1 (Nile, et al., 2016). The clonogenic experimental design was detailed in chapter 2. Figure 4.5.6 shows the survival curve of cells transfected with siRNA targeted to NuMA, or with a scrambled control. After siRNA incubations, cells were replated onto 10cm cell culture dishes and left to adhere before the addition of varying concentrations of Olaparib overnight at 37°C. Olaparib was removed and cells were left to form colonies for 10 days. The results of this preliminary experiment to determine an Olaparib treatment concentration which would not cause major cell death show that there is a slight increase in sensitivity to Olaparib in the cells which have reduced levels of NuMA. Another approach could have been to utilise siRNA. This however would have needed to be optimised and dual or even triple gene silencing within cells may not be tolerated especially well. If there was more time, a concentration of Olaparib would have been selected to use in conjunction with H₂O₂ treatment in order to perform synthetic lethality studies. Due to the TDP1 association with PARP1 and the findings that TDP1 physically interacts with NuMA, the same approach could have been used to observed synthetic lethality under a TDP1 knockdown setting. This would further consolidate the results found.

After the accumulation of further evidence to suggest NuMA has a role within the DNA damage response, it was decided to delve deeper into the structure of NuMA and the involvement of the many domains of NuMA. These studies into the protein structure allowed for the knowledge of NuMA, its structure and its function to be further elucidated in the setting of SSBR.

Chapter 5

Functional Analysis of NuMA Variants

5.1 Introduction

NuMA has been studied extensively over the past 30 years in the context of its role in the spatio-temporal arrangement of microtubules. However, in the setting of DNA damage and/or repair, along with other potential roles for the protein, limited research has been carried out. As previously described, NuMA is a very large structure of 2115 amino acids which contains many different domains, including a central coiled-coiled domain surrounded by two globular domains at the N and C termini (Kotak, et al., 2014). NuMA also contains a nuclear localisation signal (NLS) and a microtubule binding domain (MBD) both located in the C terminal region. When characterisation studies of NuMA were first undertaken (results shown in Chapter 4), potential interacting partners of NuMA were investigated. The first point of call was TDP1 and chapter 4 shows the data obtained discovering that NuMA and TDP1 physically interact. After ascertaining that NuMA and TDP1 do indeed physically interact *in vivo*, via over-expression of both TDP1 and NuMA, it was decided to try only over expressing the TDP1 and working with endogenous NuMA levels. As experiments progressed, investigations into NuMA became much more detailed and it was discovered that there was more than one isoform of NuMA. Indeed, there are many isoforms, but there seemed to be two main variants. After looking into the purchased plasmid from Addgene (Plasmid no. 81209), it was determined (by myself) that the plasmid was the short isoform as the 14 amino acid stretch present in the long isoform was missing amino acid residues 1536-1549. It was published in 2016 that there was an alternate splicing event that occurred at exon 16 which meant that there were different expression profiles (Ding, et al., 2016). In order to look at the long isoform, the 14 amino acid stretch was synthetically produced by IDT before being inserted in to the plasmid via Gibson Assembly.

As mentioned previously, NuMA is an abundant protein and has 2 detectable bands on routine western blots. These bands are not 100% defined as long and short isoform, however this seems to be the most appropriate explanation for the observed doublet. Members of the lab attempted to analyse both bands independently via mass

spectrometry. It was hoped to find that the lower band lacked the 14 amino acid stretch included in the long isoform, however due to many difficulties this could not be confirmed. There is a small chance that the occurrence of the doublet was due to a degradation event. However, great care is taken to keep all protein samples on ice, which is additional to protease inhibitors being routinely included in the lysis buffer, hence a degradation event is doubtful; although it is still possible that a post-translational modification is occurring.

5.2 Long isoform complementation rescues the NuMA depletion associated repair defect

Initial experiments with the long and short isoform were carried out by overexpressing both isoforms. However, this was overexpression additional to the endogenous levels of NuMA present in the cells. Figure 5.2.1 shows the representative levels of the long isoform and the short isoform.

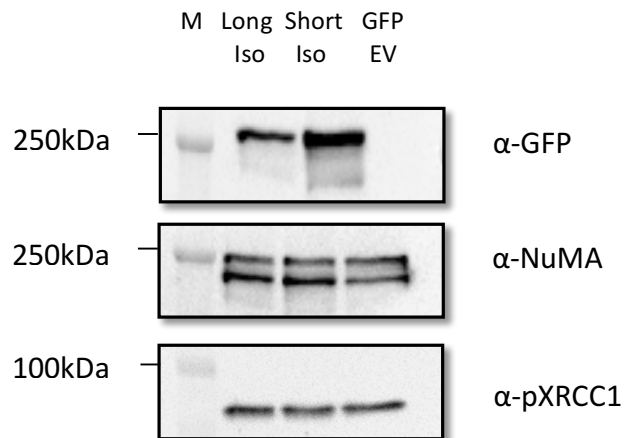


Figure 5.2.1 **The long isoform of NuMA is expressed to a lesser extent than the short isoform of NuMA.** MRC5 cells were transfected with either the long isoform of NuMA plasmid (long iso), short isoform of NuMA plasmid (short iso) or GFP-empty vector (EV) plasmid and incubated for 48 hours. Western Immunoblotting to show relative overexpression of both the short and long isoform of NuMA. phospho-XRCC1 serves as loading control. Protein sample analysis was carried out via SDS-PAGE, using 6% gel (hand poured). The gel was transferred to nitrocellulose membrane, using a Trans-Blot transfer system (Bio-Rad).

Figure 5.2.1 shows the representative level of overexpression of the long and short isoforms of NuMA, as seen in the GFP blot. The NuMA blot shows the levels of endogenous NuMA within the cells, and shows that the GFP antibody is specific due to the absence of a band in the GFP-EV lane. Phospho-XRCC1 was used as a loading control, showing equal protein levels between each sample. In order to study the specific role of each of the isoforms it was decided to make both the long and short isoforms of NuMA resistant to the siRNA. To do this effectively, each of the 4 siRNAs used in the pool were screened to ascertain which siRNA yielded the most effective knockdown. This strategy was adopted as it would be a lot of work to mutate each of the 4 distinct targeting sequences within the plasmid if one sequence provided a knockdown to a similar level to that of the pooled siRNAs. It was ascertained that sequence one provided the best knockdown and hence this sequence was chosen to make the mutations. To make a plasmid targeting resistant, silent mutations were made in the plasmid so that the coding of the protein did not change, but the plasmid would not be targeted for degradation by the siRNA. The siRNA would not target the protein for degradation as the siRNA was no longer specific to the targeted region. As the genetic code is degenerate, there only needed to be one base change in each of the codons in the targeting stretch, which allowed the protein code to be maintained and also gave a higher chance of the site directed mutagenesis (SDM) PCR working. Once the plasmid was constructed with the targeting resistant stretch, the same SDM was performed on the short isoform plasmid. This enabled the overexpression of the isoforms independently, without the plasmids being targeted for degradation by siRNA, whilst knocking down the endogenous level of NuMA. This had to be optimised once again as previous experiments had either independently overexpressed a plasmid or knocked down a protein. The optimisation involved finding a way to knockdown NuMA and overexpress the plasmid at the same time, with minimum cellular toxicity. It was also important to ensure that the siRNA was transfected twice, as previously optimised. It was finally decided that the best solution to this issue was to transfect siRNA (reagent – Dharmafect) 24 hours after plating cells, transfect DNA (reagent – GeneJuice) after 48 hours and re-transfect the siRNA after 72 hours, to be incubated for a further 24 hours before performing any experiments. This allowed for selective overexpression of the isoforms. As previously shown, depletion of NuMA results in a greater amount of initial TOP-1 linked PDBs when cells were treated with CPT, and for a significant repair defect when treated with H₂O₂, after recovery. It was thought that if it was possible to selectively

over-express both isoforms independently, that a rescue phenotype might be observed. The ideal hypothesis was that a rescue phenotype may only be exhibited by one of the isoforms, hence providing a separation of function between the two sequences. Figure 5.2.2 shows the expression profile observed.

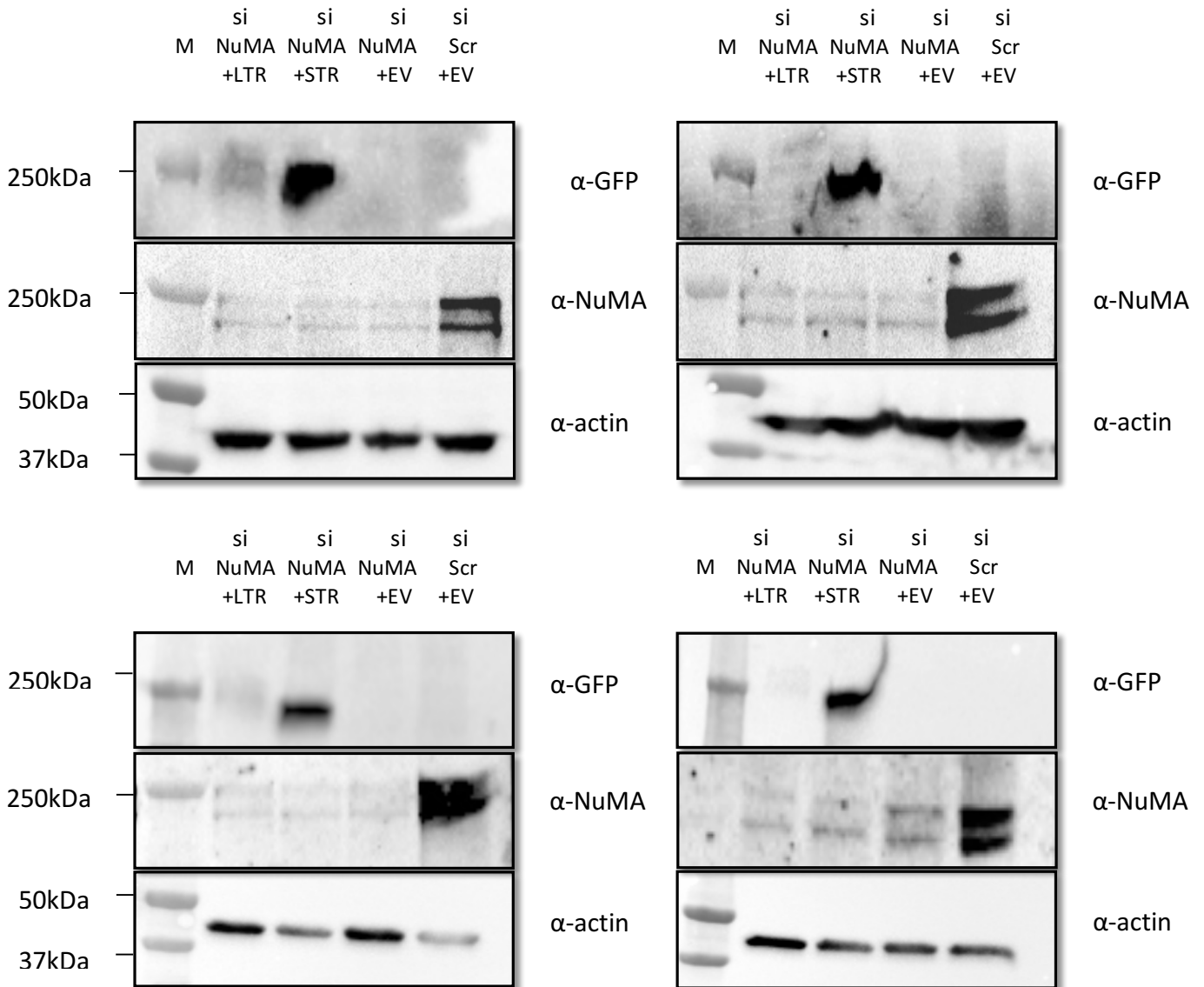


Figure 5.2.2 The **Long isoform of NuMA is expressed significantly less than the short isoform of NuMA when endogenous levels of NuMA are reduced**. MRC5 cells were transfected with specific siRNA to NuMA (siNuMA), or a scrambled control (siScr) and incubated for 24 hours. Cells were then transfected with either a long isoform (targeting resistant) plasmid (LTR), short isoform (targeting resistant) plasmid (STR) or GFP-empty vector (EV) plasmid and incubated for a further 24 hours. Cells were re-transfected with siRNA and left to incubate for a final 24 hours. Western Immunoblotting to show relative overexpression of both the short and long isoform of NuMA when endogenous levels of NuMA are reduced. Actin serves as loading control. Protein sample analysis was carried out via SDS-PAGE, using a 6% poly-acrylamide gel (hand poured). Gels were transferred to nitrocellulose membrane, using a Trans-Blot transfer system (Bio-Rad).

Figure 5.2.2 shows the expression levels of the long isoform with targeting resistance (LTR) and the short isoform with targeting resistance (STR) with NuMA depletion. The western blotting also shows two EV controls, one with NuMA depleted and one without. The above figure shows the western blotting from 4 independent experiments. It is evident that there appears to be consistently less LTR expressed in the MRC5 cells. This is an unexpected observation as the protein samples were quantified before loading. This is believed to be a true level of protein expression as the actin levels seem to be relatively even across the blots. Blots c) and d) could be seen to have slightly off-loading, however the reduced actin level seems to correlate to the STR over-expression which is still greater. Although the expression of the LTR seems to be lower than the STR, it was decided to perform alkaline comet assays on the cells in order to determine whether the LTR or STR selective over-expression can rescue the repair defect associated with NuMA depletion. The damaging agent of choice was H₂O₂. Figure 5.2.3 shows the data obtained.

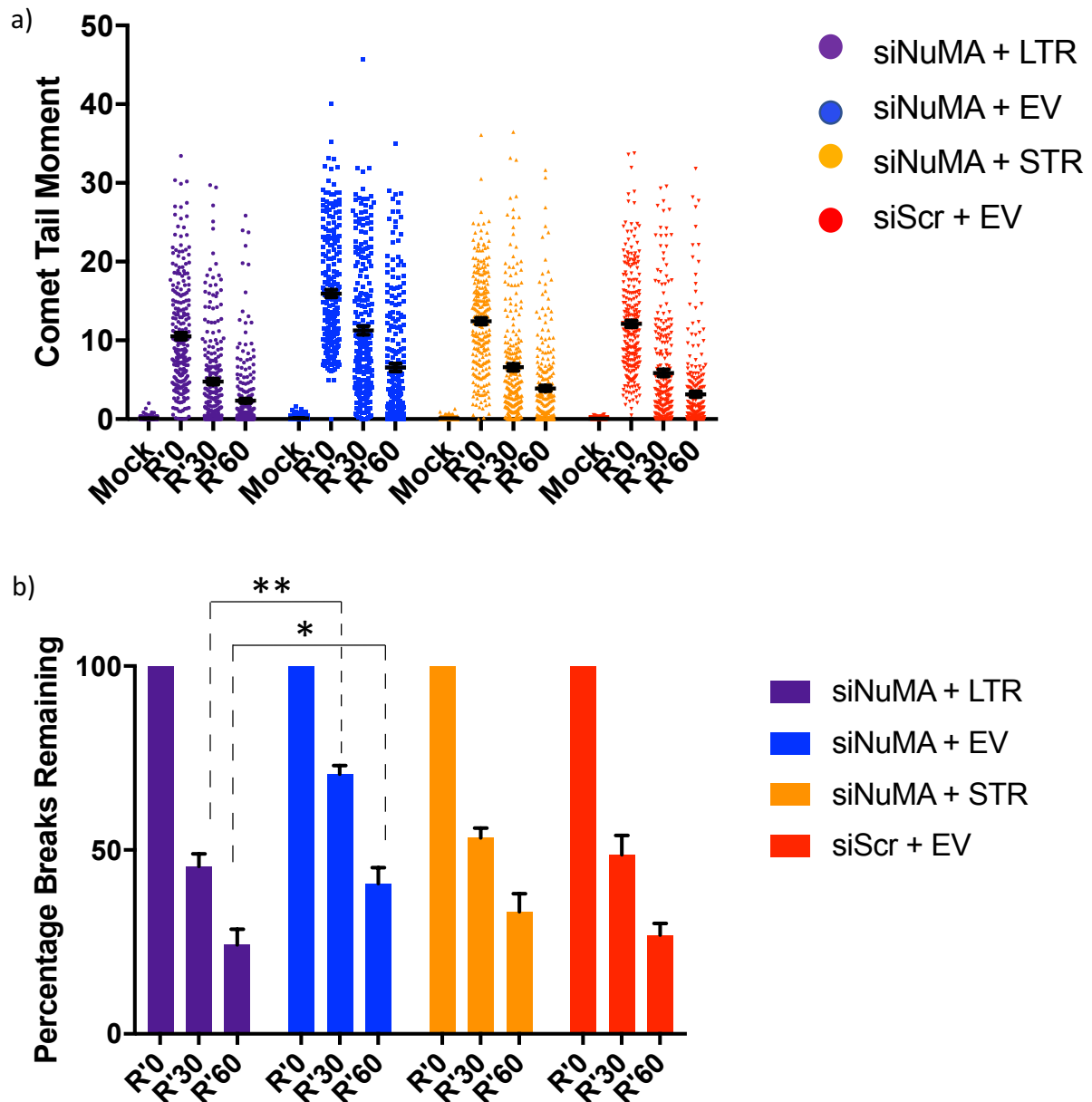


Figure 5.2.3. LTR rescues the repair defect associated with NuMA depletion to a greater extent than STR, despite being less well expressed. MRC5 cells were transfected with specific siRNA to NuMA, or a scrambled (Scr) control and left to incubate for 24 hours. Cells were then transfected with either a long isoform (targeting resistant) plasmid (LTR), short isoform (targeting resistant) plasmid (STR) or GFP-empty vector (EV) plasmid and incubated for a further 48 hours. Cells were treated with H₂O₂ (10μM) for 10 minutes on ice, followed by recovery at 37°C in complete medium for 30 or 60 minutes. Alkaline comet assay was performed to assess DNA damage in single cells after gel electrophoresis. a) Representative scatter graph showing spread of comet tail moments from 250 scored nuclei with overexpression of LTR (purple dots), overexpression of STR (yellow/orange dots), or in the presence (red dots) or absence (blue dots) of NuMA. b) The bars represent percentage breaks remaining (as a measure of average comet tail moment) after removal of oxidative stress and recovery in complete medium between cells with overexpressed LTR/STR and the presence/absence of NuMA. The error bars represent S.E.M from 5 biological repeats (n=5). * = 0.05, ** = 0.005 (Student T-test).

Figure 5.2.3 a) shows each scored comet, across 5 biological replicates (250 total). The cell populations were treated with 10 μ M H₂O₂. The scatter plots shows that the spread of comet tail moment lengths between the siNuMA + LTR, siNuMA + STR and siScr + EV complementation conditions are very similar, with the siNuMA + LTR yielding the lowest comet tail moments. The siNuMA + EV condition exhibits the largest comet tail moments, as expected. Figure 5.2.3 b) shows the representation of the data shown in a) as a repair kinetic bar chart. To note, in line with previous experiments, the siNuMA + EV and the siScr + EV conditions show a statistically significant difference (R'30; p= 0.039, R'60; p= 0.042). The siNuMA + LTR, siNuMA + STR and siScr + EV conditions have very similar repair kinetic profiles, with the siNuMA + LTR rescuing the repair defect more effectively than the STR, with only the R'30 time point in the STR over-expression exhibiting statistical significance, compared to the LTR which is significant at both (siNuMA + LTR compared to siNuMA + EV: R'30; p= 0.0029, R'60; p= 0.025, siNuMA + STR compared to siNuMA + EV: R'30; p= 0.016, R'60; p= 0.796). This is despite the evidence from figure 5.2.2 which suggests that the LTR is poorly expressed in the MRC5 cells when NuMA levels are depleted. This however does not allow for a claim that the LTR specifically rescues the repair defect associated with NuMA depletion. Notably, the repair kinetic graph suggests that there are fewer breaks remaining in the siNuMA + LTR condition than the siScr + EV (indicative of the endogenous levels of NuMA).

After the findings obtained from the comet assay experiments, it was decided to perform a similar experiment, with the output being the clonogenic survival assay. The experimental design opted for the same conditions as adopted for the comet assays and hence there was an expectation to see a similar trend; that the LTR and to some extent the STR is protective against oxidative-induced damage/more efficient in repairing oxidative-induced SSBs. Figure 5.2.4 shows the results obtained.

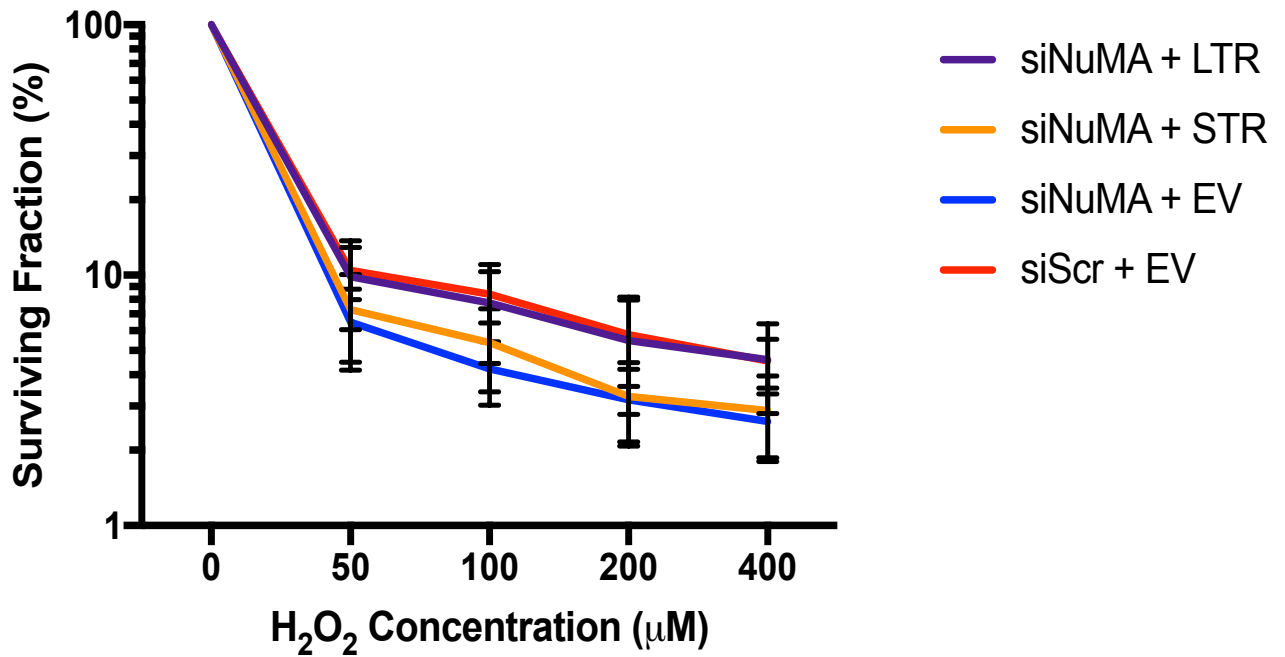
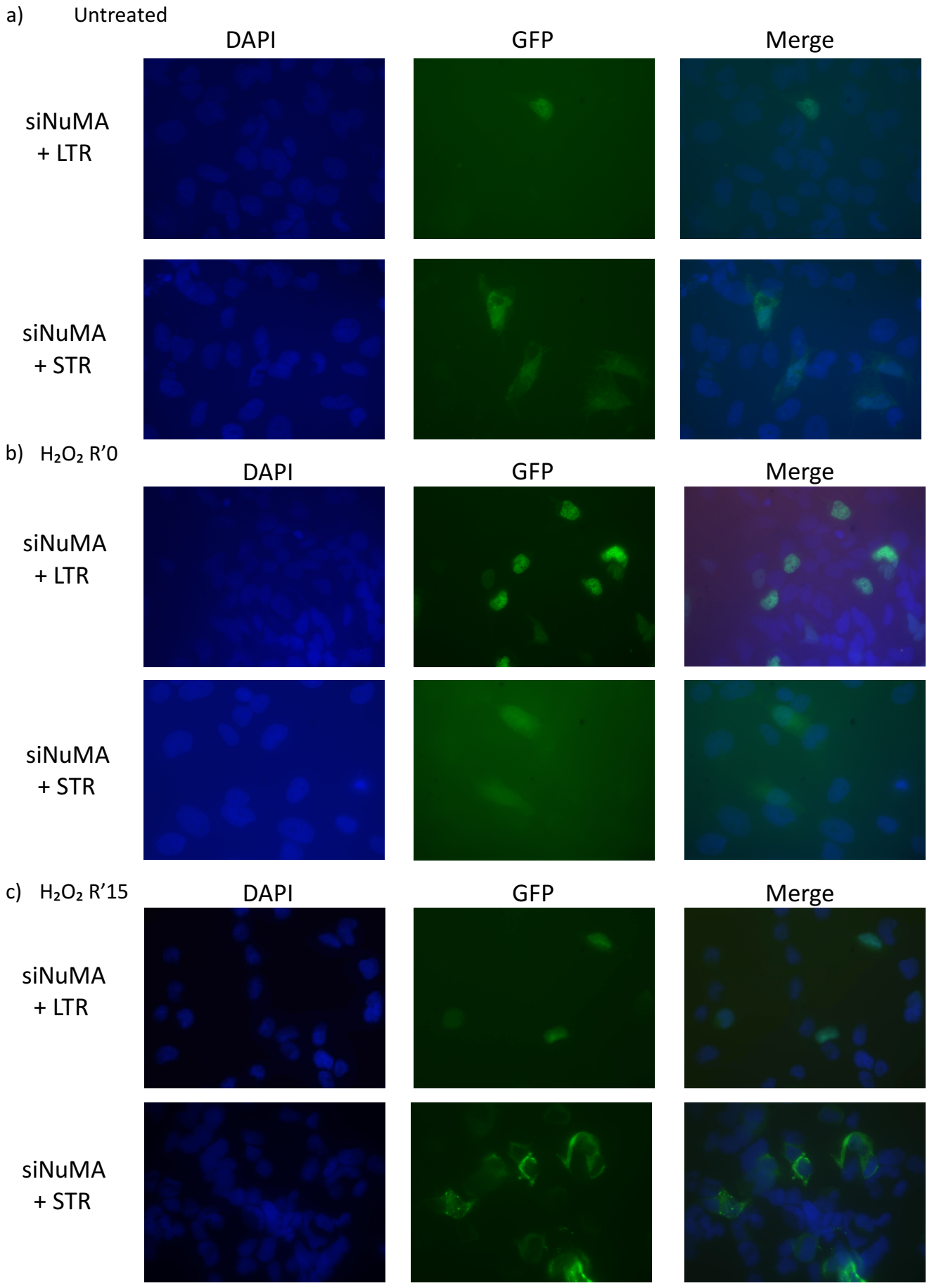


Figure 5.2.4. **Complementation with the long isoform of NuMA (LTR) rescues the repair defect associated with NuMA depletion.** MRC5 cells were transfected with specific siRNA to NuMA, or a scrambled (Scr) control and left to incubate for 24 hours. Cells were then transfected with either a long isoform (targeting resistant) plasmid (LTR), short isoform (targeting resistant) plasmid (STR) or GFP-empty vector (EV) plasmid and incubated for a further 48 hours. Cells were then treated with varying concentrations of H₂O₂ for 10 minutes on ice before washing with PBS. The medium was replaced and cells were left to form colonies for 10 days at 37°C. Log₁₀ scale graph showing the surviving cellular fractions following H₂O₂ treatment. The error bars represent S.E.M from 3 biological repeats (n=3). Statistical asterices omitted to avoid confusion.

The experiment aimed to ascertain whether the selective overexpression of the long isoform of NuMA (LTR) or the short isoform of NuMA (STR) would result in a rescue of the repair defect associated with the depletion of NuMA following oxidative-induced DNA damage. Figure 5.2.4 shows a line graph using a log₁₀ scale, detailing the percentage of surviving cells after treatment with varying concentrations of H₂O₂. The results are representative of 3 biological replicates (n=3). The results were analysed by taking plating densities and dividing by the appropriate factor to equal the same density as plated on the control plates. The graph shows that the condition which specifically overexpresses siNuMA + LTR rescues the repair defect exhibited in the siNuMA + EV condition. The extent of the rescue is almost parallel to that of the control condition (siScr + EV). The overexpression of the short isoform (siNuMA + STR) does have a certain element of rescue, with the cellular survival levels being slightly greater than that of the siNuMA depletion condition (siNuMA + EV). There is a statistical significance between the siNuMA + LTR and the siNuMA EV conditions, with all but one of the measured concentrations of H₂O₂ exhibiting statistical significance (50µM; p= 0.013, 100µM; p= 0.028, 200µM; p= 0.121, 400µM; p= 0.0295). There is however only statistical significance between the 100uM H₂O₂ concentration when comparing the siNuMA + STR and siNuMA + EV conditions (50µM; p= 0.236, 100µM; p= 0.037, 200µM; p= 0.911, 400µM; p= 0.623). To note, there is no statistical significance between the siNuMA + LTR and the siScr + EV conditions (50µM; p= 0.191, 100µM; p= 0.181, 200µM; p= 0.591, 400µM; p= 0.711). These results support the findings of the comet assay and in fact strengthen the case for the long isoform of NuMA playing a more important role in the repair of oxidative SSBs than the short isoform.

Following on from the comet assay and the clonogenic survival assay data attained, it was decided to investigate the independent isoforms further, by utilising fluorescence studies. Cells complemented with long and short isoforms (LTR and STR), which have depleted levels of NuMA were plated on to coverslips (see chapter 2). As the constructs are GFP tagged, this allowed for the visualisation of the cells under a fluorescence microscope, without having to stain with antibodies, which minimised the risk of poor staining. This allowed for the evaluation of transfection efficiency. The coverslips were mounted on to slides with a mounting medium which contained an optimised concentration of DAPI. This allowed for the determination of where the nucleus lies within the cell, and whether

either the long isoform or the short isoform localise within the nucleus. Representative images are shown in figure 5.2.5. Quantification of the fluorescence studies are shown in figure 5.2.6.



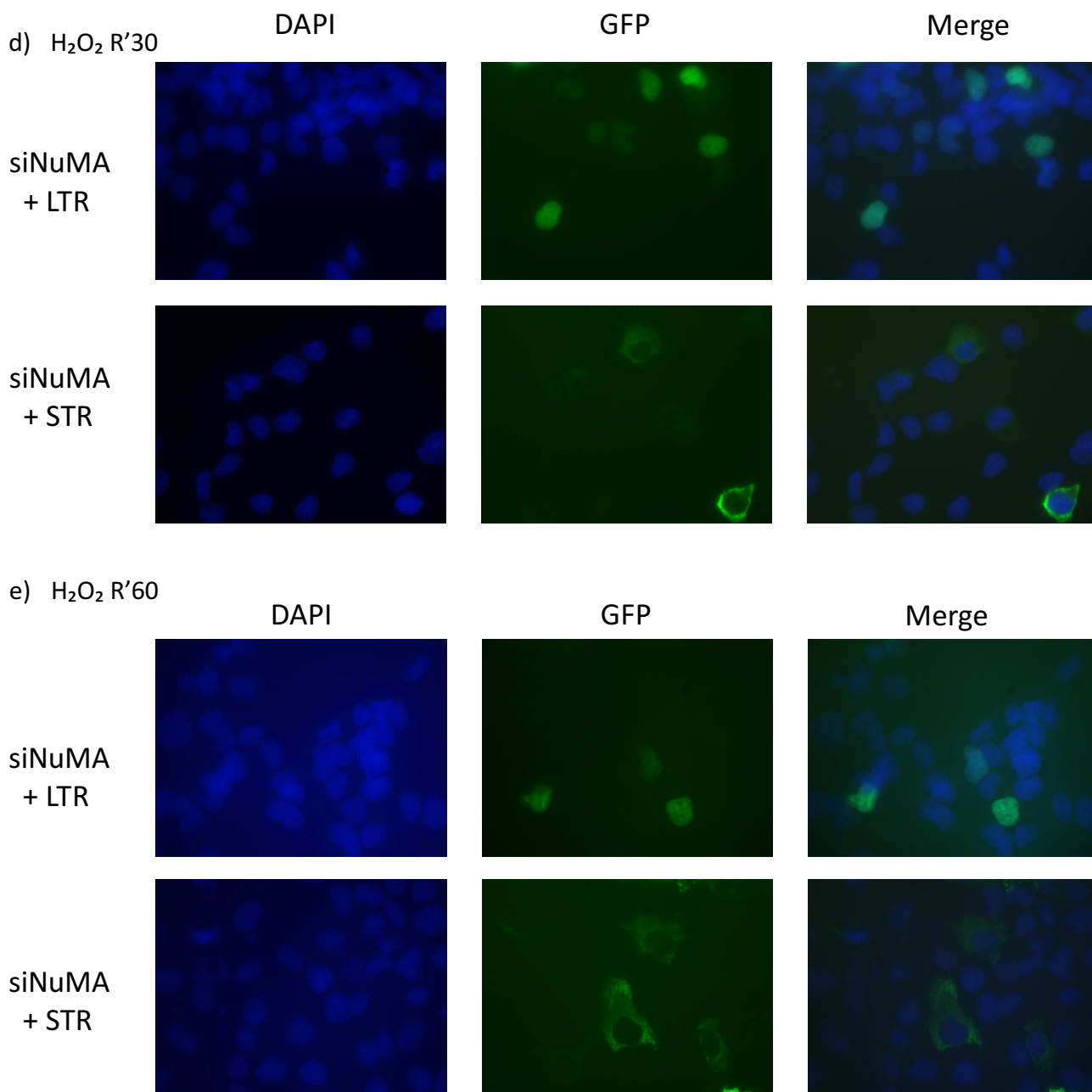


Figure 5.2.5. The long isoform of NuMA localises to nuclei whilst the short isoform of NuMA localises to the cytoplasm. MRC5 cells were plated onto coverslips before being transfected with specific siRNA to NuMA, or a scrambled (Scr) control and left to incubate for 24 hours. Cells were then transfected with either a long isoform (targeting resistant) plasmid (LTR), short isoform (targeting resistant) plasmid (STR) or GFP-empty vector (EV) plasmid and incubated for a further 48 hours. Cells were then treated with mock (a) or 10 μ M H₂O₂ for 10 minutes on ice (b), before being allowed to recover for either 15 (c), 30 (d) or 60 minutes (e) in complete media at 37°C. The coverslips were mounted on to slides with VectaShield mounting medium with DAPI, and processed using a fluorescence microscope, at magnification 63 (63x).

With reference to figure 5.2.5, it can be seen that the long isoform is predominantly localised to the nucleus, and the short isoform is predominantly located in the cytoplasm. This is the localisation pattern regardless of the damage setting; the long isoform/short isoform are situated in the nucleus/cytoplasm, respectively, in the absence of damage and after treatment with H₂O₂ (and during recovery).

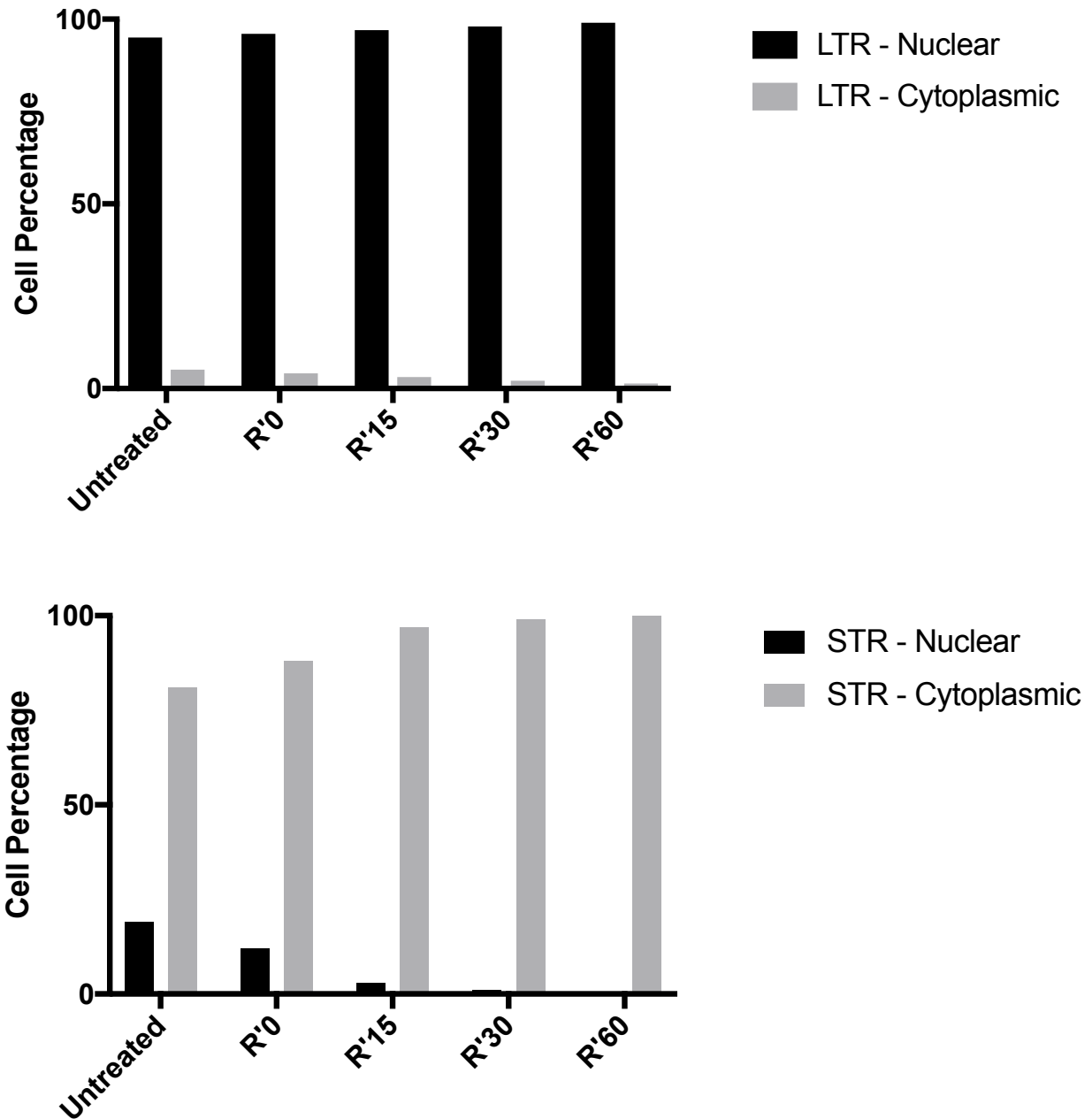


Figure 5.2.6. **The long isoform of NuMA localises to nuclei whilst the short isoform of NuMA localises to the cytoplasm.** MRC5 cells were plated onto coverslips before being transfected with specific siRNA to NuMA, or a scrambled (Scr) control and left to incubate for 24 hours. Cells were then transfected with either a long isoform (targeting resistant) plasmid (LTR), short isoform (targeting resistant) plasmid (STR) or GFP-empty vector (EV) plasmid and incubated for a further 48 hours. Cells were then treated with mock (a) or 10 μ M H₂O₂ for 10 minutes on ice (b), before being allowed to recover for either 15 (c), 30 (d) or 60 minutes (e) in complete media at 37°C. 100 cells per condition were counted and cells were assessed for the localisation of the long and short isoforms.

Referring to figure 5.2.6, quantification of 100 cells per condition was carried out. The results show a mirroring with the representative images shown in figure 5.2.5, with around 95% of cells over-expressing the LTR plasmid localising to the nucleus. Over 90% of the cells over-expressing the STR localised to the cytoplasm.

It is well documented that various genes can be up- or down-regulated in disease states such as cancer. The up-/down-regulation of genes affects protein expression and it is known that many cancer sub-types correlate with the overexpression of proteins. The expression patterns of NuMA in various tissue types were investigated by a bioinformatics PhD student in the El-Khamisy lab, Jacob Parker, to determine if there were any cancer sub-types which exhibited elevated levels of NuMA. It became apparent that there were many types of cancer which expressed increased levels of the NuMA protein (Human Protein Atlas). The cancers which exhibit the highest levels of NuMA expression are breast cancer, ovarian cancer and skin cancer (Human Protein Atlas). This led to the deliberation as to whether NuMA could be a potential drug target. After the initial studies looking at the epistasis of NuMA, TDP1 and PARP1, it was decided to use Olaparib in this context. The initial preliminary experiment looked to determine an Olaparib treatment concentration which would not cause major cell death. If there was more time, a concentration of Olaparib would have been selected to use in conjunction with H₂O₂ treatment in order to perform synthetic lethality studies. The working hypothesis for these extension studies was that if the long or the short isoform of NuMA was overexpressed, thus mimicking the phenotype in a cancer setting, selective killing of the cells could occur using Olaparib alongside a cytotoxic agent. This hypothesis worked on the assumption that as NuMA/TDP1/PARP1 had been shown to exhibit epistasis, when two proteins involved a given pathway were both affected by inhibition/depletion, there was not any additional cell death. The clonogenic survival assay was the technique adopted to investigate this. For representative expression level of plasmids, refer to figure 5.2.1. Figure 5.2.7 shows the results obtained.

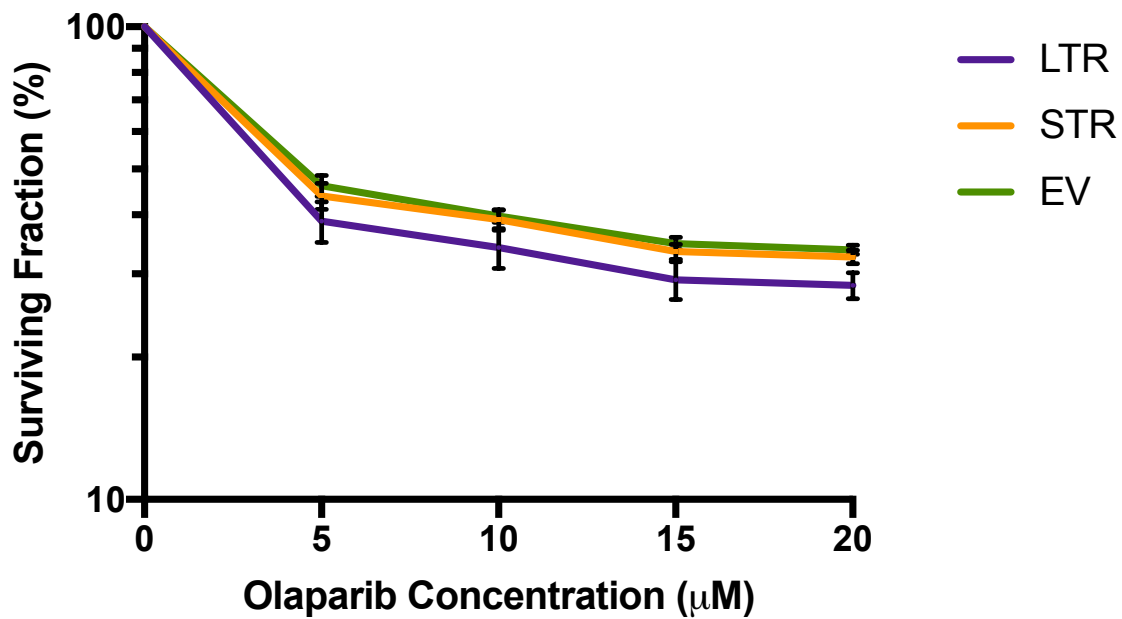


Figure 5.2.7. **Over-expression of the long isoform of NuMA results in greater cell death when treated with Olaparib.** MRC5 cells were transfected with either a long isoform (targeting resistant) plasmid (LTR), short isoform (targeting resistant) plasmid (STR) or GFP-empty vector (EV) plasmid and incubated for 72 hours. Cells were then replated on to 10cm dishes in varying cell concentrations and were left to adhere overnight. Cells treated with varying concentrations of Olaparib in media overnight at 37°C before washing with PBS. The medium was replaced and cells were left to form colonies for 10 days at 37°C. Preliminary studies to determine minimal cellular toxicity. Log10 scale graph showing the surviving cellular fractions following H₂O₂ treatment. The error bars represent S.E.M from 3 biological repeats (n=3).

Figure 5.2.7 shows a line graph using a log₁₀ scale, detailing the percentage of surviving cells after overnight treatment with varying concentrations of Olaparib. The results are representative of 3 biological replicates (n=3). The results were analysed by taking plating densities and dividing by the appropriate factor to equal the same density as plated on the control plates (over-expression of GFP-EV). The survival curve shows that the overexpression of the long isoform of NuMA (LTR) is the most sensitive to Olaparib treatment. This is evident as there are fewer surviving cells, compared to control. There is a significant statistical difference between the overexpression of the long isoform and the GFP-EV, except for at the 10 μ M concentration (5 μ M; p=0.0095, 10 μ M; p= 0.069, 15 μ M; p= 0.0015, 20 μ M; p= 0.0017). Although the overexpression of the short isoform of NuMA appears to be slightly more sensitive to Olaparib treatment than the control, this is only statistically significant at the 15 μ M treatment point (5 μ M; p=0.137, 10 μ M; p= 0.727, 15 μ M; p= 0.024, 20 μ M; p= 0.106).

5.3 Truncated versions of NuMA rescue the repair defect associated with NuMA depletion

As discussed, it came to light that there were different isoforms of NuMA. It has also been previously mentioned that NuMA has another very well documented role within cells, that of spindle orientation during mitosis. With the fact that there were two 'workable' isoforms, it was hypothesised that perhaps the different isoforms had independent cellular roles, especially due to the fact that the differential expression of the two isoforms was variable in different organs (Human Protein Atlas). As both isoforms of NuMA seemed to rescue the repair defect associated with NuMA depletion to a similar level (even though the expression of the long isoform was slightly less) a different strategy needed to be adopted. A paper published in 2014 had managed to make and successfully express various truncated forms of NuMA and hence this was the starting point (Seo, et al., 2014). It was decided to make the truncations in the targeting resistant plasmid. The truncations were made by Simona Vatavu, a Masters' student in the lab and spanned various lengths of NuMA: 1-1348, 1348-2115 and 1700-2115 (see figure 5.3.1 for schematics of truncations). It was discovered at a later date that due to time constraints and the student being unaware of the sites of mutation to create the targeting resistance, that the final 1700-2115 truncation was not made in the targeting resistant plasmid. In this case, there were two options; the truncation could be re-made by

introducing a start codon at the beginning of the 1700 stretch. The other option was to perform the SDM to make the truncation targeting resistant. It was decided that the latter was the better option as the truncation had already been tested for expression; new SDM primers were designed to bind to the specific region. Once the targeting resistant 1700-2115 truncation was made, it too was tested for expression before performing comet assay experiments. Previous experiments performed by Simona indicated that the 1-1348 truncation did not bind to PARP1 (this stretch of protein doesn't contain the nuclear localisation signal (NLS)), and hence when planning comet assay experiments, as it is already known that TDP1 and NuMA interact in a PAR dependent manner, this truncation was omitted. As the truncation expressing the 1348-2115 section of NuMA encompasses the 1700-2115 stretch, it was decided to focus on the analysis of the 1700-2115 region of NuMA. Figure 5.3.2 shows the expression profile of the truncation, as assessed by western blotting. Figure 5.3.3 shows the comet assay data.

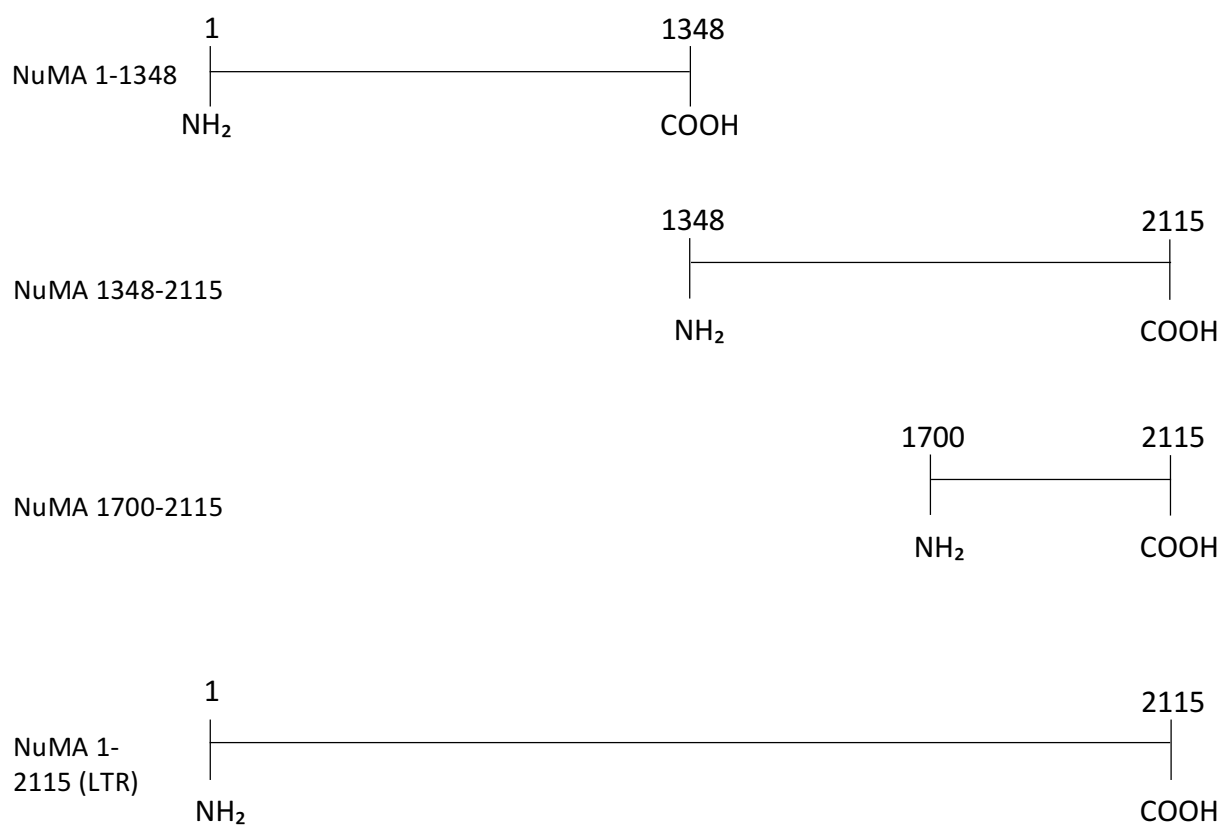


Figure 5.3.1. **Schematic of the various truncations made in the long isoform of NuMA.** Visual representation of the various truncations made within the NuMA protein. For the purpose of experiments detailed in this thesis, only the 1700-2115 (globular tail) stretch of NuMA as well as the full length LTR isoform of NuMA (1-2115) were utilised.

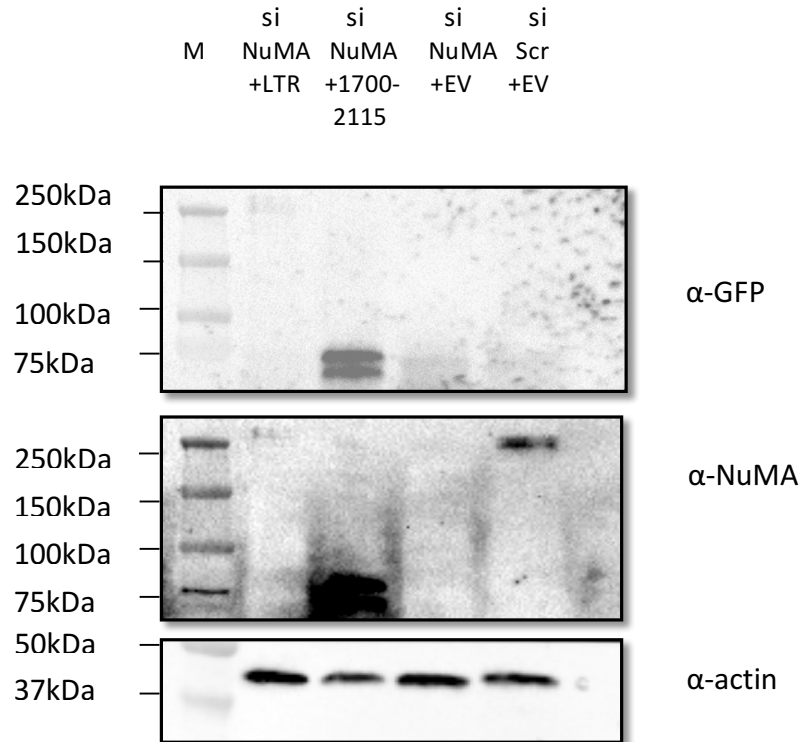


Figure 5.3.2. **The long isoform of NuMA is expressed to a lesser extent than the globular domain of NuMA.** MRC5 cells were transfected with specific siRNA to NuMA (siNuMA), or a scrambled control (siScr) and incubated for 24 hours. MRC5 cells were then transfected with either a long isoform (targeting resistant) plasmid (LTR), globular tail of NuMA (1700-2115; targeting resistant) plasmid (1700-2115) or GFP-empty vector (EV) plasmid and incubated for a further 48 hours. Western Immunoblotting to determine the overexpression profile of the long isoform of NuMA and the globular tail domain of NuMA, under knockdown conditions. Actin serves as loading control. Protein sample analysis was carried out via SDS-PAGE, using a 4-15% polyacrylamide gel (Bio-Rad). The gel was transferred to nitrocellulose membrane, using a Trans-Blot transfer system (Bio-Rad).

Figure 5.3.2 shows the expression levels of the long isoform with targeting resistance (LTR) and the 1700-2115 truncation with targeting resistance, when endogenous NuMA has been depleted. The western blotting also shows two EV controls, one with NuMA depleted and one without. It is evident that the LTR is expressed to a lesser extent than the 1700-2115 plasmid, which is concurrent with the expression of the LTR compared to the STR in figure 5.2.1. There appears to be 2 bands expressed by the 1700-2115 construct, which may suggest there is a post-translational modification or degradation event occurring. The α -NuMA blot shows the endogenous levels of NuMA in the siScr + EV condition, indicating that the endogenous NuMA has been depleted in the other conditions. This is further confirmed by the lack of a band in the control lane when probed with α -GFP.

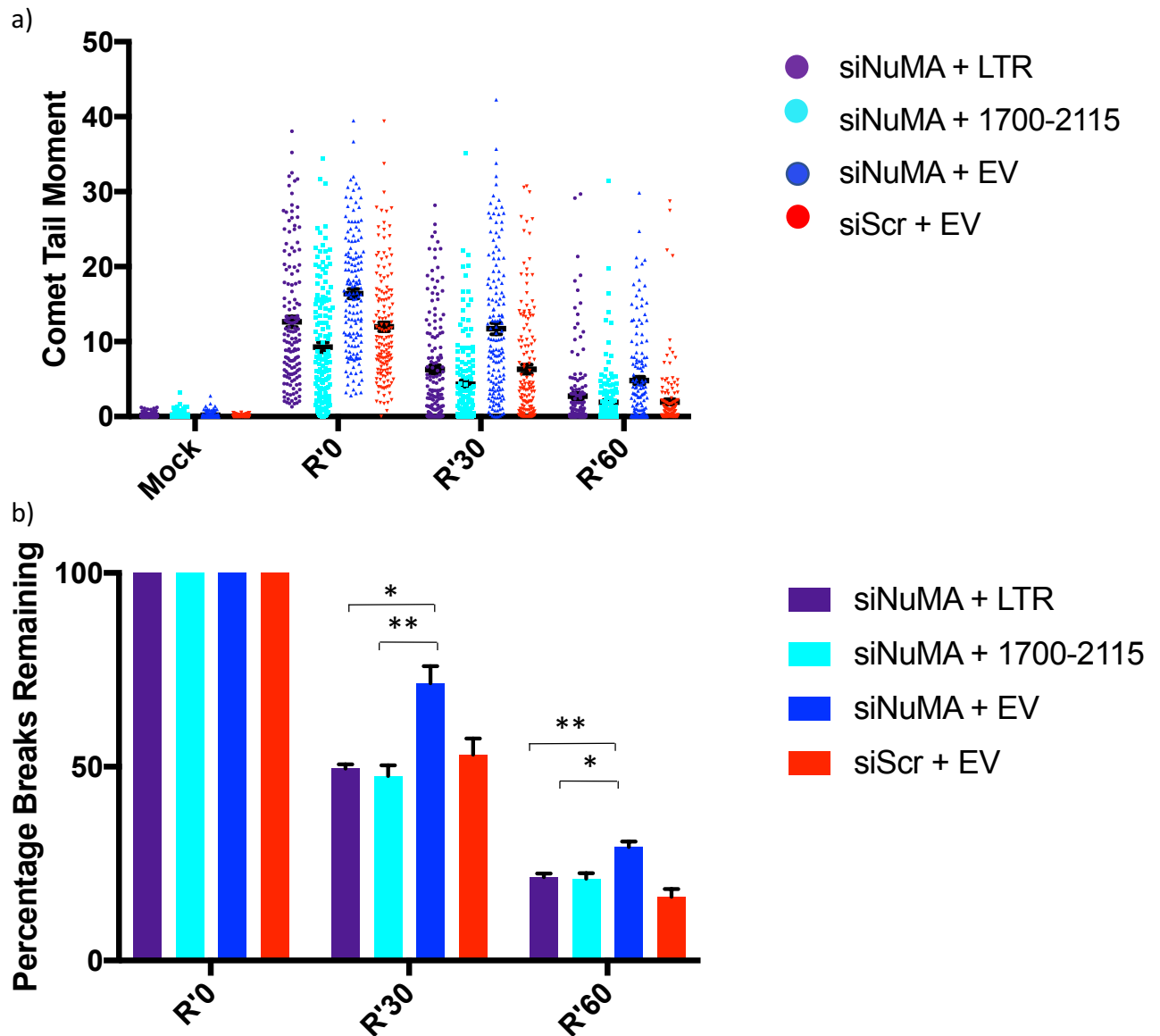


Figure 5.3.3. Over-expression of 1700-2115 stretch of NuMA rescues the repair defect associated with depletion of NuMA. MRC5 cells were transfected with specific siRNA to NuMA, or a scrambled (Scr) control and left to incubate for 24 hours. Cells were then transfected with either a long isoform (targeting resistant) plasmid (LTR), 1700-2115 truncated version of NuMA or GFP-empty vector (EV) plasmid and incubated for a further 48 hours. Cells were treated with H₂O₂ (10 μ M) for 10 minutes on ice, followed by recovery at 37°C in complete medium for 30 or 60 minutes. Alkaline comet assay was performed to assess DNA damage in single cells after gel electrophoresis. a) Representative scatter graph showing spread of comet tail moments from 150 scored nuclei with overexpression of LTR (purple dots), overexpression of 1700-2115 construct (turquoise dots), or in the presence (red dots) or absence (blue dots) of NuMA. b) The bars represent percentage breaks remaining (as a measure of average comet tail moment) after removal of oxidative stress and recovery in complete medium between cells with overexpressed LTR/globular tail domain (1700-2115) and the presence/absence of NuMA. The error bars represent S.E.M from 3 biological repeats (n=3). * = 0.05, ** = 0.005 (Student T-test).

Figure 5.3.3 a) shows each individual comet tail moment scored, across 3 biological replicates (150 total). The cell population was treated with 10 μ M H₂O₂ before being allowed to recover for the designated time periods. The comet tail moments scored from the LTR, 1700-2115 and the control samples all exhibit similar scores, with the siNuMA + EV condition exhibiting the largest comet tail moments. Figure 5.3.3 b) shows the data represented in a bar chart, detailing the repair kinetics of the different conditions. To note, the siNuMA + EV and the siScr + EV conditions which emulate the data previously detailed, exhibit statistical significance (R'30; p= 0.00000091, R'60; p= 0.0145). At the R'30 time point, it appears that the siNuMA + LTR and the siNuMA + 1700-2115 rescue the repair defect observed when NuMA levels are depleted, even to the point where there are fewer breaks remaining than exhibited in the control (siScr +EV). However, there is no statistically significant difference between the siNuMA + LTR and siNuMA + 1700-2115 conditions and the control (siNuMA + LTR compared to siScr + EV: R'30; p= 0.543; siNuMA + 1700-2115 compared to siScr + EV: R'30; p= 0.097). There are slightly fewer breaks remaining in the control sample after 60 minutes of recovery, compared to the over-expression of LTR and 1700-2115 conditions. This trend does still exhibit statistical significance compared to the siNuMA + EV condition, as well as the R'30 time points also deemed to be statistically significant (siNuMA + LTR compared to siNuMA + EV: R'30; p= 0.049, R'60; p = 0.0069; siNuMA + 1700-2115 compared to siNuMA + EV: R'30; p= 0.0062, R'60; p = 0.032).

After consideration of the data presented in figure 5.3.3 it was decided to further investigate the potential that NuMA plays a minimum of two separate roles within the cellular environment. As previously discussed, it is known that NuMA plays an important role in the correct spindle orientation during the cell cycle. Due to the nature of the role, there is an inherent involvement of the microtubules. Taking this into account, it was decided to investigate whether the removal of the microtubule binding domain (MBD) would still allow for the physical interaction with TDP1. It was also hypothesised that this mutant would still be able to rescue the repair defect associated with the depletion of NuMA when selectively over-expressed. This would convey that a MBD mutant version of NuMA is still able to carry out its role in SSBR, even when lacking the domain required for interaction with mitotic machinery. The deletion of the microtubule binding domain (MBD) (amino acids 1866-1936) was carried out by Dr Swagat Ray, a member of the El-

Khamisy lab. Co-IP experiment showed that the deletion of the MBD did not prevent the binding of TDP1 to the NuMA mutant (data not shown). The comet assay was adopted to investigate whether the overexpression of the NuMA construct which lacked the MBD rescued the repair defect. Figure 5.3.4 shows the western blotting giving a representation of the knockdown/overexpression level achieved. Figure 5.3.5 shows the results obtained from the comet assay experiments.

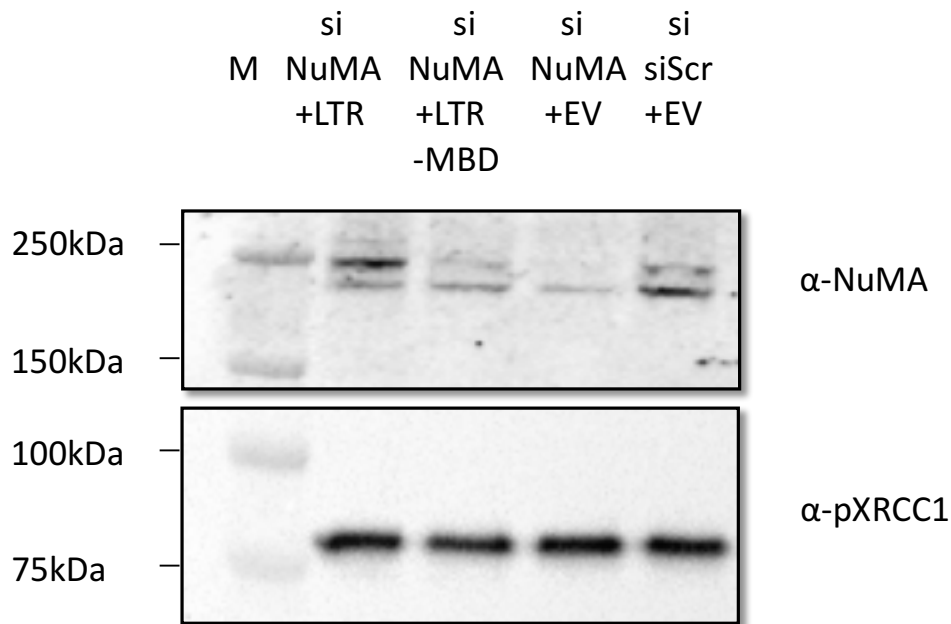


Figure 5.3.4. **Knockdown and overexpression validation of NuMA, complemented with the over-expression of LTR and the MBD deficient mutant of NuMA.** MRC5 cells were transfected with specific siRNA to NuMA (siNuMA), or a scrambled control (siScr) and incubated for 24 hours. Cells were then transfected with either a long isoform (targeting resistant) plasmid (LTR), LTR plasmid which did not include the microtubule binding domain (-MBD) or GFP-empty vector (EV) plasmid and incubated for 24 hours. Cells were re-transfected with siRNA and left to incubate for a final 24 hours. Western Immunoblotting to determine the overexpression profile of the long isoform of NuMA and the LTR less the microtubule binding domain, under knockdown conditions. phospho-XRCC1 serves as loading control. Protein sample analysis was carried out via SDS-PAGE, using a 4-15% polyacrylamide gel (Bio-Rad). The gel was transferred to nitrocellulose membrane, using a Trans-Blot transfer system (Bio-Rad).

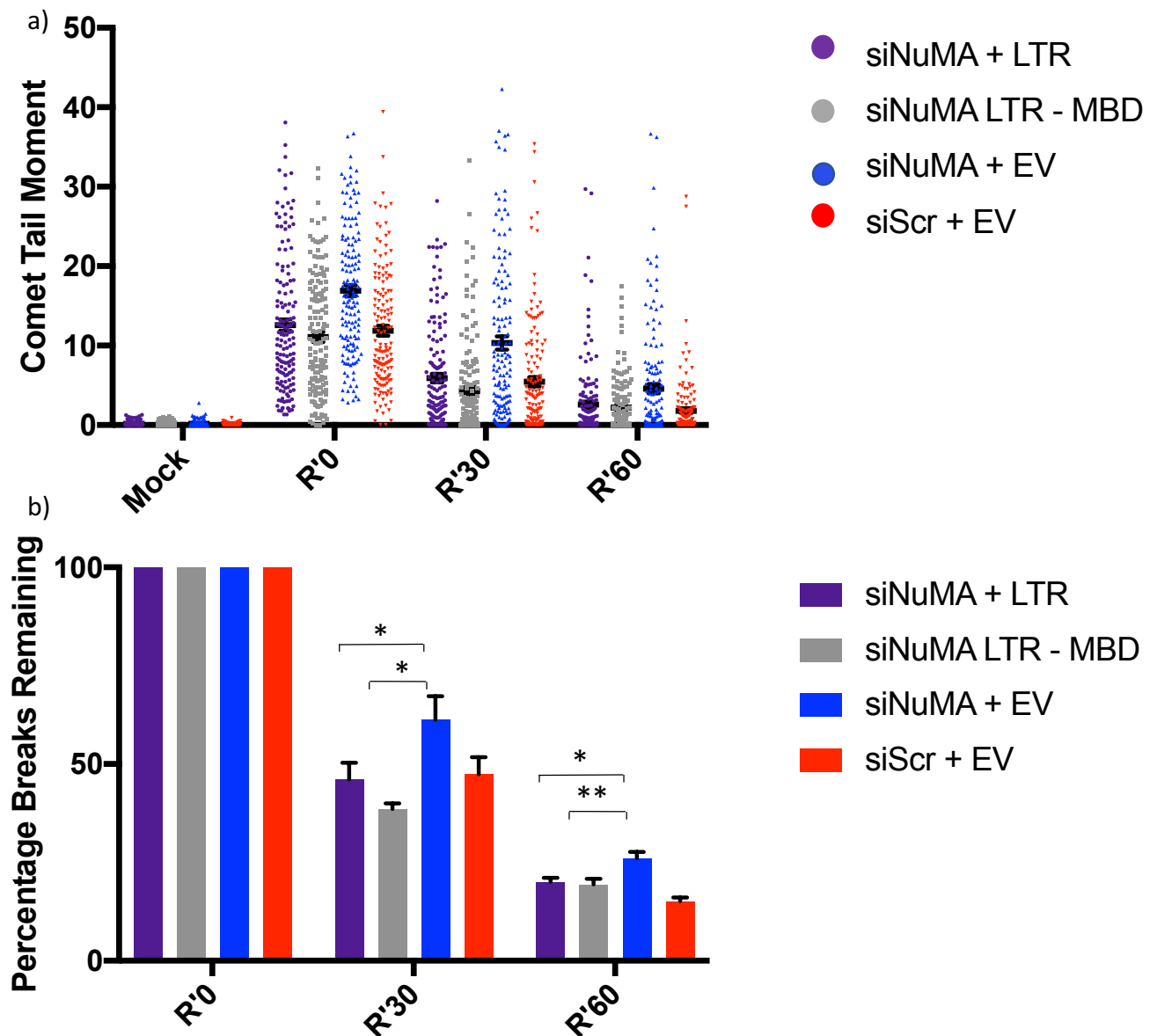


Figure 5.3.5. Over-expression of LTR and the MBD deficient mutant of NuMA rescue the defect associated with depletion of NuMA. MRC5 cells were transfected with specific siRNA to NuMA, or a scrambled (Scr) control and left to incubate for 24 hours. Cells were then transfected with either a long isoform (targeting resistant) plasmid (LTR), LTR plasmid which did not include the microtubule binding domain (MBD) or GFP-empty vector (EV) plasmid and incubated for a further 24 hours before being re-transfected with siRNA for a final 24 hour incubation. Cells were then treated with mock or 10 μ M H₂O₂ for 10 minutes on ice, before being allowed to recover for either 30 or 60 minutes in complete media at 37°C. Alkaline comet assay performed to assess DNA damage in single cells after gel electrophoresis. a) Representative scatter graph showing spread of comet tail moments from 150 scored nuclei with overexpression of LTR (purple dots), overexpression of LTR-MBD construct (grey dots), or in the presence (red dots) or absence (blue dots) of NuMA. b) The bars represent percentage breaks remaining (as a measure of average comet tail moment) after removal of oxidative stress and recovery in complete medium between cells with overexpressed LTR/LTR-MBD and the presence/absence of NuMA. The error bars represent S.E.M from 3 biological repeats (n=3). * = 0.05, ** = 0.005, n.s. = not significant (Student T-test).

Figure 5.3.4 shows the western blotting produced to determine the representative level of knockdown of NuMA as well as the NuMA knockdown with complementation of LTR and LTR minus the MBD, compared to normal endogenous levels of protein (scrambled control). It can be seen that there is an enrichment in the upper band detected on the NuMA blot when the LTR construct is over-expressed, under knockdown conditions. This indicates that the LTR is being over-expressed as expected. There also appears to be a little more enrichment in the top band in the condition with the over-expressed LTR minus the MBD compared to the siNuMA + EV. This level of knockdown/over-expression was taken as minimum and any data which did not reflect this level of knockdown was discounted.

Figure 5.3.5 a) shows each individual comet tail moment scored, across 3 biological replicates (150 total). The cell population was treated with $10\mu\text{M}$ H_2O_2 before being allowed to recover for periods of 30 or 60 minutes. There are very similar trends of comet tail moments between the over-expressed LTR, LTR minus MBD and control conditions, with the siNuMA + EV condition exhibiting a higher level of DNA damage. There is a global reduction in the comet tail moments, after 30 and 60 minutes of cellular recovery, with the siNuMA + EV condition yielding the highest comet tail moments. Figure 5.3.5 b) shows the data from a) represented as a bar chart, with averages of the 150 data points calculated; error bars represent standard error of the mean. Referring to figure 5.3.5 b) the percentage breaks remaining in the siNuMA + LTR and the control condition are similar, with the repair defect exhibited in siNuMA + EV is rescued slightly quicker in the siNuMA + LTR minus MBD condition after 30 minutes of recovery. After 60 minutes, the control cells have recovered the most, with both the siNuMA + LTR and the siNuMA + LTR minus MBD conditions have rescued the repair defect shown in the siNuMA + EV condition to a similar extent. The siNuMA + EV and the control condition exhibit statistical significance, mirroring the data shown previously in this chapter, and in chapters 3 and 4 (R'30; $p= 0.026$, R'60; $p= 0.047$). Comparing the overexpression conditions to the siNuMA + EV samples, the siNuMA + LTR shows a statistically significant difference after both 30 and 60 minutes of recovery (R'30; $p= 0.0154$, R'60; $p= 0.0176$), as does the siNuMA + LTR minus MBD (R'30; $p= 0.0417$, R'60; $p= 0.0096$). Comparing these two conditions to the control, however, show no significant difference, suggesting that they do rescue the repair defect, with cells recovering to a similar extent of the

control, with the siScr + EV condition exhibiting the fewest breaks remaining after 60 minutes of recovery (siNuMA + LTR compared to siScr + EV: R'30; p= 0.574, R'60; p= 0.130, siNuMA + LTR minus MBD compared to siScr + EV: R'30; p= 0.243, R'60; p= 0.190).

5.4 Discussion

This study set out to further investigate the NuMA protein and its potential function within the DNA damage response. This investigation stemmed from previous data collected which suggested a role for NuMA within a DNA repair setting. It was decided to explore NuMA further due to the premise that NuMA is crucial for the precise orientation of spindle poles during mitosis (Vidi, et al., 2014). After the discovery that there was a potential role for NuMA in a different setting it was of interest to attempt to determine whether, as the protein is so large, separate regions of NuMA are involved in different processes. When closer attention was given to NuMA's domains and roles of these distinct regions, it became apparent that there were two main isoforms. On inspection of the plasmid purchased, it was clear that this was the short isoform of NuMA. Ding et al., published a paper in 2016 which highlighted that there is an exon-skipping event that occurs within NuMA, resulting in the shorter isoform being expressed. This alternate splicing event can be mimicked via the use of a drug called 5-Aza-2'-deoxycytidine which inhibits DNA methylation and causes exon skipping (Ding, et al., 2016). Once it was discovered that there were two main isoforms of NuMA, it was an exciting prospect to investigate whether the two isoforms have the same role within the cellular setting, or whether they have independent roles.

In order to selectively analyse the roles of the isoforms, first a plasmid needed to be constructed which contained the additional amino acids which the short isoform plasmid purchased was lacking. Once a synthesized section of DNA was acquired, this was inserted in the correct position and expression tests were performed. There was an issue with selectively over-expressing the long and short isoforms, however. As NuMA is relatively abundant within cells, and it appeared that it was possible to detect both isoforms via western blotting, a solution to this was required. siRNA to NuMA had been utilised in many experiments (see chapter 3) and a good level of knockdown was achievable. It was decided that the siRNA was a good tool, however the siRNA would still target the plasmid DNA, if over-expressed. To overcome this, the decision was taken to

make a targeting resistant plasmid. This involved the adoption of SDM to make silent mutations within a specific region which would not alter the coding sequence of the protein but would prevent the binding of siRNA to cause a knockdown of the protein level. As previously mentioned in section 5.1, there was a screening step carried out in order to select a single siRNA sequence to mutate, rather than mutating the 4 different sequences within the pooled siRNA. Once this had taken place, specific primers were purchased and the SDM was carried out in both the long and short isoform plasmids. This then allowed for selective over-expression of each isoform independently. With reference to figure 5.2.1, the western blotting indicates the typical level of over-expression of the long isoform with targeting resistance (LTR) and the short isoform with targeting resistance (STR). This western blotting was performed to check that after the SDM had been performed, the proteins still expressed appropriately. In this case, the over-expression was additional to the endogenous levels of NuMA. The blots were probed with a-GFP antibody to detect the over-expressed proteins only, as they were generated in a GFP-backbone. Once expression was considered adequate, the knockdown experiments began.

Figure 5.2.2 shows several western blots supporting the same trend; that the LTR is expressed to a greatly reduced level, compared to the STR, when endogenous NuMA levels were depleted. This was an unexpected discovery and one which is hard to explain. The only difference between the 2 constructs is the addition of the 14 amino acid stretch. The SDM had been carried out on the same site in both plasmids. It was strange that something within the added amino acid stretch could allow for the very poor over-expression, nevertheless the results obtained were consistent. However, with reference to figures 5.2.3 and 5.2.4, despite the much reduced expression levels of the LTR compared to the STR, the LTR construct appears to rescue the repair defect associated with depleted levels of NuMA, to a greater extent than the STR. This could suggest that the specific over-expression of the LTR plays a more specific and important role in repairing oxidative-induced SSBs than the endogenous pool which contains both the long and short isoform. This is due to the greater rescue of the repair defect despite the poor expression. There was indeed a rescue of the repair defect when the STR was over-expressed however, which rules out the statement that complementation with the long

isoform rescues the repair defect and the short isoform doesn't. This resulted in additional work being needed to elucidate a separation of function mutant.

Following on from the comet assay and clonogenic survival assay results with the selective over-expression of the long and short isoforms. The immunofluorescence data obtained (figure 5.2.5) suggests that the long isoform localises to the nucleus, whereas the short isoform localises to the cytoplasm, in the absence, presence and recovery from oxidative damage. This suggest that perhaps the long isoform is required in the repair of SSBs and the short isoform is not. The presence of the long isoform of NuMA in the nucleus in the untreated samples could be due to the relatively high level of endogenous SSBs which occur in cells on a daily basis which are required to be repaired to maintain genomic stability. The quantification of the cells shown in figure 5.2.6 confirms the observations from the analysis of the immunofluorescence images, with a larger population of cells analysed (100 per condition).

Another approach to make a separation of function mutant was to make truncations in the NuMA protein. The initial strategy was to make various truncations within the protein in order to find a section of NuMA which doesn't interact with TDP1. Seo, et al., published a paper in 2014 which detailed truncations in NuMA, which were shown to express well and hence we decided to make the same truncations. This was because it can sometimes be difficult to express certain sections of protein, due to loss of various domains. It was a starting point and once the truncations had been made and co-IP experiments were performed, and interactions had been analysed, the truncations were deemed sufficient to work with, for further investigations. Comet assays were adopted as the output reading of these investigations. It was hoped that the truncated versions of NuMA would not be able to rescue the repair defect associated with the depletion of NuMA. This would allow for the narrowing down of the section of NuMA which is required to help protect the cells from damage/repair the cells more quickly after insult. With reference to figure 5.3.3, it can be seen that the over-expression of the 1700-2115 stretch of protein was sufficient for the rescue of the repair defect, with cells recovering to a point where the damage levels are almost parallel to those in the control condition. However, referring to figure 5.3.2, it can be seen that the 1700-2115 stretch is expressed to a higher level than the LTR

plasmid. Due to this section of NuMA being sufficient for rescue, it enabled the narrowing down of the region of NuMA which was responsible for the rescue of the repair defect.

After the truncation comets, it was decided to attempt to mutate a region which is required for the known function of NuMA, the involvement with mitotic spindle fibres. This region was the microtubule binding domain (MBD). It was of interest if the deletion of this region would prevent the rescue observed when the knockdown cells are complemented with the long isoform and/or the truncations. The MBD was deleted (deletion of amino acids 1866-1936). The cloning was performed by another member of the lab, before the comet assays could begin. Referring to figure 5.3.5, the over-expression of the plasmid which contained the MBD deletion still facilitated the rescue of the repair defect associated with depleting NuMA. This meant that the deletion of the MBD had resulted in the maintenance of the SSBR function of NuMA, even with the microtubule interacting domain deleted. This could be classed as a separation of function mutant. As the 1700-2115 region was sufficient to allow rescue of the repair defect, this was the region which seemed the most attractive to further explore. The data seems to suggest that there are residues within this region which may play a role within the DNA damage response. As this is a relatively recent finding and these experiments were some of the last to be performed, there is a need for greater exploration into the putative residues that may be required for the rescue of the repair defect.

Another area which was of interest was the potential link between NuMA, a nuclear structural protein and the association of mechanical stress with such proteins. A novel approach to applying stress was adopted.

Chapter 6

Functional Analysis of the Effect of Mechanical Stress on Mammalian Cells

6.1 Introduction

Over recent years, there has been advances in the linking of biochemical processes to structural proteins. Work from the Foiani group (IFOM, Italy) suggests that ATR mediates the mechanical response to membrane stress (Kumar, et al. 2014). ATR responds to mechanical forces occurring at the nuclear envelope. It is believed that this membrane stress response could be caused by chromatin dynamics and is hence important for genome integrity (Kumar, et al. 2014). If mechanical stress is active, it is thought that it could affect the biochemical signalling pathways; if the nuclear matrix proteins are under stress, signalling to the ECM may be prevented and hence this could affect genome order and gene activity (Radulescu & Cleveland, 2010).

Evidence suggests that structural proteins can accumulate under mechanical stress in processes such as cytokinesis, and that filament proteins can accumulate in the nucleus in response to DNA damage (Srivastava & Robinson, 2015; Belin, et al., 2015). Taking this into account, it was hypothesised that other structural proteins are involved in the coordination between mechanical stress and the DNA damage response. Nuclear Mitotic Apparatus Protein 1 (NuMA) is a protein related to lamins and has been investigated for its potential role in SSBs. Second to this, it was found that NuMA interacts with TDP1, hence it was decided NuMA was an ideal candidate to investigate in a mechanical stress setting, providing a link to structural and biochemical processes.

6.2 Mechanical stress increases the level of SSBs

Taking into account the growing evidence arising with regards to cellular processes and mechanical stress, it was decided to look at whether applying mechanical stress to cells increases the amount of SSBs and/or whether it impairs the ability of cells to recover. The decision was made to use both CPT and H₂O₂ (independently) as damaging agents to induce the SSBs during the addition of mechanical stress. Specially designed plastic

inserts, with small holes at the base were designed courtesy of Dr. Jason King (King Lab, Department of Biomedical Science, University of Sheffield, UK) which allowed for the compression studies to be carried out (see materials and methods, section 2.7). Briefly, a very thin layer of 1% agarose (dissolved in media) was carefully placed on cells. The plastic insert was then positioned on top of the agarose disc in order to apply compression, which was additional to genotoxic stress (see materials and methods, section 2.7) The amount of pressure applied was small at around 0.1kPa. This pressure is sufficient to differentiate mesenchymal stem cells into neuronal precursors (Mousavi & Doweidar, 2015). There were many optimisation steps required to transfer the premise of 'mechanical stress' into a mammalian cell system; Dr Jason King and members of his lab have previously performed these types of experiments on *Dictyostelium discoideum*. Dr. King explained the concept of short burst mechanical stress and longer treatments and it was initially opted to try a medium time length incubation, with 30 minutes of mechanical stress selected. CPT was chosen as the damaging agent for the preliminary experiments, with the comet assay selected for the experimental read-out. Figure 6.2.1 shows the results.

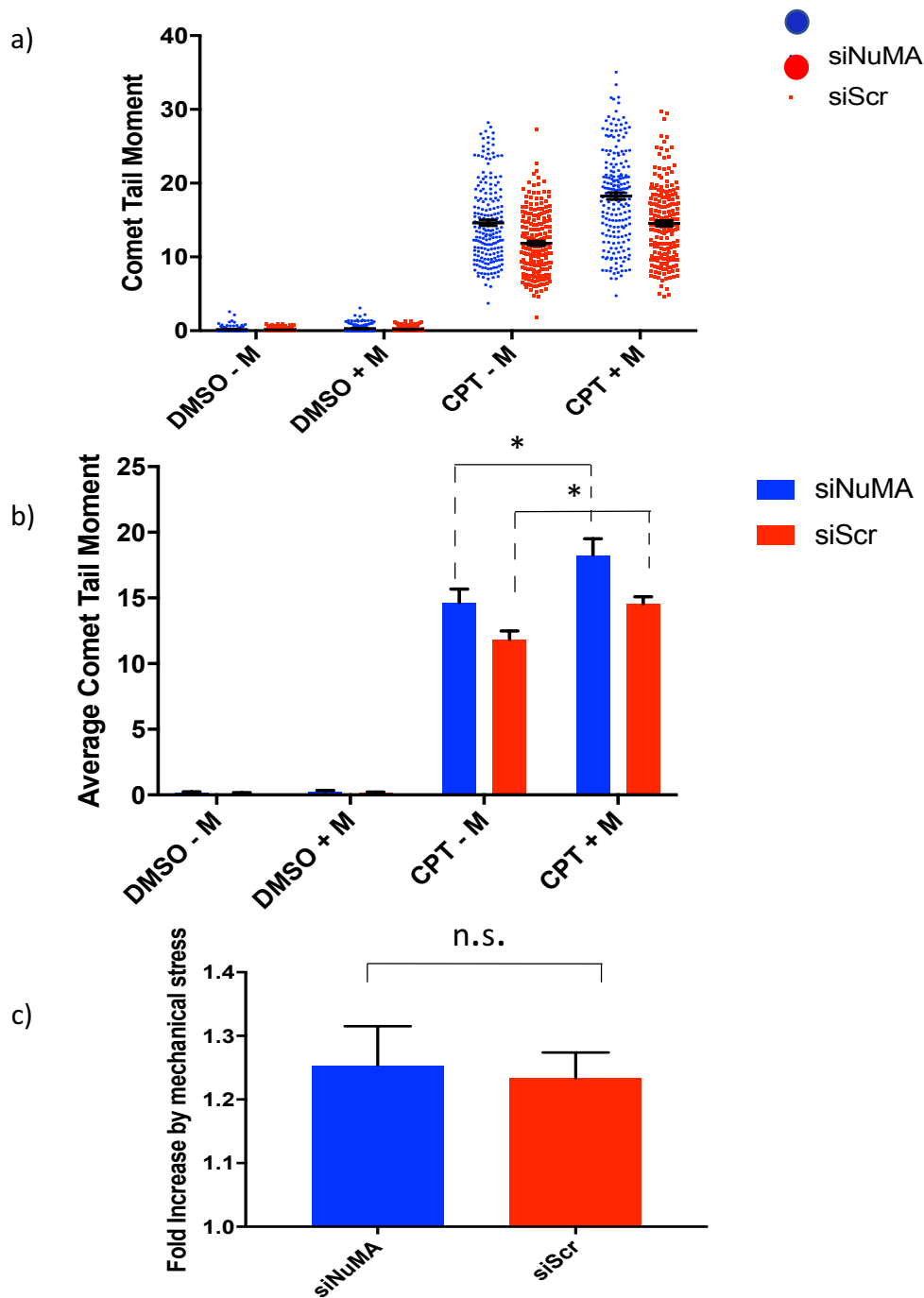


Figure 6.2.1 Mechanical stress increases CPT-induced SSBs independently of the presence or absence of NuMA. MRC5 cells were transfected with either scrambled (siScr) or NuMA (siNuMA) siRNA (50nM) for 72 hours. Cells were treated with CPT (50 μ M) for 30 minutes in the presence or absence of mechanical stress (M) before harvest. Alkaline comet assay was performed to assess DNA damage in single cells after gel electrophoresis. a) Representative scatter graph showing spread of comet tail moments from 200 scored nuclei in presence (red squares) or absence of NuMA (blue dots). b) The bars represent average comet tail moments in presence (+M) or absence (-M) of applied mechanical stress. c) The bars represent fold increase in mechanical stress-induced comet tail moment between siScr and siNuMA transfected cells, when compared to corresponding cells with no mechanical stress applied. The error bars represent S.E.M from 4 biological repeats (n=4). * = <0.05, n.s. = not significant (Student T-test).

Figure 6.2.1 a) shows each individual data point scored across 4 biological replicates (200 total), represented as dots. The data represents 50 μ M CPT treated MRC5 cells, which have had agarose discs added to each well, with + M samples representing the cell populations which have had mechanical stress applied. The scatter plot shows the data spread, with error bars representing the standard error of the mean. Figure 6.2.1 b) shows the individual data points represented as a bar chart, exhibiting the data as average comet tail moment. There is an increase in the average comet tail moment of both NuMA depleted cells and the control cells when treated with CPT, however the statistical significance remains after the application of mechanical stress between the NuMA depleted cells and control (siNuMA compared to siScr: -M p= 0.048; +M p= 0.019). However, when mechanical stress is applied there seems to be no dependence on presence/absence of NuMA. Figure 6.2.1 c) shows a bar chart representing the fold increase in average comet tail moment when mechanical stress is applied. This data was calculated by assigning the respective cell pool which did not have mechanical stress applied as 1. The graph shows that the control cells exhibit approximately a 1.2-fold increase by mechanical stress and a very similar fold increase value is noted in the NuMA depleted cells. There is a significant increase in the siNuMA conditions with both mechanical stress applied, and not, which is also exhibited in the siScr conditions (siNuMA -M compared with +M: p= 0.021; siScr -M compared with +M: p= 0.047).

After the treatment with CPT, it was decided to perform a very similar experiment with H₂O₂ as the damaging agent. As in previous experiments, the H₂O₂ comet assays assessed the initial damage point (R'0) along with a recovery condition, in this case R'30. For the cell compression studies to be carried out effectively, the cells were required to be treated as adherent cells. As the mechanical stress incubation time selected was 30 minutes, this meant that the previous treatment of 10 μ M H₂O₂ on ice (with cells in suspension) was inappropriate. This led to the decision to use H₂O₂ dissolved in media. This is less than ideal, due to the media containing glucose. Glucose is required for cell maintenance as an important energy source. However, for glucose to be utilised as an energy source, it is metabolised to pyruvate before being further metabolised to ATP. Unfortunately, pyruvate reacts with H₂O₂ in a non-enzymatic manner, to produce carbon dioxide, H₂O and acetic acid (Troxell, et al., 2014). This reaction enables the cells to protect against oxidative damage and hence reduces the efficacy of the H₂O₂. As 10 μ M H₂O₂ usually yields

significant oxidative damage, it was thought that even if the cells were defending against the oxidative damage in some capacity, as the treatment time had been extended to account for this, a significant amount of damage should be able to be detected. Figures 6.2.2 and 6.2.3 show the results.

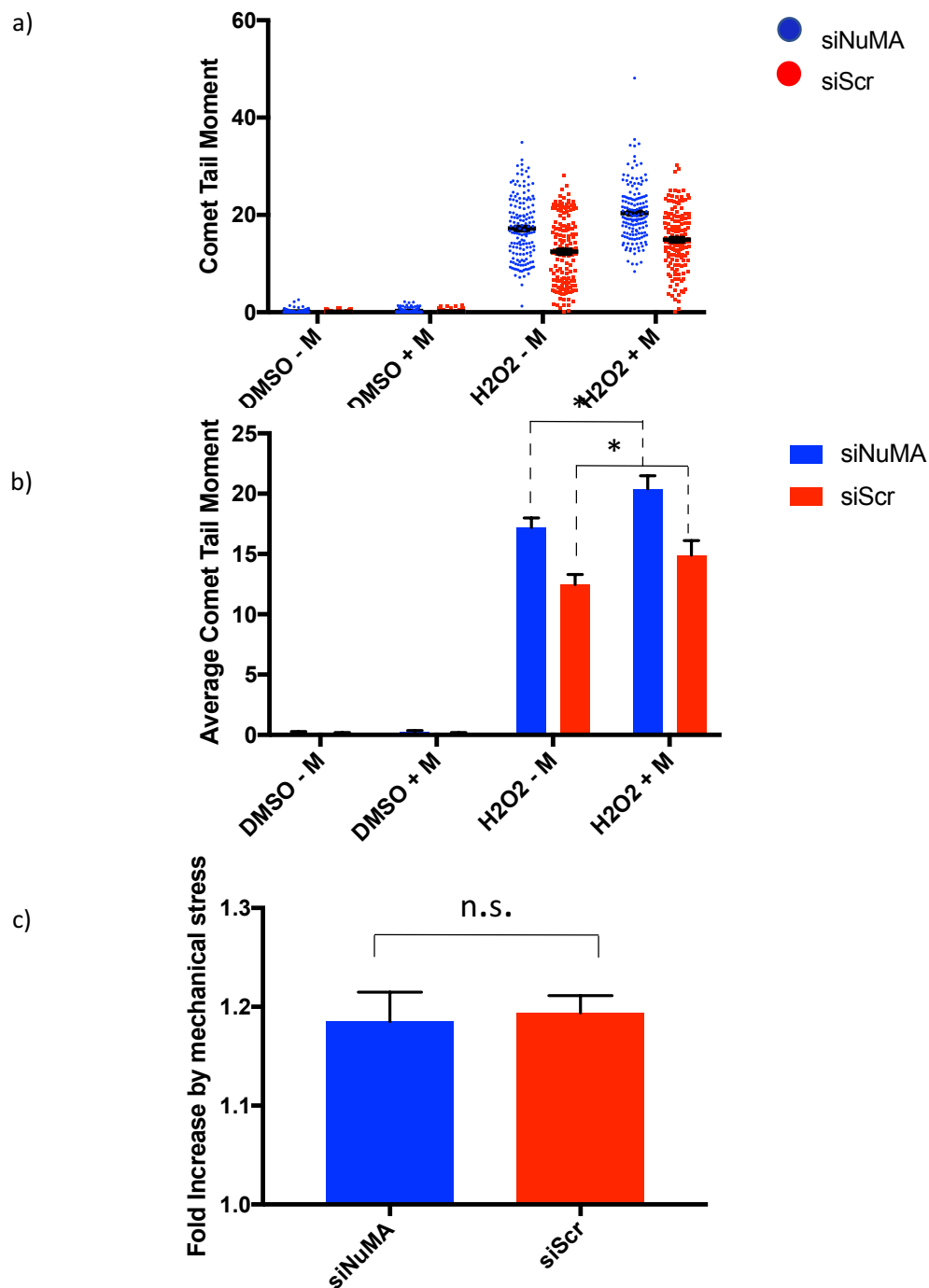


Figure 6.2.2. Mechanical stress increases oxidative stress-induced SSBs independently of the presence or absence of NuMA. MRC5 cells were transfected with either scrambled (siScr) or NuMA (siNuMA) siRNA (50nM) for 72 hours. Cells were treated with H₂O₂ (10μM) for 30 minutes in the presence or absence of mechanical stress (M) before harvest. Alkaline comet assay was performed to assess DNA damage in single cells after gel electrophoresis. a) Representative scatter graph showing spread of comet tail moments from 200 scored nuclei in presence (red squares) or absence of NuMA (blue dots). b) The bars represent average comet tail moments in presence (+M) or absence (-M) of applied mechanical stress. c) The bars represent fold increase in mechanical stress-induced comet tail moment between siScr and siNuMA transfected cells, when compared to corresponding cells with no mechanical stress applied. The error bars represent S.E.M from 4 biological repeats (n=4). * = <0.05, n.s. = not significant (Student T-test).

Figure 6.2.2 a) shows each individual data point scored across 3 biological replicates (150 total), represented as dots. The data represents 10 μ M H₂O₂ treated MRC5 cells, which have had 1% agarose discs added to each well (reconstituted in media), with +M samples representing the cell populations which have had mechanical stress applied. The scatter plot shows the data spread, with error bars representing the standard error of the mean. Figure 6.2.2 b) shows the individual data points represented as a bar chart, exhibiting the data as average comet tail moment. There is an increase in the average comet tail moment of both NuMA depleted and control cells with a significance difference exhibited between the respective conditions when comparing compressed cells to those which haven't been mechanically stressed (siNuMA compared to siScr: -M p= 0.015; +M p= 0.0015). Figure 6.2.2 c) shows a bar chart representing the fold increase in average comet tail moment when mechanical stress is applied. The values were calculated in the same way described in figure 6.2.1. Upon the application of mechanical stress, the NuMA depleted and the control cells exhibited a very similar fold increase in comet tail moments. This figure was 1.85 for the NuMA depleted cells and 1.9 in the siScr condition, therefore there was a marginally greater fold increase in the control cells. The fold change in both conditions was not significant (p= 0.81), hence further supporting the data from figure 6.2.1 that the application of mechanical stress increases the amount of SSBs detected, regardless of NuMA depletion (siNuMA -M compared with +M: p= 0.026; siScr -M compared with +M: p= 0.023).

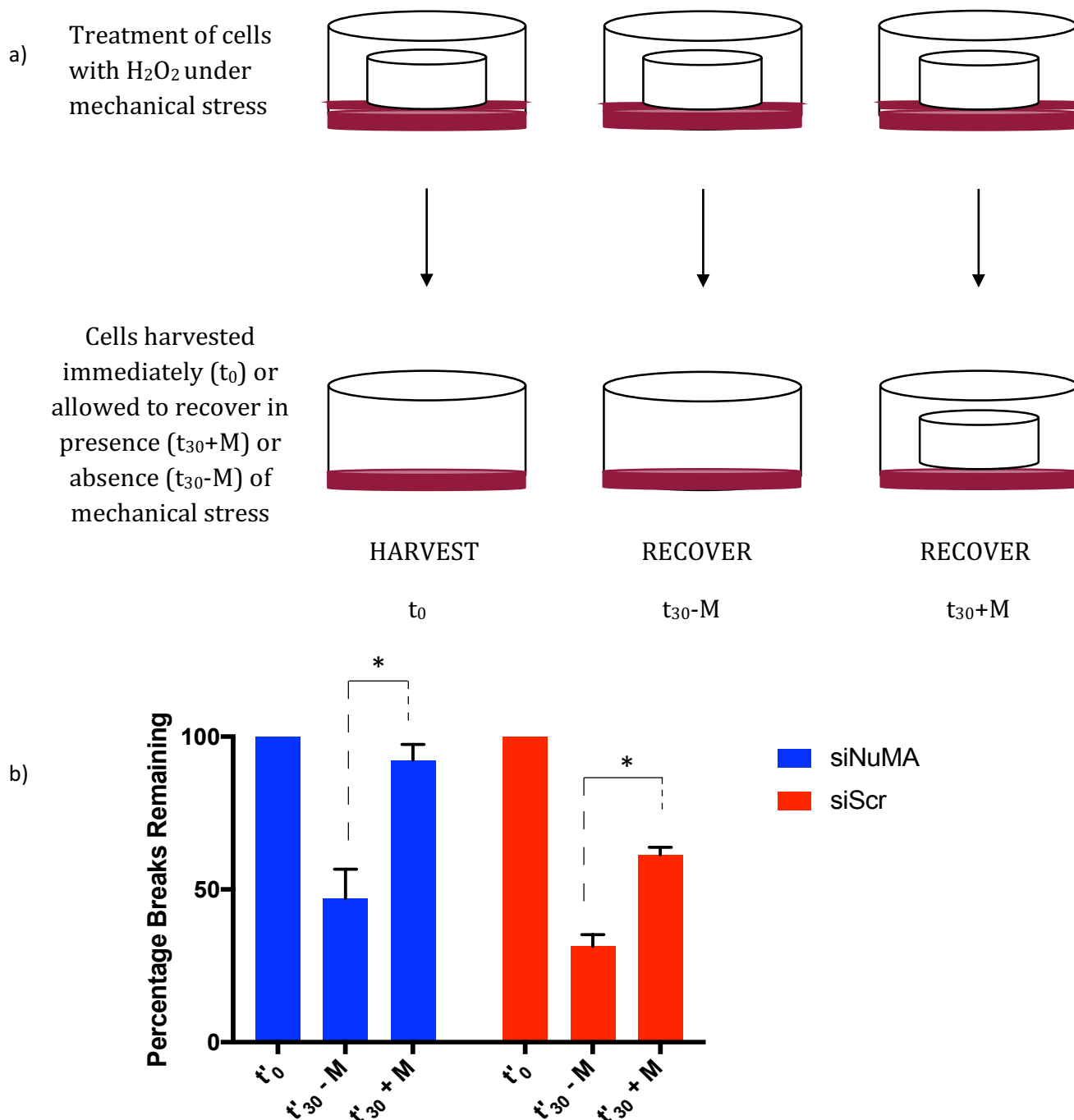


Figure 6.2.3. **Mechanical stress significantly prevents the repair of NuMA depleted cells after the introduction oxidative stress-induced SSBs.** MRC5 cells were transfected with either scrambled (siScr) or NuMA (siNuMA) siRNA (50nM) for 72 hours. Cells were treated with H₂O₂ (10 μ M) for 30 minutes along with mechanical stress applied. Cells were then harvested immediately (t_0) or allowed to recover in complete medium without H₂O₂ in the continued presence of mechanical stress (t_{30+M}) or in its absence (t_{30-M}) for 30 minutes before harvest. Alkaline comet assay was performed to assess DNA damage in single cells after gel electrophoresis. a) Simplified diagram explaining the treatments of cells in this experiment. b) The bars represent percentage SSBs remaining (as a measure of average comet tail moments having assigned $t_0=100$) between cells recovered with continued mechanical stress and ones without it. The error bars represent S.E.M from 4 biological repeats ($n=4$). * = <0.05 (Student T-test).

Figure 6.2.3 a) shows a simplified schematic diagram detailing the treatment of cells in this experiment. Figure 6.2.3 b) shows a bar chart representing the cells scored at a point of maximal damage (t'_0) and cells scored after 30 minutes of recovery in complete media at 37°C, both with and without continued mechanical stress. All the conditions were initially treated with 10 μ M H₂O₂ and were subjected to mechanical stress for 30 minutes. The bar chart shows that when cells were recovered under normal conditions (i.e. mechanical stress wasn't applied) both the NuMA depleted and control cells recover to a similar level to previous comet assay experiments, with the control cells recovering slightly quicker. This can be inferred due to a smaller percentage of breaks remaining after 30 minutes of recovery. The difference in the amount of percentage breaks remaining between the NuMA depleted cells and the control ($t'_{30} -M$) is not statistically significant ($p= 0.303$). There is however a statistical significant difference between respective conditions which have been recovered under mechanical stress and those which haven't (siNuMA $t'_{30} -M$ compared with $t'_{30} +M$: $p= 0.033$; siScr $t'_{30} -M$ compared with $t'_{30} +M$: $p= 0.041$). Figure 6.2.3 b) takes the continued mechanical stress recovery data from a) and represents it in an easier to compare format, omitting the data showing the cells which had been treated with mechanical stress before being recovered without additional stimuli. It shows that NuMA depleted cells which have been allowed to recover under maintained mechanical stress manage very little recovery, with around 92% of percentage breaks remaining after the 30-minute recovery period. The control cells are still able to recover, however to a lesser extent than when the recovery period was performed without mechanical stress. The difference in recovery rates between the NuMA depleted and control cells after the maintenance of mechanical stress during recovery is statistically significant ($p= 0.0102$).

6.3 Imaging of cells after application of mechanical stress

After the findings of the comet assays, it was exciting to have found a potential role for NuMA in linking mechanical stress to the cellular DNA damage response. It was decided to investigate further by performing immunofluorescence on both NuMA depleted and control cells. The cells were treated with 10 μ M CPT (50 μ M too high for immunofluorescence analysis) or 10 μ M H₂O₂ in media (in order to mimic the comet assay experimental set up) and included recovery conditions with cells treated with H₂O₂. All conditions were treated with mechanical stress. It was hoped to observe variations in the

cell morphology or immunostaining patterns in cells which had depleted levels of NuMA when treated with cytotoxic drugs and mechanical stress was applied. The immunofluorescence studies were carried out using the method detailed in chapter 2 (section 2.6.3) and were stained with α -NuMA antibody, before being mounted on to slides with mounting medium containing DAPI. Figures 6.3.1 and 6.3.2 shows the results obtained.

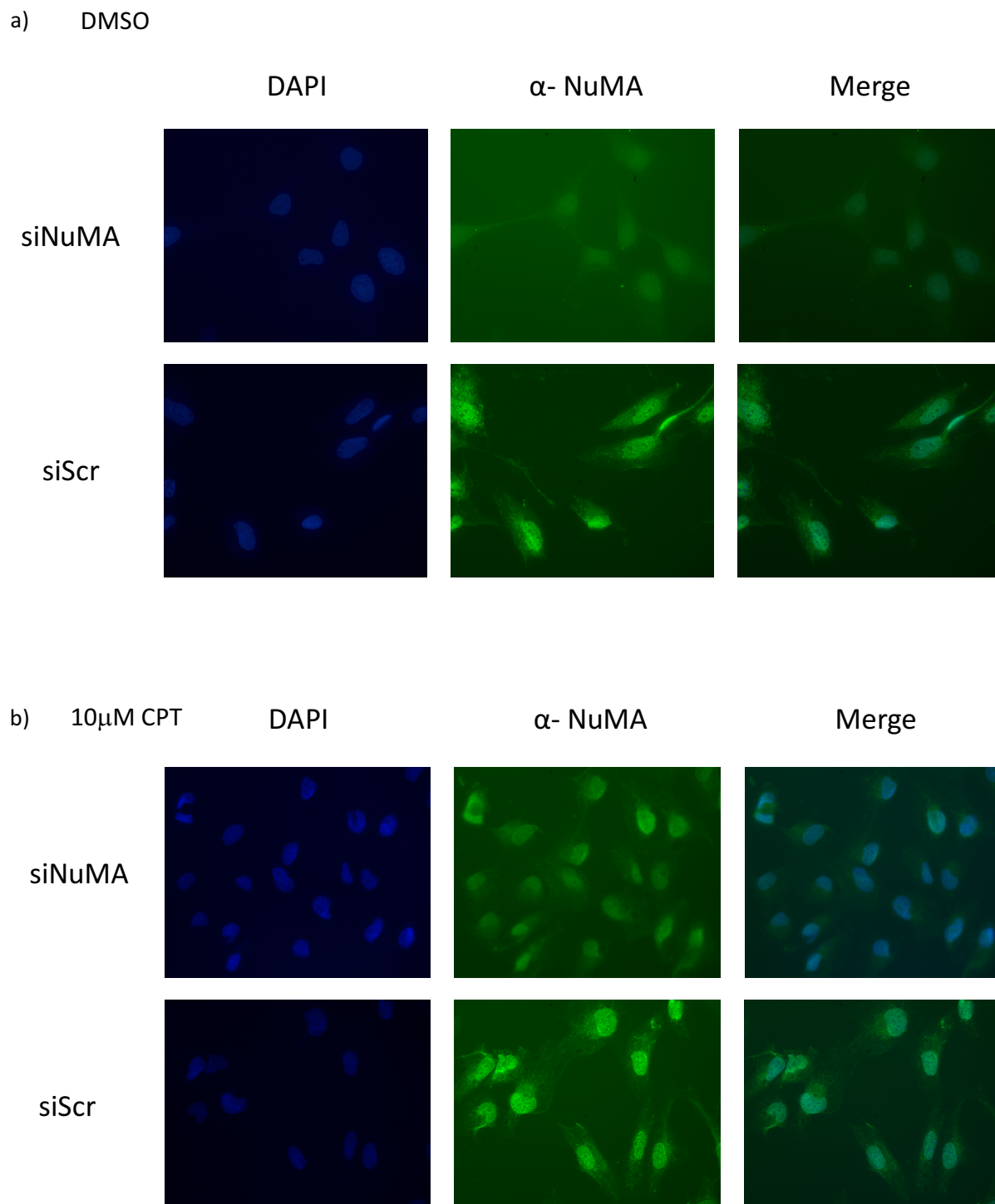


Figure 6.3.1. **Treatment with CPT and mechanical stress in NuMA depleted cells does not show an obvious difference in cell morphology compared to mechanical stress alone.** MRC5 cells were plated onto coverslips before being transfected with specific siRNA to NuMA, or a scrambled (Scr) control and left to incubate for 72 hours. Cells were treated with a) DMSO or b) 10 μ M CPT for 30 minutes in complete media at 37 $^{\circ}$ C. Cells were treated with mechanical stress during the incubation period. The coverslips were mounted on to slides with VectaShield mounting medium with DAPI, and processed using a fluorescence microscope, at magnification 63 (63x).

Figure 6.3.1 a) shows representative immunofluorescence images of MRC5 cells mock treated with DMSO whilst mechanical stress was applied. The NuMA signal is greatly reduced in both the cytoplasm and the nucleus when transfected with siRNA specific to NuMA, with nuclear position determined by the DAPI staining. The siScr cells show that NuMA is diffuse across the cells, with NuMA detected in both the nucleus and the cytoplasm, with a slightly increased intensity in the nucleus. This is to be expected as NuMA is predominantly a nuclear protein. To note, in both figure 6.3.1 a) and b) the blue (DAPI) and green channel (α -NuMA) images were exposed for the same length of time (4ms and 250ms respectively). b) shows representative immunofluorescence images of MRC5 cells treated with 10 μ M CPT whilst mechanical stress was applied. As shown in figure 6.3.1 a) there is a global decrease in the intensity of NuMA in siNuMA treated samples, which is an expected observation. In comparison to a) there appears to be less NuMA signal in nuclei in the CPT-treated condition in the NuMA depleted cells, however this needs further validation as the DAPI signal seems to be stronger and this could be occluding the weak NuMA signal. The siScr condition appears to have a slight increase in the intensity of the NuMA signal in the nuclei compared to the equivalent condition in a). The NuMA localisation in the siScr condition appears to be punctate, with lots of small focal accumulation of NuMA signal compared to a diffuse signal across the nucleus.

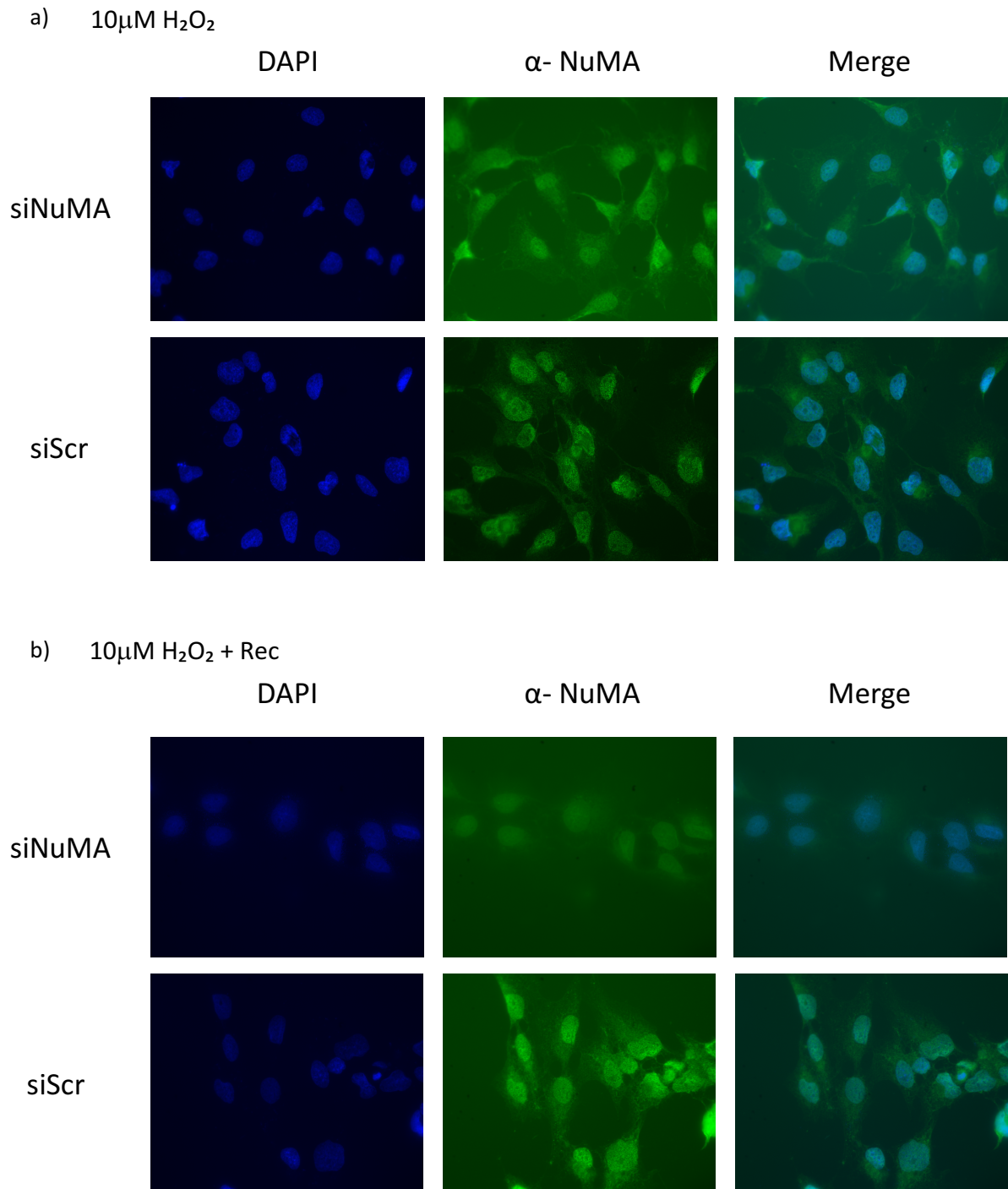


Figure 6.3.2. **Maintained mechanical stress during recovery from H₂O₂ treatment in NuMA depleted cells results in fragmented nuclei.** MRC5 cells were plated onto coverslips before being transfected with specific siRNA to NuMA, or a scrambled (Scr) control and left to incubate for 72 hours. Cells were treated with 10 μ M H₂O₂ for 30 minutes in complete media at 37^oC. Cells were treated with mechanical stress during the incubation period. b) Cells were recovered for 30 minutes in complete media after removal of H₂O₂. During this period, mechanical stress was maintained. The coverslips were mounted on to slides with VectaShield mounting medium with DAPI, and processed using a fluorescence microscope, at magnification 63 (63x).

Figure 6.3.2 a) shows representative immunofluorescence images of MRC5 cells treated with 10 μ M H₂O₂ whilst mechanical stress was applied. There is decreased NuMA signal in the NuMA depleted cells, as expected. The siScr cells show that NuMA signal is diffuse across the cells, with NuMA detected in both the nucleus and the cytoplasm. It appears that there is a greater localisation of NuMA in the nuclei in the siScr condition, compared to the NuMA depleted condition. This was also observed in the CPT samples. There is little difference in respective cell conditions when comparing the H₂O₂ samples to the mock or CPT samples in figure 6.3.1. As in figure 6.3.1, in both a) and b) the blue (DAPI) and green channel (α -NuMA) images were exposed for the same length of time (4ms and 250ms respectively). b) shows representative immunofluorescence images of MRC5 cells treated with 10 μ M H₂O₂ whilst mechanical stress was applied, before recovering cells in media with mechanical stress re-applied. After maintained mechanical stress, the NuMA signal is decreased to a greater level than previously observed in the NuMA knockdown condition, with the NuMA signal in the siScr cells of a similar level to those shown in the DMSO, CPT and H₂O₂ conditions. It is also noticeable that the NuMA depleted cells appear to have fragmented nuclei. This is inferred due to the DAPI staining of nuclear material outside the nucleus. This is not detectable in the siScr condition.

Another technique which was initially employed in the hope to further understand what was preventing the repair of cells treated with H₂O₂ and continued mechanical stress was that of live cell imaging. The optimisation of this technique for the specific application was very difficult and something which had not been tried in mammalian cells, at least in the El-Khamisy lab, or the King lab. The spinning disk microscope was utilised for all live cell imaging experiments. Due to many unforeseen problems, accurate and reliable data could not be obtained.

6.4 Discussion

The emerging area of the link between biochemical cellular processes and mechanical stresses within a cellular setting was of great interest. This was mainly due to the novel findings relating to the structural protein NuMA. It is known that NuMA is a protein related to lamins. Lamins and lamin-processing defects are recognised to cause a sub-set of diseases called laminopathies, which can result in progeria and genome instability, to name just a few. Initial investigations were tests to establish whether the technique of cell compression developed in the lab of Dr. Jason King was transferrable to a mammalian

cell system, that involved gene silencing and additional genotoxic stresses. To clarify, 'mechanical stress' refers to cells which were subjected to a 30-minute incubation with a specially made plastic insert with an average weight of 7.5g, which applies an average pressure of 0.1kPa. This mechanical stress produces compression of cellular organelles, which can cause cellular blebbing, most commonly within the nucleus. This can affect various cellular processes and can lead to apoptosis, however there is little evidence to show how the blebbing occurs and its biological significance (Funkhouser, et al., 2013). With reference to figure 6.2.1, application of mechanical stress increases the amount of CPT-induced breaks in both the siNuMA and siScr conditions. This increase is of a similar extent in both conditions, suggesting that mechanical stress increases the amount of CPT-induced SSBs regardless of whether NuMA levels are depleted. This means that NuMA depletion doesn't significantly exacerbate the increase in breaks caused by the application of mechanical stress.

Following on from these experiments, H₂O₂ was the chosen drug to induce SSBs. The issue with setting up the experiments as previously explained was that the cells needed to be treated adherently so H₂O₂ dissolved in PBS on ice wasn't an option. The solution to this was to extend the incubation period of H₂O₂ in media, whilst keeping the concentration at 10µM. This allowed for a mirrored experiment with the CPT treatment. One way to overcome the cells' protection against the oxidative damage gained due to the non-enzymatic reaction taking place within the media would be to use the H₂O₂ analogue *tert*-Butyl hydroperoxide (TBH). TBH is known for its greater stability than H₂O₂, however due to the time associated with optimisation of concentration of TBH, H₂O₂ was opted for. Referring to figure 6.2.2, the average comet tails increase in both the NuMA depleted and control cells upon treatment with H₂O₂ and mechanical stress. As was the case with the CPT treated cells, the increase attributed to the application of mechanical stress was not significantly greater in the NuMA depleted cells compared to the control, suggesting that there is no dependence on the knockdown of NuMA in this scenario. As with previous experiments that adopted H₂O₂ as the damaging agent, it was decided to formulate a repair kinetic profile. This involved treating cells with mechanical stress and then allowing cells to recover for 30 minutes either with no additional treatment, or the re-application of mechanical stress during the recovery period. With reference to figure 6.2.3, it is evident that after the initial treatment with mechanical stress, if the stimulus is removed and cells are allowed to recover without stress, around 50% of the NuMA

depleted cells recovered within 30 minutes compared to the control cells, which had around an additional 25% recovery compared to the siNuMA transfected cells. This suggests that cells with depleted levels of NuMA that have been exposed to H₂O₂ and mechanical stress for a period of 30 minutes have a repair defect compared to control when allowed to recover without mechanical stress. This points to a role for NuMA within the setting of repairing oxidative stress-induced breaks exacerbated by mechanical stress. This is backed up further by the cells which were allowed to recover under maintained mechanical stress. This was facilitated by re-applying the inserts to the cells during the 30-minute recovery period. In this situation, it is apparent that the NuMA depleted cells almost wholly fail to recover during the 30-minute incubation period, with only around a 2% reduction in percentage cell survival compared to the maximal damage point (t'_0). This is compared to around 60% of breaks remaining in the control samples. There are more breaks remaining in the control samples when cells were recovered under mechanical stress, however there is a marked reduction in the amount of cells exhibiting damage compared to the NuMA depleted cells. This further suggests that there is an important role for NuMA in the repair of oxidative-induced SSBs which are intensified by the application of continued mechanical stress.

To further investigate the role of NuMA in the repair of CPT- and oxidative-induced SSBs and the lack of repair observed with the maintenance of mechanical stress, immunofluorescence studies were undertaken. One adaptation from the comet assay experiments was the use of a lower dose of CPT. The concentration chosen was 10 μ M, as this had previously been optimised for use in the immunostaining setting. The other conditions were directly comparable to the ones used for the comet assays. The results in figure 6.3.1 show that the NuMA knockdown can be further validated using immunofluorescence. In figure 6.3.1 a) there is an evident reduction in the signal in the siNuMA samples, as shown by the representative images. The reduction in intensity of the NuMA signal in the NuMA knockdown condition is comparable to the siScr condition as the exposure time used to capture the images remained consistent between samples. Figure 6.3.1 b) shows the images of cells treated with CPT. The treatment with CPT initially didn't seem to have much of a difference on the cells, when compared to the DMSO control. Second to the pan reduction of NuMA signal in the knockdown condition, on closer inspection, it appeared that the signal is of equal intensity between the

cytoplasm and the nucleus and hence when the images are merged, it is difficult to detect NuMA signal in the nucleus. This is converse to the siScr condition where it appears the NuMA signal is quite diffuse across both the nucleus and cytoplasm, with a more intense, punctate NuMA signal within the nucleus. As mentioned in 6.3, this may need further investigations as the NuMA signal in the siScr condition is much more intense. Taking this information into account, it is possible that the patterns may be parallel between conditions but as the NuMA signal in the siNuMA condition is heavily reduced it is very difficult to visualise the punctate signal. However, it could be that this punctate configuration after CPT treatment and mechanical stress observed in the siScr condition is the physiological response to stress. In this case, the NuMA knockdown prevents this accumulation in the nucleus. The data shown in figure 6.3.2. a) also supports observation noted in the CPT treated samples. This provides additional sustenance that this could be a physiological process, as two different drug treatments with applied mechanical stress substantiates the same pattern. With reference to figure 6.3.2 b), the cells were treated with H₂O₂ and mechanical stress for a period of 30 minutes, before the removal of the H₂O₂ and the addition of complete media. The cells were then recovered for 30 minutes, under maintained mechanical stress. The results show that there is a heavily reduced signal of NuMA in the siNuMA condition, which is of a greater reduction than the other conditions analysed. The NuMA signal which remains seems to be of equal intensity in the cytoplasm and the nucleus. The NuMA depleted cells may have reduced intensity of NuMA (compared to control) as the cells could be entering programmed cell death. It is possible that with a reduced level of NuMA in the cells that they are not able to cope with the H₂O₂ insult and the maintained mechanical stress and the nuclear blebbing that may be caused as a result and hence they enter apoptosis. In the comparable siScr condition, the pattern observed is very similar to the CPT and H₂O₂ with mechanical stress conditions, with a punctate NuMA expression within the nucleus, which is more intense than in the cytoplasm.

It was alluded to in section 6.3 that there was much time spent attempting live cell imaging experiments to ascertain the cause of the cells lacking repair when levels of NuMA were depleted after the application of mechanical stress. Unfortunately this was to no avail, despite many attempts. Live cell imaging involved plating cells at a very specific density on glass bottomed cell culture plates, or individual wells. The dishes also needed

to be poly-D lysine coated, which also required optimisation. The wells were just large enough to allow for the plastic insert to be placed on the cells, but as the cells were to be assessed whilst still alive, agarose gel disc needed to just cover the glass coverslip. This proved to be a difficult task and with help from a PhD student in the King lab, it was determined that a portion of the cells were not being precisely compressed and hence any results obtained could not be trusted. It was decided to attempt making a thicker agarose disc, with a composition of 2% agarose, which would hopefully raise up the insert and hence apply direct mechanical pressure to the glass cover-slip. However, as the gel insert was denser and smaller, the removal of the inset and the gel in order to image the cells proved too harsh on the cells and resulted in cellular shearing and the removal of a high percentage of the seeded cells. This made analysis almost impossible. Another issue encountered was the staining of nuclei. In immunofluorescence experiments when cells are fixed, DAPI was the stain of choice. However, in order for the DAPI stain to be taken up by the nucleus, cells need to be permeabilised. As the cells were still alive, a different approach needed to be taken. Hoechst 33342 was utilised as this is very cell permeable, however optimisation was required as high concentrations can be cytotoxic. This did however allow for the calculation of the deformation of the nucleus when mechanical stress was applied. Through Z-stack analysis of the cells (parameters set to take a measurement every 5 microns) allowed for the calculation of the height of the nucleus of a compressed cell compared to that of an untreated cell. The calculation pointed to a reduction in the height of the nucleus by around 50%, albeit this may not be trusted evidence as there were issues with the spread of the mechanical stress from the insert. This was due to the insert failing to lie flat on the dish and hence lead to uneven spread of the pressure. This could mean that the cells analysed via Z-stack were being compressed more than the kPa value quoted, or less. This could mean that the 50% decrease in nuclear height could be unrepresentative, and could be a lower or higher value.

Secondly, initial experiments were planned to emulate the exact conditions of the comet assay experiments in a live cell imaging platform. This would hopefully give an indication of what was preventing the cells from recovery. However, the glass dishes required were smaller than standard wells of a 6 well plate and siRNA optimisation needed to be reassessed. It was decided that the knockdown, treatment, compression of the cells and

then staining whilst the cells were still alive would be too difficult, as it hadn't been shown that the NuMA antibody available worked for the experimental output of live cell imaging. It was decided that the easiest way to get further insight into the cells with live cell studies was to create stable cell lines, expressing GFP-NuMA. This was completed, but it was decided that as it would not provide enough specific understanding of why the NuMA depleted cells could not recover after sustained mechanical stress, that these experiments were not a priority. Unfortunately, due to time constraints and the interesting nature of other projects which didn't require as much optimisation, the live cell imaging experiments failed to be followed up.

This aspect of the project is something that, given more time, would be an exciting area to explore. Given that there is such a striking observation with the lack of recovery in cells which are treated with maintained mechanical stress and have depleted levels of NuMA, this is an exciting prospect to gain further insight to.

Chapter 7

General Discussion

7.1 NuMA is involved in SSBR

The initial research into NuMA within a DDR background focused on DSBs and their repair. The data obtained suggested that NuMA depletion did increase the number of foci of both the DSB repair markers, albeit there was only an average increase of 1.69 53BP1 and 2.17 γ H2AX foci per cell when NuMA was depleted. This led to the investigations into the role of NuMA within a SSBR context, using both CPT and H₂O₂ as damaging agents, using alkaline comet as the predominant read-out. The results showed a role for NuMA in CPT-mediated DNA damage, with the depletion of NuMA resulting in greater accumulation of both SSBs and DSBs (El-Khamisy & Caldecott, 2006; El-Khamisy, et al., 2009). The use of H₂O₂ as the damaging agent to induce predominantly single strand breaks (Nakamura, et al., 2003; Ismail, et al., 2005) resulted in NuMA depleted cells exhibiting a slower level of repair of oxidative induced breaks, compared to control. This was illustrated by the higher level of breaks remaining at given time points when NuMA levels had been reduced. Following on from these results, it was decided to determine whether the accumulation of breaks observed in both CPT and H₂O₂ treated cells was dependent on transcription. To study this, the transcription-stalling drug DRB was utilised to halt transcription prior to (and during) the drug treatments. The results were consistent across both treatment types; the stalling of transcription resulted in a reduction of the accumulation of SSBs in NuMA depleted cells. There were still slightly more SSBs present in the condition with NuMA depleted, compared to control, but this was not to a statistically significant level. This result led to the conclusion that the accumulation of SSBs associated with the reduction in NuMA levels is dependent on transcription. Second to testing the effect of the stalling of transcription, the stoppage of replication was also tested. Conversely, the stalling of replication (via treatment with aphidicolin) in cells treated with CPT still resulted in the statistical significance between cells with depleted levels of NuMA and control. This observation was supported by the usage of SH-SY5Y cells, with H₂O₂ as the damaging agent. These cells are able to grow as an undifferentiated population (derived from neuroblastoma tissue), which have the

ability to differentiate into neuronal cells, under specific conditions (Gordon, et al., 2013). The parallel nature of both sets of data confirms that the accumulation of SSBs related to NuMA depletion is independent of replication. This could have a significant impact if engaged in a post-mitotic neuron background. This is due to inability for these types of cells to re-enter the cell cycle and hence damage is not repaired, which can lead to neurodegenerative diseases (Iyama & Wilson, 2013). The implication of NuMA in the setting of SSBs and their repair was further confirmed by the sensitivity of NuMA depleted cells to both CPT and H₂O₂, via assessment by clonogenic survival. These results showed that there was an increase in the sensitivity of cells with decreased levels of NuMA to damaging agents. This result, taken with the previous comet assay data points to a novel role for NuMA in a DNA damage background, with specificity for SSBs and subsequent repair.

7.2 NuMA interacts with TDP1, a key player in resolution of PDBs

After the discovery of a role for NuMA in the repair of SSBs, and given that TDP1 has an important, established role in the resolution of PDBs, it was decided to test for a physical interaction with NuMA, to test if there was a link with SSBR machinery. Co-IP experiments showed a physical interaction between NuMA and TDP1, with the proven interaction of TDP1 and PARP1 being used as a positive control (Das, et al., 2014). A subset of experiments which over-expressed both Myc-TDP1 and GFP-NuMA seemed to exhibit a reduction in PARP1 binding. This led to the hypothesis that perhaps NuMA and PARP1 were competing for the same binding site on TDP1. Following the production of two truncated versions of TDP1 (plasmids containing the residues 150-608 and 168-608 of TDP1, respectively), it was ascertained that the 150-608 section of TDP1 was sufficient to bind both PARP1 and NuMA, however the 168-608 stretch of TDP1 cannot bind PARP1, but is still able to bind NuMA. This suggested that the hypothesis that PARP1 and NuMA were competing for the same binding site was incorrect and that they bind to distinct regions of TDP1. Noting that within the co-IP experiments a physical interaction was detected it was decided to attempt to ascertain whether NuMA and TDP1 were epistatic for the repair of SSBs. This was explored using the tools of alkaline comet assay and clonogenic survival assays. The simultaneous knockdown of both NuMA and TDP1 did not result in a significant increase in accumulation of SSBs or a significantly greater repair defect when either CPT or H₂O₂ was used as the damaging agent, respectively, when

compared to single NuMA/TDP1 knockdown alone. Additional to the use of H₂O₂ alone, DRB was adopted to stall transcription. As found with the NuMA depletion alone, the depletion of TDP1 and the simultaneous knockdown of NuMA and TDP1 after transcription-stalling, there was no longer a statistically significant difference between the knocked-down conditions and control and there was also no significant difference between single and simultaneous knockdowns. Following on from the data suggesting TDP1 and NuMA were epistatic in the repair of SSBs, it was decided to explore this area in greater detail, by adopting the PARP1 inhibitor Olaparib. Olaparib is a catalytic inhibitor of PARP1, and it was hypothesised that if PARP1 was also epistatic for the repair of SSBs and functioned along the same pathway as TDP1 and NuMA then there would be no further sensitivity of NuMA knockdown cells when treated with Olaparib (Zhang, et al., 2011; Murai, et al., 2012; Das, et al., 2014; Alagoz, et al., 2014). The results confirmed the hypothesis and showed that there was no significant difference in the sensitivity of NuMA depleted cells compared with control when treated with Olaparib. As TDP1 functions in the same pathway as PARP1, the hypothesis was formulated that TDP1 depletion or a simultaneous NuMA/TDP1 knockdown would also result in no further sensitivity to Olaparib treatment, when compared with control cells (Zhang, et al., 2011; Das, et al., 2014; Alagoz, et al., 2014).

7.3 Long isoform of NuMA rescues the repair defect observed when NuMA is depleted to a greater extent than the short isoform

Whilst studying the structure of NuMA at a DNA sequence level, it was realised (with reference to UniProt) that there were many different isoforms of NuMA. During the course of the PhD studies, the two major isoforms were studied further. After it was realised that initial overexpression studies in chapter 3 had been carried out with the short isoform (plasmid purchased from Addgene) the cloning of the missing amino acid stretch into the existing short isoform occurred, to create the long isoform of NuMA. Subsequently, mutating residues to make each plasmid resistant to specific siRNA allowed for specific over-expression of each isoform. Comet assay experiments showed that the over-expression of the long isoform of NuMA rescues the repair defect exhibited by NuMA depleted cells. The over-expression of the short isoform of NuMA rescues the repair defect to a lesser extent than the long isoform, despite the much greater level of

over-expression of the shorter isoform, detected via western blotting. This suggests that although the long isoform is very poorly expressed, this level of protein expression enables greater rescue than the short isoform with 45% and 24% of breaks remaining after 30 and 60 minutes of recovery, respectively. This is compared with the short isoform, which exhibited 53% and 33% of breaks remaining after 30 and 60 minutes of recovery, respectively. Clonogenic survival assays confirmed this finding, with the long isoform rescuing the surviving fraction of cells to a similar level of control cells. This rescue was of a significant level, compared with the NuMA depleted cells. The long isoform rescue was also to a significantly greater, when compared with the rescue level exhibited by the short isoform over-expression. This suggested that there was a more pertinent role of the long isoform of NuMA (rather than the short isoform) in SSBR. Following on from the epistasis studies, which established that when NuMA levels were depleted, there was no additional sensitivity to the cells when treated with the PARP1 inhibitor, Olaparib. This result was explained by the pathway already having a defective element (NuMA depletion). This led to the investigation into whether the over-expression of long and short isoforms of NuMA are sensitive to Olaparib. The theory behind this was that through PARP inhibition, there would be suppression of an over-activated pathway upon which cells rely to survive. The results from clonogenic survival assays showed that the over-expression of the long isoform of NuMA was the most sensitive to Olaparib, when comparing with the over-expression of the short isoform and the control (over-expression of GFP-EV). This suggests that the hypothesis of epistasis between NuMA, TDP1 and PARP1 has been further confirmed. More excitingly, it points to a potential role to target NuMA in cancer therapy, as many types of cancer exhibit elevated levels of NuMA, including endometrial cancers and head and neck cancers (Human Protein Atlas; Brüning-Richardson, et al., 2012).

7.4 The globular tail domain of NuMA is sufficient to rescue the repair defect associated with NuMA depletion

Truncated versions of NuMA were produced, in an attempt to narrow down specific regions of the protein involved in SSBR. The data shows that both regions 1348-2115 and 1700-2115 of NuMA when over-expressed selectively (both containing a targeting resistant region) are able to rescue the repair defect associated with the knockdown of

NuMA. Due to the 1348-2115 region encompassing the 1700-2115 region, it was decided to focus on the 1700-2115 region, which is the globular tail domain (Compter, et al., 1992). There is additional work required to further narrow down specific regions within the globular domain which may be essential, or putative residues which facilitate the rescue of the repair defect.

7.5 The deletion of the microtubule binding domain still allows for the rescue of the repair defect associated with the knockdown of NuMA

The well documented role of NuMA is the function of the interaction with microtubules and the facilitation of the correct spindle orientation during mitosis (Radulescu & Cleveland, 2014). For this role to be carried out, the microtubule binding domain (MBD) (residues 1866-1936) is imperative for NuMA's interaction with the mitotic apparatus (Seldin, et al., 2106). It was decided to investigate whether the deletion of the MBD would interfere with the proposed role for NuMA within SSB. Co-IP experiments showed that the deletion of this domain did not perturb the binding of the mutant NuMA to TDP1. Following this, it was hypothesised that the over-expression of the plasmid with the MBD deleted would still facilitate the rescue of the repair defect. This was reflected in the comet assay results. These results indicate that there is a role for NuMA in SSB, even when the domain required for the interaction with microtubules is deleted. This could be classified as a separation of function mutant, however, confirmation that aberrant spindle orientation and/or insufficient tethering of microtubules occurs in this mutant is required.

7.6 Mechanical stress prevents the repair of TOP1-linked and oxidative-induced SSBs

The emerging area of linking structural proteins to biochemical cellular processes was something of interest, especially in the context of mechanical stress in processes such as cytokinesis (Srivastava & Robinson, 2015). This led to the assessment of the effect of mechanical stress on mammalian cells when it was applied additionally to treatment with both CPT and H₂O₂. This was of keen interest as there are many cells within the body which are subjected to mechanical stress, such as endothelial cells which line the blood vessels and skin cells which are the first contact of external mechanical stress, amongst

others (Levy Nogueira, et al., 2015; Goldstein & Sanders, 1998). It has also been detailed that one major hallmark of Hutchinson-Gilford Progeria Syndrome (HGPS) (see section 1.7.3) is the abnormal reaction to mechanical stress, probably due to defective lamin production resulting in an improper extra-cellular matrix (ECM) (Jalouk & Lammerding, 2009; DuFort, et al., 2011). The mechanical stress didn't have a greater effect on NuMA depleted cells when compared with control after 30 minutes of CPT and H₂O₂ treatment. However, when NuMA depleted cells treated with H₂O₂ were recovered for 30 minutes under maintained mechanical stress, there was only a minimal reduction in the percentage breaks still remaining after recovery. Conversely, the control cells exposed to the same conditions recovered around 50% of breaks. This points to a novel role for NuMA in the repair of SSBs induced by H₂O₂ whilst cells are exposed to mechanical stress. Immunofluorescence studies of the H₂O₂ condition with maintained mechanical stress condition showed a reduction of NuMA staining, compared to the NuMA depleted condition which was DMSO treated with 30 minutes of mechanical stress. The recovery of H₂O₂ treated, NuMA depleted cells under mechanical stress also showed fragmented nuclei. This data together suggests there is a possible role for NuMA in the repair of oxidative-induced SSBs which were introduced whilst cells were being compressed. These results could also suggest that the depletion of NuMA along with both chemical and mechanical insults was too much damage for the cell to recover, and they enter apoptosis. The level of NuMA, however is the key factor in this, as control cells could still recover after the application of the same chemical and mechanical stresses.

7.7 Future Work

There are many aspects of the project which, had time permitted, would have been investigated further. Further defining the binding domains of PARP1 and NuMA on TDP1 would have been of interest. The glutamic acid (Glu) at residue 150 on TDP1 could potentially be the putative binding site of PARP1, as Glu residues are the main acceptors of PAR chains and therefore a major site of post-translational modification. Although there are several amino acid residues which are ADP-ribosylated including arginine, lysine and aspartic acid, glutamic acid residues are known to be the primary sites of PARylation (Zhang, et al. 2013). Site directed mutagenesis of this site could allow the disruption of the interaction between TDP1 and PARP1 (due to potential abrogation of

PARylation) and hence narrow down the PARylation site on TDP1. With reference to NuMA, it was shown that NuMA binds to TDP1 within the 168-608 region. The production of additional truncated versions of TDP1 would help to narrow down the binding site of NuMA on TDP1.

Following on from the comet assay experiments exploring the rescue of the repair defect associated with NuMA depletion via the 1700-2115 stretch of NuMA, clonogenic experiments would have been performed in order to further confirm the observation. The finding that the depletion of the MBD still allowed for the rescue of the repair defect associated with the reduction of NuMA levels still requires more attention. It would have been interesting to perform live cell imaging with cells stably expressing NuMA, to see if NuMA still accumulates at the spindle poles during mitosis. As the rescue role is still applicable to the MBD-deficient mutant, it was hypothesised that perhaps the PARylation of glutamic acid residue(s) may be essential for the rescue. The proposed site of PARylation was the glutamic acid residue at amino acid 1993. If there was more time, co-IP experiments would have been performed to see if mutating this site would have perturbed the binding of NuMA to TDP1, before performing comet assays to determine whether this mutation would prevent the rescue of the repair defect.

The association of PARP1 with both TDP1 and NuMA has been shown, however another member of the PARP family, PARP3, has been shown to interact with NuMA in a complex with Tankyrase 1 (Boehler, et al., 2011). PARP3 has also been shown to respond to DSB along with PARP1. Given that there is an association with PARP3 in both spindle assembly and DNA damage settings, experiments could be performed in order to determine whether the PARP3 plays a role in the interaction between TDP1 and NuMA (Boehler, et al., 2011; Vidi, et al., 2014; Aydin, et al., 2014). These experiments could be performed by siRNA knockdown of PARP3 before continuing with a co-IP assay.

Given that it was shown that the repair defect associated with NuMA depletion was dependent on the process of transcription, if time permitted, the genome-wide mapping of the accumulating breaks in NuMA depleted cells would have been performed. The main purpose of this experiment would have been to check to see if the breaks co-localised with sites of transcription, such as co-localisation with RNA polymerase II (Baranello, et al., 2016). This could have been analysed via the experimental processes of TOP1-ChIP (Topoisomerase 1-Chromatin Immunoprecipitation) or γ H2AX-ChIP, with the utilisation

of CPT to trap TOP1 on DNA and a specific inducer of DSB, such as IR, respectively (Baranello, et al., 2016; Seo, et al., 2012; Husain, et al., 2016). The results of the ChIP experiments could have been sequenced and mapped against sites of transcriptional activity, such as promoter sites with the hope to determine the map of the NuMA depletion-associated breaks and give a better idea of which areas these breaks occur (Baranello, et al., 2016).

The mechanical stress section to the project is something which required much more time to further investigate the role of mechanical stress and NuMA's implication in SSBR. As mentioned in chapter 6, efforts to optimise live cell imaging were made. If more time was available, the optimisation process would have been completed and the idea was to ascertain the cellular process in real time. This would have helped elucidate the reason behind the lack of repair when mechanical stress was maintained during recovery.

7.8 Conclusion

To conclude, this project has unveiled a role for the structural protein NuMA in the repair of SSBs, via the tool of gene silencing. As mentioned in chapter 3, a fellow lab member attempted to attain a CRISPR knockout NuMA cells line, to no avail. This may be due to the essential need for NuMA in cellular processes; specific residues in NuMA have been found to be essential in murine embryonic development (Silk, et al., 2009). NuMA has been shown to physically interact with the PDB repair protein TDP1, and function within the same pathways as both TDP1 and PARP. This has the potential for targeting NuMA over-expression in a cancer setting with Olaparib. NuMA has different isoforms, of which the long isoform appears to have a more pronounced role in SSBR, with over-expression able to rescue the repair defect to a greater level than the short isoform. It has also been shown that the globular tail domain of NuMA is sufficient for the rescue of the repair defect, as well as a MBD mutant still being able to perform the rescue. Lastly, it has been shown that there is a role for NuMA in the repair of SSBs when created under mechanical stress.

References

- Abbas, T., and Dutta, A. (2009). p21 in cancer: intricate networks and multiple activities. *Nature Reviews Cancer*, 9(6) pp. 400-414.
- Abbotts, R., and Wilson III, D.M. (2017). Coordination of DNA single strand break repair. *Free Radical Biology and Medicine*, 107 pp. 228-244.
- Abraham, R.T. (2001). Cell cycle checkpoint signaling through the ATM and ATR kinases. *Genes & Development*, 15(17) pp. 2177-2196.
- Alagoz, M., Wells, O., and El-Khamisy, S.F. (2014). TDP1 deficiency sensitizes human cells to base damage via distinct topoisomerase I and PARP mechanisms with potential applications for cancer therapy. *Nucleic Acids Research*, 42(5) pp. 3089-3103.
- Allers, T., and Lichten, M. (2001). Differential timing and control of non-crossover and crossover recombination during meiosis, *Cell*. 106(1) pp. 47-57.
- Ashour, M.E., Atteya, R., and El-Khamisy, S.F. (2015). Topoisomerase-mediated chromosomal break repair: an emerging player in many games. *Nature Reviews. Cancer*, 15(3) pp. 137-151.
- Aydin, Ö.Z., Vermeulen, W., and Lans, H. (2014). ISWI chromatin remodeling complexes in the DNA damage response. *Cell Cycle*, 13(19) pp. 3016-3025.
- Bakr, A., Oing, C., Köcher, S. Borgmann, K., Dornreiter, I., Petersen, C., Dikomey, E., and Mansour, W.Y. (2015). Involvement of ATM in homologous recombination after end resection and RAD51 nucleofilament formation. *Nucleic Acids Research*, 43(6) pp. 3154-3166.
- Baranello, L., Wojtowicz, D., Cui, K., Devaiah, B.N., Chung, H.J., Chan-Salis, K.Y., Guha, R., Wilson, K., Zhang, X., Zhang, H., Piotrowski, J., Thomas, C.J., Singer, D.S., Pugh, B.F., Pommier, Y., Przytycka, T.M., Kouzine, F., Lewis, B.A., Zhao, K., and Levens, D. (2016). RNA Polymerase II Regulates Topoisomerase 1 Activity to Favor Efficient Transcription. *Cell*, 165(2) pp. 357-371.
- Baranovskiy, A.G., Babayeva, N.D., Suwa, Y., Gu, J., Pavlov, Y.I., and Tahirov, T.H. (2014) Structural basis for inhibition of DNA replication by aphidicolin. *Nucleic Acids Research*, 42(22) pp. 14013-14021.
- Barboro, P., D'Arrigo, C., Diaspro, A., Mormino, M., Alberti, I., Parodi, S., Patrone, E., and Balbi, C. (2002). Unraveling the organization of the internal nuclear matrix: RNA-dependent anchoring of NuMA to a lamin scaffold. *Experimental Cell Research*, 279(2) pp. 202-218.
- Baum, B., and Kunda, P. (2005). Actin Nucleation: Spire — Actin Nucleator in a Class of Its Own. *Current Biology*, 15(8) pp. R305-R308.
- Baumli, S., Endicott, J.A., and Johnson, L.N. (2010). Halogen Bonds Form the Basis for Selective P-TEFb Inhibition by DRB. *Chemistry and Biology*, 17(9) pp. 931-936.
- Belin, B.J., Lee, T., and Mullins, R.D. (2015). DNA damage induces nuclear actin filament assembly by Formin -2 and Spire-1/2 that promotes efficient DNA repair. *Elife*, 4: e07735.

- Beranek, D.T. (1990). Distribution of methyl and ethyl adducts following alkylation with monofunctional alkylating agents. *Mutation Research*, 231(1) pp. 11-30.
- Bermejo, R., Doksani, Y., Capra, T., Katou, Y-K., Tanaka, H., Shirahige, K., and Foiani, M. (2007). Top1- and Top2-mediated topological transitions at replication forks ensure fork progression and stability and prevent DNA damage checkpoint activation. *Genes & Development*, 21(15) pp. 1921-1936.
- Blower, M.D., Nachury, M., Heald, R., and Weis, K. (2005). A Rae1-containing ribonucleoprotein complex is required for mitotic spindle assembly. *Cell*, 121(2) pp. 223-234.
- Boehler, C., Gauthier, L.R., Mortusewicz, Biard, D.S., Saliou, J.M., Bresson, A., Sanglier-Cianferani, S., Smith, S., Schreiber, V., Boussin, F., and Dantzer, F. (2011). Poly(ADP-ribose) polymerase 3 (PARP3), a newcomer in cellular response to DNA damage and mitotic progression. *Proceedings of the National Academy of Sciences of the United States of America*, 108(7) pp. 2783-2788.
- Bohgaki, T., Bohgaki, M., and Hakem, R. (2010). DNA double strand break signaling and human disorders. *Genome Integrity*, 1(1): 15.
- Broers, J.L., Ramaekers, F.C., Bonne, G., Yaou, R.B., and Hutchison, C.J. (2006). Nuclear lamins: laminopathies and their role in premature ageing. *Physiological Reviews*, 86(3), pp. 967-1008.
- Brooks, C.L., and Gu, W. (2010). New insights into p53 activation. *Cell Research*, 20(6) pp. 614-621.
- Brüning-Richardson, A., Bond, J., Alsiary, R., Richardson, J., Cairns, D.A., McCormac, L., Hutson, R., Burns, P.A., Wilkinson, N., Hall, G.D., Morrison, E.E., and Bell, S.M. (2012). NuMA overexpression in epithelial ovarian cancer. *PLoS One*, 7(6): e38945.
- Bugreev, D.V., Huang, F., Mazina, O.M., Pezza, R.J., Voloshin, O.N., Daniel Camerini-Otero, R., and Mazin, A.V. (2014). HOP2-MND1 modulates RAD51 binding to nucleotides and DNA. *Nature Communications*, 5; 4198.
- Cadet, J., Davies, K.J.A., Medeiros, H.G., Di Mascio, P., and Wagner, J.R. (2017). Formation and repair of oxidatively generated damage in cellular DNA. *Free Radical Biology and Medicine*, 107 pp. 13-34.
- Caldecott, K.W. (2008). Single-strand break repair and genetic disease. *Nature Reviews. Genetics*, 9(8) pp. 619-631.
- Cannan, W.J., Pederson, D.S. (2016). Mechanisms and Consequences of Double-Strand DNA Break Formation in Chromatin. *Journal of Cellular Physiology*, 231(1) pp. 3-14.
- Ceccaldi, R., Parmar, K., Mouly, E., Delord, M., Kim, J.M., Regairaz, M., Pla, M., Vasquez, N., Zhang, Q.S., Pondarre, C., Peffault de Latour, R., Gluckman, E., Cavazzana-Calvo, M., Leblanc, T., Larghero, J., Grompe, M., Socié, G., D'Andrea, A.D., and Soulier, J. (2012). Bone marrow failure in Fanconi anemia is triggered by an exacerbated p53/p21 DNA damage response that impairs hematopoietic stem and progenitor cells. *Cell Stem Cell*, 11(1) pp. 36-49.
- Champoux, J.J. (2001). DNA topoisomerases: structure, function, and mechanism. *Annual Review of Biochemistry*, 70: pp.369-413.

- Chang, H.H.Y., Pannunzio, N.R., Adachi, N., and Lieber, M.R. (2017). Non-homologous DNA end joining and alternative pathways to double-strand break repair. *Nature Reviews. Molecular Cell Biology*, 18(8) pp. 495-506.
- Chang, W., Dynek, J.N., and Smith, S. (2005). NuMA is a major acceptor of poly(ADP-ribose)ylation by tankyrase 1 in mitosis. *The Biochemical Journal*, 391(Pt 2) pp. 177-184.
- Chapman, J.R., Taylor, M.R.G., and Boulton, S.J. (2012). Playing the End Game: DNA Double-Strand Break Repair Pathway Choice. *Molecular Cell*, 47(4) pp. 497-510.
- Cheung, V.G., and Ewens, W.J. (2006). Heterozygous carriers of Nijmegen Breakage Syndrome have a distinct gene expression phenotype. *Genome Research*. 16(8) pp. 973-979.
- Chiang, S.C., Carroll, J., and El-Khamisy, S.F. (2010). TDP1 serine 81 promotes interaction with DNA ligase IIIalpha and facilitates cell survival following DNA damage. *Cell Cycle*, 9(3) pp. 588-595.
- Chiang, Y.J., Hsiao, S.J., Yver, D., Cushman, S.W., Tessarollo, L., Smith, S., and Hodes, R.J. (2008). Tankyrase 1 and Tankyrase 2 Are Essential but Redundant for Mouse Embryonic Development. *PLoS One*, 3(7): e2639.
- Ciccia, A., and Elledge, S.J. (2010). The DNA damage response: making it safe to play with knives. *Molecular Cell*, 40(2) pp. 179-204.
- Cleaver, J. E., Feeney, L., and Revet, I. (2011). Phosphorylated H2Ax is not an unambiguous marker for DNA double-strand breaks, *Cell Cycle*, 10(19), pp. 3223-3224
- Cleveland, D.W. (1995). NuMA: a protein involved in nuclear structure, spindle assembly, and nuclear re-formation. *Trends in Cell Biology*, 5(2) pp. 60-64.
- Collins, A.R., Oscoz, A.A., Brunborg, G., Gaivão, I., Giovannelli, L., Kruszewski, M., Smith, C.C., and Štětina, R. (2008). The comet assay: topical issues. *Mutagenesis*, 23(3) pp. 143-151.
- Cooper, D.N., Mort, M., Stenson, P.D., Ball, E.V., and Chuzhanova, N.A. (2010). Methylation-mediated deamination of 5-methylcytosine appears to give rise to mutations causing human inherited disease in CpNpG trinucleotides, as well as in CpG dinucleotides. *Human Genomics*, 4(6) pp. 406-410.
- Cristini, A., Park, J-H., Capranico, G., Legube, G., Favre, G., and Sordet, O. (2016) DNA-PK triggers histone ubiquitination and signaling in response to DNA double-strand breaks produced during the repair of transcription-blocking topoisomerase I lesions. *Nucleic Acids Research*, 44(3) pp. 1161-1178.
- Cui, H., Kong, Y., and Zhang, H. (2012). Oxidative Stress, Mitochondrial Dysfunction, and Aging. *Journal of Signal Transduction*, 2012: 646354.
- Curtin, N.J. (2005). PARP inhibitors for cancer therapy. *Expert reviews in Molecular Medicine*, 7(4) pp. 1-20.

- de Boer, J., and Hoeijmakers, H.J. (2000). Nucleotide excision repair and human syndromes. *Carcinogenesis*, 21(3) pp. 453-460.
- De Bont, R., and van Larebeke, N. (2004). Endogenous DNA damage in humans: a review of quantitative data. *Mutagenesis*, 9(3) pp. 169-185.
- de Laat, W.L., Jaspers, N.G., Hoeijmakers, J.H. (1999). Molecular mechanism of nucleotide excision repair. *Genes & Development*, 13(7) pp. 768-785.
- De Lorenzo, S.B., Patel, A.G., Hurley, R.M., and Kaufmann, S.H. (2013). The Elephant and the Blind Men: Making Sense of PARP Inhibitors in Homologous Recombination Deficient Tumor Cells. *Frontiers in Oncology*, 3: 228.
- Das, B.B., Antony, S., Gupta, S., Dexheimer, T.S., Redon, C.E., Garfield, S., Shiloh, Y., and Pommier, Y. (2009). Optimal function of the DNA repair enzyme TDP1 requires its phosphorylation by ATM and/or DNA-PK. *The EMBO Journal*, 28(23) pp.3667-3680.
- Das, B.B., Dexheimer, T.S., Maddali, K., and Pommier, Y. (2010). Role of tyrosyl-DNA phosphodiesterase (TDP1) in mitochondria. *Proceedings of the National Academy of Sciences of the United States of America*, 107(46), pp. 19790–19795.
- Das, B.B., Huang, S.Y.N., Murai, J., Rehman, I., Amé, J.C., Sengupta, S., Das, S.K., Majumdar, P., Zhang, H., Biard, D., Majumder, H.K., Schreiber, V., and Pommier, Y. (2014). PARP1–TDP1 coupling for the repair of topoisomerase I-induced DNA damage. *Nucleic Acids Research*, 42(7) pp. 4434-4449.
- Deans, A.J., and West, S.C. (2011). DNA interstrand crosslink repair and cancer. *Nature Reviews Cancer*, 11(7) pp. 467-480.
- Denissenko, M.F., Pao, A., Pfeifer, G.P., and Tang, M. (1998). Slow repair of bulky DNA adducts along the nontranscribed strand of the human p53 gene may explain the strand bias of transversion mutations in cancers. *Oncogene*, 16(10) pp. 1241-1247.
- Desai, S.D., Zhang, H., Rodriguez-Bauman, A., Yang, J.M., Wu, X., Gounder, M.K., Rubin, E.H., and Liu, L.F. (2003). Transcription-dependent degradation of topoisomerase I-DNA covalent complexes. *Molecular and Cellular Biology*, 23(7) pp. 2341-2350.
- Dexheimer, T.S., Antony, S., Marchand, C., and Pommier, Y. (2008). Tyrosyl-DNA Phosphodiesterase as a Target for Anticancer Therapy. *Anti-cancer agents in medicinal chemistry*, 8(4) pp. 381-389.
- Ding, X.L., Yang, X., Liang, G., and Wang, K. (2016). Isoform switching and exon skipping induced by the DNA methylation inhibitor 5-Aza-2'-deoxycytidine. *Scientific Reports*, 6: 24545.
- Dominguez, R., and Holmes, K.C. (2011). Actin Structure and Function. *Annual Review of Biophysics*, 40 pp. 169-186.
- Drabløs, F., Feyzi, E., Aas, P.A., Vaagbø, C.B., Kavli, B., Bratlie, M.S., Peña-Díaz, J., Otterlei, M., Slupphaug, G., Krokan, H.E. (2004). Alkylation damage in DNA and RNA- repair mechanisms and medical significance. *DNA Repair*, 3(11) pp. 1389-1407.
- DuFort, C.C., Paszek, M.J., and Weaver, V.M. (2011). Balancing forces: architectural control of mechanotransduction. *Nature Reviews. Molecular Cell Biology*. 12(5) pp. 308-319.

Edenberg, E.R., Downey, M., and Toczyski, D. (2014). Polymerase stalling during replication, transcription and translation. *Current Biology*, 24(10) pp. R445-R452.

Ehrenhofer-Murray, A.E. (2004). Chromatin dynamics at DNA replication, transcription and repair. *European Journal of Biochemistry*, 271(12) pp. 2335-2349.

El-Khamisy, S.F., Saifi, G.M., Weinfeld, M., Johansson, F., Helleday, T., Lupski, J.R., and Caldecott, K.W. (2005). Defective DNA single-strand break repair in spinocerebellar ataxia with axonal neuropathy-1. *Nature*, 434(7029) pp. 108-113.

El-Khamisy, S.F., and Caldecott, K.W. (2006). TDP1-dependent DNA single-strand break repair and neurodegeneration. *Mutagenesis*, 21(4) pp. 219-224.

El-Khamisy, S.F., Katyal, S., Patel, P., Ju, L., McKinnon, P., and Caldecott, K.W. (2009). Synergistic decrease of DNA single-strand break repair rates in mouse neural cells lacking both Tdp1 and aprataxin. *DNA Repair*, 8(6) pp. 760-766.

Fairbairn, D.W., Olive, P.L., and O'Neill, K.L. (1995). The comet assay: a comprehensive review. *Mutation Research*, 339(1) pp. 37-59.

Falck, J., Mailand, N., Syljuåsen, R.G., Bartek, J., and Lukas, J. (2001). The ATM-Chk2-Cdc25A checkpoint pathway guards against radioresistant DNA synthesis. *Nature*, 410(6830) pp. 842-847.

Felgentreff, K., Du, L., Weinacht, K.G., Dobbs, K., Bartish, M., Giliani, S., Schlaeger, T., DeVine, A., Schambach, A., Woodbine, L.J., Davies, G., Baxi, S.N., van der Burg, M., Bleesing, J., Gennery, A., Manis, J., Pan-hammarström, Q., and Notarangelo, L.D. (2014). Differential role of nonhomologous end joining factors in the generation, DNA damage response, and myeloid differentiation of human induced pluripotent stem cells. *Proceedings of the National Academy of Sciences of the United States of America*, 111(24) pp. 8889-8894.

Fernández-Marcelo, T., Frías, C., Pascua, I., de Juan, C., Head, J., Gómez, A., Hernando, F., Jarabo, J.R., Díaz-Rubio, E., Torres, A.J., Rouleau, M., Benito, M., and Iniesta, P. (2014). Poly (ADP-ribose) polymerase 3 (PARP3), a potential repressor of telomerase activity. *Journal of Experimental and Clinical Cancer Research*, 33: 19.

Frade, J.M., and Ovejero-Benito, M.C. (2015) Neuronal cell cycle: the neuron itself and its circumstances. *Cell Cycle*, 14(5) pp. 712-720.

French, S.L., Sikes, M.L., Hontz, R.D., Osheim, Y.N., Lambert, T.E., El Hage, A., Smith, M.M., Tollervey, D., Smith, J.S., and Beyer, A.L. (2011). Distinguishing the Roles of Topoisomerases I and II in Relief of Transcription-Induced Torsional Stress in Yeast rRNA Genes. *Molecular and Cell Biology*, 31(3) pp. 482-494.

Freudenthal, B.D., Beard, W.A., Shock, D.D., and Wilson, S.H. (2013). Observing a DNA Polymerase Choose Right from Wrong. *Cell*, 154(1) pp. 157-168.

Fronza, G., and Gold, B. (2004). The biological effects of N3-methyladenine. *Journal of Cellular Biochemistry*, 91(2) pp. 250-257.

Funkhouser, C.M., Sknepnek, R., Shimi, T., Goldman, A.E., Goldman, R.D., and Olvera de la Cruz, M. (2013). Mechanical model of blebbing in nuclear lamin meshworks. *Proceedings of the National Academy of Sciences of the United States of America*, 110(9) pp. 3248-3253.

- García-Muse, T., and Aguilera, A. (2016). Transcription-replication conflicts: how they occur and how they are resolved. *Nature Reviews. Molecular Cell Biology*, 17(9) pp. 553-563.
- Garner, E., and Smogorzewska, A. (2011). Ubiquitylation and the Fanconi anemia pathway. *FEBS Letters*, 585(18) pp. 2853-2860.
- Gary, R., Kim, K., Cornelius, H.L., Park, M.S., and Matsumoto, Y. (1999). Proliferating cell nuclear antigen facilitates excision in long-patch base excision repair. *The Journal of Biological Chemistry*, 274(7) pp. 4354-4363.
- Gates, K.S. (2009). An Overview of Chemical Processes That Damage Cellular DNA: Spontaneous Hydrolysis, Alkylation, and Reactions with Radicals. *Chemical Research in Toxicology*, 22(11) pp. 1747-1760.
- Ghilarov, D., and Shkundina, I. (2012). DNA topoisomerases and their functions in a cell. *Molecular Biology*, 46(1) pp. 47-57.
- Ghosh, S., and Zhou, Z. (2014). Genetics of aging, progeria and lamin disorders. *Current Opinion in Genetics and Development*, 26, pp. 41-46.
- Goldstein, B., and Sanders, J. (1998). Skin response to repetitive mechanical stress: A new experimental model in pig. *Archives of Physical Medicine and Rehabilitation*, 79(3) pp. 265-272.
- Gordon, J., Amini, S., and White, M.K. (2013). General overview of neuronal cell culture. *Methods in Molecular Biology*, 1078: 1-8.
- Gruenbaum, Y., and Foisner, R., (2015). Lamins: nuclear intermediate filament proteins with fundamental functions in nuclear mechanics and genome regulation. *Annual Review of Biochemistry*, 84; pp. 131-164.
- Groh, M., and Gromak, N. (2014). Out of balance: R-loops in human disease. *PLoS Genetics*, 10(9): e1004630.
- Hakem, R. (2008). DNA-damage repair; the good, the bad, and the ugly. *The EMBO Journal*, 27(4) pp. 589-605.
- Hang, B. (2010). Formation and Repair of Tobacco Carcinogen-Derived Bulky DNA Adducts. *Journal of Nucleic Acids*, 2010: 709521.
- Harel, A., and Forbes, D.J. (2004). Importin beta: conducting a much larger cellular symphony. *Molecular Cell*, 16(3) pp. 319-330.
- Haren, L., and Merdes, A. (2002). Direct binding of NuMA to tubulin is mediated by a novel sequence motif in the tail domain that bundles and stabilizes microtubules. *Journal of Cell Science*, 115(Pt 9) pp. 1815-1824.
- Hawkins, A.J., Subler, M.A., Akopiants, K., Wiley, J.L., Taylor, S.M., Rice, A.C., Windle, J.J., Valerie, K., and Povirk, L.F. (2009). In vitro complementation of Tdp1 deficiency indicates a stabilized enzyme-DNA adduct from tyrosyl but not glycolate lesions as a consequence of the SCAN1 mutation. *DNA Repair*, 8(5) pp. 654-663.
- Haynes, B., Saadat, N., Myung, B., and Shekhar, M.P. (2015). Crosstalk between Translesion Synthesis, Fanconi Anemia Network, and Homologous Recombination Repair Pathways in Interstrand DNA Crosslink Repair and Development of Chemoresistance. *Mutation Research. Reviews in Mutation Research*, 763: pp. 258-266.

- Hedge, M.L., Hazra, T.K., and Mitra, S. (2008). Early steps in the DNA base excision/single strand interruption repair pathway in mammalian cells. *Cell Research*, 18(1) pp. 27-47.
- Hentze, H., Latta, M., Küntzle, G., Dhakshinamoorthy, S., Ng, P.Y., Porter, A.G., and Wendel, A. (2004). Topoisomerase inhibitor camptothecin sensitizes mouse hepatocytes in vitro and in vivo to TNF-mediated apoptosis. *Hepatology*, 39(5) pp. 1311-1320.
- Holmström, K.M., Finkel, T. (2014). Cellular mechanisms and physiological consequences of redox-dependent signalling. *Nature Reviews. Molecular Cell Biology*, 15(6). pp. 411-421.
- Hombauer, H., Campbell, C.S., Smith, C.E., Desai, A., and Kolodner, R.D. (2011). Visualization of eukaryotic DNA mismatch repair reveals distinct recognition and repair intermediates. *Cell*, 147(5) pp. 1040-1053.
- Hong, Z., Jiang, J., Hashiguchi, K., Hoshi, M., Lan, L., and Yasui, A. (2008). Recruitment of mismatch repair proteins to the site of DNA damage in human cells. *Journal of Cell Science*, 121(19) pp. 3146-3154.
- Hsieh, P., and Yamane, K. (2008). DNA mismatch repair: molecular mechanism, cancer, and ageing. *Mechanisms of ageing and development*, 129(7-8) pp. 391-407.
- Huang, S.N., Pommier, Y., and Marchand, C. (2011). Tyrosyl-DNA Phosphodiesterase 1 (Tdp1) inhibitors. *Expert Opinion on Therapeutic Patents*, 21(9) pp.1285-1292.
- Hubert Jr, L., Lin, Y., Dion, V., and Wilson, J.H. (2011). Topoisomerase 1 and Single-Strand Break Repair Modulate Transcription-Induced CAG Repeat Contraction in Human Cells. *Molecular and Cellular Biology*, 31(15) pp. 3105-3112.
- Hudson, J.J., Chiang, S.C., Wells, O.S., Rookyard, C., and El-Khamisy, S.F. (2012). SUMO modification of the neuroprotective protein TDP1 facilitates chromosomal single-strand break repair. *Nature Communications*, 3: 733.
- Husain, A., Begum, N.A., Taniguchi, T., Taniguchi, H., Kobayashi, M., Honjo, T. (2016). Chromatin remodeller SMARCA4 recruits topoisomerase 1 and suppresses transcription-associated genomic instability. *Nature Communications*, 7: 10549.
- Ikejima, M., Noguchi, S., Yamashita, R., Ogura, T., Sugimura, T., Gill, D.M., and Miwa, M. (1990). The zinc fingers of human poly(ADP-ribose) polymerase are differentially required for the recognition of DNA breaks and nicks and the consequent enzyme activation. Other structures recognize intact DNA. *The Journal of Biological Chemistry*, 265(35) pp. 21907-21913.
- Interthal, H., Pouliot, J.J., and Champoux, J.J. (2001). The tyrosyl-DNA phosphodiesterase Tdp1 is a member of the phospholipase D superfamily. *Proceedings of the National Academy of Sciences of the United States of America*, 98(21) pp. 12009-12014.
- Ismail, I.H., Nyström, S., Nygren, J., and Hammarsten, O. (2005). Activation of ATM by DNA strand break-inducing agents correlates closely with the number of DNA double-strand breaks. *The Journal of Biological Chemistry*, 280(6) pp. 4649-4655.
- Jaalouk, D.E., and Lammerding, J. (2009). Mechanotransduction gone awry. *Nature Reviews. Molecular Cell Biology*, 10(1) pp. 63-73.

- Jackson, S.P., and Bartek, J. (2009). The DNA-damage response in human biology and disease. *Nature*, 461(7267) pp. 1071-1078.
- Jacobs, A.L., and Schär, P. (2012). DNA glycosylases: in DNA repair and beyond. *Chromosoma*, 121(1) pp. 1-20.
- Jasin, M., and Rothstein, R. (2013). Repair of Strand Breaks by Homologous Recombination. *Cold Spring Harbor Perspectives in Biology*, 5(11): a012740.
- Kakarougkas, A., Ismail, A., Klement, K., Goodarzi, A.A., Conrad, S., Freire, R., Shibata, A., Lobrich, M., and Jeggo, P.A. (2013). Opposing roles for 53BP1 during homologous recombination. *Nucleic Acids Research*, 41(21) pp. 9719-9731.
- Kamat, A.K., Rocchi, M., Smith, D.I., and Miller, O.J. (1993). Lamin A/C gene and a related sequence map to human chromosomes 1q12.1-q23 and 10. *Somatic Cell and Molecular Genetics*, 19(2) pp. 203-208.
- Kass, E.M., Helgadottir, H.R., Chen, C.C., Barbera, M., Wang, R., Westermarck, U.K., Ludwig, T., Moynahan, M.E., and Jasin, M. (2013). Double-strand break repair by homologous recombination in primary mouse somatic cells requires BRCA1 but not the ATM kinase. *Proceedings of the National Academy of Sciences of the United States of America*, 110(14) pp. 5564-5569.
- Kastan, M.B., and Bartek, J. (2004). Cell-cycle checkpoints and cancer. *Nature*, 432(7015) pp. 316-323.
- Katyal, S., El-Khamisy, S.F., Russell, H.R., Li, Y., Ju, L., Caldecott, K.W., and McKinnon, P.J. (2007). TDP1 facilitates chromosomal single-strand break repair in neurons and is neuroprotective in vivo. *The EMBO Journal*, 26(22) pp. 4720-4731.
- Kim, Y.J., and Wilson III, D.M. (2012). Overview of base excision repair biochemistry. *Current Molecular Pharmacology*, 5(1) pp. 3-13.
- Kingsbury, W.D., Boehm, J.C., Jakas, D.R., Holden, K.G., Hecht, S.M., Gallagher, G., Caranfa, M.J., McCabe, F.L., Faucette, L.F., Johnson, R.K., and Hertzberg, R.P. (1991). Synthesis of water-soluble (aminoalkyl)camptothecin analogs: inhibition of topoisomerase I and antitumor activity. *Journal of Medicinal Chemistry*, 34(1) pp. 98-107.
- Klapacz, J., Meira, L.B., Luchetti, D.G., Calvo, J.A., Bronson, R.T., Edelman, W., and Samson, L.D. (2009). O6-methylguanine induced death involves exonuclease 1 as well as DNA mismatch recognition in vivo. *Proceedings of the National Academy of Sciences of the United States of America*, 106(2) pp. 567-581.
- Knezevic, C.E., Wright, G., Rix, L.L.R., Kim, W., Kuenzi, B.M., Luo, Y., Watters, J.M., Koomen, J.M., Haura, E.B., Monteiro, A.N., Radu, C., Lawrence, H.R., and Rix, U. (2016). Proteome-wide Profiling of Clinical PARP Inhibitors Reveals Compound-Specific Secondary Targets. *Cell Chemical Biology*, 23(12) pp. 1490-1503.
- Krishnakumar, R., and Kraus, W.L. (2010). The PARP side of the nucleus: molecular actions, physiological outcomes, and clinical targets. *Molecular Cell*, 39(1) pp. 8-24.
- Köhne, C.H., De Greve, J., Hartmann, J.T., Lang, I., Vergauwe, P., Becker, K., Braumann, D., Joosens, E., Müller, L., Janssens, J., Bokemeyer, C., Reimer, P., Link, H., Späth-Schwalbe, E., Wilke, H.J., Bleiberg, H., Van Den Brande, J., Debois, M., Bethe, U., and Van Cutsem, E. (2008). Irinotecan combined with infusional 5-fluorouracil/folinic acid or capecitabine

plus celecoxib or placebo in the first-line treatment of patients with metastatic colorectal cancer. EORTC study 40015. *Annals of Oncology*, 19(5) pp. 920-926.

Kotak, S., Busso, C., and Gönczy, P. (2013). NuMA phosphorylation by CDK1 couples mitotic progression with cortical dynein function. *The EMBO Journal*, 32(18) pp. 2517-2529.

Lassmann, M., Hänscheid, H., Gassen, D., Biko, J., Meineke, V., Reiners, C., and Scherthan, H. (2010). In Vivo Formation of γ -H2AX and 53BP1 DNA Repair Foci in Blood Cells After Radioiodine Therapy of Differentiated Thyroid Cancer. *The Journal of Nuclear Medicine*, 51(8), pp.1318-25.

Lee, A.Y., Chiba, T., Truong, L.N. Cheng, A.N., Do, J., Cho, M.J., Chen, L., Wu, X. (2012). Dbf4 is a direct downstream target of ataxia telangiectasia mutated (ATM) and ataxia telangiectasia and Rad3-related (ATR) protein to regulate intra-S-phase checkpoint. *The Journal of Biological Chemistry*, 287(4) pp. 2531-2543.

Legarza, K., and Yang, L.X. (2006). New molecular mechanisms of action of camptothecin-type drugs. *Anticancer Research*, 26(5A) pp. 3301-3305.

Levy Nogueira, M., da Veiga Moreira, J., Baronzio, G.F., Dubois, B., Steyaert, J.M., and Schwartz, L. (2015). Mechanical Stress as the Common Denominator between Chronic Inflammation, Cancer, and Alzheimer's Disease. *Frontiers in Oncology*, 5: 197.

Li, G.M. (2008). Mechanisms and functions of DNA mismatch repair. *Cell Research*, 18(1) pp. 85-98.

Liao, W., McNutt, M.A., and Zhu, W-G. (2009). The comet assay: A sensitive method for detecting DNA damage in individual cells. *Methods*, 48(1) pp. 46-53.

Lin, K.Y., and Kraus, W.L. (2017). PARP Inhibitors for Cancer Therapy. *Cell*, 169(2), pp. 183.

Lindahl, T., and Nyberg, B. (1972). Rate of depurination of native deoxyribonucleic acid. *Biochemistry*, 11(19) pp. 3610-3618.

Lindahl, T. (1993). Instability and decay of the primary structure of DNA. *Nature*, 362(6422) pp. 709-715.

Lomax, M.E., Gulston, M.K., and O'Neill, P. (2002). Chemical Aspects of Clustered DNA Damage Induction by Ionising Radiation. *Radiation Protection Dosimetry*, 99(1-4) pp. 63-68.

Loseva, O., Jemth, A.S., Bryant, H.E., Schöler, H., Lehtiö, L., Karlberg, T., and Helleday, T. (2010). PARP-3 is a mono-ADP-ribosylase that activates PARP-1 in the absence of DNA. *The Journal of Biological Chemistry*, 285(11) pp. 8054-8060.

Ludérus, M.E., den Blaauwen, J.L., de Smit, O.J., Compton, D.A. and van Driel, R. (1994). Binding of Matrix Attachment Regions to Lamin Polymers Involves Single-Stranded Regions and the Minor Groove. *Molecular and Cellular Biology*, 14(9) pp. 6297-6305.

Luo, Y., Deng, X., Cheng, F., Li, Y., and Qui, J. (2013). SMC1-Mediated Intra-S-Phase Arrest Facilitates Bocavirus DNA Replication. *Journal of Virology*, 87(7) pp. 4017-4032.

- Lydersen, B.K., and Pettijohn, D.E. (1980). Human-specific nuclear protein that associates with the polar region of the mitotic apparatus: distribution in a human/hamster hybrid cell. *Cell*, 22(2 Pt 2) pp. 489 – 499.
- Ma, W., Westmoreland, J.W., Gordenin, D.A., and Resnick, M.A. (2011) Alkylation Base Damage Is Converted into Repairable Double-Strand Breaks and Complex Intermediates in G2 Cells Lacking AP Endonuclease. *PLoS Genetics*, 7(4) e1002059.
- Maréchal, A., and Zou, L. (2013). DNA damage sensing by the ATM and ATR kinases. *Cold Spring Harbor perspectives in biology*, 5(9): a012716.
- Martin, L., Marples, B., Coffey, M., Lawler, M., Hollywood, D., and Marignol, L. (2009). Recognition of O6MeG lesions by MGMT and mismatch repair proficiency may be a prerequisite for low-dose radiation hypersensitivity. *Radiation Research*, 172(4) pp. 405-413.
- Masai, H., Matsumoto, S., You, Z., Yoshizawa-Sugata, N., and Oda, M. (2010). Eukaryotic chromosome DNA replication: where, when and how? *Annual Review of Biochemistry*, 79: pp. 89-130.
- Matos, J., and West, S.C. (2014). Holliday junction resolution: regulation in space and time. *DNA Repair*, 19: pp. 176-181.
- Maynard, S., Schurman, S.H., Harboe, C., de Souza-Pinto, N.C. and Bohr, V.A. (2009). Base excision repair of oxidative DNA damage and association with cancer and aging. *Carcinogenesis*, 30(1) pp. 2-10.
- Meas, R., and Smerdon, M.J. (2016). Nucleosomes determine their own patch size in base excision repair. *Scientific Reports*, 6: 27122.
- Mehta, A., and Haber, J.E. (2014). Sources of DNA Double-Strand Breaks and Models of Recombinational DNA Repair. *Cold Spring Harbor Perspectives in Biology*, 6(9): a016428.
- Melis, J.P., van Steeg, H., and Luijten, M. (2013). Oxidative DNA damage and nucleotide excision repair. *Antioxidants & Redox Signaling*, 18(18) pp. 2409-2419.
- Merdes, A., Heald, R., Samejima, K., Earnshaw, W. C., and Cleveland, D.W. (2000). Formation of Spindle Poles by Dynein/Dynactin-Dependent Transport of Numa. *The Journal of Cell Biology*, 149(4) pp. 851-862.
- Mohammed, M.Z., Vyjayanti, V.N., Laughton, C.A., Dekker, L.V., Fischer, P.M., Wilson III, D.M., Abbotts, R., Shah, S., Patel, P.M., Hickson, I.D., and Madhusudan, S. (2011). Development and evaluation of human AP endonuclease inhibitors in melanoma and glioma cell lines. *British Journal of Cancer*, 104(4) pp. 653-663.
- Mousavi, S.J., and Doweidar, M.H. (2015). Role of Mechanical Cues in Cell Differentiation and Proliferation: A 3D Numerical Model. *PLoS One*, 10(5): e0124529
- Murai, J., Huang, S.Y., Das, B.B., Renaud, A., Zhang, Y., Doroshov, J.H., Ji, J., Takeda, S., and Pommier, Y. (2012). Differential trapping of PARP1 and PARP2 by clinical PARP inhibitors. *Cancer Research*, 72(21) pp. 5588-5599.

- Murai, J., Marchand, C., Shahane, S.A., Sun, H., Huang, R., Zhang, Y., Chergui, A., Ji, J., Doroshov, J.H., Jadhav, A., Takeda, S., Xia, M., and Pommier, Y. (2014). Identification of novel PARP inhibitors using a cell-based TDP1 inhibitory assay in a quantitative high-throughput screening platform. *DNA Repair*, 21 pp.177-182.
- Murakami, H., and Keeney, S. (2008). Regulating the formation of DNA double-strand breaks in meiosis. *Genes & Development*, 22(3) pp. 286-292.
- Musich, P.R., and Zou, Y. (2011). DNA-damage accumulation and replicative arrest in Hutchinson-Gilford progeria syndrome. *Biochemical Society Transactions*, 39(6) pp. 1764-1769.
- Nakamura, J., Purvis, E.R., and Swenberg, J.A. (2003). Micromolar concentrations of hydrogen peroxide induce oxidative DNA lesions more efficiently than millimolar concentrations in mammalian cells. *Nucleic Acids Research*, 31(6) pp. 1790-1795.
- Neil, A.J., Belotserkovskii, B.P., and Hanawalt, P.C. (2012). Transcription Blockage by Bulky End Termini at Single-Strand Breaks in the DNA Template: Differential Effects of 5' and 3' Adducts. *Biochemistry*, 51(44) pp. 8964-8970.
- Nikolova, T., Ensminger, M., Löbrich, M., and Kaina, B. (2010) Homologous recombination protects mammalian cells from replication-associated DNA double-strand breaks arising in response to methyl methanesulfonate. *DNA Repair*, 9(10) pp. 1050-1063.
- Nile, D.L., Rae, C., Hyndman, I.J., Gaze, M.N., and Mairs, R.J. (2016). An evaluation in vitro of PARP-1 inhibitors, rucaparib and olaparib, as radiosensitisers for the treatment of neuroblastoma. *BMC Cancer*. 16:621
- Nilsen, L., Førstrom, R.J., Bjørås, M., and Alseth, I. (2012). AP endonuclease independent repair of abasic sites in *Schizosaccharomyces pombe*. *Nucleic Acids Research*, 40(5) pp. 2000-2009.
- Nitiss, K.C., Malik, M., He, X., White, S.W., and Nitiss, J.L. (2006). Tyrosyl-DNA phosphodiesterase (Tdp1) participates in the repair of Top2-mediated DNA damage. *Proceedings of the National Academy of Sciences of the United States of America*, 103(24) pp. 8953-8958.
- Nitiss, J.L., and Nitiss, K.C. (2013). Tdp2: A Means to Fixing the Ends. *PLoS Genetics*, 9(3): e1003370.
- O'Leary, J., and Muggia, F.M. (1998). Camptothecins: a review of their development and schedules of administration. *European Journal of Cancer*, 34(10) pp. 1500-1508.
- Olive, P.L., and Banáth, J.P. (2006). The comet assay: a method to measure DNA damage in individual cells. *Nature Protocols*, 1(1) pp. 23-29.
- Ostling, O., and Johanson, K.J. (1984). Microelectrophoretic study of radiation-induced DNA damages in individual mammalian cells. *Biochemical and Biophysical Research Communications*, 123(1) pp. 291-298.

- Parsons, J.L., Preston, B.D., O'Connor, T.R., and Dianov, G.L. (2007). DNA polymerase δ -dependent repair of DNA single strand breaks containing 3'-end proximal lesions. *Nucleic Acids Research*, 35(4) pp. 1054-1063.
- Patel, A.G., Flatten, K.S., Schneider, P.A., Dai, N.T., McDonald, J.S., Poirier, G.G., and Kaufmann, S.H. (2012). Enhanced killing of cancer cells by poly(ADP-ribose) polymerase inhibitors and topoisomerase I inhibitors reflects poisoning of both enzymes. *The Journal of Biological Chemistry*, 287(6) pp. 4198-4210.
- Patil, M., Pabla, N., and Dong, Z. (2013). Checkpoint kinase 1 in DNA damage response and cell cycle regulation. *Cellular and molecular life sciences*, 70(21) pp. 4009-4021.
- Peltomäki, P., (2001). Deficient DNA mismatch repair: a common etiologic factor for colon cancer. *Human Molecular Genetics*. 10(7) pp. 735-740.
- Perovanovic, J., Dell'Orso, S., Gnoch, V.F., Jaiswal, J.K., Sartorelli, V., Vigouroux, C., Mamchaoui, K., Mouly, V., Bonne, G., and Hoffman, E.P. (2016). Laminopathies disrupt epigenomic developmental programs and cell fate. *Science Translational Medicine*, 8(335): 335ra58.
- Pfeifer, G.P., You, Y.H., and Besaratinia, A. (2005). Mutations induced by ultraviolet light. *Mutation Research*, 571(1-2) pp. 19-31.
- Pfister, S.X., Ahrabi, S., Zalmas, L.P., Sarkar, S., Aymard, F., Bachrati, C.Z., Helleday, T., Legube, G., La Thangue, N.B., Porter, A.C., and Humphrey, T.C. (2014). SETD2-Dependent Histone H3K36 Trimethylation Is Required for Homologous Recombination Repair and Genome Stability. *Cell Reports*, 7(6) pp. 2008-2016.
- Pileur, F., Andreola, M.L., Dausse, E., Michel, J., Moreau, S., Yamada, H., Gaidamakov, S.A., Crouch, R.J., Toulmé, J.J., and Cazenave, C. (2003). Selective inhibitory DNA aptamers of the human RNase H1. *Nucleic Acids Research*, 31(19) pp. 5776-5788.
- Pommier, Y., Redon, C., Rao, V.A., Seiler, J.A., Sordet, O., Takemura, H., Antony, S., Meng, L., Liao, Z., Kohlhagen, G., Zhang, H., and Kohn, K.W. (2003). Repair of and checkpoint response to topoisomerase I-mediated DNA damage. *Mutation Research*, 532(1-2) pp. 173-203.
- Pommier, Y. (2013). Drugging topoisomerases: lessons and challenges. *ACS Chemical Biology*, 8(1) pp. 82-95.
- Pommier, Y., Huang, S.Y., Gao, R., Das, B.B., Murai, J., and Marchand, C. (2014). Tyrosyl-DNA-phosphodiesterases (TDP1 and TDP2). *DNA Repair*, 19: pp. 114-129.
- Pommier, Y., Sun, Y., Huang, S.N., and Nitiss, J.L. (2016). Roles of eukaryotic topoisomerases in transcription, replication and genomic stability. *Nature Reviews. Molecular Cell Biology*, 17(11) pp. 703-721.
- Prasad, R., Dianov, G.L., Bohr, V.A., and Wilson, S.H. (2000). FEN1 stimulation of DNA polymerase beta mediates an excision step in mammalian long patch base excision repair. *The Journal of Biological Chemistry*, 275(6) pp. 4460-4466.
- Radulescu, A.E., and Cleveland, D.W. (2010). NuMA after 30 years: the Matrix Revisited. *Trends in Cell Biology*, 20(4) pp. 214-222.

- Rastogi, R.P., Richa, Kumar, A., Tyagi, M.B., and Sinha, R.P. (2010). Molecular mechanisms of ultraviolet radiation-induced DNA damage and repair. *Journal of Nucleic Acids*, 2010: 592980.
- Ray Chaudhuri, A., and Nussenzweig, A. (2017). The multifaceted roles of PARP1 in DNA repair and chromatin remodelling. *Nature Reviews. Molecular Cell Biology*, Epub ahead of print.
- Reynolds, P., Cooper, S., Lomax, M., and O'Neill, P. (2015). Disruption of PARP1 function inhibits base excision repair of a sub-set of DNA lesions. *Nucleic Acids Research*, 43(8) pp. 4028-4038.
- Robertson, A.B., Klungland, A., Rogenes, T., and Leiros, I. (2009). DNA repair in mammalian cells: Base excision repair: the long and short of it. *Cellular and Molecular Life Sciences*, 66(6) pp. 981-993.
- Rodgers, K., and McVey, M. (2016). Error-Prone Repair of DNA Double-Strand Breaks. *Journal of Cellular Physiology*, 231(1) pp. 15-24.
- Roedgaard, M., Fredsoe, J., Pedersen, J.M., Bjergbaek, L., and Andersen, A.H. (2015) DNA Topoisomerases Are Required for Preinitiation Complex Assembly during GALGene Activation. *PLoS One*, 10(7): e0132739.
- Rothkamm, K., and Löbrich, M. (2003). Evidence for a lack of DNA double-strand break repair in human cells exposed to very low x-ray doses. *Proceedings of the National Academy of Sciences of the United States of America*, 100(9) pp. 5057-5062.
- Rouleau, M., Patel, A., Hendzel, M.J., Kaufmann, S.H., and Poirier, G.G. (2010). PARP inhibition: PARP1 and beyond. *Nature Reviews. Cancer*, 10(4) pp. 293-301.
- Rulten, S.L., Fisher, A.E., Robert, I., Zuma, M.C., Rouleau, M., Ju, L., Poirier, G., Reina-San-Martin, B., and Caldecott, K.W. (2011). PARP-3 and APLF function together to accelerate nonhomologous end-joining. *Molecular Cell*, 41(1) pp. 33-45.
- Sartori, A.A., Lukas, C., Coates, J., Mistrik, M., Fu, S., Bartek, J., Baer, R., Lukas, J., and Jackson, S.P. (2007). Human CtIP promotes DNA end resection. *Nature*, 450(7169), pp.509-514.
- Sattler, U., Frit, P., Salles, B., and Calsou, P. (2003). Long-patch DNA repair synthesis during base excision repair in mammalian cells. *EMBO Reports*, 4(4) pp. 363-367.
- Sbodio, J.I., and Chi, N.W. (2002). Identification of a tankyrase-binding motif shared by IRAP, TAB182, and human TRF1 but not mouse TRF1. *The Journal of Biological Chemistry*, 277(35) pp. 31887-31892.
- Schärer, O.D. (2005). DNA interstrand crosslinks: natural and drug-induced DNA adducts that induce unique cellular responses. *Chembiochem*, 6(1) pp. 27-32.
- Schärer, O.D. (2013). Nucleotide excision repair in eukaryotes. *Cold Spring Harbor Perspectives in Biology*, 5(10): a01209.
- Schimmel, J., Eifler, K., Sigurösson, J.O., Cuijpers, S.A.G., Hendriks, I.A., Verlaan-de Vries, M., Kelstrup, C.D., Francavilla, C., Medema, R.H., Olsen, J.V., and Vertegaal, A.C. (2014). Uncovering SUMOylation Dynamics during Cell-Cycle Progression Reveals FoxM1 as a Key Mitotic SUMO Target Protein. *Molecular Cell*, 53(6) pp. 1053-1066.

Schneider-Poetsch, T., Ju, J., Eyler, D.E., Dang, Y., Bhat, S., Merrick, W.C., Green, R., Shen, B., and Liu, J.O. (2010) Inhibition of Eukaryotic Translation Elongation by Cycloheximide and Lactimidomycin. *Nature Chemical Biology*, 6(3) pp. 209-217.

Sclafani, R.A., and Holzen, T.M. (2007). Cell cycle regulation of DNA replication. *Annual Review of Genetics*, 41 pp. 237-280.

Seldin, L., Poulson, N.D., Foote, H.P., and Lechler, T. (2013). NuMA localization, stability, and function in spindle orientation involve 4.1 and Cdk1 interactions. *Molecular Biology of the Cell*, 24(23) pp. 3651-3662.

Seldin, L., Muroyama, A., and Lechler, T. (2016). NuMA-microtubule interactions are critical for spindle orientation and the morphogenesis of diverse epidermal structures. *eLife*, 5: e12504.

Seo, J., Kim, S.C., Lee, H.S., Kim, J.K., Shon, H.J., Salleh, N.L., Desai, K.V., Lee, J.H., Kang, E.S., Kim, J.S., and Choi, J.K. (2012). Genome-wide profiles of H2AX and γ -H2AX differentiate endogenous and exogenous DNA damage hotspots in human cells. *Nucleic Acids Research*, 40(13) pp. 5965-5974.

Seo, J.S., Kim, H.N., Kim, S.J., Bang, J., Kim, E.A., Sung, K.S., Yoon, H.J., Yoo, H.Y., and Choi, C.Y. (2014). Cell cycle-dependent SUMO-1 conjugation to nuclear mitotic apparatus protein (NuMA). *Biochemical and Biophysical Research Communications*, 443(1) pp. 259-265.

Shah Punatar, R., Martin, M.J., Wyatt, H.D., Chan, Y.W., and West, S.C. (2017). Resolution of single and double Holliday junction recombination intermediates by GEN1. *Proceedings of the National Academy of Sciences of the United States of America*, 114(3) pp. 443-450.

Shipley, M.M., Mangold, C.A., and Szpara, M.L. (2016). Differentiation of the SH-SY5Y Human Neuroblastoma Cell Line. *Journal of Visualised Experiments*, (108): 53193.

Shrivastav, M., De Haro, L.P., Nickoloff, J.A. (2008). Regulation of DNA double-strand break repair pathway choice. *Cell Research*, 18(1) pp. 134-147.

Silk, A.D., Holland, A.J., and Cleveland, D.W. (2009). Requirements for NuMA in maintenance and establishment of mammalian spindle poles. *The Journal of Cell Biology*, 184(5) pp. 677-690.

Singh, N.P., McCoy, M.T., Tice, R.R., and Schneider, E.L. (1988). A simple technique for quantification of low levels of DNA damage in individual cells. *Experimental Cell Research*, 175(1) pp. 184-191.

Singh, S.K., Szulik, M.W., Ganguly, M., Khutsishvili, I., Stone, M.P., Marky, L.A., and Gold, B. (2011). Characterization of DNA with an 8-oxoguanine modification. *Nucleic Acids Research*, 39(15) pp. 6789-6801.

Sproul, C.D., Rao, S., Ibrahim, J.G., Kaufmann, W.K., and Cordeiro-Stone, M. (2013). Is activation of the intra-S checkpoint in human fibroblasts an important factor in protection against UV-induced mutagenesis? *Cell Cycle*, 12(22) pp. 3555-3563.

- Solier, S., Zhang, Y.W., Ballestrero, A., Pommier, Y., Zoppoli, G. DNA damage response pathways and cell cycle checkpoints in colorectal cancer: current concepts and future perspectives for targeted treatment. *Current cancer drug targets*, 12(4) pp. 356-371.
- Soll, J.M., Sobol, R.W., and Mosammamarast, N. (2017). Regulation of DNA Alkylation Damage Repair: Lessons and Therapeutic Opportunities. *Trends in Biochemical Sciences*, 42(3) pp. 206-218.
- Sørensen, C.S., Syljuåsen, R.G., Falck, J., Schroeder, T., Rønnstrand, L., Khanna, K.K., Zhou, B.B, Bartek, J., and Lukas, J. (2003). Chk1 regulates the S phase checkpoint by coupling the physiological turnover and ionizing radiation-induced accelerated proteolysis of Cdc25A. *Cancer Cell*, 3(3) pp. 247-258.
- Srivastava, V., and Robinson, D.N. (2015). Mechanical stress and network structure drive protein dynamics during cytokinesis. *Current Biology*, 25(5) pp. 663-670.
- Staker, B.L., Hjerrild, K., Feese, M.D., Behnke, C.A. and Stewart, L. (2002). The mechanism of topoisomerase I poisoning by a camptothecin analog. *Proceedings of the National Academy of Sciences of the United States of America*, 99(24), pp. 15387-92
- Stoimenov, I., and Helleday, T. (2009). PCNA on the crossroad of cancer. *Biochemical Society Transactions*, 37(3) pp. 605-613.
- Strumberg, D., Pilon, A.A., Smith, M., Hickey, R., Malkas, L., and Pommier, Y. (2000). Conversion of Topoisomerase I Cleavage Complexes on the Leading Strand of Ribosomal DNA into 5'-Phosphorylated DNA Double-Strand Breaks by Replication Runoff. *Molecular Cell Biology*, 20(11) pp. 3977-3987.
- Swift, J., Ivanovska, I.L., Buxboim, A., Harada, T., Dingal, P.C., Pinter, J., Pajeroski, J.D., Spinler, K.R., Shin, J.W., Tewari, M., Rehfeldt, F., Speicher, D.W., and Discher, D.E. (2013). Nuclear lamin-A scales with tissue stiffness and enhances matrix-directed differentiation. *Science*, 341(6149): 1240104.
- Sykora, P., Croteau, D.L., Bohr, V.A and Wilson III, D.M. (2011). Aprataxin localizes to mitochondria and preserves mitochondrial function. *Proceedings of the National Academy of Sciences of the United States of America*, 108(18) pp. 7437-7442.
- Takahashi, T., Tada, M., Igarashi, S., Koyama, A., Date, H., Yokoseki, A., Shiga, A., Yoshida, Y., Tsuji, S., Nishizawa, M., and Onodera. (2007). Aprataxin, causative gene product for EAOH/AOA1, repairs DNA single-strand breaks with damaged 3'-phosphate and 3'-phosphoglycolate ends. *Nucleic Acids Research*, 35(11) pp. 3797-3809.
- Troxell, B., Zhang, J.J., Bourret, T.J., Zeng, M.Y., Blum, J., Gherardini, F., Hassan, H.M., and Yang, X.F. Pyruvate Protects Pathogenic Spirochetes from H₂O₂ Killing. *PLoS One*, 9(1): e84625.
- Truebestein, L., and Leonard, T.A. (2016). Coiled-coils: The long and short of it. *Bioessays*, 38(9) pp. 903-916.
- Tuduri, S., Crabbé, L., Conti, C., Tourrière, H., Holtgreave-Grez, H., Jauch, A., Pantesco, V., De Vos, J., Thomas, A., Theillet, C., Pommier, Y., Tazi, J., Coquelle, A., and Pasero, P. (2009).

Topoisomerase I suppresses genomic instability by preventing interference between replication and transcription. *Nature Cell Biology*, 11(11) pp. 1315-1324.

Turinetto, V., Porcedda, P., Orlando, L., De Marchi, M., Amoroso, A., and Giachino, C. (2009). The cyclin-dependent kinase inhibitor 5, 6-dichloro-1-beta-D-ribofuranosylbenzimidazole induces nongenotoxic, DNA replication-independent apoptosis of normal and leukemic cells, regardless of their p53 status. *BMC Cancer*, 9: 281.

Uchida, C., Hattori, T., Takahashi, H., Yamamoto, N., Kitagawa, M., and Taya, Y. (2014). Interaction between RB protein and NuMA is required for proper alignment of spindle microtubules. *Genes to Cells*, 19(2) pp. 89-96.

Uziel, T., Lerenthal, Y., Moyal, L., Andegeko, Y., Mittelman, L., and Shiloh, Y. (2003). Requirement of the MRN complex for ATM activation by DNA damage. *The EMBO Journal*. 22(20) pp. 5612-5621.

Vermeulen, K., Van Bockstaele, D.R., and Berneman, Z.N. (2003). The cell cycle: a review of regulation, deregulation and therapeutic targets in cancer. *Cell Proliferation*, 36(3) pp. 131-149.

Vermeulen, W., and Fousteri, M. (2013). Mammalian Transcription-Coupled Excision Repair. *Cold Spring Harbor Perspectives in Biology*, 5(8): a012625.

Vidi, P.A., Liu, J., Salles, D., Jayaraman, S., Dorfman, G., Gray, M., Abad, P., Moghe, P.V., Irudayaraj, J.M., Weismüller, L., and Lelièvre, S.A. (2014). NuMA promotes homologous recombination repair by regulating the accumulation of the ISWI ATPase SNF2h at DNA breaks. *Nucleic Acids Research*, 42(10) pp. 6365-6379.

Walker, C., Herranz-Martin, S., Karyka, E., Liao, C., Lewis, K., Elsayed, W., Lukashchuk, V., Chiang, S.C., Ray, S., Mulcahy, P.J., Jurga, M., Tsagakis, I., Iannitti, T., Chandran, J., Coldicott, I., De Vos, K.J., Hassan, M.K., Higginbottom, A., Shaw, P.J., Hautbergue, G.M., Azzouz, M., and El-Khamisy, S.F. (2017). C9orf72 expansion disrupts ATM-mediated chromosomal break repair. *Nature Neuroscience*, 20(9) pp. 1225-1235.

Walker, S., Meisenberg, C., Bibby, R.A., Askwith, T., Williams, G., Rininsland, F.H., Pearl, L.H., Oliver, A.W., El-Khamisy, S., Ward, S., and Atack, J.R. (2014). Development of an oligonucleotide-based fluorescence assay for the identification of tyrosyl-DNA phosphodiesterase 1 (TDP1) inhibitors. *Analytical Biochemistry*, 454: pp. 17-22.

Wang, J.C. (2002). Cellular roles of DNA topoisomerases: A molecular perspective. *Nature Reviews. Molecular Cell Biology*, 3(6) pp. 430-440.

Ward, J.M., and La Spada, A.R. (2015). Ataxin-3, DNA Damage Repair, and SCA3 Cerebellar Degeneration: On the Path to Parsimony? *PLoS Genetics*, 11(1): e1004937.

Warren J.J., Forsberg L.J., and Beese, L.S. (2006). The structural basis for the mutagenicity of O⁶-methyl-guanine lesions. *Proceedings of the National Academy of Sciences of the United States of America*, 103(52) pp. 19701-19706.

Wells, O and El-Khamisy, S.F. (2014). *Animal Models of Movement Disorders: Second Edition*, Mark S. LeDoux eds. (Elsevier Inc.).

- Whitaker, A.M., Schaich, M.A., Smith, M.R., Flynn, T.S., and Freudenthal, B.D. (2017). Base excision repair of oxidative DNA damage: from mechanism to disease. *Frontiers in Bioscience*, 22 pp. 1493-1522.
- Willis, N., and Rhind, N. (2009). Regulation of DNA replication by the S-phase DNA damage checkpoint. *Cell Division*, 4:13.
- Wong, R.W., Blobel, G., and Coutavas, E. (2006). Rae1 interaction with NuMA is required for bipolar spindle formation. *Proceedings of the National Academy of Sciences of the United States of America*, 103(52) pp. 19783-19787.
- Woodbine, L., Gennery, A.R., and Jeggo, P.A. (2014). Reprint of "The clinical impact of deficiency in DNA non-homologous end-joining". *DNA Repair*. 17: pp. 9-20.
- Xu, Y., Wu, X., and Her, C. (2015). hMSH5 facilitates the repair of camptothecin-induced double-strand breaks through an interaction with FANCD1. *The Journal of Biological Chemistry*, 290(30) pp. 18545-58.
- Yang, C.H., Lambie, E.J., and Snyder, M. (1992). NuMA: an unusually long coiled-coil related protein in the mammalian nucleus. *The Journal of Cell Biology*, 116(6) pp. 1303-1317.
- Yarden, R.I., Pardo-Reoyo, S., Sgagias, M., Cowan, K.H., and Brody, L.C. (2002). BRCA1 regulates the G2/M checkpoint by activating Chk1 kinase upon DNA damage. *Nature Genetics*, 30(3) pp. 285-289.
- Yokoyama, H., and Gruss, O.J. (2013). New Mitotic Regulators Released from Chromatin. *Frontiers in Oncology*, 3: 308.
- Zandomeni, R., Mittleman, B., Bunick, D., Ackerman, S., and Weinmann, R. (1982). Mechanism of action of dichloro-f8-D-ribofuranosylbenzimidazole: Effect on *in vitro* transcription. *Proceedings of the National Academy of Sciences of the United States of America*, 79(10) pp. 3167-3170.
- Zhang, Y.W., Regairaz, M., Seiler, J.A., Agama, K.K., Doroshov, J.H., and Pommier, Y. (2011). Poly(ADP-ribose) polymerase and XPF-ERCC1 participate in distinct pathways for the repair of topoisomerase I-induced DNA damage in mammalian cells. *Nucleic Acids Research*, 39(9) pp. 3607-3620.
- Zhang, Y., Wang, J., Ding, M., Yu, Y. (2013) Site-specific characterization of the Asp- and Glu-ADP-ribosylated proteome. *Nature Methods*, 10(10) pp. 981-984.
- Zhao, X.B., Wu, D., Wang, M.J., Goto, M., Morris-Natschke, S.L., Liu, Y.Q., Wu, X.B., Song, Z.L., Zhu, G.X., and Lee, K.H. (2014). Design and synthesis of novel spin-labeled camptothecin derivatives as potent cytotoxic agents. *Bioorganic & Medicinal Chemistry*, 22(22) pp. 6453-6458.
- Zhou, B.B., and Elledge, S.J. (2000). The DNA damage response: putting checkpoints in perspective. *Nature*, 408(6881) pp. 433-439.